AN ENVIRONMENT-DEPENDENT APPROACH TO WIDEBAND MODELLING AND COMPUTER SIMULATION OF UHF MOBILE RADIO PROPAGATION IN BUILT-UP AREAS

BY

Olutumininu Olufolabomi Kafaru, B.Sc(Hons), M.Sc.

Thesis submitted in accordance with the requirements of the University of Liverpool for the degree of Doctor in Philosophy.

The Department of Electrical
Engineering and Electronics,
The University of Liverpool.

February 1989

ABSTRACT

A statistical multipath model for the echo amplitudes, time delays and carrier phase shifts caused by multipath propagation in a mobile radio channel has been derived. The model, based on a scattering approach, is directly dependent on the stochastic processes associated with the characterising parameters of the environment, namely the scatterer locations and sizes. The model uses an optical analogy which is well justified at UHF. Specifically, a geometric 'wave' optics approach provides a high frequency approximation for the behaviour of the electromagnetic wave.

Multipath propagation is fundamentally a function of the nature of the local environment of the mobile and hence the model parameters are environment-related. A quantitative classification of the various types of environments encountered in a typical mobile radio service area has been undertaken and the relationship between the nature of multipath and the environment established.

A simulation package has been developed which uses the model, together with environment-dependent parameters generated stochastically and extracted from Ordnance Survey community maps, to produce a wideband impulse response of the channel. The frequency and delay dispersion in a particular radio channel environment can be obtained by appropriate processing of the simulated impulse response as shown in this work.

ACKNOWLEDGEMENT

I would like to express my appreciation to the individuals and organisations who have made it possible for me to complete this project.

Firstly, my gratitude goes to my Heavenly Father for His steadfast love and abundant blessings to me, and His strength which upheld me right through the studies.

I am most grateful to Prof. J.D Parsons, my supervisor for his invaluable contributions to the success of this work. His constant encouragement, assistance and guidance have been very much a blessing. My thanks also go to Dr A.S Bajwa for his interest in the work and his various comments and suggestions. The contributions made by Dr A.M Turkmani are also gratefully acknowledged. I would like to thank Mr D.A Demery who provided the experimental data used in this study.

My gratitude also goes to my family for their loving and prayerful support, and to my friends , in particular David, Yinka, Emmanuel and the Africa Christian Fellowship, Liverpool branch for their support and also to my colleagues, particularly L. Wang.

I gratefully acknowledge the scholarship received from the Association of Commonwealth Universities for the period from October 1984 to September 1987, and the financial assistance from other organisations including the IEE, Cellnet, Leche Trust for the period from October 1987 to date.

Finally, I wish to thank Mrs B. Lussey for her help and encouragement, and for typing some of the lengthy equations and thanks to Yetunde who patiently converted the manuscript into typscript.

Dedicated to

my mother, Adebisi.

To God be the glory for His blessing.

Table of Contents

LIST OF PRINCIPAL SYMBOLS

a_k	amplitude associated with k^{th} propagation path
$\hat{A}_T$	range vector of transmitter location with respect to model origin
$\hat{A}_S$	range vector of scatterer location with respect to model origin
$\hat{A}_m$	range vector of mobile location with respect to model origin
$\hat{A}_i$	range vector of scatterer location with respect to mobile
A_{os}	test square
A_{bs}	total area occupied by buildings in test square A_{os}
A_v	area covered by vegetation in test square A_{os}
A_R	area covered by roads and pavements in test square A_{os}
$b(\tau)$	measuring system filters
B	bandwidth of channel sounder
B_c	coherence bandwidth of channel
B_d	Doppler spread of channel
c_i	amplitude associated with i^{th} scatterer
C_n	normalised amplitude of n^{th} component in electric field E_z
d	average excess delay
d_z	average excess delay for location z
D	average separation between scatterers
E_z	electric field component of mobile received signal
E_o	common amplitude of signal components in electric field E_z
E_i	field incident on scatterers (μV/m)
f_d	Doppler frequency shift (Hz)
f_c	carrier frequency (Hz)
$g(t, \tau)$	lowpass complex impulse response of the channel
$G(f, v)$	output Doppler spread function for a deterministic channel
$G(s)$	curvature of wavefront at point s on a ray

$h(t, \tau)$	bandpass complex impulse response of the channel
H	scatterer height
$I_k(\tau)$	inphase component of amplitude a_k at delay τ
$I_n(\tau_k)$	inphase component of impulse response envelope at delay τ_k
Nb	number of buildings in test square A_{os}
Nm	number of spatial measurement locations
$p(\tau)$	bandlimited approximation to an impulsive probing signal
P_{oc}	probability of echo path occupancy
p(R)	probability density distribution of scatterer range location R
p (ϕ)	probability density distribution of scatterer azimuth location ϕ
p(H)	probability density distribution of scatterer height H
$p_n(\tau_k)$	instantáneous power density at location m and delay τ_k
$P_s(\eta, \xi)$	time-delay cross power spectral density (W/s)
$P_s(\xi)$	average power output of the channel (W/s)
$P_G(\Omega, \xi)$	frequency/Doppler-shift cross power spectral density (W/Hz)
$P_G(\xi)$	Doppler power spectrum
$P_V(\xi, \mu)$	time-delay/Doppler-shift cross power spectral density (W/s/Hz)
$P_z(\tau_k)$	average power density at location z and delay τ_k
$Q_k(\tau)$	quadrature component of amplitude a_k at delay τ
$Q_n(\tau_k)$	quadrature component of impulse response envelope at delay τ_k
r_i	distance of i^{th} scatterer from mobile (metres)
$r(t)$	envelope of mobile received signal
R_i	distance of i^{th} scatterer from model origin (meters)
$R(\tau)$	autocorrelation function of a process
$R_g(t, s; \tau, \xi)$	autocorrelation function of the time-variant impulse response $g(t, \tau)$
$R_T(f, l; t, s)$	autocorrelation function of the time-variant transfer function $T(f, t)$

$R_G(f, l; \nu, \mu)$	autocorrelation function of the output Doppler spread function $G(f, \nu)$
$R_V(\tau, \xi; \nu, \mu)$	autocorrelation function of the delay-Doppler spread function $V(\tau, \nu)$
$R_s(\tau)$	autocorrelation function of probing signal
$R_T(\Omega)$	frequency correlation for zero spatial separation of observation points
$R_T(\Omega, \eta)$	spaced two-frequency correlation function
$R_{yx}(\tau)$	cross correlation function of x and y variables at time lag τ
s	excess delay spread
s_b	building size
s_z	excess delay spread for location z
s_i	size of i^{th} scatterer
s_{av}	average scatterer size
$s(t)$	complex bandpass input signal
S_i	i^{th} scatterer
$S(f)$	complex spectrum of input signal s(t)
$S(f, t)$	bandpass complex transfer function of the channel
T	time period of pseudo random binary sequence
$T_c(t)$	inphase component of electric field E_z
$T_s(t)$	quadrature component of electric field E_z
$T(f, t)$	lowpass complex transfer function of the channel
$u(t)$	complex lowpass input signal
$U(f)$	complex spectrum of lowpass input signal u(t)
V	vehicle speed
$V(\tau, \nu)$	delay-Doppler spread function for a deterministic channel
w	dimensions of the scatterer walls
W	canyon width of street
$y(t)$	complex bandpass output signal
$Y(f)$	complex spectrum of bandpass output signal y(t)
$z(t)$	complex lowpass output signal
$Z(f)$	complex spectrum of lowpass output signal z(t)

α_i	angle of wave arrival of i^{th} scattered component
β	phase constant
$\Delta\gamma$	relative phase change
Δm	sampling distance between two measurement locations
$\Delta\tau$	incremental propagation time interval
ε_H	standard deviation of building height distribution BHD
ε_s	standard deviation of building size distribution BSD
ε_ϕ	standard deviation of azimuth location distribution BLD (ϕ)
ε_R	standard deviation of range location distribution BLD (R)
γ_i	phase shift associated with i^{th} scatterer
γ_o	initial phase of scattered component
λ	carrier wavelength (meters)
Λ	average number of scatterers per unit area
μs	microseconds
μ_s	mean of building size distribution BSD
μ_R	mean of range location distribution BLD (R)
μ_ϕ	mean of azimuth location distribution BLD (ϕ)
μ_H	mean of building height distribution BHD
Ψ	wave function
$\Psi_{inc}(r)$	incident plane electromagnetic wave
$\Psi_{ref}(r)$	reflected plane electromagnetic wave
ρ_i	reflection coefficient of i^{th} scatterer
$\rho_n(t)$	attenuation factor for n^{th} path in channel
$\sigma(\xi, \mu)$	time-delay/Doppler shift scattering function
τ_i	propagation time delay associated with i^{th} scatterer
$\tau_n(t)$	propagation time delay for n^{th} path in channel
τ_k	time delay associated with k^{th} propagation path
τ_g	gross delay of resolvable propagation path
$\tau_{(xi}(t)$	excess delay due to i^{th} scatterer
τ_o	minimum arrival delay

θ_k	phase shift associated with k^{th} propagation path
$\otimes$	convolution symbol
$< . >$	ensemble average notation
DF	double Fourier transform notation
DF^{-1}	inverse double Fourier transform notation
$E_x[.]$	exponential function notation
$F[.]$	Fourier transform notation
$F^{-1}[.]$	Inverse Fourier transform notation
$Re\{.\}$	Real part notation
BAI	building area index
BHD	building height distribution
BLD	building location distribution
BSD	building size distribution
RI	road index
SI	storey index
TI	terrain index
VI	vegetation index

LIST OF ABBREVIATIONS

AM	Amplitude modulation
APDP	Average power delay profile
B_c	Coherence bandwidth
B_d	Doppler spread
BER	Bit Error Rate
BS	Base station
CPU	Central Processor Unit
dB	Decibel
e.m	Electromagnetic
FCF	Frequency correlation function
FFT	Fast Fourier Transform
FM	Frequency modulation
FSF	Frequency selective fading
GIS	Geographic Information Systems
ISI	Intersymbol Interference
kHz	Kilohertz
km	kilometers
LOS	Line of sight
LTV	Linear Time-Varying
MHz	Megahertz
MRC	Mobile Radio Communication
MS	Mobile station
NG	National Grid
ns	nanoseconds
OS	Ordnance Survey
PDP	Power delay profile
prbs	pseudo random binary sequence

rms	root mean square
SSB	Single sideband
SW	Southwest
UHF	Ultra High Frequency
US	Uncorrelated scattering
VHF	Very High Frequency
WB	Wideband
WSS	Wide sense stationary
WSSUS	Wide sense stationary uncorrelated scattering

CHAPTER ONE

1. INTRODUCTION

In the beginning God created the heavens and the earth...
..... and God said to man," Be fruitful and multiply,
fill the earth and subdue it .
Genesis 1:28

1.1 Prologue

Nature and man, singly or acting together are the sources of all engineering problems. Man's insatiable need to communicate instantly and reliably whether on the move or otherwise has led to the use of the natural medium for radio communications. This of course has led to the unavoidable involvement with and the desire to overcome the random changeability which often accompanies natural phenomena. This involvement has resulted in engineering feats, one of which is mobile radio communications.

The use of radio for communications with people on the move dates back to 1897 when Marconi sent a transmission to a tugboat over an 18 mile path from Needles on the Isle of Wight. The first land mobile radio telephone system was installed in 1921 in Detroit, USA operating in the 2 MHz frequency band [1]. As needs increased and technology improved, so service was extended and use was made of higher frequencies where spectrum availability was greater. The mobile telephone system initially provided service to specialized groups, the military and public safety services. This was extended to the industrial and land transportation class e.g taxi cabs and finally to the private sector where considerable interest was shown initially by business executives who needed to be constantly accessible to colleagues and clients. Today, the service has been extended to the travelling public on trains, coaches, etc.

The increasing demand for service (man's need) has led to congestion of the frequency bandwidth in the regions of the spectrum (natural resource) where technology can provide economical systems. Man is therefore continually pitting his wits against nature in order to make the best use of the available resources. Efficient use of the available frequency spectrum is therefore of utmost importance to the systems designer. This has resulted in the Federal Communications Commission (FCC) reducing channel spacing from

50KHz to the present 25KHz [1] while research is being carried out by various interested groups into radio schemes which will maximise the use of available spectrum while providing efficient and reliable service to customers. In the battle of wits between nature and man, a compromise is often achieved.

1.2 Land Mobile Radio Systems Considerations

In a typical mobile radio communications system, one terminal is stationary while the other is moving. In towns and cities where the majority of these system operate, transmission from the base station to the mobile is often obstructed by buildings so that the mode of propagation is by way of diffraction, reflection and scattering from the buildings in the general vicinity of the mobile. The signal at the mobile is composed of a number of these scattered waves and their mutual interference causes random fluctuations in the received signal level of up to 40dB at a rate of several times per second at VHF and above [1,2]. These random fluctuations, referred to as fast or multipath fading, are manifest as space and frequency selective fading in radio transmissions. Space selective fading can seriously impair intelligibility of speech in analogue transmissions. In digital systems, these phenomena cause errors and an increase in transmitter power is largely ineffective in mitigating their effects. Frequency selective fading, apparent in the form of Intersymbol Interference (ISI) causes irreducible errors with different forms of modulation schemes and thus sets the performance limit for digital mobile radio.

In order to design systems for optimum performance under the conditions established by the propagation channel, it is absolutely essential for the systems designer to have a good understanding of the behaviour of the channel. The fundamental mechanisms of propagation must be understood and suitable propagation models developed for use in the analysis of the channel. The

use of theoretical models for radio propagation channel analysis is of fundamental importance in the advancement of radio science and such models are of considerable engineering value. Several workers have in the past developed multipath propagation models and some of these will be examined in chapter 3. The inadequacy of these models however lies in their omission of environment dependent parameters to describe the behaviour of the radio channel. Previous work by Cox[4] and Bajwa[9] has shown the dependence of the channel characteristics on the local environment of the mobile. This work seeks to overcome the aforementioned limitation by using an environment-dependent approach in the channel modelling. The various types of environments encountered in the operational domain of a mobile radio communication system ensure that the channel behaves randomly so that statistical methods are best suited for use in the channel analysis.

1.3 Radiowave Propagation in Built Up Areas.

Mobile radio propagation in built up areas is primarily via random scatterers along the path within the environment. In a typical system, the transmitting antenna or base station (BS) is situated atop a high building to give a clear view of the operational area while the receiving antenna or mobile station (MS) is located atop the vehicle. All communication is therefore essentially at ground level. In addition to the propagation path losses that are encountered by other types of atmospheric propagations, mobile radio signals are also affected by various types of scattering and multipath phenomena which cause severe signal fading and are attributable to the propagation medium [10]. In built-up areas, the received signal at the mobile is therefore subject to multipath propagation in addition to long term shadow effects and noise. The long term shadow effect, evident as variations in the mean received signal strength, is caused by changes in the gross features of the environment through which

the mobile moves. A lot of work has been done on this aspect as recorded in literature [1,11,12,16,17,18,23,29,30,32, 34,64,65,74-78]. Noise is an additive effect which originates from nature or man. (Nature and man causing yet more problems !). Atmospheric noise is due to nature while man-made noise is found in the guise of vehicle ignition noise, receiver equipment noise and interference from transmissions by other radio users within the service area of the mobile. Urban noise has been studied and modelled by Middleton [72,73].

Multipath propagation has also been studied and characterised by several workers [1-9,26,27,31,43,63-70,79,80]. Although some of these studies have shown the dependence of the multipath phenomena on the environment, very little work has been done [25,70] to model the environment-dependent nature of the mobile radio channel. A review of the fundamental mechanisms of propagation is obligatory in this study, as a first step towards developing an environment-dependent multipath model.

1.3.1 Propagation Mechanisms

In the 800/900 MHz band, propagation usually takes place via space waves. At these frequencies ground waves are attenuated very rapidly with distance and sky waves pass readily through the ionosphere with little energy being reflected back to earth. For the relatively short service ranges of land mobile systems using this band of frequencies, propagation is achieved by means of space waves travelling between transmitting and receiving antennas, and in some cases diffraction over terrain irregularities such as hills. Following is a discussion of the propagation mechanisms which have been found to be prevalent in the mobile radio propagation channel at these frequencies [11,12].

1.3.1.1 Atmospheric Propagation

In free space propagation, electromagnetic (e.m) energy spreads out uniformly in all directions from the source. The amount of energy available to the receiving antenna is inversely proportional to the square of the distance from the source [13,82,83]. Generally, free space conditions are deemed to occur if there is a clearance for the first Fresnel Zone for the path between transmitter and receiver. In land mobile system operations this condition rarely exists but work done by Ikegami et al [11] and Bertoni et al [12] has shown that free space propagation takes place place between the BS and the roof tops of the buildings in the vicinity of the mobile. For large distances the signals at this level comprise of plane uniform-phase e.m waves.

1.3.1.2 Diffraction

Diffraction of the e.m waves is affected by the frequency and polarisation of the waves and the geometry of the propagation path. Diffraction occurs when the propagation path is obstructed by features of the intervening terrain or by the buildings between the transmitting and receiving antennas. This is a mechanism whereby the e.m waves are caused to bend around the obstruction before continuing on to the receiver, resulting in attenuation of the waves. The severity of signal attenuation depends on whether the obstruction extends through the propagation path or merely approaches the line of sight (LOS) path. The extent of the clearance of the obstruction may be assessed in terms of Fresnel Zone Ellipsoids drawn around the path terminals. Methods of calculating diffraction loss by knife edge methods are well documented [14-17].

Figure (1.1) shows a situation in which a hill results in the mobile antenna being located in a local shadow zone. The strength of the received field in

the shadow zone, calculated using knife edge methods, will be less than the free space field for the same distance from the transmitter. The deeper the antenna is in the shadow, the less the field strength and for a given situation, the loss of field strength increases with higher frequencies [71]. The service area on the leeward side of the hill is said to have diffraction coverage while the windward side receives direct coverage.

1.3.1.3 Scattering/Reflection.

Scattering of radiowaves occur from the surfaces of the obstructing buildings. Specular reflection occurs when the surface is smooth and it follows Snell's Law. Diffuse reflection occurs when the surface is roughly textured, (the roughness being comparable with the wavelength of the radiated signal) causing the reflected e.m waves to follow divergent paths and therefore scattering the energy. In the UHF frequency band, such scattering is predominant because the wavelengths at these frequencies are very small. The buildings are therefore referred to as scatterers. Huygen's principle can be used to explain the properties of scattering by diffuse reflections [14,15,54,57,84]. Attenuation of the reflected signal occurs because the scatterer walls are not prefect reflectors. The reflective property of the scatterers is measurable and in any mobile radio environment, needs to be appraised. In a given situation, a reflection from an individual building may be dominant because of the building height, size or orientation with respect to the antennas. Reflections may make high signals available in areas deeply shadowed. The gain produced by a large reflecting surface can even result in signals in excess of free space values [18].

In addition to reflections from the walls of buildings, terrain features such as hills or even the ground can reflect radio waves as shown by rays A and B in Figure (1.1). The reflection coefficient in this case is dependent on the

dielectric constant and conductivity of the type of terrain (e.g sandy, rocky etc), the transmission frequency, plane of polarisation and angle of incidence of the wave [71,85].

1.3.1.4 Channelling / Ducting.

When the mobile moves along a street radially oriented with respect to the transmitter and with buildings along both sides of the road, the waves can be trapped in the canyons formed by the buildings and channelled down the street. This is illustrated in Figure (1.2).

Having examined these propagation mechanisms, it is seen that multipath is caused primarily by reflections and scattering either from terrain features or from buildings. This study will therefore consider reflection/scattering as the main propagation mechanism in built up areas. In addition, the model to be developed will be based on flat terrain only. We now look further at a typical mobile radio scenario in a built-up area.

1.3.2 A Typical Mobile Radio Propagation Situation

A typical situation of propagation in built up areas is shown in Figure (1.3). The plane waves arriving at the cluster of buildings arrive by way of free space propagation (path A), reflection from (path B) or diffraction around (path C) a large non local scatterer. These waves have propagation times and amplitudes that are random variables. At the cluster of buildings the waves break up into subpaths as shown. Subpaths 1 and 2 result from single reflection while subpath 3 results from possible multiple reflection. Thus the received signal at the mobile consists of a large but finite number of waves with different propagation time delays and carrier phases due to the varying propagation

path lengths travelled, and random angles of arrival relative to the direction of vehicle motion due to the varying locations of the scatterers. These waves interfere, either constructively or destructively depending on the distribution of the carrier phases, to produce a received signal which exhibits random variations in both amplitude and phase. The fades are deep and rapid for systems operating at UHF and microwave frequencies.

In a dynamic situation where the mobile moves from one location to another, the path lengths become time variant because for each path associated with a distinct physical scatterer, as the mobile moves so will the location of the associated scatterer. The electrical lengths of the paths for the scatterers are sufficiently different so that signals starting out simultaneously on each ray path can be distinguished as arriving sequentially. However, paths with the same propagation time delay but different angles of wave arrival cannot be distinguished by path length alone. Figure (1.4) shows a situation in which three waves subject to single scattering arrive at the receiver. The propagation time is identical for the paths located on a particular elliptical surface of revolution with the transmitter and receiver as foci. Each such ellipse defines a different transmitter-receiver propagaton time delay. It is, therefore, possible to distinguish between paths with the same propagation time and different angles of arrival (BPM and BQM), and paths with the same angle of arrival by their different propagation times (BRM and BQM).

Another consequence of the random motion of the mobile is that different scatterers and terrain along the route constitute a constantly changing environment which in turn changes the plane waves incident on the mobile receiver. Thus, superimposed on the rapid fading are slow variations in the mean field strengths of the received signals. The long term variations are referred to as shadow effects.

1.3.2.1 Discrete Point Scatterer Channel Representation

The mobile radio channel representation in which propagation takes place through single scattering is shown to comprise a set of discrete independent scatterers or 'blobs' [22] as in Figure (1.5). The propagation path via scatterer i causes the i^{th} wave to arrive τ_i seconds after the signal is transmitted. For a static situation, τ_i is related to the distance d_i travelled by the i^{th} wave as:

$$\tau_i = \frac{d_i}{c} \qquad (1.1)$$

where c is the velocity of wave propagation in the medium. The energy received from this wave is related to the scattering cross section σ where :

$$\sigma = |\rho^2| \qquad (1.2)$$

The factor ρ is defined as the reflection coefficient of the scatterer and determines the amplitude of the wave received from the i^{th} scatterer.

For a dynamic situation when the location of the scatterer changes as the mobile moves, τ_i becomes a function of time and can be expressed as

$$\tau_i = \mu_i + \Delta\mu_i \qquad (1.3)$$

where μ_i is the gross delay and $\Delta\mu_i$ is the delay perturbation component due to the time variation associated with path i. This time variant term appears as a phase fluctuation in the received signal and is specified such that the phase factor $2\pi f_c \Delta\mu_i$ takes values in the range $-\pi$ to $+\pi$ and is apparent as a frequency shift f_d about the carrier frequency of the transmitted signal.

1.3.3 The Doppler Effect

When the mobile (or transmitter) is moving, it moves at various rates of speed and in various directions so that arriving waves, in addition to the random variations in signal amplitude and phase, also experience a frequency shift caused by the Doppler Effect. For a component wave, the Doppler frequency shift f_d is a function of the mobile speed v and the angle of arrival α which propagation vector makes with the mobile velocity vector and is given by :

$$f_d = \frac{v}{\lambda} \cos \alpha \qquad (1.4)$$

where λ is the carrier wavelength. The situation is shown in Figure (1.6). The Doppler shifts can be used to identify the location of the scatterers. A positive shift indicates that the scatterer is ahead of the mobile while a negative shift indicates that the scatterer is behind. The maximum possible shift is $(\frac{v}{\lambda})$. Even though a knowledge of the Doppler frequency shifts can be used in the identification of scatterers, ambiguities still exist for those situated to the left or right of the mobile. This difficulty can be overcome with the use of semi-omnidirectional antennas for each side.

With the knowledge of the propagation mechanisms in built up areas and the ability to identify individual scatterers, the behaviour of the mobile radio propagation medium can be effectively studied, characterised and modelled.

1.4 Radio Reception in the Prescence of Multipath

In the mobile radio propagation channel in built up areas, several distinguishable paths exist from transmitting to receiving antenna. This multipath phenomenom results in fading of the received signal as the

attenuated, delayed and phase shifted replicas of the transmitted signal combine. In a fading environment the received signal fluctuates as the vehicle moves, thus distorting speech and data transmitted by conventional methods. Two distinct types of signal fading can be observed in the channel - space and frequency selective fading.

1.4.1 Space Selective Fading

Space selective fading occurs as a result of the movement of the mobile. The relative path lengths of the scattered waves vary due to the spatial movement of the mobile thereby introducing relative phase shifts depending on the carrier wavelength. The multiple signal phasors combine to produce a resultant phasor with a random amplitude and phase.

In narrowband transmission where the propagation delays are extremely small compared to the inverse of the signal bandwidth, the fading of the signal envelope is rapid and severe and the statistics of the envelope conform to a Rayleigh distribution. In AM and AM-related (e.g SSB) systems the fast fading causes loss of synchronisation between the received signal carrier and the local oscillator used for coherent detection. Envelope (non-coherent) detection is degraded due to frequent dropouts. In FM systems, the time varying phase of the fading signal results in random frequency modulation which appears as random noise at the output of an FM demodulator.

1.4.2 Frequency Selective Fading

In wideband transmission the signal bandwidth is large, comprising of a band or packet of frequencies. Two frequency components in the packet with a small separation in frequency will tend to fade in a correlated manner because

the phasors for the multipath echos are alike. With increasing frequency separation, the sets of phasors at one frequency tend to decorrelate with the set at the other. This occurs because the relative phase positions of the frequency components which depend strongly on the carrier frequency become random. The severity of the decorrelation depends on the time delay spread of the multipath echos which in turn depend on the excess path lengths travelled by the component waves. The signal phase, critically sensitive to path length, changes by the order of 2π radians as the path length changes by a wavelength. Hence for large delay spreads, the phases will vary over many radians for smaller frequency separations[9,17]. This results in uncorrelated fading and ultimately a distorted frequency spectrum. This phenomenom is termed frequency selective fading (FSF) and is the dual of space selective fading.

In digital radio transmission where the signal transmitted is a pulse train, this phenomenom causes errors. The individual pulses tend to spread out and overlap, a condition known as Intersymbol Interference (ISI). This effect becomes more pronounced as the data rate increasingly approaches the inverse of the delay spread. The multipath delay spread thus sets a limit on the irreducible bit error rate (BER) performance of the channel.

Various methods of combatting these channel impairments have been developed. Different types of diversity techniques such as space, frequency, time and polarisation diversity have been successfully employed in voice and low speed data (up to 2400 b/s) transmission [1]. In Wideband transmission, in addition to diversity techniques, signal waveform shaping, message coding and adaptive equalisation techniques have been utilised in reducing the effect of ISI [16]. In recent years spread spectrum has enjoyed increased usage in mitigating against multipath effects [52].

1.5 Scope of present study

Establishing a workable MRC system is a tough task due to the vulnerability of the propagation medium to multipath. In a communications system, once the transmitter and receiver sites have been chosen , if the propagation medium is well characterised and modelled, the transmitter and receiver can be designed in such a manner as to reduce the effects of the channel disturbances. The channel can be characterised by performing extensive measurements and preparing a model of the channel on the basis of the measurements. This method can be very costly and time consuming. Another approach is to develop a realistic theoretical model which can be used in a computer simulation of the channel, with the purpose of predicting, via simulation, the response of the channel to any transmitted signal. This approach eliminates the need to carry out the costly process of field trials.

The work presented in the study involves the channel simulation approach. Whereas previous work [19] has neglected to include the environment directly in the modelling and simulation, this study specifically approached the modelling from an environment-dependent viewpoint. The model includes parameters which are obtained from the local environment of the mobile. In addition, the simulation process is based on the physical environment. The behaviour of the channel is determined in terms of statistics pertaining to the random time varying behaviour of the equivalent channel filter [20,21,22]

Hitherto, in propagation studies for mobile radio links, the environment is qualitatively described as rural, suburban, urban etc. These terms are imprecise and open to different interpretations by different users. A qualitative classification of the various types of environments encountered in a mobile radio service area is here proposed. This classification is based on the building sizes, heights and density distribution, building location distributions and the

percentage of the area covered by buildings. A quantitative relationship between the nature of multipath and the environment is thus established.

In order to simulate the received signal at the mobile, it is necessary to superimpose signals scattered from various points in the environment. To do this superposition, the phase of the component signals must be specified. This leads to the use of phasors to describe the signals and of complex algebra to process them in the simulation. In chapter 2, the statistical methods that are applicable to the channel characterisation are discussed. The correlation functions which are relevant to study of the system behaviour are derived. The central core of the channel simulation is the model that describes the propagation phenomena. Chapter 3 describes the environment-dependent approach to the modelling of the channel. The stochastic model is derived as are the system functions for the mobile radio propagation channel. In chapter 4, we discuss the simulation technique used in this study. and the principles of the programming. The relevance of the environment to the propagation phenomena cannot be over emphasised. As such, in chapter 5, a new method of classifing the environment is presented. In chapter 6, the results of the simulation in the various environments are discussed and compared with some measured data where available. Finally the conclusions drawn from this work, together with proposals for further study are presented in chapter 7.

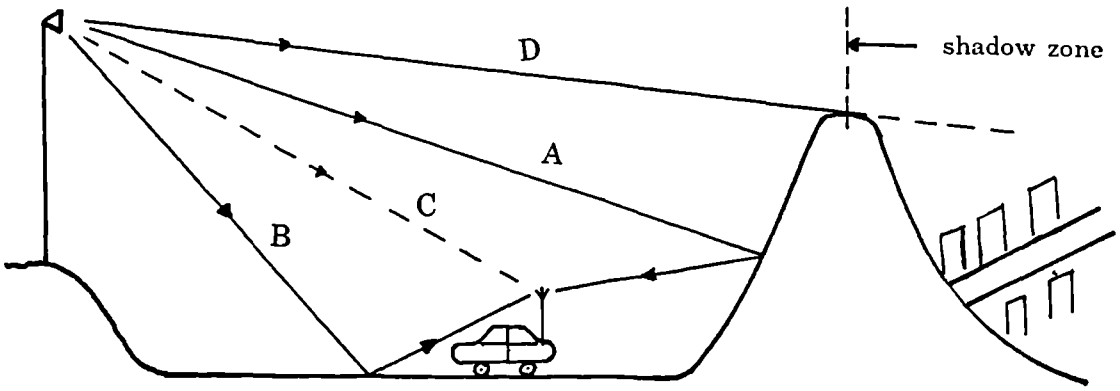

Figure (1.1) Multipath radio propagation mechanisms.

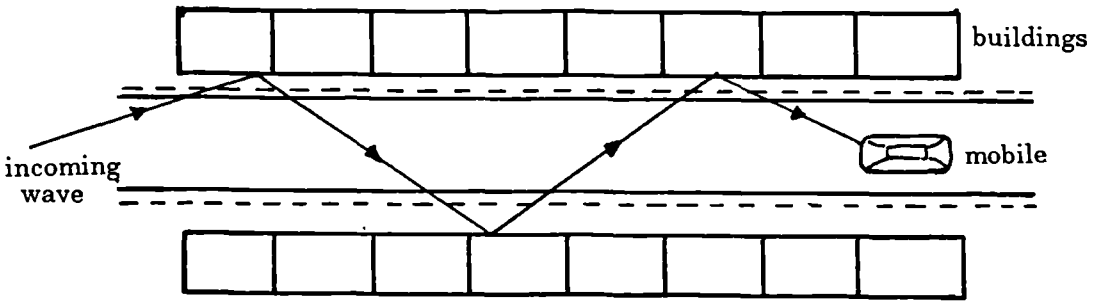

Figure (1.2) Channelling of radio waves.

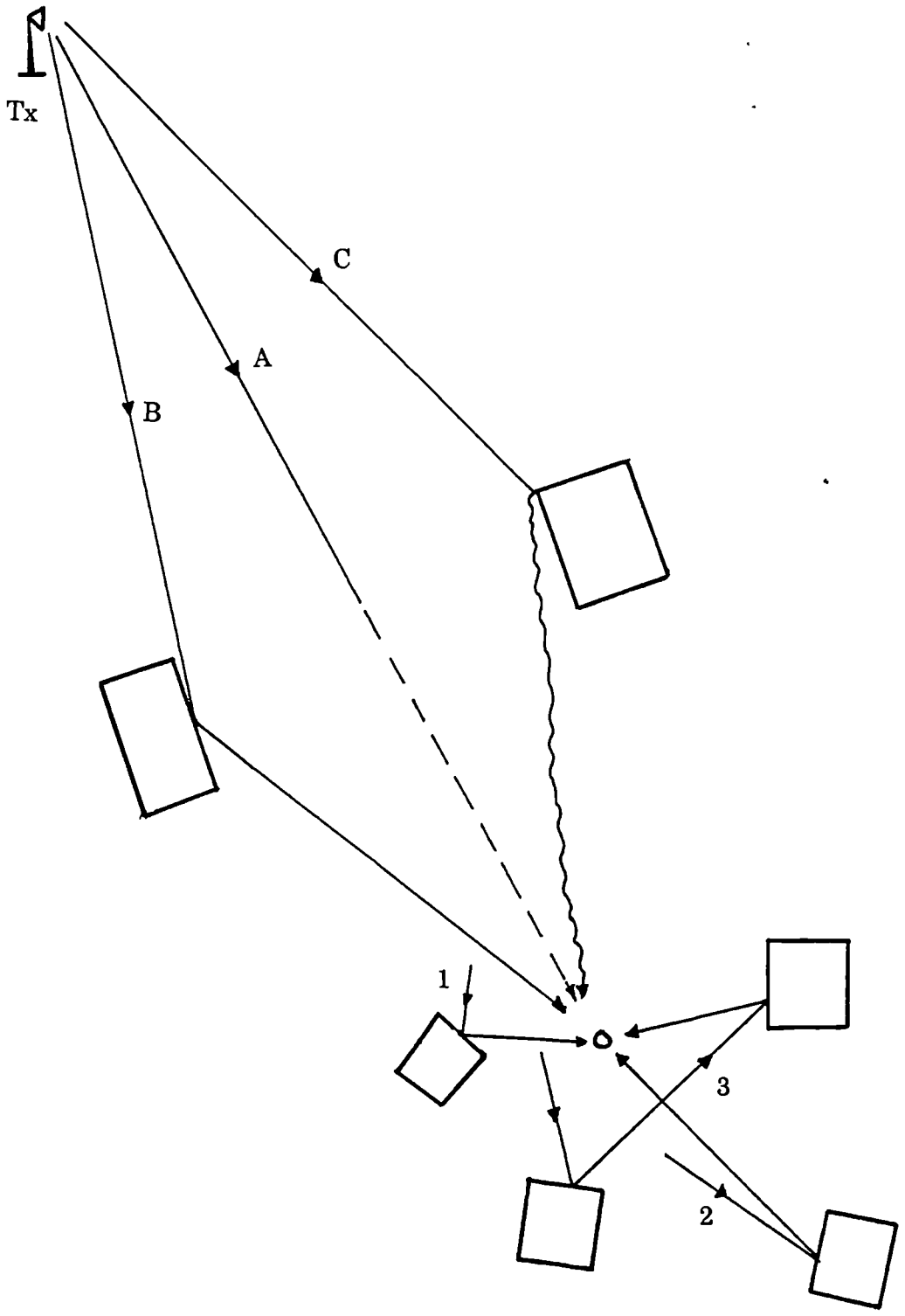

Figure (1.3) Propagation in built-up areas.

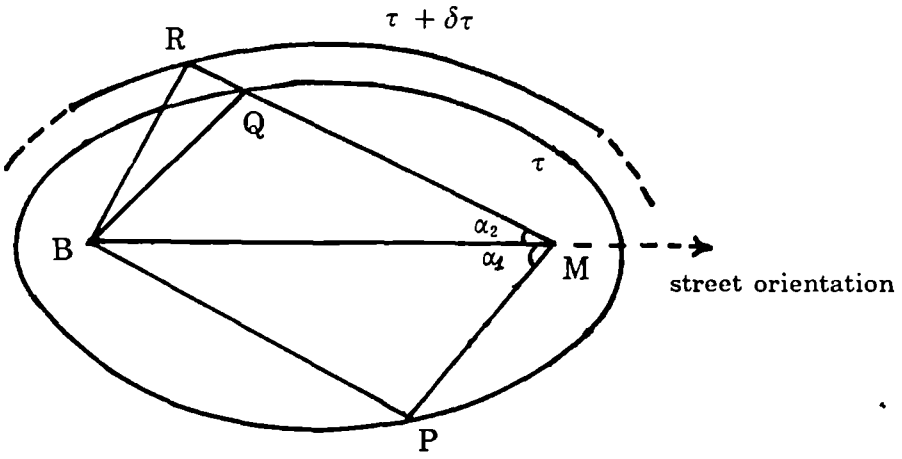

B = base station

M = mobile

α = angle of wave arrival

τ = propagation time delay

Figure (1.4) Differentiation of single scattered waves

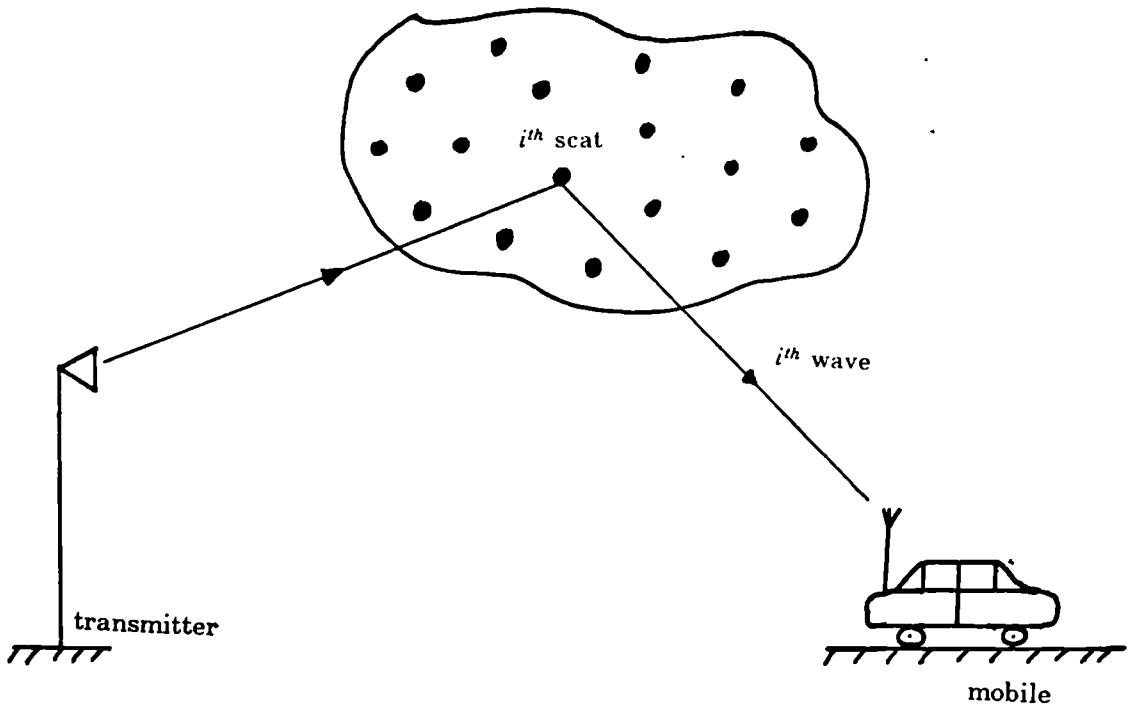

Figure (1.5) Point scatterer model.

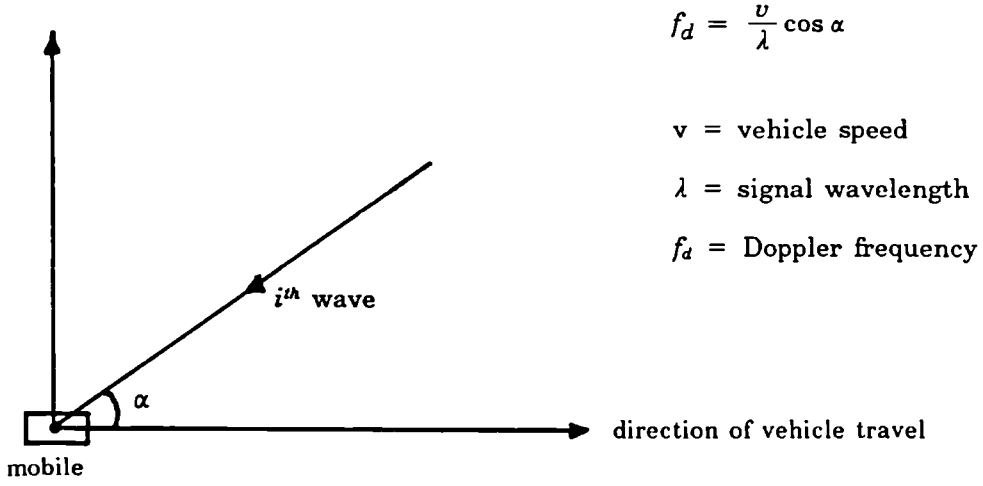

Figure (1.6) Doppler effect

CHAPTER TWO

2. CHARACTERISATION OF THE WIDEBAND MOBILE RADIO PROPAGATION CHANNEL.

For out of the abundance of the heart,
the mouth speaks.
Matthew 12:34

2.1 General Description of the Fading Dispersive Channel.

A radio communications system is required to perform a function involving the transmission of various forms of information from one location to another. The performance of such a system is largely dependent on the behaviour of the propagation medium. In mobile radio communications, the propagation path is a system element whose characteristics are beyond the control of the design engineer. It is therefore apparent that these characteristics should be determined as thoroughly as possible so that the other system elements can be designed for optimum operation under the conditions established by the propagation path.

Fading dispersive radio communication channels are best described as random linear time variant (LTV) filters [3,20,21,22]. These channels are most conveniently and usually quite adequately studied through their system functions, that is, their reponses to "elementary" signals, usually time-impulses (delta functions) or frequency impulses (sinusoidal tones). The random behaviour of the channel leads to a statistical characterisation in terms of correlation functions for the various system functions. The characterisation of LTV networks was first treated by Zadeh [24]. Since then, extensive work has been done by Kailath [21] and Bello [20] with emphasis on communication channel characterisation. Some of this work is applied in this present study.

The MR propagation channel can generally be represented as a random LTV filter. By classifying the channel using statistical descriptions based on the physical propagation characteristics, a more exact characterisation can be obtained. The characterising function is expected to provide an insight into the physical mechanisms which dominate the channel behaviour.

2.2 Linear Time Variant Description of Propagation Channel.

The propagation channel converts the signal at the output ports of the transmitter (input port of channel) into a roughly equivalent but much reduced signal at the input terminals of the receiver (output port of channel). If an ideal impulse (delta function) is transmitted over the channel, the received signal will appear as a train of delayed impulses separated in time depending on the particular environment. The characteristics of these impulses which occupy a certain length of time before falling to an undetectable level, change as a function of time. If the delayed impulses overlap, the channel is called continuous whereas if they are confined within certain non-overlapping ranges in time, it is termed a discrete multipath channel. The channel is seen to operate as a linear time-varying filter with the property of introducing several components, including the main one. The filter can be described in the time or frequency domains or a combination of both [40]. (The terms filter and channel will be used interchangeably in the following discussions). The signal representation to be employed in this study is now discussed.

2.2.1 Complex Signal Representation

The filter input signal s(t) whose spectral components cover a band of frequencies which is small compared to any frequency in the band may be expressed as

$$s(t) = Re\{u(t)\exp(j2\pi f_c t)\} \tag{2.1}$$

where

$$u(t) = b(t)\exp(j\Theta) \tag{2.2}$$

Re {.} is the real part notation, f is some frequency within the band, and u(t) is the complex envelope of s(t). The name for u(t) derives from the fact that the magnitude $|u(t)|$ is the conventional envelope of s(t), while the angle Θ of u(t) is the conventional phase of s(t) measured with respect to the carrier phase ($2\pi f_c t$) [40]. s(t) is called a narrowband or bandpass signal, while u(t) is called the equivalent lowpass signal of s(t) because its frequency contents are centered around f = 0.

Equation (2.1) is a time domain representation of the complex signal. The frequency domain representation S(f) and s(t) are related through the Fourier Transform relationship. If F denotes the forward transform and F^{-1} the inverse transform, then,

$$s(t) = F^{-1}[S(f)] = \int S(f) \exp(j2\pi ft)df \tag{2.3}$$

and

$$S(f) = F[s(t)] = \int s(t) \exp(-j2\pi ft)dt \tag{2.4}$$

The time and frequency domain representations as well as the complex envelope signal representation will be employed in the following discussions of the filter and channel characterisations.

2.2.2 Bandpass Representation of the Linear Time Variant Filter.

A bandpass filter is a system whose amplitude characteristic has significant values only in an interval not containing the origin [41]. The system impulse

response h(t) and output function y(t) can be obtained in terms of their equivalent lowpass representations.

2.2.2.1 System Response.

The impulse response h(t) is the time domain response of the system to an input signal s(t), while the frequency domain response H(f) is called the transfer function of the system and are given by [41] :

$$h(t) = F^{-1}[H(f)] = \int H(f) \exp(j2\pi ft) df \tag{2.5}$$

and

$$H(f) = F[h(t)] = \int h(t) \exp(-j2\pi ft) dt \tag{2.6}$$

The complex bandpass representation of h(t) is also given by [41]

$$h(t) = Re\{\ g(t) \exp(j2\pi f_c t)\ \} \tag{2.7}$$

where g(t), the equivalent lowpass signal is

$$g(t) = \int G(f) \exp(j2\pi ft) df \tag{2.8}$$

2.2.2.2 Output Function.

The signal y(t) at the output of the filter can be obtained from the convolution integral [41]

$$y(t) = s(t) \otimes h(t) = \int s(t-\tau)h(t)dt \qquad (2.9)$$

or from the frequency domain multiplication

$$Y(f) = S(f)H(f) \qquad (2.10)$$

where

$$S(f) = \int s(t) \exp(-j2\pi f_c t)dt \qquad (2.11)$$

s(t) is as defined in (2.1) with u(t) having a low pass spectrum U(f) given by

$$U(f) = \int u(t) \exp(-j2\pi ft)dt \qquad (2.12)$$

substituting s(t) in (2.1) into (2.11)

$$S(f) = \int Re\{ u(t) \exp(j2\pi f_c t) \} \exp(-j2\pi f_c t)dt \qquad (2.13)$$

If $Re\{A\} = \frac{1}{2}[A + A^{\times}]$, where $A^{\times}$ is the complex conjugate of A, then

$$S(f) = \frac{1}{2}[U(f-f_c) + U^{\times}(-f-f_c)] \qquad (2.14)$$

Now,

$$Y(f) = \frac{1}{2}[U(f-f_c) + U^{\times}(-f-f_c)][G(f-f_c) + G^{\times}(-f-f_c)] \qquad (2.15)$$

For a linear narrowband system,

$$U(f-f_c) = 0 \qquad f < 0 \qquad (2.16a)$$

$$G(f-f_c)=0 \qquad f<0 \tag{2.16b}$$

hence expanding (2.15) and using (2.16)

$$Y(f)=\frac{1}{2}\left[U(f-f_c)G(f-f_c)\ +\ U^{\times}(-f-f_c)G^{\times}(-f-f_c)\right] \tag{2.17}$$

Let

$$Z(f)=U(f)G(f) \tag{2.18}$$

then

$$Y(f)=\frac{1}{2}\left[Z(f-f_c)\ +\ Z^{\times}(-f-f_c)\right] \tag{2.19}$$

Taking the inverse Fourier Transform of (2.19)

$$y(t)=Re\{\,z(t)\exp(j2\pi f_c t)\,\} \tag{2.20}$$

From (2.18) it is seen that the complex low pass output of the channel is given by

$$z(t)=\ u(t)\otimes g(t)\ =\ \int u(t-\tau)g(t)dt \tag{2.21}$$

Representing the real bandpass signals and systems by their equivalent lowpass responses ensures the removal of the carrier frequency from the ensuing mathematical processing. This form of representation allows the filter processes to be described simply and conveniently and in addition, the full flavour of the time-frequency duality of such an approach can be fully exploited. In using complex envelope notation, it is understood that there is always implied

the existence of the carrier frequency via which, equations such as (2.7) and (2.20), converts the complex time functions into physical narrowband signals. The behaviour of the linear time-varying filter can be obtained either deterministically for one time instant, or statistically over a period of time during which the system behaviour varies randomly. The system functions which describes this behaviour are derived using the signal representations introduced in this section. In addition, the bandpass and complex envelope notations will be used interchangeably in the function equations.

2.2.3 The System Functions

The general behaviour of the linear time-variant channel can be described basically in the time or frequency domains. In addition, the dispersive behaviour, which is of particular interest in this work, is best expressed in the time-delay or Doppler-shift domains or both. The four basic system functions used for the description of the deterministic behaviour of the filter has been derived by Bello [20] and is summarised below.

2.2.3.1 Time - Time Delay System Function

The time domain description of the channel is given by the time impulse response of the system. Associated with each of the N multiple paths in the channel is a propagation time delay $\tau_n(t)$ and an attenuation factor $\rho_n(t)$ both of which are functions of time. The received bandpass signal may be expressed as

$$y(t) = \sum_n \rho_n(t)\, s[t - \tau_n(t)] \tag{2.22}$$

substituting (2.1) in (2.22), the equivalent low pass received signal is observed to be

$$z(t) = \sum_n \rho_n(t)\, u[t - \tau_n(t)]\ \exp[-j2\pi f_c \tau_n(t)] \tag{2.23}$$

Since z(t) is the response of an equivalent low pass channel to the equivalent low pass signal u(t), it follows that the equivalent low pass channel is described by the time variant impulse response

$$g(t, \tau) = \sum_n \rho_n(t)\, \delta[t - \tau_n(t)]\ \exp[-j2\pi f_c \tau_n(t)] \tag{2.24}$$

The transmission function $g(t, \tau)$ represents the response of the channel at time t to an impulse applied at time $t - \tau$. It shows that the linear time-varying channel may be interpreted as a continuum of nonmoving scintillating scatterers.

2.2.3.2 Time-Frequency System Function.

If the channel is cissoidally excited, it is observed that different outputs are produced for different frequencies of the input signal. This implies a channel modification as a function of frequency. The relationship between the output signal in time and the spectrum of the input signal is expressed by the lowpass channel transfer function T(f,t) where

$$T(f,t) = \sum_n \rho_n(t) \exp[-j2\pi(f + f_c)\tau_n(t)] \tag{2.25}$$

T(f,t) is the Fourier transform of $g(t, \tau)$ [20].

2.2.3.3 Frequency - Doppler System Function.

The frequency domain description of the channel is obtained through G(f,v), the output Doppler spread function. This function, a dual of the impulse response, relates the input frequency spectrum to the output signal spectrum of the channel. Due to the relative motion of the receiver with respect to the transmitter, additional frequency components v are introduced into the output spectrum due to the Doppler effect discussed in section 1.3.3. This frequency shift causes a smear or spread of the spectrum around the carrier frequency, called the Doppler Spread. With U(f) as the spectrum of the complex envelope of the input signal and Z(f) the corresponding output signal spectrum, the relationship between U(f) and Z(f) is given by

$$Z(f) = \int U(f - v)G(f - v, v)dv \tag{2.26}$$

$G(f, v)$ and T(f,t) are related through the Fourier transform as

$$G(f, v) = \int T(f,t) \exp(-j2\pi vt)dt \tag{2.27}$$

Function G(f,v) explicitly describes the frequency dispersive behaviour of the multipath channel. It shows that the channel can be interpreted as a continuum of Doppler shifting elements.

2.2.3.4 Time delay - Doppler System Function.

A description which shows the dispersiveness of the channel in both the time and frequency domains simultaneously is obtained through the delay - Doppler system function $V(\tau, \nu)$. Functions $V(\tau, \nu)$ and $g(t, \tau)$ are related through the Fourier transform as

$$V(\tau, \nu) = \int g(t, \tau) \exp(-j2\pi\nu t) dt \tag{2.28}$$

that is, $V(\tau, \nu)$ is the spectrum of the impulse response $g(t, \tau)$. If the time dispersiveness is restricted to the input port of the channel while the frequency dispersiveness is constrained to the output port, then z(t) the lowpass output function is obtained as

$$z(t) = \int\int V(\tau, \nu) u(t - \tau) \exp(j2\pi\nu t) d\nu d\tau \tag{2.29}$$

Equation (2.29) shows that the output is represented as a sum of delayed and then Doppler shifted elements. Signals in the delay range $(\tau, \tau + d\tau)$ with Doppler shifts in the range $(\nu, \nu + d\nu)$ have a differential scattering amplitude of $V(\tau, \nu) d\nu d\tau$.

This function gives the best description of the physical behaviour of the scatterers in the channel.

The relationships between the four system functions which describe the deterministic behaviour of scattering in the multipath channel is shown diagramatically in Figure (2.1).

For a randomly time variant linear channel, a deterministic approach to the channel characterisation as discussed above cannot be used since the exact

output at any time cannot be predicted. The output of the equivalent channel filter is a series of random signals so that the channel can be described as a stochastic process. Characterisation is best achieved using stochastic methods, specifically description in terms of correlation functions.

2.2.4 The System Correlation Functions

In general, a randomly time variant linear channel has a mixed deterministic and random behaviour. These may be separated into the sum of a purely random part, and a deterministic part which is equal to the ensemble average. A purely random process has a zero ensemble average and corresponds to a Gaussian process. For the random time variant channel, the system functions of section 2.2.3 become stochastic processes. In order to obtain an exact description for such channels, a knowledge of the multidimensional probability density distributions of the random variables is required, a situation highly unlikely in real physical situations. A more practical but less exact approach involves statistical characterisation in terms of the correlation functions for the various system functions since these correlation functions make it possible to obtain the autocorrelation functions of the channel output.

In general, for a random signal comprising an ensemble of sample components, complete information about it is unavailable, hence it is best described in terms of ensemble averages. The autocorrelation function $R(\tau)$ is a measure of the rapidity of variation of a given signal. If the signal contains predominantly low frequencies, it varies slowly while the converse is true for high frequency components. Hence for slowly varying signals, $R(\tau)$ is sizeable even for large values of τ. For rapidly varying signals, $R(\tau)$ becomes small and dies out quickly. Generally, $R(\tau)$ decays with τ and eventually goes to zero.

In defining the autocorrelation function of the complex envelope of a random process, two correlation functions are needed in order to uniquely specify the $R(\tau)$ of the original real process. Thus for a process $\mathrm{Re}\{w(t)\exp(j2\pi f_c t)\}$ the required functions are

$$r_1(t,s) = < w^{\times}(t)w(s) > \tag{2.30a}$$

$$r_2(t,s) = < w(t)w(s) > \tag{2.30b}$$

$< >$ denotes ensemble average. In most applications, especially wide sense stationary processes, $r_2(t,s) = 0$, so that the autocorrelation function is completely defined by $< w^{\times}(t)w(s) >$. So if $s = t + \tau$, then

$$R(\tau) = < w^{\times}(t)w(t+\tau) > \tag{2.31}$$

Correlation functions for the general random linear time variant channel are given below. It is assumed that the system response is a Gaussian process so that the system functions of section 2.2.3, have a zero ensemble average. The corresponding autocorrelation functions are defined as:

$$R_g(t,s;\tau,\xi) = < g^{\times}(t,\tau)g(s,\xi) > \tag{2.32}$$

$$R_T(f,l;t,s) = < T^{\times}(f,t)T(l,s) > \tag{2.33}$$

$$R_G(f,l;\nu,\mu) = < G^{\times}(f,\nu)G(l,\mu) > \tag{2.34}$$

$$R_V(\tau,\xi;\nu,\mu) = < V^{\times}(\tau,\nu)V(\xi,\mu) > \tag{2.35}$$

These correlation functions are related through the Fourier Transform relationships. They also provide a tool for classifying the various types of channels encountered in radio communications.

2.3 Classification of Propagation Channels

Classification of propagation channels can be done on the basis of the character of the distortions associated with them. The distortions often encountered include temporal variations in the fading statistics and time and frequency dispersiveness. The three representative classes of channels which are of interest in radio propagation have been treated extensively in literature [20,22] and are briefly discussed below :

2.3.1 The Wide Sense Stationary (WSS) Channel.

In many physical channels it may be assumed that the fading statistics are time invariant (or stationary) over some definable time interval. This behaviour leads to the classification of such a channel as a Wide Sense Stationary channel. This means that the channel correlation functions are invariant under a translation in time and therefore related in time only through the time difference. For example,

$$R_g(t,s;\tau,\xi) = R_g(t,t+\eta;\tau,\xi) \equiv R_g(\eta;\tau,\xi) \tag{2.36}$$

where s is related to t through the time difference η, i.e $s = t + \eta$.

The channel is said to be dispersive only in time. One of the physical scattering properties inherent in the WSS channel is that contributions from differential

scatterers with different Doppler shifts are uncorrelated, that is, the correlation functions have a singular behaviour in the Doppler shift variables. The WSS channel is said to comprise of a continuum of scintillating scatterers.

2.3.2 The Uncorrelated Scattering (US) Channel.

Some physical channels (e.g troposcatter) may be modelled as a continuum of uncorrelated scatterers. This implies that the amplitudes of two different scatterers are uncorrelated if they cause different time delays. This class of channels are called Uncorrelated Scattering Channels [20]. They are singular in the time delay variable and dispersive only in frequency. This means that the channel correlation functions are invariant under a translation in frequency and therefore related in frequency only through the frequency shift, that is

$$R_G(f,l;\nu,\mu) = R_G(f,f+\Omega;\nu,\mu) \equiv R_G(\Omega;\nu,\mu) \tag{2.37}$$

where l is related to f through the frequency shift Ω i.e, $l = f + \Omega$.

The manifestation of frequency dispersion is sometimes called time-selective fading [40].

2.3.3 The Wide Sense Stationary Uncorrelated Scattering (WSSUS) Channel.

There exist channels which are dispersive both in time and frequency. This class of channels, the simplest to describe in terms of channel correlation functions, are of practical interest and are called WSSUS channels. The channel correlation functions are of the form characteristic to the WSS channel and the US channel. The WSSUS channel provides a complete understanding of the physical distribution and behaviour of scatterers in the channel.

Classification of the mobile radio propagation channel as WSSUS provides a realistic approach to the study of the channel behaviour. For this class of channnels the correlation functions can be expressed in terms of the corresponding cross power spectral densities as:

$$R_g(t, t+\eta; \tau, \xi) = P_g(\eta, \xi)\delta(\tau - \xi) \tag{2.38}$$

$$R_T(f,l;t, t+\eta) = R_T(\Omega, \eta) \tag{2.39}$$

$$R_G(f, f+\Omega; \nu, \mu) = P_G(\Omega, \xi)\delta(\nu - \mu) \tag{2.40}$$

$$R_V(\tau, \xi; \nu, \mu) = P_V(\xi, \mu)\delta(\nu - \mu)\delta(\tau - \xi) \tag{2.41}$$

Equation (2.38) called the delay spread function, shows that for the WSSUS channel, $g(t, \tau)$ exhibits uncorrelated scattering in the time delay domain and WSS behaviour in time. The correlation function of (2.39) exhibits wide sense stationarity in both time and frequency domains. This function can be used to evaluate the frequency coherence of two signals. Equation (2.40) is called the Doppler spread function and it shows the channel as exhibiting uncorrelated scattering in the Doppler shift variable and WSS statistics in the frequency domain. Finally, equation (2.41) the delay Doppler spread function, shows that the channel exhibits uncorrelated scattering in both time delay and frequency shift variables. This implies that the WSSUS channel can be represented as a collection of scintillating uncorrelated scatterers which cause different delays and Doppler shifts. The relationships between these autocorrelation functions are shown in Figure (2.2).

The scattering phenomenom observed in a mobile radio channel is similar to that exhibited by the WSSUS channel. This obsrvation has led to the

classification of the mobile radio channel as a WSSUS channel, thus simplifying its characterisation.

2.4 Characterisation of the Mobile Radio Propagation Channel.

In the mobile radio channel, due to the presence of buildings and other obstacles between the transmitter and receiver stations, propagation is by way of diffraction and scattering via these obstacles. Each propagation path can be viewed as a ray path along which electromagnetic energy travels. Associated with each ray path is a path variable set $\{a_k, \tau_k, \phi_k\}$ where a_k is the amplitude, τ_k is the propagation time delay and ϕ_k is the carrier phase shift. The buildings within the service area are of different types and sizes, and at varying locations from the mobile. Each significant scatterer will give rise to a scattered wave whose amplitude charactristics are independent of the other contributions. The various scatterer locations result in different propagation time delays while the movement of the mobile introduces Doppler shifts into the phases of the waves. At the receiver, these delayed, attenuated and phase shifted replicas of the transmitted signal, combine as phasors to produce a fading signal. The nature of the local environment of the mobile is random so that as the mobile moves from one location to another, the fading signal statistics become random, behaving in a non stationary manner. Characterisation of such a channel can be simplified if assumptions of stationarity can be made.

Refering to the discussions in previous sections, it is noted that the mobile radio channel behaves as a linear time variant filter, therefore it can be treated as a WSSUS channel where the contributions from different scatterers with different propagation time delays and Doppler shifts are uncorrelated [4,9,20,22]. In order to account for the mixture of environments within a proposed service

area, small scale characterisation is possible over short spatial distances of a few tens of wavelengths (up to 10m at 900 MHz) where the mean field strength and significant scatterers remain unchanged. A large scale or global characterisation can then be produced by averaging the small scale statistics over the service area. This is an approach suitable for system design where the designer is interested mainly in knowing the bounds of the variation of the channel parameters over the service area. This two stage characterisation process has been successfully employed by Cox [4] and Bajwa [9] and will also be used in this simulation study.

A good description of the multipath channel can be obtained from its complex impulse response measured as a function of distance along the direction of vehicle travel. Appropriate processing yields useful statistical descriptions such as the power delay profile and the frequency correlation function from which descriptors such as the average delay, delay spread and coherence bandwidth, which are very useful system design parameters, are obtained. The statistical processing is done using the four correlation functions derived previously.

2.4.1 Small Scale Characterisation Using the Correlation Functions.

2.4.1.1 Time - Time Delay function

Characterisation in the time domain is achieved using the delay spread function of equation (2.38) which presents the power in the envelope as a delay cross power spectral density $P_g(\eta, \xi)$. When the time separation between observations is zero, i.e $\eta = 0$, then $P_g(\eta, \xi)$ reduces to a power spectral density:

$$P_g(\eta, \xi) \equiv P_g(\xi) = < g(\xi) > \qquad (2.42)$$

$P_g(\xi)$ is the average power output of the channel as a funtion of delay ξ. This function is called the power impulse response [42] or Power Delay Profile PDP [4,9]. If $P_g(\xi)$ is considered as a statistical distribution of echo strengths, then the average delay d is the first central moment of the distribution while the delay spread s is the square root of the second central moment.

The delay spread s, is a measure of the time dispersion encountered in the channel. In digital data systems, time dispersion causes intersymbol interference as the data rate approaches the inverse of the delay spread. s thus sets a bound on the maximum signalling rate and the BER rate performance of the channel. The average delay d is a performance parameter for use in the design of vehicle location systems.

2.4.1.2 Time - Frequency function

The frequency domain description of the channel can be obtained from equation (2.39) and $P_g(\eta, \xi)$ as [9,20]

$$R_T(\Omega, \eta) = \int P_g(\eta, \xi) \exp(-j2\pi\Omega\xi) d\xi \tag{2.43}$$

When the time separation between observations is zero, i.e $\eta = 0$, then (2.43) becomes

$$R_T(\Omega) = \int P_g(\xi) \exp(-j2\pi\Omega\xi) d\xi \tag{2.44}$$

This function is called the spaced frequency correlation function [41] or the Frequency Correlation Function FCF [4,9]. The FCF is a measure of the

correlation between the frequency components of the received signal spectrum and hence explicitly gives an indication of the frequency selective behaviour of the channel. The FCF can be obtained by Fourier transforming the PDP.

A useful system design parameter obtainable from the FCF is the Coherence bandwidth B_c This is a measure of the maximum frequency difference for which signal spectrum components remain correlated, in other words, the frequency separation beyond which samples of the Fourier transform of the PDP are independent. Correlation bandwidths can be defined for suitable values of correlation, and usual values are 0.5 and 0.9 [4,9]. In an ideal channel, B_c and s are related through an inverse relationship [4].

2.4.1.3 Frequency - Doppler Function

The function $P_G(\Omega, \xi)$ of (2.40) can be expressed as

$$P_G(\Omega, \xi) = \int R_T(\Omega, \eta) \exp(-j2\pi\mu\eta) d\eta \qquad (2.45)$$

When the frequency separation is zero, i.e $\Omega = 0$, then (2.45) becomes

$$P_G(0, \xi) \equiv P_G(\xi) \qquad (2.46)$$

This function is called the Doppler power spectrum [20]. Parameter B_d, the Doppler spread can be obtained from $P_G(\xi)$ and is defined in a similar manner to B_c.

2.4.1.4 Delay - Doppler Function

The function $P_V(\xi, \mu)$ of (2.41) is a 2-dimensional power spectrum as a function of time delay ξ and Doppler shift μ. It has been identified as the scattering function $\sigma(\xi, \mu)$ of a scatterer (identical to the radar target scattering function [41]). $\sigma(\xi, \mu)$ may be regarded as the fraction of the scatterer cross section contributed by scatterers in the vicinity of delay ξ and Doppler shift μ, i.e

$$\sigma(\xi, \mu) = \int P_g(\eta, \xi) \exp(-j2\pi\mu\eta) d\eta \qquad (2.47)$$

$\sigma(\xi, \mu)$ gives an insight into the physical mechanism of the channel by which it is possible to identify (i) the path lengths of the delayed signal components associated with the scatterers and (ii) the scatterer locations by the angle of wave arrival. An example of a scattering function obtained from one of the simulation runs is shown in Figure (2.3).

2.4.2 Large Scale Characterisation Using the Correlation Functions.

Within a large service area, the multipath channel exhibits temporal nonstationarity due to the spatial inhomogeneity of the environment. To obtain the large scale characterisation, the scattering functions can be used over consecutive spatially homogeneous , wide sense stationary locations so that these correlation functions become dependent only on the variations due to the temporal nonstationarity. The large scale description can be accomplished in two ways, by direct data reduction methods or by global probability density distributions of the path variables amplitude a, delay τ, Doppler shifts ν and carrier phase shifts ϕ.

2.4.2.1 Direct data reduction

This method is applied to the small scale parameters average delay, delay spread and correlation bandwidth described in section 2.5.1. The power delay profile PDP is obtained at M consecutive locations on a small section of the mobile route. The average power delay profile (APDP) for this section is the ensemble average of the M power profiles and the parameters d and s for the small section are defined as :

$$d = \frac{\int \tau P(\tau) d\tau}{\int P(\tau) d\tau} \tag{2.48}$$

and

$$s = \left[\frac{\int (\tau - d)^2 P(\tau) d\tau}{\int P(\tau) d\tau} \right]^{\frac{1}{2}} \tag{2.49}$$

The coherence bandwidth B_c is obtained from the corresponding FCF. The set of d, s and B_c obtained over the large area provide the large scale characteristics.

2.4.2.2 Global probability density distributions

The propagation channel can be described by the set of path parameters $\{a_k, \tau_k, \phi_k\}$ defined previously. A complete description would be in terms of the joint probability density distributions. On the basis of the WSSUS assumption, it is more appropriate to regard these parameters as independent

variables so that the density distributions of the independent sets $\{a_k\}$, $\{\tau_k\}$ and $\{\phi_k\}$ should be used in the large scale description. This approach has been employed by Turin et al [3] and Suzuki [8], and by Hashemi [19] in his simulation of the propagation channel. None of these authors however included the angle of wave arrival α in their studies.

The characterisation approach outlined in this section has been adopted by previous workers to enable them make simplifying assumptions about the propagation channel. This approach, though well tried and proven, still leaves the question of the environment dependency unanswered. Simulation offers the solution to the problem. Referring to the point-scatterer model of Figure (1.5), it is seen that if this model is implemented in software, then it is possible to vary the location, size and other attributes of the scatterers, so that the various scenarios obtainable in real physical situations can be simulated for use in system performance evaluations. The first step toward this goal is the development of a suitable propagation model. This is carried out in the next chapter.

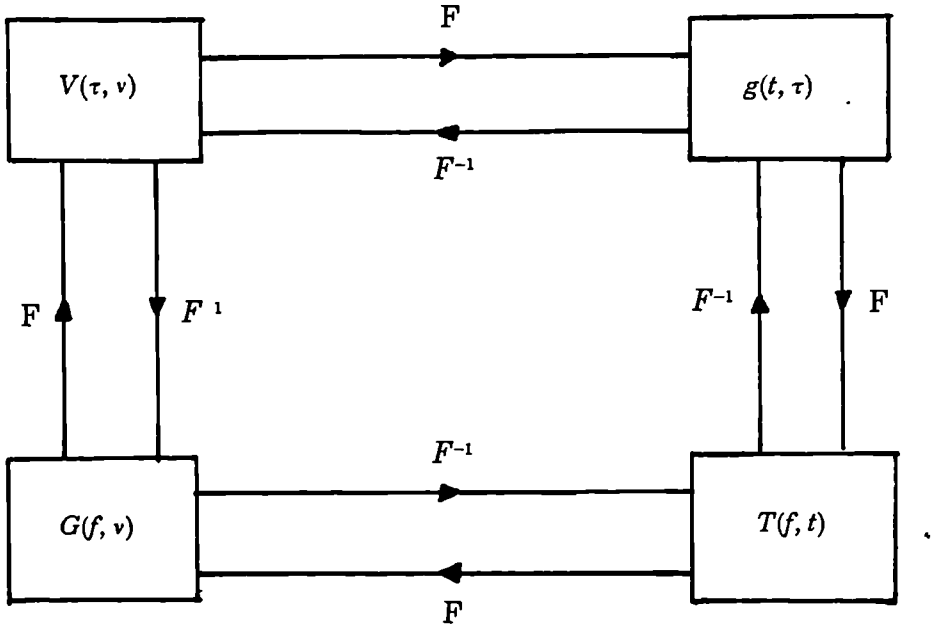

Figure (2.1) Relationships between the channel system functions.

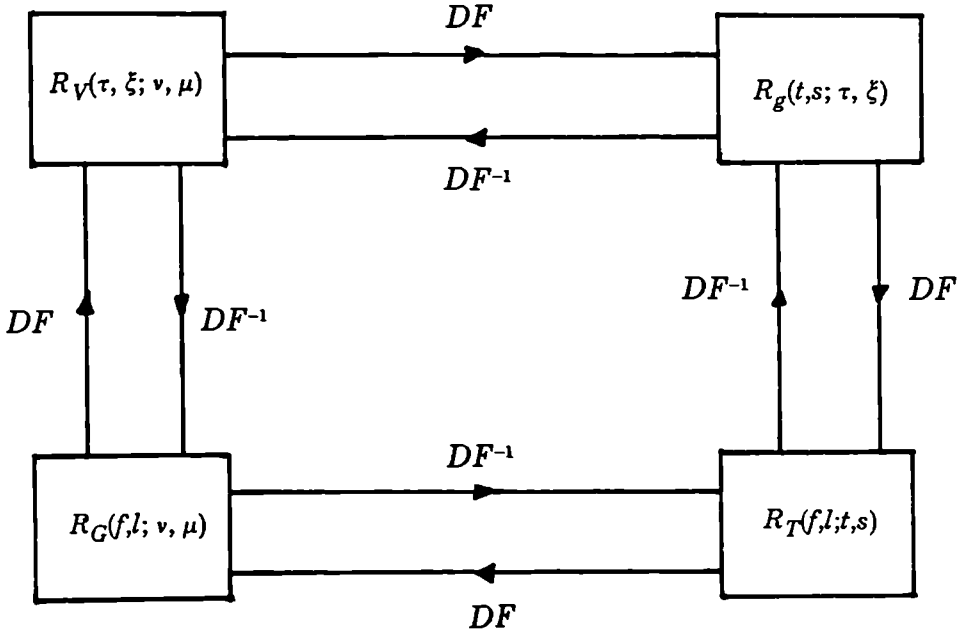

Figure (2.2) Relationships between the channel correlation functions.

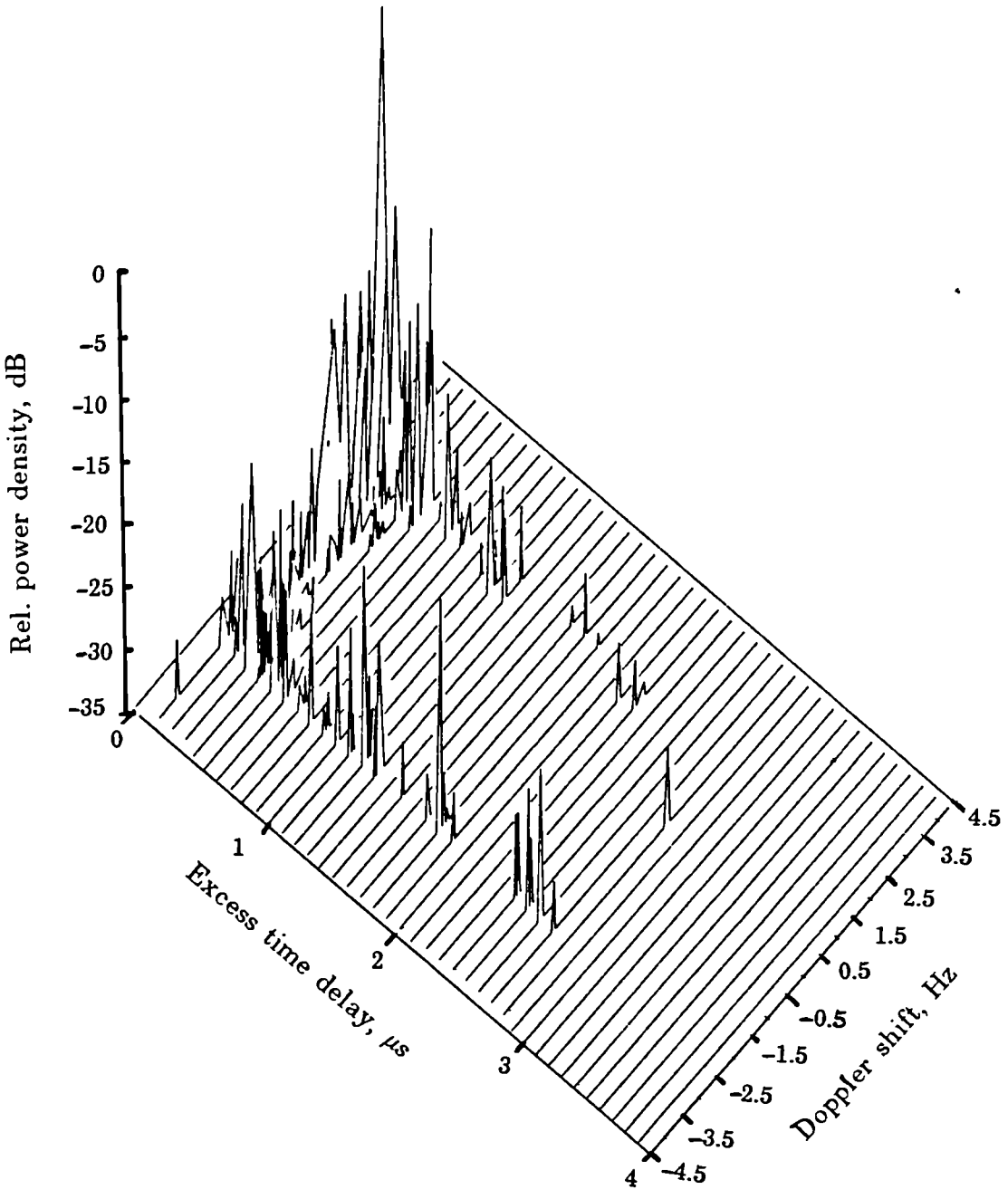

Figure (2.3) Scattering function for mobile radio channel.

CHAPTER THREE

3. THE ENVIRONMENT - DEPENDENT MULTIPATH PROPAGATION MODEL

Now the body is not made up of one part but of many.
So that there should be no division in the body....
..its parts should have equal concern for each other.
1 Corinthians 12:14,25

Multipath propagation as introduced previously causes rapid variations in the received signal at the mobile station and is directly dependent on the nature of the local environment of the mobile station. A model of the propagation channel will, for the sake of completeness and accuracy, need to include parameters which are functions of the environment. This need, previously omitted by workers who have attempted to model the channel, is now addressed in this study.

3.1 Factors affecting channel modelling.

Various factors influence the choice of method of developing a channel propagation model. A simple and obvious objective is to develop a model that is very reliable and affordable by the service providers. This objective involves considerations such as accuracy in representing the propagation mechanism, ease of use and others which are discussed below.

3.1.1 Applicability

In general system design, such as when systems are being developed that will operate in many locations, propagation models that apply to a wide variety of locations but in a limited frequency band and for limited distances are needed. On the other hand, when a given performance objective is to be met in a known location, the specific system design requires a propagation model that accounts for relevant environmental and /or topographical information.

3.1.2 Model Basis

The basis for a model may be either theoretical or empirical or a combination of both. Theoretical models allow (i) a recognition of the fundamental relationships that apply over a broad range of circumstances and (ii) the definition of relationships that exist among any combination of input parameters. Empirical models are derived from measurement and observation, and offer an advantage in that all environmental influences are implicit in the results regardless of whether or not they can be separately recognized and theoretically studied. In addition, they offer the opportunity to provide probabilistic descriptions of the propagation phenomena. However, the validity of such models is limited by the accuracy with which measurements are made and the extent to which the environment of the measurements adequately represent the physical environment in which the model is to be applied.

3.1.3 Model Form

Whatever the basis for the model, it may take one of two forms - Analytic or Graphical.

Analytic models consist of mathematical expressions and explicit procedures such as an analytic fit to measurements [23]. They allow a certain degree of accuracy, precision, breadth of application and can account for the interaction of many variables. Analytic models give consistent results when applied by different users and are readily implemented as computer programs.

Graphical models such as the Bullington nomograms [24] allow problem solution without the need for computational machinery or skills, thus they can be applied by less skilled personnel. However, graphical methods are limited

in practice as to the number, range and inter-relationships of input variables that can be represented and are of limited accuracy.

3.1.4 Accuracy and Validity.

Accuracy is a function of the fundamental design of the model and not the precision with which computations are made. It is the ability of the model to predict received signal statistics in a given environment, and is primarily dependent on the inclusion of the important modes of propagation to be found in the physical environment in which the model is to be applied.

3.1.5 Input Parameters and Supporting Data.

Models should be developed with due consideration for the availability of input data for each input parameter and the extent of the formers' influence on the prediction results. Some important input parameters include base station antenna height and location, mobile antenna height and building dimensions and locations. The model development, evaluation and application stages depend on supporting data such as

(i) Environmental data - to which radio propagation is sensitive. The prominent environmental factors include buildings, topography, other man made structures and foliage. Building and topographic data is obtainable from the Ordnance Survey and is available in conventional map or digitised form. The data should be affordable by the users of the model and its quality need not be better than that to which the model is reasonably sensitive.

(ii) Propagation measurements - sometimes in the form of experiments conducted in a particular location with a specific system. Such data is desirable for the development and evaluation of a propagation model since they contain the detail needed for quantitative analysis.

3.1.6 Convenience of Use.

Model development must consider the extent to which the method is convenient to use by the individuals and organisations expected to apply it. Ease of use and simplicity can be achieved by sacrificing other characteristics of the method but not to such an extent as to compromise the accuracy of the model.

3.2 A Review of Previous Models

Over the years, various propagation models have appeared in the literature. Some develop the model from a scattering / reflection viewpoint [5,7] while others treat the signal fading as a stochastic process [1,3,25]. Furthermore, the characterisation has been mostly in the form of a narrowband process with some experimental results having been reported for wideband characterisation [3,9,26,27].

Ossanna [7] first proposed a modelling approach based on deterministically placed, perfectly conducting vertical plane reflectors. He assumed that reflection occurs at the flat sides of the houses and that the mobile would receive only two waves simultaneously - one direct wave and one randomly oriented reflected wave. The waves interfere to produce a standing wave pattern (with successive nulls occuring half wavelengths apart) through which the

mobile moves. With the direction of vehicle motion and the direction to the transmitter as parameters, he then used numerical iteration to calculate the theoretical power spectra of the fading signal which he was able to show had good correlation with experimental spectra. This model is basically a reflection model and is rather inflexible in that for every reflected wave, there exists a direct wave incident on the mobile station and of equal power. This situation is not always valid and the assumption also fixes the ratio of coherent to incoherent power in the received signal.

Gilbert [6] proposed three mathematical models for his study of energy reception in mobile radio. One feature common to all three models was the assumption that the phases of the waves were independent, random and uniformly distributed from 0 to 2π. In the first model, he considered N waves arriving at the mobile with azimuthal angles of arrival equally spaced around the unit circle and having complex amplitudes with a Gaussian distribution. In the second model, the angles of arrival were allowed to occur at random with equal probability for any direction but the amplitudes were assumed to be constant. The third model was an extension of the second to include the case of a random distribution of amplitudes. He showed that for sufficiently large N, the second and third models were equivalent to the first.

Clarke's model [5] is the same as Gilbert's second model, with the angles of wave arrival distributed uniformly over the range $(0,2\pi)$. He also assumed that the transmitted signal is vertically polarised, remaining unchanged on scattering so that the received signal is also vertically polarised. Although their models are essentially statistical, Gilbert and Clarke approached the modelling from a scattering viewpoint but have not included the environmental situation directly in the models.

Turin et al. [3] first considered the response of the propagation channel to a train of impulses. A series of experiments was carried out in San Francisco to measure the impulse response of the channel. By regarding the channel as a linear filter they supposed that if the transmitted signal is $Re\{s(t)\exp(j2\pi f_c t)\}$, the received signal will be $Re\{r(t)\exp(j2\pi f_c t)\}$ where

$$r(t) = \sum_k a_k s(t - t_k)\exp(j\theta_k) \quad + \quad n(t)$$

a_k is the amplitude, t_k is the arrival time and θ_k the carrier phase of the individual pulses. The impulse response of the propagation medium is then described by the set of path variables [a_k, t_k, θ_k] and the complex-valued lowpass additive noise n( ). From the experimental results, a revised model was presented which models the time delay sequence $[t - t_k]$ as a Poisson sequence, the amplitudes a_k with a lognormal distribution and the carrier phases θ_k with a uniform distribution over $(0,2\pi)$. All the a_k and θ_k are independent. This model is based on a relatively sparse environment compared with the range of localities over which it is expected to be used. The model is however suitable for software simulators and such a simulator has been developed by Hashemi [19].

Suzuki [8] devised a refined model based on the experiments conducted by Turin et al. He analysed the path strength statistics and path arrival time by curve fitting of the experimental data to some distributions. The final model describes the distribution of the path strengths of initial paths by a Nakagami distribution which becomes a lognormal distribution as the excess delay becomes large. The path arrival time was modelled as a modified Poisson process. There has been no inclusion of parameters directly related to the environment to account for the statistics observed.

Recently, Zander [25] proposed a simple optical approach based on randomly placed and randomly scintillating scatterers. The model includes path length related phase differences but omits the wave intensity variations due to wave divergence. He was however able to derive the transfer function of the channel in terms of an environment-dependent parameter, the location distribution of the scatterers.

3.2.1 The Basic Rayleigh Model.

A general model which has been applied to the mobile radio communication channel over the years is the Rayleigh model. Theoretical and experimental work has shown that the envelope of the mobile radio signal is Rayleigh distributed when measured over distances where the mean field strength is constant. The model assumes that at any point, the received field is made up of a number of plane electromagnetic waves with random amplitudes and angles of wave arrival. The phases of the waves are uniformly distributed over $(0,2\pi)$ [5]. If the transmitted signal is vertically polarised, the electric field component E_z of the received signal is given by:

$$E_z = E_o \sum_{n=1}^{\infty} C_n \cos(2\pi f_c t + \theta_n) \tag{3.1}$$

Following the work of Rice [44], E_z can be expressed as

$$E_z = T_c(t) \cos(2\pi f_c t) - T_s(t) \sin(2\pi f_c t) \tag{3.2}$$

where

$$T_c(t) = E_o \sum_{n=1}^{\infty} C_n \cos(2\pi f_d t + \phi_n) \tag{3.3}$$

$$T_s(t) = E_o \sum_{n=1}^{\infty} C_n \sin(2\pi f_d t + \phi_n) \tag{3.4}$$

and from equation (1.4)

$$\omega_n = 2\pi f_d t = \beta v \cos \alpha_n \tag{3.5}$$

$T_c(t)$ and $T_s(t)$ are the inphase and quadrature components of E_z respectively. Since α_n and ϕ_n are assumed to be uniformly distributed and the C_n are either all equal or Gaussian variables, then by the Central Limit Theorem as $N \to \infty$, $T_c(t)$ and $T_s(t)$ become Gaussian processes. The envelope r(t) of the received signal is then given by :

$$r(t) = E_z = \left[\{T_c(t)\}^2 + \{T_s(t)\}^2 \right]^{\frac{1}{2}} \tag{3.6}$$

and tends to follow the Rayleigh distribution given by [4] :

$$p(r) = \left(\frac{r}{\sigma^2} \right) \exp\left(\frac{-r^2}{2\sigma^2} \right) \quad r \geq 0 \tag{3.7}$$

where $\sigma^2 = \frac{E_o^2}{2}$ is the mean power.

The cumulative distribution is given by

$$P(r \leq R) = \int_0^{\infty} p(r)dr = 1 - \exp\left(\frac{-R^2}{2\sigma^2} \right) \tag{3.8}$$

Gilbert [6] has shown that with three component waves, i.e N = 3, the envelope follows the Rayleigh distribution, however it is more usual to have a model with at least six independent waves [45,46].

It has been observed, however by Cox [4] and Bajwa [9] in their wideband channel sounding experiments that the signal envelope at some delays deviates from the Rayleigh model in some environments. This will correspond to the situation where the basic assumptions for α_n and C_n become invalid.
The majority of the previous work done to simulate the mobile radio channel, in both hardware and software, has produced simulations based on the pure Rayleigh fading approach [47-51]. The approach in this study does not determine apriori, the amplitude distribution, but obtains the amplitude of the scattered waves in terms of the reflective properties of the buildings.

3.3 The Multipath Channel.

The principal mode of propagation in this model is ***single scattering.*** By considering the propagation path as a ray path over which e.m energy travels from the transmitter to the receiver, it is possible to use optical methods in the model development. This approach is well justified in the UHF range of the frequency spectrum. In electromagnetic wave theory, when the surface of the scatterer is smooth and large compared to the wavelength of the source, the method of geometrical or ray optics is the most satisfactory way to calculate the scattered field. The term smooth is usually defined to mean that the minimum radius of curvature is large in terms of the wavelength [53-57].
At 900 MHz, the wavelength of the source is much smaller than the dimensions of the buildings which produce the scattering in a mobile radio environment.

The main aims of this study are

(i) to develop a multipath propagation model with environment-dependent parameters, which is simple and adequately represents the multipath phenomenon in built-up areas.

(ii) to implement the model in a computer simulation of the multipath mobile radio channel.

Therefore, to simplify the modelling process, some basic assumptions were made, taking into consideration the modelling factors discussed in section 3.1.

3.3.1 The Model Assumptions.

Assumption 1

The principal mode of propagation is ***single scattering.*** If multiple scattering is considered, there will, in general, be an infinite number of ray paths, resulting in a complex model. However, it is assumed that the multi-scattered rays are very weak compared with the singly-scattered rays and as such can be ignored.

Assumption 2

The location of the scatterers are random and can be modelled by a suitable stochastic process.

Assumption 3

Each scatterer acts as an omnidirectional secondary source of radio waves, or more precisely the scatterer reradiates incident e.m energy.

Assumption 4

On the basis of assumption 3, each scatterer has a reflection coefficient ρ , which is a measure of its reradiating capabilities since some energy is invariably absorbed by the scatterer. ρ is the ratio of the scattered to incident energy. For the ideal case $\rho = 1$ and for the worst case, $\rho = 0$.

Assumption 5

The reflection coefficients ρ depend only on the physical size of the scatterer. They are randomly distributed and can be modelled by a suitable stochastic process.

Assumption 6

The local environment of the model is homogeneous. This follows from the discussions in section 2.4.2.

Assumption 7

The location and height of the transmitter are fixed and known

Assumption 8

The receiver location is known, though constantly changing as the mobile moves along the streets.

Assumption 9

The terrain of the local environment of the model is flat.

With these simplifying assumptions in hand, the multipath model can now be derived.

3.3.2 Geometry of the Multipath Model.

The two coordinate geometry of the general mobile radio situation is shown in Figure (3.1) while the path geometry of one ray is depicted in Figure (3.2). The scatterers S_i, i = 1,2....N are assumed to be randomly located around an arbitrary origin O(0,0) at distances R_i, i = 1,2....N. The mobile M is situated at a distance m from the origin and the transmitter at T, a distance Z from the origin.

The model is essentially local and so is valid for the case when

$$Z >> R_i >> m \tag{3.9}$$

For small movements of the mobile, the angle which the transmitter makes with respect to the direction of vehicle motion is constant so that the transmitter appears fixed. The scatterer S_i is at a distance r_i from the mobile at an azimuth of α_i with respect to the direction of motion of the mobile. Thus α_i is the angle of arrival of the i^{th} ray as shown in section 1.3.3. The angles θ and ϕ are the azimuth locations of the mobile and scatterer respectively with respect to the origin O. Now, the buildings, usually a combination of concrete, brick, wood and glass materials, have surfaces that are rough and irregular. At UHF, the signal wavelength λ is less than 1 metre and sufficiently small compared with the dimensions of and the distances to the scatterers. Hence, the irregular surfaces result in random scattering of the incident e.m energy with the receiver not always in the main lobe of the scattered field. The scatterer is therefore ascribed a reflection coefficient ρ_i.

The scatterer i introduces a delay in the propagation time so that the i^{th} ray arrives with propagation time τ_i. The amplitude and phase shift associated with this ray are designated c_i and γ_i. The received signal comprises the sum

of the time delayed, attenuated and phase shifted echos. The geometric expressions for the path variables τ_i, c_i and γ_i for the i^{th} echo are now obtained.

3.3.3 The Echo Propagation Time Delay.

To obtain the delay time, reference is made to the geometric representation in Figure (3.2). Let $\hat{A}_T$, $\hat{A}_S$, $\hat{A}_M$ be the range vectors for the transmitter, scatterer and mobile with respect to the origin and $\hat{A}_i$ for the scatterer with respect to the mobile. The corresponding polar coordinates are :

$$\hat{A}_T \sim (Z, \zeta) \tag{3.10a}$$

$$\hat{A}_S \sim (R_i, \phi_i) \tag{3.10b}$$

$$\hat{A}_M \sim (m, \eta) \tag{3.10c}$$

$$\hat{A}_i \sim (r_i, \alpha_i) \tag{3.10d}$$

For the situation in which the mobile is located close to the origin, the propagation time τ_i via the reflector at $\hat{A}_S$ is

$$\tau_i = \frac{1}{c}\left[|\hat{A}_T - \hat{A}_S| + |\hat{A}_S - \hat{A}_M| \right] \tag{3.11}$$

c is the velocity of light.

Using the condition in equation (3.9) and Fig (3.2)

$$w = |\hat{A}_T - \hat{A}_S| = Z + R_i \cos\phi_i \tag{3.12}$$

$$r_i = |\hat{A}_S - \hat{A}_M| = R_i - m\cos(\phi_i - \eta) \tag{3.13}$$

The total path length is

$$w + r_i = Z + R_i(1 + \cos\phi_i) - m\cos(\phi_i - \eta) \qquad (3.14)$$

and the total propagation time τ_i is

$$\tau_i = \frac{1}{c}[Z + R_i(1 + \cos\phi_i) - m\cos(\phi_i - \eta)] \qquad (3.15)$$

The full derivation of this equation is discussed in Appendix A.

3.3.4 The Echo Amplitude.

To obtain an expression for the echo amplitude which includes the wave divergence of electromagnetic waves, recourse is made to optics. Two methods may be used, the first a ray optic approach using Huygen's Principle and the second is a modified geometric optics method.

3.3.4.1 Ray Optics Method.

Huygen's Construction Principle states that as an e.m wave traverses a medium, every element of volume of the medium that is influenced by the wave may be considered as the source of a secondary spherical wave which propagates through the medium just as the radiation from an isolated source [54]. This principle is easily extended to the problem of scattering of a base station transmitted signal by a group of scatterers in the vicinity of the mobile. The base station signal is the primary wave while the reflected signal from the scatterer is the secondary wave.

In the model, the base station transmitter is located at a large distance from the receiving mobile. The signal which is incident on the scatterers can thus be said to comprise of plane e.m waves. A wave function Ψ which describes the interaction of the radiation field and the scatterers can be separated into two parts which describe an incident plane wave and a scattered wave. Ψ must satisfy certain boundary conditions imposed by the prescence of the scatterer; i.e it must assume some certain value at the scatterer surface, the value dictated by the physical nature of the situation.

In general, a plane wave will not fulfill such conditions and it is necessary to introduce an additional wave so that interference between the two waves will produce the desired result at the surface. Clearly, this additional wave must be an outgoing wave and, since we must account for the energy carried off in this manner, the outgoing wave must be a portion of the incident wave which is reflected by the scatterer. A reflection coefficient ρ ascribed to the scatterer will indicate the proportion of the incident wave that is reflected. Let the incident plane wave be described by

$$\Psi_{inc}(r) = E \exp(-jkz) \tag{3.16}$$

which is a plane wave of amplitude E moving in the z direction. According to Huygen's principle, the interaction of the plane waves with the scattering volume will produce outgoing spherical waves. The reflected wave is given by

$$\Psi_{ref}(r) \sim \frac{\{\rho E \exp(-jkr)\}}{r} \tag{3.17}$$

The coefficient ρ can be a function of the azimuth angle to describe any angular dependence of the scattered wave.

The complete wave function Ψ described earlier is given by

$$\Psi(r) = \Psi_{inc}(r) + \Psi_{ref}(r) \tag{3.18}$$

From equation (3.17), it is seen that the amplitude is a function of the reflection coefficient and the inverse of the distance r_i.

3.3.4.2 Geometric Optics Method.

The second method is that of geometrical optics. It is well known that the geometrical optics field gives a good approximate representation of the time varying high frequency electromagnetic field. Specifically, Kirchoff showed that for sources with small wavelengths (or high frequencies), the wave field in the prescence of an obstacle approaches the field by geometric optics. Sommerf eld and Runge also showed that plane e.m waves exhibit some of the properties of geometric optics. Though classical geometric optics ignores the polarisation and wave nature of the e.m field, a modified geometric 'wave' optics approach first introduced by Luneberg includes this information. Luneberg introduced the subject of asymptotic series solution of time harmonic fields. The variable in the series is the frequency ω or the wavelength λ of the source and the series is said to be asymptotic to the exact time harmonic solutions for large ω or small λ. These series present an improvement on geometric optics approxiation to e.m problems because the terms of the series contain the phase factor $\exp(-jk\psi)$. The geometric optics field is the leading term in the asymptotic high frequency solution of Maxwell's equations [15,55-57].

From Maxwell's equations in a source-free isotropic, homogeneous medium, the electric field satisfies the Helmholtz equation [56]

$$\nabla^2\hat{E} + k^2\hat{E} = 0 \tag{3.19}$$

subject to the condition that

$$\nabla.\hat{E} = 0 \tag{3.20}$$

where

k = phase constant $\left(\frac{2\pi}{\lambda}\right) = \frac{\omega}{c}$

ω = angular frequency of the source

λ = wavelength of the source

c = speed of light

The asymptotic expansion of the electric field for k, apart from the time factor $\exp(j\omega t)$ is of the form

$$\hat{E}(x,y,z) \sim \exp(-jk\psi)\sum_n (jk)^{-n}\hat{E}_n(x,y,z) \tag{3.21}$$

The high frequency limit of interest, the geometric optics term, is obtained for n = 0. Substituting (3.21) in (3.19) and solving the resulting recursive equations for n=0 gives

$$\hat{E} \sim \exp\{-jk\psi(s)\}\hat{E}_n(s_o)\left[\frac{G(s)}{G(s_o)}\right]^{\frac{1}{2}} \tag{3.22}$$

where

G(s) = the curvature of the wavefront at the point s on a ray

(or the Gaussian curvature)

s_o = the reference point.

Using the assumption that the scatterers are located at a large distance from the transmitting station, the waves incident on the scatterers are plane e.m waves of the form

$$\hat{E}(x, y, z) \sim \exp\{-jk\psi(x)\}\hat{E}_o(y, z) \tag{3.23}$$

If the time coordinate is selected such that the secondary wavefront appears to have its beginning at the point r = 0 at t = 0 , then

$$\psi(r, \theta, \phi) \equiv r \tag{3.24}$$

The wavefronts r = ct represent a spherical wave propagating outward from r = 0 with its curvature given by

$$G(r) = \frac{1}{r^2} \tag{3.25}$$

Substituting equations (3.23), (3.24), (3.25) in (3.22) and solving, gives the electric field of the reflected wave component at distance r from the scatterer as

$$\hat{E}^r(r) = \left[\frac{\rho \hat{E}_o^{\,i}(r_o)}{r} \right] \exp[-jk(\psi(r_o) + \psi(r))] \tag{3.26}$$

The field at r is thus specified in terms of the known incident field $\hat{E}_i$ at r_o. The term $\exp\{-jk\psi(r_o)\}$ is a reference phase which can be suppressed. Hence the echo amplitude is given by

$$c_i = \frac{\rho_i E_i}{r_i} \tag{3.27}$$

which is of the same form as equation (3.17).
The full derivation of this parameter is shown in Appendix B.

3.3.5 The Echo Phase shift.

To obtain the Doppler induced phase shift γ, reference is made to equation (1.4) and Figure (3.3). Let γ_o be the phase at location m_1. The mobile moving from point $(m_1,0)$ to point $(m_2, 0)$, a distance Δm in time $\Delta\tau_i$ undergoes a relative phase change of

$$\Delta\gamma = \int_0^{\Delta\tau} 2\pi f_d \, d\tau_i = 2\pi f_d \Delta\tau_i \tag{3.28}$$

where f_d is as defined in equation (1.4).

For vehicle speed V m/s, $\Delta m = V\Delta\tau_i$ so that

$$\Delta\gamma = \left(\frac{2\pi}{\lambda}\right)\Delta m \cos\alpha = \beta(\Delta m)\cos\alpha_i \tag{3.29}$$

The phase at m_2 is thus

$$\gamma_i = \gamma_o + \Delta\gamma = \gamma_o + \beta(\Delta m)\cos\alpha_i \tag{3.30}$$

The distribution of α is dependent on the distribution of the scatterers around the origin.

Equations (3.15), (3.27) and (3.30) give the relationship between the path variables and the local environment of the mobile through the environment related parameters R, ϕ, r, α and ρ. The distribution of these parameters is generally random and unknown so it is necessary to derive stochastic processes which describe the random variables.

3.4 The Stochastic Multipath Model.

The complete description of the environment is obtained through the parameters R, ϕ in two dimensions and R, ϕ, H in three dimensions, where H is the height of the scatterer. The echo path variables may be obtained when the stochastic processes R(ϕ) and H(ϕ) are known where R denotes the distance to the first scatterer at angle ϕ with height H. The probability density distribution (pdf) of the scatterer location is p(R,ϕ) and of the height p(H) with H independent of R and ϕ.

3.4.1 The Scatterer Location.

If it is assumed that range R is independent of azimuth ϕ and that the scatterers are equally likely to be located all around the mobile in each possible direction, then the joint pdf becomes

$$p(R, \phi) = p(R)p(\phi) \tag{3.31}$$

where

$$p(\phi) = \frac{1}{(2\pi)} \tag{3.32}$$

The assumption in equation (3.32) is valid in built up environments but in a less restrictive sense, p(ϕ) is allowed to assume a distribution other than the uniform distribution.

To obtain p(R), reference is made to the point process discussed in section 1.3.2.1. The scattering volume constitutes a Poisson process with each of the points being the centre of the square reflecting object of dimensions 2r x 2r.

The points are homogeneously located according to the planar Poisson process in a street with canyon width W and the average scatterer per unit area is Λ. Then, referring to Figure (3.4) and using cartesian coordinates, the probability of a scatterer being placed in the infinitesimal area $A = (x + dx,\ y + dy)$ shaded in the figure is

$$Pr[\,one\ scatterer\ in\ A\,] = \Lambda dxdy \tag{3.33}$$

By definition, the probability of more than one scatterer lying in this area is zero. Thus the probability of no scatterer lying in A is

$$Pr[no\ scatterer\ in\ A\,] = 1 - \Lambda dxdy \tag{3.34}$$

A scatterer is said to be found in A if and only if its centre lies in area A. R is the random variable denoting the distance along the x-axis of the first scatterer from the mobile which for convenience is located at the origin. $F(R \leq \upsilon)$ is the cumulative distribution of the process where υ is the distance to the nearest scatterer intersecting the x-axis and lying in the area A. So

$$F(R \leq \upsilon) = \int_0^{\upsilon} p(R)dR = Pr[\,at\ least\ one\ scatterer\ in\ A] \tag{3.35}$$

then

$$F(R \leq \upsilon) = 1 - Pr[\,no\,point\ in\ A\,] = 1 - [1 - \Lambda dxdy] \tag{3.36}$$

Area A can be divided into L incremental areas dA = dxdy so that

$$Ldxdy = \left[(\upsilon + r) - \frac{W}{2}\right]2r = (2\upsilon - W)r + 2r^2 \tag{3.37}$$

and (3.36) becomes

$$F(R \leq \upsilon) = 1 - [1 - \Lambda dxdy]^L \tag{3.38}$$

substituting for dxdy from equation (3.37)

$$F(R \leq \upsilon) = 1 - \left[1 - \frac{\Lambda}{L}\{(2\upsilon - W)r + 2r^2\}\right]^L \tag{3.39}$$

When $L \rightarrow \infty$, the series approximation exp(-x) = 1 - x is used to obtain

$$F(R \leq \upsilon) = 1 - \exp[\Lambda(2\upsilon - W)r + 2r^2\Lambda] \tag{3.40}$$

since p(R) = $\frac{d}{dR}[F(R \leq \upsilon)]$, then differentiating (3.40) we obtain

$$p(\upsilon) = 2r\Lambda \exp[\Lambda 2\upsilon r - Wr\Lambda] \tag{3.41}$$

Define D as the average separation between scatterers, given by

$$D = \frac{1}{2r\Lambda} \tag{3.42}$$

and using (3.42) for D in (3.41) gives

$$p(\upsilon) = \frac{1}{D}\exp\left(\frac{W}{2D}\right)\exp\left(\frac{-\upsilon}{D}\right) \tag{3.43}$$

which is the desired density distribution for the location R of the scatterer.

3.4.2 The Scatterer Reflection Coefficient.

The scattering properties of a scatterer are described in terms of a scattering cross section similar to the well known radar cross section. From equation (1.2) a complete reflection coefficient ρ can be defined as

$$\rho = \sqrt{\sigma}\ \exp(jz) \tag{3.44}$$

where exp(jz) accounts for any phase changes that occur on reflection. In a typical mobile radio environment, the scatterers are of varying dimensions so that it is reasonable to regard ρ as a random variable independent of R, and can be described by the pdf $p(\rho)$.

The process $\rho(\phi)$ is thus modelled as a zero mean stationary second order complex valued stochastic process, i.e

$$< \rho(\phi) > \ = 0 \tag{3.45}$$

and

$$< \rho(\phi)\rho(\psi) > \ = \sigma^2\delta(\phi - \psi) \tag{3.46}$$

The process thus has the character of non stationary white noise and corresponds to the representation of the channel as a continuum of uncorrelated randomly scintillating scatterers as in section 2.4.3. In addition, the quadrature components $\rho_c(\phi)$ and $\rho_s(\phi)$ of the waves scattered at angle ϕ are independent, i.e

$$< \rho_c(\phi)\rho_s(\phi) > \ = 0 \tag{3.47}$$

It seems reasonable to assume that the density function of the reflection coefficient should follow a cosine law as in some optical systems [58]. This approach is justified as the modelling has been based on optical methods. If the scatterer is considered as a square, given that the dimension of each side is w meters and its height H metres, then the scatterer aspect or size can be expressed in two dimensional form as

$$s = w \times w \tag{3.48a}$$

and in three dimensional form, with height consideration as

$$s = H \times w \tag{3.48b}$$

Now from Assumption 5 in section 3.3.1, $\rho \propto s$ so that

$$\rho = ks \tag{3.49}$$

where k = constant of proportionality

It is expected that the s distribution will vary from $s = 0$ (open space) to $s = s_{max}$, concentrating around an average size s_{av}. Therefore we let

$$p(s) = A \sin\left(\frac{\pi s}{2s_{av}}\right) \quad 0 < s < 2s_{av} \tag{3.50}$$

Using the transformation

$$p(\rho)d\rho = p(s)ds$$

as shown in Appendix C, we obtain

$$p(\rho) = \frac{\pi}{2}\sin(\pi\rho) \qquad 0 < \rho < 1 \tag{3.51}$$

The stochastic model is thus completely defined by p(R), p(ϕ) and p(ρ). As shown in sections 2.2 and 2.3, the behaviour of a channel can be studied through its system and correlation functions. The influence of the environmental parameters on the behaviour of the mobile radio propagation channel can now be studied through its system and correlation functions derived in the following sections.

3.4.3 The Channel Impulse Response.

Following equation (2.24), the time-variant bandpass impulse response of the channel is given by

$$h(t, \tau) = \sum_{k=0}^{\infty} a_k(\tau)\delta[t - \tau_k(t)] \exp(-j\theta_k) \exp(-j2\pi f_c t) \qquad (3.52)$$

where k numbers the resolvable echo paths, a, τ, and θ are the path variables $\theta_k = 2\pi f_c \tau_k(t)$. In a physically realisable experimental situation, the k^{th} echo path is received within the finite time interval $\Delta\tau = (\tau_k, \tau_k + \Delta\tau)$ which is the time delay resolution of the channel sounding equipment used for measuring the channel impulse response. This situation is depicted in Figure (1.2). $\Delta\tau = \frac{1}{B}$ where B is the bandwidth of the sounder. The size of $\Delta\tau$ is small enough to be represented by a gross delay τ_k. The resultant contributions from all scatterers within this shell can be identified as the path echo. This resultant is the superposition of the i = 1,2.....N subpaths within the delay bin interval, therefore,

$$a_k = \sum_{i=1}^{N} c_i(\tau) \exp(-j\gamma_i) \qquad (3.53)$$

and in terms of the environmental parameters

$$a_k = \sum_{i=1}^{N} \frac{\rho E_i}{r_i} \exp[\, -j(\gamma_o + \beta(\Delta m) \cos \alpha_i)] \tag{3.54}$$

The inphase $I_k(\tau)$ and quadrature $Q_k(\tau)$ components of a_k are

$$I_k(\tau) = \sum_{i=1}^{N} \frac{\rho E_i}{r_i} \cos[\, -j(\gamma_o + \beta(\Delta m) \cos \alpha_i)] \tag{3.55}$$

$$Q_k(\tau) = \sum_{i=1}^{N} \frac{\rho E_i}{r_i} \sin[\, -j(\gamma_o + \beta(\Delta m) \cos \alpha_i)] \tag{3.56}$$

so that

$$\theta_k = \tan^{-1}\left[\frac{Q_k(\tau)}{I_k(\tau)} \right] \tag{3.57}$$

Now substituting equation (3.15) in the expression $\theta_k = 2\pi f_c \tau_k(t)$, we have

$$\theta_k = \frac{2\pi f_c}{c} [Z + R_i(1 + \cos \phi_i) - m \cos(\phi_i - \eta)] \tag{3.58}$$

It is noted that $\frac{2\pi f_c Z}{c}$ represents the absolute phase which can be ignored. The phase due to the excess delay $\tau_{xi}(t)$ is thus

$$\theta_k = \frac{2\pi f_c}{c} [\, R_i(1 + \cos \phi_i) - m \cos(\phi_i - \eta)] \tag{3.59}$$

then from (3.52)

$$h(t, \tau) = \sum g(t, \tau) \exp(-j2\pi f_c t) \tag{3.60}$$

where g(t,τ) is the lowpass channel impulse response given by

$$g(t, \tau) = \sum_k a_k(\tau)\delta[t - \tau_{xi}(t)] \exp[-j2\pi f_c \tau_{xi}(t)] \tag{3.61}$$

The impulse response of the channel is very useful means of studying the time dispersive behaviour of the channel as has been shown by the work of Cox [4] and Bajwa [9] and is a useful simulation tool as shown by Hashemi [19]. The frequency domain behaviour is best studied through the channel transfer function, derived in the following section.

3.4.4 The Channel Transfer Function.

The frequency characteristics of the channel can be studied through the transfer function. By considering the contributions from all scatterers and following equation (2.25), we can express the model bandpass transfer function as

$$S(f, t) = \sum_{i=1}^{N} c_i(\tau) \exp[-j2\pi(f_d + f_c)\tau_i(t)] \exp(j2\pi f_c t) \tag{3.62}$$

f_d are the frequencies measured around f_c which result from the Doppler effect. Expanding (3.62) and taking the first two terms only [59], we have

$$S(f, t) = S^o(t) - jS^1(f, t) \tag{3.63}$$

where

$$S^o(t) = \sum_{i=1}^{N} c_i(\tau) \exp[-j2\pi f_c \tau_i(t)] \tag{3.64}$$

$$S^1(f, t) = 2\pi f \sum_{i=1}^{N} c_i(\tau)\tau_i \exp[-j2\pi f_c \tau_i(t)] \tag{3.65}$$

Equation (3.64) is the frequency-independent term of the transfer function which would correspond to distortionless propagation if it completely represented $S(f, t)$. This condition implies that the differential time delay over several paths is small relative to the reciprocal of the signal bandwidth. That is

$$f_c \tau_i(t) << 1 \tag{3.66}$$

Equation (3.65) is the frequency-dependent term of the transfer function. To complete the criteria for the reception of an undistorted signal, the condition

$$\frac{S^1(f, t)}{S^o}(t) << 1 \tag{3.67}$$

must be met. In multipath propagation, however, if the condition in (3.66) is fulfilled while that of (3.67) is not, then selective fading will be observed. This situation would occur when the combination of the phasors in equation (3.62) is close to zero resultant (ie. destructive interference). The channel will therefore be selective in its response to various frequency components within the signal bandwidth.

In a manner similar to that used for the impulse response derivations, the bandpass transfer function can be expressed in terms of the absolute delay and lowpass transfer function T(f,t):

$$S(f, t) = \sum T(f, t) \exp(j2\pi f_c t) \tag{3.68}$$

where T(f,t) is the lowpass channel transfer function given by

$$T(f, t) = \sum_{i=1}^{N} c_i(\tau) \exp[-j2\pi f \tau_{xi}(t)] \tag{3.69}$$

where $f = f_a + f_c$, and c_i and $\tau_{xi}(t)$ as given in equations (3.27) and (3.59) contain the parameters R, ϕ and ρ.

For a wideband system, the frequency selective behaviour of the channel is of paramount interest. Since the channel is randomly time-varying, this behaviour is best studied using the autocorrelation function R_T of the transfer function.

3.4.5 The Autocorrelation Function of the Transfer Function.

If we let the low pass transfer function T(f,t) depend on the location m of the mobile where

$$\bar{x} = \bar{r}(t) \tag{3.70}$$

and r(t) denotes the position of the mobile at time t, then

$$T(f,t) \equiv T(f,\bar{x})$$

$$= \int_0^{2\pi} \left[\frac{E_i\,\rho(\phi)\exp\left\{ \frac{(-j2\pi f)}{c}[R(\phi)(1 + \cos\phi) - m\cos(\phi-\eta)] \right\}}{[R(\phi) - m\cos(\phi-\eta)]} \right] d\phi \tag{3.71}$$

Now the autocorrelation function R_T is defined as

$$R_T(f_1, f_2; \bar{x}_1, \bar{x}_2) = < T(f_1, \bar{x}_1)\, T^{\times}(f_2, \bar{x}_2) > \tag{3.72}$$

$T^{\times}(f_2, \bar{x}_2)$ is the complex conjugate of $T(f_2, x_2)$ and is defined as

$$T^{\times}(f_2, \bar{x}_2) = \int_0^{2\pi} \left[\frac{E_i\,\rho(\psi)\exp\left\{ \frac{(j2\pi f_2)}{c}[R(\psi)(1 + \cos\psi) - m\cos(\psi-\eta_2)] \right\}}{[R(\psi) - m\cos(\psi-\eta_2)]} \right] d\psi \tag{3.73}$$

Then, as shown in Appendix D,

$$R_T = E_i^{\,2} k^2 \int_0^{2\pi} \exp[j2\pi\{z_1\cos(\phi - \eta_1) - z_2\cos(\phi - \eta_2)\}] \times < \left[\frac{\exp\left[\left(\frac{j2\pi\Delta f}{c} \right) R(\phi)(1 + \cos\phi) \right]}{[R(\phi) - m\cos(\phi-\eta)]^2} \right] > d\phi \tag{3.74}$$

The evaluation of the expectation in (3.74) requires the probability density function of R. For the planar Poisson process of section 3.4.1, the density function given in equation (3.43) is substituted in (3.74), yielding

$$R_T = E_i^2 k^2 \int_0^{2\pi} \exp[j2\pi\{z_1 \cos(\phi - \eta_1) - z_2 \cos(\phi - \eta_2)\}]$$
$$\times \frac{\exp\left(\frac{W}{2D}\right)}{D} \exp\left[-\frac{W}{2D} - \left\{1 - \frac{j2\pi\Delta f}{c} D(1 + \cos\phi)\right\}\right]$$
$$+ \left[\frac{1}{D} - \frac{j2\pi\Delta f}{c}(1 + \cos\phi)\right] \cdot E_x\left[\frac{W}{2}\left\{\frac{1}{D} - \frac{j2\pi\Delta f}{c}(1 + \cos\phi)\right\}\right] d\phi \quad (3.75)$$

E_x is the exponential function.

Equation (3.75) is the generalised expression for the autocorrelation function R_T. This integral is complex and difficult to handle analytically. Another approach to the study of the frequency dispersive behaviour of the channel is to consider frequency selective fading as a feature of the echo time delays caused by multipath propagation. The existence of the different time delays in the various waves that constitute the total received signal causes the statistical properties of two signal components of different frequencies to become uncorrelated if the frequency separation is large enough. Using the dual relationships between the time and frequency domain representations of the radio channel, the computer simulation of the channel can be carried out to obtain the channel impulse response from which the appropriate correlation functions can be calculated using Fourier Transform techniques.

The environment-dependent model has been developed and its system correlation functions derived. However, these functions which are suitable for studying the channel behaviour are difficult to handle analytically. The computer simulation of the model is an alternative approach which will be used in the study as shown in the next chapter.

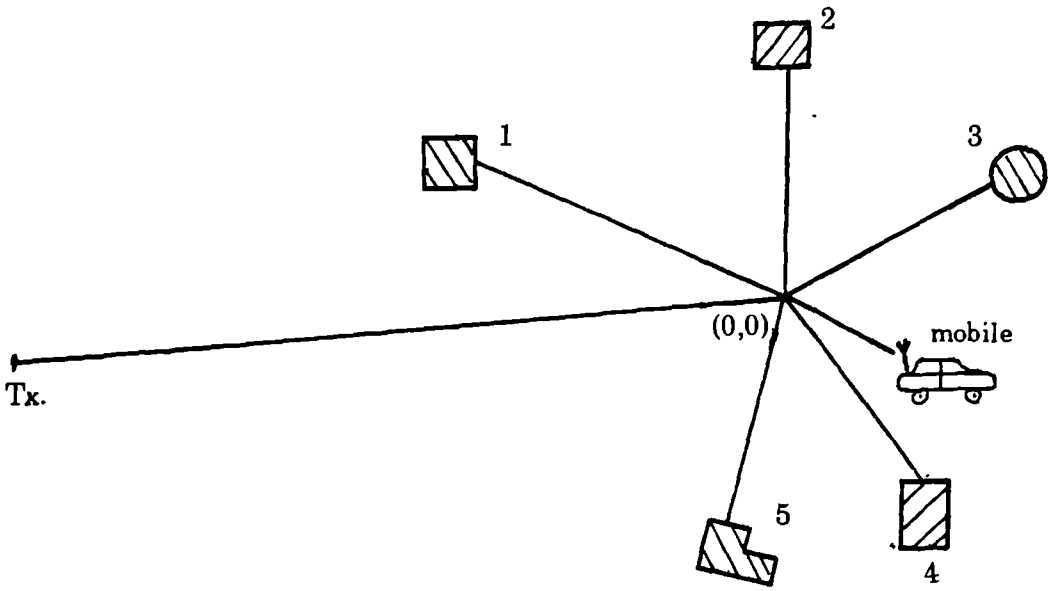

Figure (3.1) Geometry of general mobile radio situation

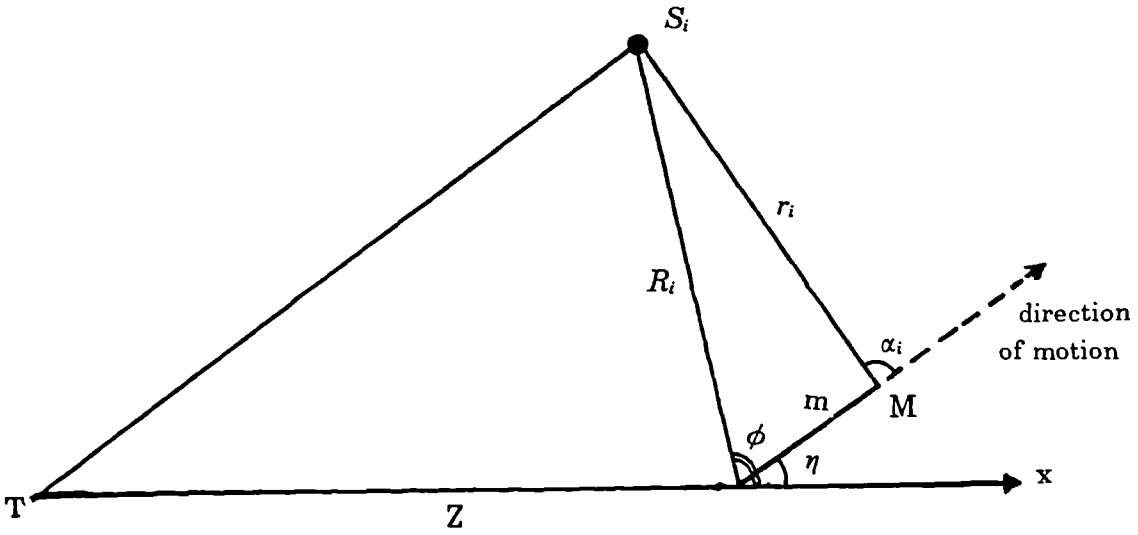

Figure (3.2) Path geometry for one ray

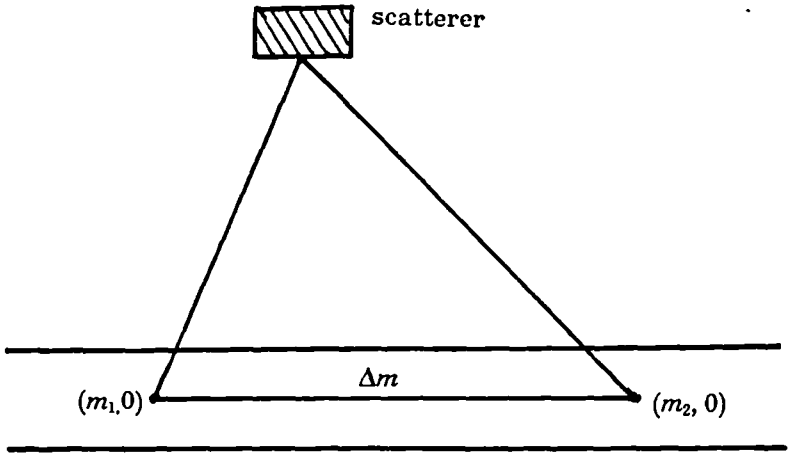

Figure (3.3) Illustration of Doppler induced phase shift

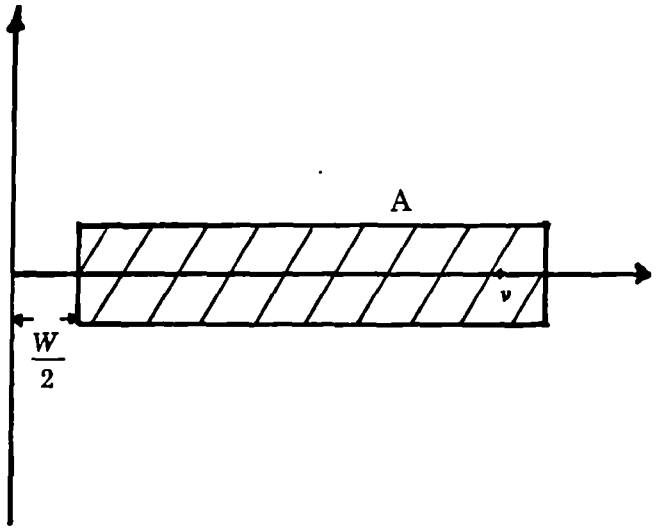

Figure (3.4) Two dimensional location of scatterers

CHAPTER FOUR

4. SIMULATION OF THE MULTIPATH RADIO CHANNEL

By wisdom a house is built, and through understanding
it is established.
Proverbs 24:3

4.1 The Simulation Choice

A simulation is the imitation of the operation of a real system over a time for the purpose of understanding the behaviour of the system within the limits imposed by a set of criteria [60,61]. The simulation process implies the construction of a suitable simulation model which, may be deterministic or stochastic, and can be implemented either in hardware or computer software. Many real systems, including mobile radio communications systems, are so complex that they are virtually impossible to model mathematically. In this instance, numerical computer-based simulation can be used to imitate the behaviour of the system over time. From the simulation, data *are collected* as if a real system were being observed. This simulation-generated data can then be used to estimate the measures of performance of the system. The availability of special purpose simulation languages, massive computing facilities at a decreasing cost per operation and advances in simulation methodologies have made simulation one of the most widely used and accepted tools in systems analysis.

The model that has been developed in this work is for use in the study of the dependence of the multipath phenomenon at 900 MHz on the nature of the mobile environment and ultimately for predicting the dispersion in such an environment. However, the correlation functions developed for this purpose are complex and difficult to handle analytically. The model itself is simple and thus lends itself to computer simulation. An examination of the merits of simulation will show why this option is suitable.

4.1.1 Advantages of Simulation

Although simulation is an appropriate tool of analysis in many instances, it is prudent to consider its advantages and disadvantages before pursuing the methodology in a particular instance. The primary advantages of simulation are:

(1) It enables the study of, and experimentation with the radio propagation channel.

(2) It allows the use of more input variables than a mathematical problem-solving approach could accommodate since the process is not constrained by the type of simplifying assumptions required for analytic methods.

(3) By changing simulation inputs (model parameters), and observing resulting outputs, valuable insights may be gained into which parameters are most important and how these interact.

(4) The process of performing an extensive set of measurements for the purpose of characterising the channel is expensive. Simulation data are much less costly and offer huge savings in cost, time and personnel usage.

(5) The simulation generated data can be used to estimate any number of system performance parameters for use in system design.

(6) The simulation can be used to predict the response of the channel to any transmitted signal.

(7) A software package is easily updated to suit the changing needs of the user simply by adding or removing lines of code. If the model were

implemented in hardware, its parameters would be fixed and it may need to be redesigned and rebuilt if changes are necessary. This can be expensive.

In as much as the case for simulation is good, it does have its drawbacks, some of which are listed below.

4.1.2 Disadvantages of Simulation

(1) Simulation is not a completely precise process. Analysis of the sensitivity of the model to changing parameter values can overcome this difficulty to a large extent.

(2) Simulation results are usually numerical, and given to any chosen degree of accuracy. Thus there arises the danger of 'deification of the numbers', i.e attributing to the numbers a greater degree of validity than is justified.

(3) The user may become so familiar with the simulation methods as to forget the theories supporting any analytic solution of the same problem.

It is seen that the merits of simulation far outweigh the demerits, hence its increased use in problem solving today.

4.2 Review of Previous Software Simulations.

Previous simulations have sought to represent the mobile radio channel with the pure Rayleigh model. The most fundamental of these forms its Rayleigh distributed fading signal by adding two Gaussian noise sources in quadrature. A schematic diagram of this process is shown in Figure (4.1). The two noise

sources are uncorrelated, and each have a zero mean Gaussian amplitude distribution with equal rms values. The rms frequency of the Gaussian shaped power spectra determines the fading rate. Frequency selective fading may be produced by combining several delayed fading signals.

A second widely used method is the multiple oscillator system shown in Figure (4.2). It operates on the principle of summing several vectors of constant amplitude but varying phase. The signal envelope is thus given by

$$E(t) = \sum_{m=1}^{\infty} A_m v_i \cos[2\pi(f + f_m)t] \qquad M > 6$$

v_i is the input signal and A_m is the attenuation for path m. The low frequency oscillators produce the small doppler shifts (or frequency offsets) f_m. The oscillator frequencies are chosen to distribute the M vectors approximately uniformly over a given bandwidth. Additional frequency components can be accomodated by including more oscillators [1,90,91,92]. The amplitude distribution for this system is approximately Rayleigh although the power spectrum deviates appreciably from Gaussian.

Smith [47] developed a simulation for obtaining the amplitude of the fading signal envelope. He however shaped the spectra of the noise sources to take into account the frequency band-limiting inherent in equations (3.68) and (3.69).

Hashemi [19] developed a simulation program for the wideband response of the propagation channel. He used the mathematical model suggested by Turin. His aim was to achieve a simulation program that generated multipath profiles having statistics close to those empirically determined by Turin and Suzuki [3,8]. The vehicle motion is taken into account by generating the path profiles at spatial points along the street. The path arrival times were simulated

based on the modified Poisson process of Suzuki. The path amplitudes were generated according to a lognormal distribution and the phases according to an independent uniform $(0,2\pi)$ distributions. His simulation included temporal and spatial correlation factors for successive paths.

Gladstone and McGeehan [51] based their simulation on the statistical plan of the locality. The method also accounts for vehicle movement through a particular environment. They also made provision for shadowing and coherent waves. The simulation was however based on a purely reflection model similar to that of Ossanna [7]. The received narrowband signal was obtained as the resultant of the waves reflected by the scatterers. The latter are represented on the map as rectangles with the centres as the effective scattering points. However, the amplitudes of the reflected waves were chosen to have a narrow Gaussian distribution as suggested by Gilbert [6], leading to Rayleigh type signal statistics. Gladstone and McGeehan were able to show good correlation between their simulation and experimental data.

Davies [70], recently applied physical ray optics methods to the determination of wideband channel characteristics. His simulation, based on the statistical plan of the route along which the mobile travels, obtains the delay-Doppler response function $h(\tau, \nu)$ (or scattering function) of the channel as a limiting set of weighted impulses in the relative delay, Doppler shift domain (τ, ν) domain. The simulation, carried out for a single mobile location, was subject to some simplifying conditions some of which are:

(a) the row of buildings on either side of the street are continous

(b) the building walls are flat and behave as lossy reflectors

(c) the relevant propagation modes are edge diffraction at roof level and up to seven multiple reflections between the walls parallel and adjacent to the street

In comparing some of his results with data published by Bajwa and Parsons [66], he was able to show good correlation and further confirmation of the dependence of the echo amplitude statistics on the street orientation. This simulation method does not however allow for mobile movement, or features such as open spaces between buildings, nor does it consider buildings not directly located on the street.

The simulation described in this study is for the wideband response of the channel, following the approach in [19], and is based on the direct influence of the mobile radio environment. Going a step further than [51], the path amplitudes are dependent on the scattering aspect of the buildings. For the first time, the Doppler related phase shifts are included in a simulation model of the mobile radio propagation channel.

4.3 The Simulation Technique.

For a known transmitted signal and the measured received waveform, the channel impulse response can be obtained as discussed in section 2.2.3.1. The simulation technique is therefore based on a real physical channel sounding experiment, illustrated in Figure (4.3). For the chosen service area, a test route (or set of routes) is selected for the experiment. In this simulation, the mobile is empowered to move and travels at a constant speed, measuring the channel response to a pulse transmission. The spatial locations n = 1,...,Nm at which this measurement is made are separated by a constant distance Δm. At point n = 1, an echo path profile is generated as follows:

(1) First, a set of propagation delay times τ_i for all scatterers which are identified by ray tracing techniques as contributing to the scattering phenomena.

(2) In addition to the propagation times, the angles of wave arrival α_i with respect to the direction of vehicle motion are obtained.

(3) Then, for each validated path with arrival time τ_i, the echo amplitude c_i is calculated using equation (3.40).

(4) Finally, the echo phase shifts γ_i, caused by the motion of the mobile and the Doppler effect, are calculated using equation (3.43).

Subscript i numbers the scatterers which contribute to the multipath scattering and are located within an area of 250 metre radius of the mobile, referred to in this study as the occupational domain. Experiments have shown that most of the significant scattering originates within this range of the mobile.[4,9,11]. The process outlined in steps (1) to (4) above is repeated for all consecutive sampling locations and the data stored for further processing which yields the channel characterising parameters, eg. delay spreads and coherence bandwidths. The sampling distance Δm is chosen such that it is small enough to give some correlation between two consecutive profiles, but large enough to ensure that changes in the path variables due to spatial movement of the mobile are exhibited. In generating these profiles, it is assumed that

(a) the transmitted signal is an impulse, enabling the exact time of arrival to be determined.

(b) all the scatterers are equally illuminated.

(c) contributions from different scatterers are uncorrelated.

We now examine the process in more detail.

4.4 The Area Plan

The core of this simulation process is the plan or map of the service area under consideration, as in Figure (4.4). The scatterer locations are obtained both stochastically, using the density distributions associated with parameters R, ϕ and ρ, and determinstically by extraction from Ordnance Survey (OS) maps.

4.4.1 Ordnance Survey Map Derived Plan

The location data extracted from OS maps comprise of the 2-dimensional coordinates of the building corners with respect to the National Grid (NG) coordinate of the south west corner of the map. This form of representation is discussed in more detail in chapter 5. The building centre is considered as the effective scattering point. The location parameters (R,ϕ) can be calculated with respect to any suitable reference point or origin on the map. R is measured as the distance between the building centre and the reference point, while ϕ is measured anticlockwise with respect to the positive x-axis direction. The building size is the area enclosed by the building coordinates, while the building orientation is measured as for ϕ. The advantage of using a real physical environment is that the simulation generated data can be compared with experimental data obtained in the same locality.

4.4.2 Statistical Plan

The statistical plan is obtained as follows :

(1) First, a set of distances {R} is generated using a random number generator of a suitable distribution (Gaussian, Uniform or Poisson).

(2) Next, a corresponding set of Uniformly distributed angles $\{\phi\}$ in the range $[0,2\pi)$ are generated.

(3) Then, the sinusoidally distributed reflection coefficients are obtained by applying the transformation

$$\rho = \left| \left(\frac{1}{\pi}\right) \cos^{-1}(2x) - 1 \right| \qquad -0.5 < x < 0.5 \tag{4.1}$$

to the a set of uniformly distributed numbers in the range [0,1)

(4) The map boundary is defined in a similar manner to the OS maps and on determining the number of scatterers to be accomodated within this area, each scatterer i is assigned a descriptive set $\{R_i, \phi_i, \rho_i\}$ and laid out on the map.

In order to make this statistical plan more representative of the OS map, the scatterers can be drawn as squares or rectangles, rather than points, with the edges representing the building walls. Assigning a value to s_{max} defined in section 3.4.2, the sizes are obtained as

$$s_i = w \times w \tag{4.3}$$

If on the other hand, a rectangular shape is desired with the ratio (length:depth) of (x:y), then

$$s_i = yw \times xw \tag{4.4}$$

where

$$w = \sqrt{\left[\frac{s_i}{(x \times y)} \right]} \tag{4.5}$$

The building in this form allows the inclusion of the shadowing effect, a feature exhibited by real channels, in the channel simulation. To complete its set of attributes, each building is assigned an orientation and a height. Program DATAGEN generates the data required for the statistical plan.

4.4.3 Multiple-Map Plan

A typical service area is much larger than the area defined by the 500m × 500m square maps described above. In addition, to reduce the edge effects encountered if a street is located at the extreme edge of a map, additional map areas will need to be created adjacent to the core map. If OS maps are being used, the extra maps can be purchased and the required data extracted. However, this is not strictly necessary. If the statistical description of the test square is known, and can be regarded as typical of the locality, ie. a sample of the ensemble of squares in the area, then, suitable transformations can be applied to the known building coordinates to obtain the location distributions for other squares.

To illustrate this process, the core map is designated map A such that a pair of building location coordinates is defined as (xa,ya). Then to obtain the equivalent in four other maps B, C, D and E, the following transformations are applied:

$$[B] \quad \begin{aligned} xb &= 500 - ya \\ yb &= xa \end{aligned} \tag{4.6}$$

$$[C] \quad \begin{aligned} xb &= 500 - xa \\ yb &= 500 - ya \end{aligned} \tag{4.7}$$

$$[D] \quad \begin{aligned} xb &= ya \\ yb &= 500 - xa \end{aligned} \tag{4.8}$$

$$[E] \quad \begin{aligned} xb &= ya \\ yb &= 500 - ya \end{aligned} \tag{4.9}$$

The transformations are applied to each building on map A, and the five maps thus obtained can be arranged in a 9-map plan illustrated in Figure (4.5), in a manner which ensures that no two similar squares are co-located. The location distributions p(R) of the core map and the that of the transformed enlarged map with area 1500m × 1500m are shown in Figure (4.6). It is seen that the distributions are very similar. The ordinate shows the probability of finding a scatterer at a given location.

This method is also applicable to the statistically derived plan, and is of immense potential as a tool for reducing expenditure on the maps that may be needed for a particular task. A mixture of areas can also be generated by using core maps of different distributions. An entire city can be mapped out along the categories discussed in chapter 5, once the statistical description of the different classes of environments are determined.

Two programs have been developed for generating this multiple-map plan. Program TRANSCOD applies the coordinate transformations while TRANS-MAP arranges the maps on the multiple grid.

4.4.4 Data Structure For Maps

The individual maps contain on average up to 200 buildings. A large mass of data is thus required for the simulation, and these must be stored and managed efficiently. Each building is defined by the coordinates of its centre, its area, length, width, height and orientation. These are stored as one data record using the format shown in Table (4.1). The data for each map are stored in different files, with the NG index of the map as the file identifier. The data are stored in direct access mode so that the simulation program can read or write any desired record from or into the file. Each building has a unique identifier, so that its identity is preserved even if moved to a different location on the map.

The map can be viewed on screen using program PLANPLOT developed for that purpose. Changes can thus be made, if necessary, before the main process is begun. With the area plans well prepared, the channel simulation can then proceed as shown in the next section.

4.5 Generation of Echo Path Profiles.

The channel impulse response if fully described by the path variable set $\{\tau_i, c_i, \gamma_i\}$. Therefore, these variables are generated for every building identified as contributing to the multipath phenomenom.

At the start of the simulation, a control data file is set up with the initial values of control parameters such as the radius of the occupational domain, vehicle route and speed, carrier frequency, number of profiles to be generated etc.. The mobile is then positioned at the starting location, and as it moves

at the selected speed along the route, the profiles are generated as explained below.

4.5.1 Scatter Selection

The mobile can receive a wave scattered only once from any of the scatterers. In order to introduce shadowing, a wave is not allowed to pass through a building except that which causes a valid echo. Using ray tracing techniques, each possible path is traced backwards from the mobile. The building walls are represented as vectors, as is the potential ray path between the mobile and the scattering centre of the building. Each building within the occupational domain is considered in turn in determining which are significant to the multipath phenomenom. A scatterer is a valid contributor if the vector connecting the mobile and the scattering centre is not intersected by any of the wall vectors. In order to include the effect of tall buildings which may be at a long distance but visible to the mobile, if an intersection occurs within the lengths of either path or wall vector, then the height of the obstructing building is checked. The ray path is thus valid only if the obstructing scatterer height is shorter than that of the scatterer being checked by at least one storey.

On a plan with 200 scatterers, there would be as many ray paths to be traced with each path requiring 199 x 4 wall vectors to be checked to ensure it is not shadowed. This means that a possible 160000 checks are required at every spatial sampling point. These points are spaced 0.2λ metres (=6 cm) apart, a distance small enough to ensure correlation between spatially adjacent profiles, but large enough to show the change in the multipath structure. One simulation run to generate up to 1000 profiles will require over 100 million checks! It is imperative therefore, that the ray tracing routine algorithm and programming be efficient. Although, a profile is generated every 6cm, it was observed that the principal scatterers remained the same for mobile movement

up to 10 metres ($\sim 30\lambda$). Therefore, the check for significant scatterers is made once at the start of a 10 metre section of the route, thus reducing computation time immensely. Subroutine DOMAIN in conjunction with SELEKT and PRIWAV determines the valid ray paths. Each scatterer is assigned a marker which is set if its path is valid and reset otherwise, enabling identification during the interval between checks. The distributions p(R), p(ϕ), p(H) and p(ρ) of the significant scatteres are also obtained. Having determined the contributory scatterers, the path variables are then calculated.

4.5.2 Echo Path Variables.

The path variables τ_i, c_i, γ_i are calculated using equations (3.15), (3.40) and (3.43) respectively in subroutine ECHGEN. The propagation time delays are calculated to the nearest nanosecond value in order that the individual contributions can be identified, and for the envelope processing at a later stage. The incident field E_i is assigned at the start of the run. For the first measurement location, the initial path phases are deterministically assigned from a uniformly distributed set of random phases within the range $(0,2\pi)$. For subsequent locations, the phases are obtained as in equation (3.43). When a set of scatterers is selected at the start of 10 metre section, those that were valid in the previous section retain the phase shift values attributed to them up until then, while new ones are assigned phase shift values deterministically from the set mentioned previously. This ensures continuity of the process.

The time delay resolution of the simulation is 100 ns (or 0.1μs), which is the pulse width of the probing signal. The pulse width defines the scatterer resolution capability of the simulation and for the specified width, scatterers with differential path lengths of 30 metres can be resolved. This figure has been used by Cox and Bajwa in their sounding equipment, and most recently by Demery, at Liverpool University, who has provided some of his experimental

data for comparisons with the simulation generated data for validation of the model. This figure has been selected because the radio propagation channel characterisation is over a 10 MHz bandwidth which is adequate for most applications. The generated set of path variables are then processed to obtain the envelope of the impulse response.

4.5.3 Signal Processing for Path Variables.

To obtain the instantaneous impulse response at a sampling location, the time delay axis is made discrete by dividing it into 100-ns intervals or delay bins numbered k = 1,127. Bin 0 is centred on the LOS or shortest delay, and subsequent bins on multiples of 100ns such that

$$\tau_{k+1} - \tau_k = 0.1\mu s \tag{4.10}$$

This allows measurement of delays up to 12.7μs beyond the minimum delay. For the L number of distinct echoes arriving within a delay bin interval, the composite echo amplitude a_k and phase shift θ_k for the bin k is theoretically obtained as a vectorial sum:

$$\begin{aligned} a_k(\tau) &= \sum_{i=1}^{L} c_i \exp(j\gamma_i) \\ &= \sum_{i=1}^{L} c_i \cos\gamma_i \; + \; j\sum_{i=1}^{L} c_i \sin\gamma_i \end{aligned} \tag{4.11}$$

and

$$\theta_k(\tau) = \tan^{-1}\left[\frac{\sum_{i=1}^{L} c_i \sin \gamma_i}{\sum_{i=1}^{L} c_i \cos \gamma_i}\right] \qquad (4.12)$$

However, experiments have shown that the probing pulse modifies the echoes arriving at the reciever terminals in such way that the resultant of two echoes close together is not a vectorial sum, nor an algebraic addition, but some other function. This led to the investigation of the signal processing methods employed in channel sounding equipments.

Wideband channel sounding techniques applied in the measurement of the channel impulse response over the years include : periodic pulse sounding [3,93], swept time-delay cross correlation [4,94] and the convolution type pulse sounding [9]. The first method involves periodically sounding the channel with very short pulses sufficiently spaced in time to obtain a series of snapshots of the multipath structure. It however discards the relative phase of the signal which contains information on the angle of wave arrivals in the form of Doppler shifts. The other two methods are very similar, utilising the correlation properties of maximal length pseudo-random sequences which are used as the sounding waveform. Such a waveform is shown in Figure (4.7). Coherent quadrature detection is used to enable extraction of the Doppler shifts which are embedded in the signal as the rate of change of relative phase of the carrier. The common feature of these methods is that the received waveform is the convolution of the pulse sounding waveform with the impulse response of the propagation medium.

It was decided to apply the cross correlation method for reasons explained in the following discussion.

For a time-invariant linear system, the cross correlation function $R_{yx}(\tau)$ the output y(t) and input x(t) waveforms is related to the autocorelation function $R_x(\tau)$ of the input waveform :

$$R_{yx}(\tau) = R_x(\tau) \otimes h(\tau) \tag{4.13}$$

where $h(\tau)$ is the impulse response of the system. It can be seen that if $R_x(\tau)$ is a dirac delta function through appropriate choice of the sounding signal, the impulse response of the linear system at a delay τ is obtained. For the mobile radio channel which exibits WSSUS behaviour, the relationship of equation (4.13) becomes

$$R_{yx}(\tau) = R_x(\tau) \otimes < h(\tau) > \tag{4.14}$$

Therefore, this method provides a sample of the average impulse response for an excitation of the channel τ seconds in the past. For the linear system representation of the propagation measurement shown in Figure (4.8) and following Cox [63] as in Appendix E, the complex bandpass impulse response envelope $E(\tau)$ is

$$E(\tau) = p(\tau) \otimes g(\tau) \tag{4.15}$$

$g(\tau)$ is the impulse response of the multipath medium and $p(\tau)$, the bandlimited approximation to an impulsive probing signal, is the same as the correlation function $R_s(\tau)$ of the probing pulse sequence convolved with the filters $b(\tau)$ of the system, that is

$$p(\tau) = b(\tau) \otimes R_s(t - \tau) \tag{4.16}$$

The inphase and quadrature components of the envelope are therefore

$$I(\tau) = \sum_{i=1}^{L} c_i R_s(t - \tau_i) \cos \gamma_i \tag{4.17}$$

$$Q(\tau) = \sum_{i=1}^{L} c_i R_s(t - \tau_i) \sin \gamma_i \tag{4.18}$$

The envelope of the impulse response can thus be derived from $R_s(\tau)$ which is easy to generate, and the echo path variables. The probing signal shown in Figure (4.7b) is generated by subroutine HPROBE, with values obtained for each nanosecond width of the pulse. The path variables generated by routine ECHGEN are sorted in increasing order of delay in IMPSOT to obtain the discrete quadrature channel impulse response which is then convolved in subroutine CONVOL. The impulse response envelope generated is stored in files for processing to obtain the small and large scale channel characteristics using methods outlined in the following section.

4.6 Data Processing.

The channel impulse response envelopes obtained as described in section 4.5 were processed using a set of data processing programs developed for that purpose. A two stage analysis, as discussed in chapter 2, was carried out. The first stage analyses the small scale behaviour over distances up to 24 metres while the large scale analysis is over distances of 72 metres or more of the channel. The complex impulse response envelopes are stored as lowpass quadrature components $I_n(\tau_k)$ and $Q_n(\tau_k)$. In each profile, there are 127 time delay cells of 0.1μs duration, which implies that excess delays up to 12.7μs can be measured.

4.6.1 Small scale characterisation.

The small scale characteristics are obtained from a maximum of 300 individual impulse responses. This corresponds to a 24-metre section over which the channel is expected to exhibit WSS behaviour. The analysis is carried out in the time domain, frequency domain and time delay - Doppler shift domain.

4.6.1.1 Time Domain Analysis.

Individual power delay profiles $p_n(\tau_k)$ are computed from the quadrature components of the impulse response envelope by:

$$p_n(\tau_k) = I_n^2(\tau_k) + Q_n^2(\tau_k) \tag{4.19}$$

where subscript n orders the set of profiles along the street, and k the delay samples of each profile. $p_n(\tau_k)$ represents the power in the envelope $E_n^2(\tau_k)$ of the complex impulse response. Thus

$$p_n(\tau_k) = E_n^2(\tau_k) = |I_n(\tau_k) + jQ_n(\tau_k)|^2 \tag{4.20}$$

The average power delay profile $P(\tau_k)$ for a small 6 cm section of the channel is computed from 100 consecutive individual power delay profiles. $P(\tau_k)$ is the bandlimited estimate of $< h(t, \tau)h^*(t, \tau) >$ assuming the data is ergodic [4,9]. Therefore,

$$P_z(\tau_k) = \frac{1}{100}\sum_{n=1}^{100}\left[I_n^2(\tau_k) + Q_n^2(\tau_k)\right] = < |h_n(\tau_k)|^2 > \tag{4.21}$$

Subscript z orders each small 6 metre area. The first and second central moments of the average power profile are parameters which are of interest in assessing the performance of communication systems in the presence of multipath [1,4,9]. The average delay d or first central moment (with respect to the minimum arrival delay τ_o is calculated in terms of the simulated data as

$$d_z = \frac{\sum_{n=1}^{100} \tau_k P(\tau_k)}{\sum_{n=1}^{100} P(\tau_k)} - \tau_o \qquad (4.22)$$

The second central moment or delay spread s is a measure of the width of the profile and is calculated by

$$s_z = \left[\frac{\sum_{n=1}^{100} (\tau_k - d_z)^2 P(\tau_k)}{\sum_{n=1}^{100} P(\tau_k)} \right]^{\frac{1}{2}} \qquad (4.22)$$

4.6.1.2 Frequency Domain Analysis.

For a WSSUS channel, a frequency domain equivalent of the average impulse response is the magnitude of the autocorrelation function $R_T(f, f+\Omega)$. It has been shown that $R_T(\Omega)$ and P(τ) are related through the Fourier transform relationship [20], hence from equation (4.21)

$$\begin{aligned} R_T(\Omega) &= \int P(\tau)\ \exp(-j2\pi\Omega\tau)\, d\tau \\ &= \int <\ |h_n(\tau_k)|^2\ >\ \exp(-j2\pi\Omega\tau)\, d\tau \end{aligned} \qquad (4.24)$$

The correlation function is obtained by applying the Fast Fourier Transform (FFT) to the measured power profile P(τ). The number of discrete points for the FFT are determined by the number of time delay cells in the power profile. For this analysis 128 delay cells corresponds to a frequency separation resolution of 78 KHz. The resolution can be increased by zero padding.

4.6.1.3 Delay - Doppler domain analysis.

The delay-Doppler scattering function describes the scattering phenomenom in a three dimensional pictorial manner. Scattered signals arriving at the receiver with the same delay will be Doppler shifted by different amounts depending on the angle of wave arrival with respect to the direction of vehicle motion. Thus it is useful in resolving the multipath structure of the media. The n^{th} complex envelope of the impulse response at delay τ_k is

$$h_n(\tau_k) = I_n(\tau_k) + jQ_n(\tau_k) \tag{4.25}$$

and for a uniform sampling interval Δm, equation (4.25) becomes

$$h_n(k\Delta m) = I_n(k\Delta m) + jQ_n(k\Delta m) \tag{4.26}$$

where k numbers the delay intervals and $\tau_k = k\Delta m$. For a periodic sequence with time period T, (4.26) can be rewritten as

$$h_n(nT + k\Delta m) = I_n(nT + k\Delta m) + jQ_n(nT + k\Delta m) \tag{4.27}$$

If the time series for the analysis is composed of N echo profiles, then the record length is NT seconds, resulting in a resolvable frequency of $\left(\frac{1}{NT}\right)$ Hz. The scattering function is obtained by complex Fourier transforming the $I(\tau)$ and $Q(\tau)$ components. This process can be expressed as

$$\sigma\left(k\Delta m, \frac{m}{NT}\right) = \sum\{I_n(nT + k\Delta m) + jQ_n(nT + k\Delta m)\} \exp\left[-j2\pi\left(\frac{mn}{N}\right)\right]^2 \tag{4.28}$$

where m numbers the discrete Doppler frequency shifts and takes the values $0, +1, +2, \ldots, +(\frac{N}{2} - 1), -\frac{N}{2}$. The record length N is chosen to be 256, which allows a maximum Doppler frequency resolution of 0.1 Hz.

4.6.2 Large scale characterisation.

In the large scale analysis, 1200 or more individual impulse responses obtained over a number of channel sections is used to calculate the probability of echo path occupancy and distribution of echo strengths at fixed excess delays.

4.6.2.1 Probability of echo path occupancy.

The probability distribution of echo path occupancy as a function of excess delay is a measure of the relative frequency of occurrence of echoes occupying a particular time delay cell. It is defined as

$$P_{oc} = Pr[\textit{ at least one echo in interval } (\tau, \tau + d\tau)] \tag{4.29}$$

where the time delay cell or bin is as defined in equation (4.10). It is obtained by counting the number of echo profiles in which a bin was occupied and dividing by the total number of profiles analysed. An amplitude threshold was set to 25dB below the peak amplitude in the profile set. At least 1200 profiles selected from various sections along a route travelled by the mobile.

4.6.2.2 Cumulative amplitude distributions at fixed delays.

The series of complex impulse response envelopes show amplitude fluctuations or fading at all delays. This phenomenom, observed by some previous workers [3,4], is due to RF phase cancellations among signals propagating along unresolved paths within a time delay bin. The amplitude distributions at fixed delays are obtained as a cumulative distribution and compared with the theoretical Rayleigh and lognormal distributions. For the Rayleigh comparisons, the amplitudes are normalised either to the mean or median value of the data set.

4.6.2.3 The scatterer distributions.

In order to examine the effect of the environment on the multipath phenomenom in quantitative terms, the location distributions of the scatterers within the occupational domain are derived. In addition, distributions for the significant scatterers are also obtained. Comparisons are made between the two sets of distributions. These distributions are useful in illustrating the gross changes that occur in the channel as the mobile moves through it.

4.7 Programming.

The simulation package, called CHANSIM, is written in FORTRAN 77 language and implemented on the IBM3081 mainframe computer at Liverpool University. This is a high-level language and was selected for use because it is a universal programming language, widely used in the fields of scientific, numerical and technical applications. It is very well supported by a large library of documentation and applications packages, and is available on a large number of computer systems. Furthermore, unlike assembly language

programming which is dependent on the computer architecture, high-level language programming is procedure-oriented or problem-oriented. Therefore the software package can be used on any type of computer.

A critical factor in the design of the simulation package is the design methodology. Using the method of Top-Down design, the program has been written in modular form, a system of developing programs as a set of interrelated individual units or modules which are linked to form the complete program [95]. This strategy involves expressing the program algorithm in very broad terms, and then breaking each block down into successively more detailed sub-blocks or subprograms. Each individual subprogram performs a particular defined task. On identification of the 'irreducible' tasks, a subprogram is written, coded and then tested to ensure it performs correctly. When linked together, the subprograms communicate by passing data from one to another mainly through the Fortran COMMON facility. This ensures the maximisation of storage space and the minimisation of the number of variables used.

One of the great advantages of modular programming is that it produces small sections of easily reusable and/or replaceable coding. A single module can very simply be 'lifted' from an existing program and used elsewhere, or replaced with another module. Closely related to this advantage is the ability to simplify, elaborate, or modify a module in particular, and the program in general.

The package is divided into two : a simulation section which generates the envelope of the channel impulse response, and an analysis section which carries out the small and large scale characterisation. The module linkage chart of the simulation process is shown in Figure (4.9) and the functions of each of the main subprograms are briefly described in the next section. A simulation

run to generate 1200 impulse response profiles requires 20 CPU minutes and 4 Megabytes of storage.

4.7.1 Channel Simulation Programs.

4.7.1.1 Subroutine SETUP

This subprogram sets up the input control parameters and data to be used by the package. It accesses a control data file, which contains the map data, route identity, transmitter location etc.. In addition, it initialises the channel sounding signal processing parameters such as the probing signal width and operating carrier frequency.

4.7.1.2 Subroutine DOMAIN

The scatterers which fall into the defined occupational domain are determined by this subroutine. It reads the landcover data for all the maps to be used in the simulation (the data format is as shown in Table (4.1.) and using the scatterer location coordinates and the coordinates of the mobile location, selects buildings located within the boundaries of the occupational domain and stores their attributes in the appropriate arrays. The flow chart for the subprogram is given in Appendix F

4.7.1.3 Subroutine SELEKT

This routine selects the scatterers which contribute to the multipath phenomenom. The data output from DOMAIN is the input data for this routine. Each building in the occupational domain is assigned a marker which is set

if is a valid scatterer and reset otherwise. The flow chart for the subprogram is given in Appendix F

4.7.1.4 Subroutine COORDS

In order to select the contributory scatterers, the 4 sets of coordinates which define the building plan are required. These are calculated by subroutine COORDS. The input data are the coordinates of the building centre, the dimensions of the walls and the building orientation.

4.7.1.4 Subroutine PRIWAV

This is a ray tracing routine used by SELEKT. It sets up the vector representation of the mobile-scatterer path and of the buildings walls. It then finds the intersection, if any, between the former and any one of the latter. The flow chart for the subprogram is given in Appendix F

4.7.1.5 Subroutine ECHGEN

This subprogram generates the echo path variables for the buildings marked by SELEKT as valid scatterers. It moves the mobile along the designated route, measuring the channel response. The flow chart for the subprogram is given in Appendix F

4.7.1.6 Subroutine IMPSOT

This is the signal processing routine that orders the echo paths in increasing order of delay and splits the profile into quadrature components before convolving with the probing signal.

4.7.1.7 Subroutine CONVOL

The inphase and quadrature components of the echo profiles are convolved with the probing signal to obtain the complex envelope of the channel impulse response.

4.7.1.8 Subroutine PDF

The scatterer location and size distributions are generated by this routine. It also calculates the mean and standard deviations of the distributions.

4.7.2 Data Processing Programs.

Following is a brief description of the programs developed for calculating both small and large scale channel characteristics.

4.7.2.1 Program POWCOR

The small scale time and frequency domain analysis of the channel characteristics are performed by this program. The three main subprograms are described below.

POWDEL uses the quadrature components of the complex impulse response envelopes to obtain the average power delay profiles as discussed in section 4.5.1. It also calculates the average delay and delay spread for each profile.

FRQCOR applies the Discrete Fourier Transform to the average power delay profile to obtain the correponding frequency correlation function.

CORBW is a linear interpolation routine for estimating the 0.5 and 0.9 coherence bandwidths.

These profiles are stored in appropriate data files by POWCOR and are plotted by program SSPLOT using plotting routines from the GINO library which is available on the computer.

4.7.2.2 Program DOPLA3D

This program calculates the three dimensional scattering function which is then plotted by DOPDRA.

4.7.2.3 Program PATHOCC

The echo path occupancy distribution is calculated using this program. The distribution is plotted by PATHPLOT.

4.7.2.4 Program AMPDIST

The cumulative amplitude distributions at fixed delays are calcuted by AMPDIST and plotted on Rayleigh type coordinated by RAYLPLOT.

The channel simulation results obtained using the techniques outlined in this chapter are presented and discussed in chapter 6. However, the environmental classes and the methods of classification employed in this simulation are discussed in the following chapter.

Parameter	Data type	Description
RKX(i)	F10.2	X-coordinate of centre of ith block
RKY(i)	F10.2	Y-coordinate of centre of ith block
SIZEK(i)	F8.2	Base area of ith block
BLENTH(i)	F6.2	Length of block
BDEPTH(i)	F6.2	Width of block
IHAIT(i)	I3	Height of ith block
BANGLE(i)	F6.2	Orientation of ith block

Table 4.1 Data file format for map data

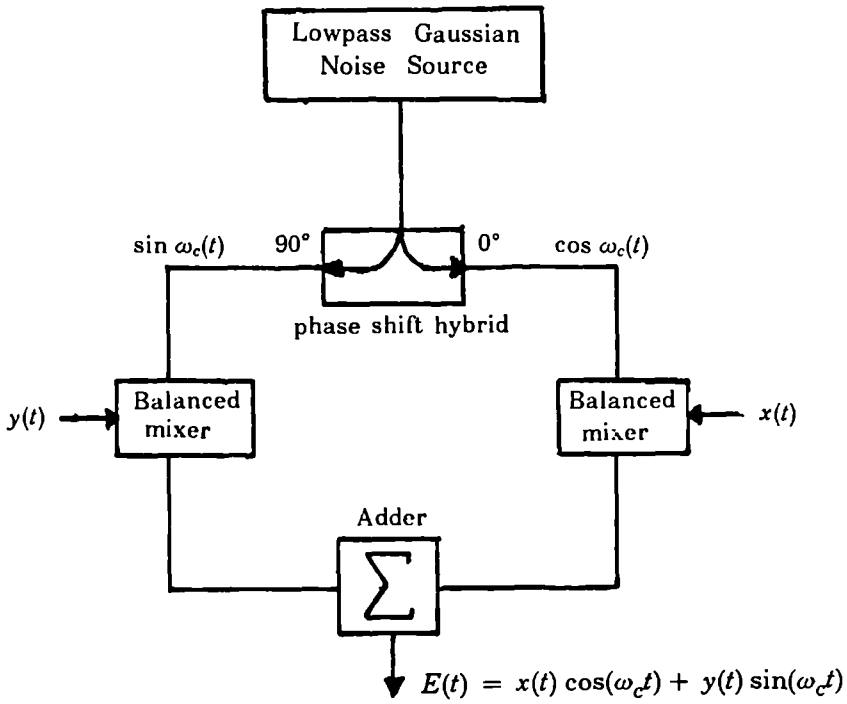

Figure (4.1) Rayleigh fading simulator : Quadrature Gaussian noise method.

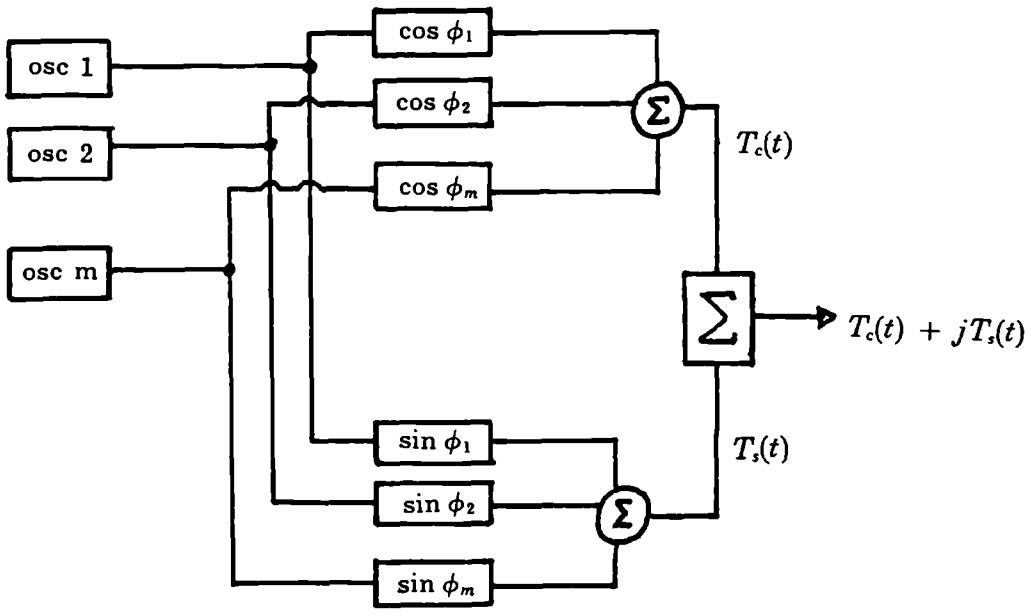

Figure (4.2) Rayleigh fading simulator : Multiple oscillator method.

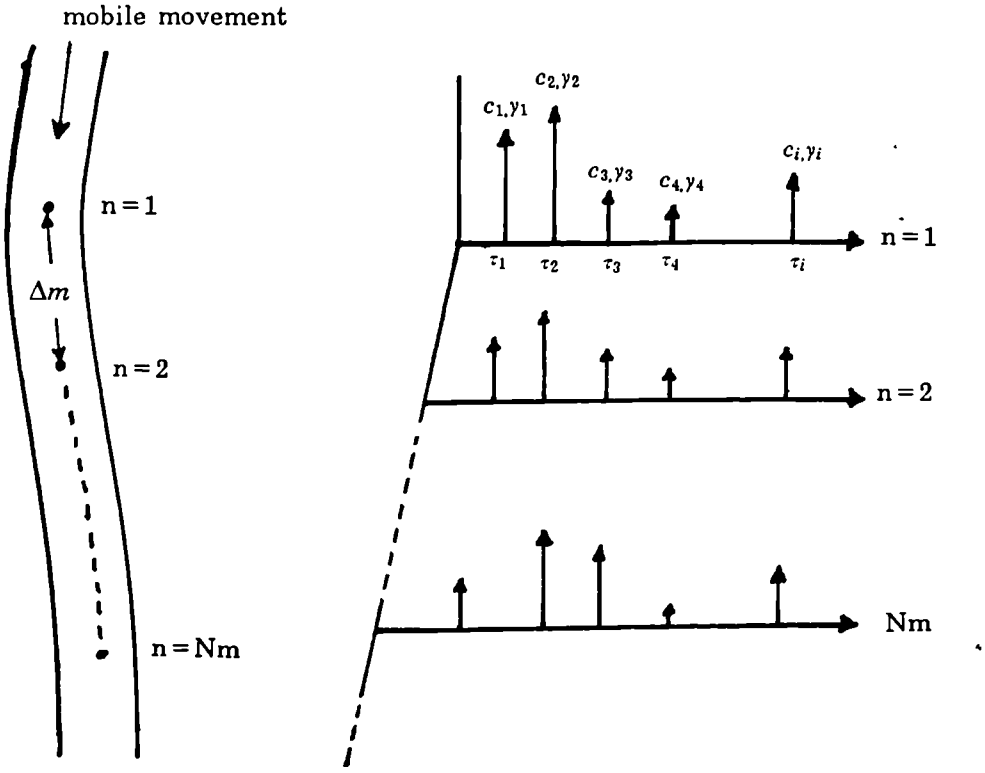

Figure (4.3) Illustration of channel sounding experiment.

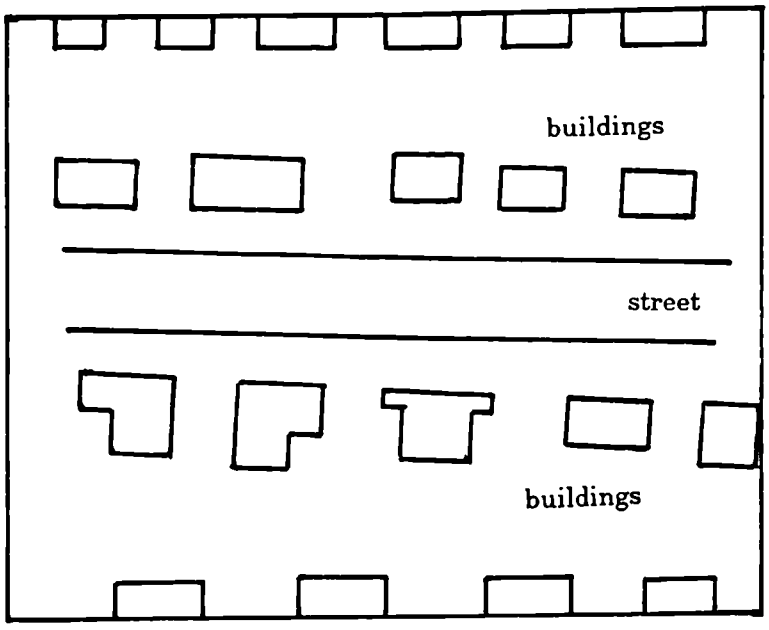

Figure (4.4) Plan of simulation location.

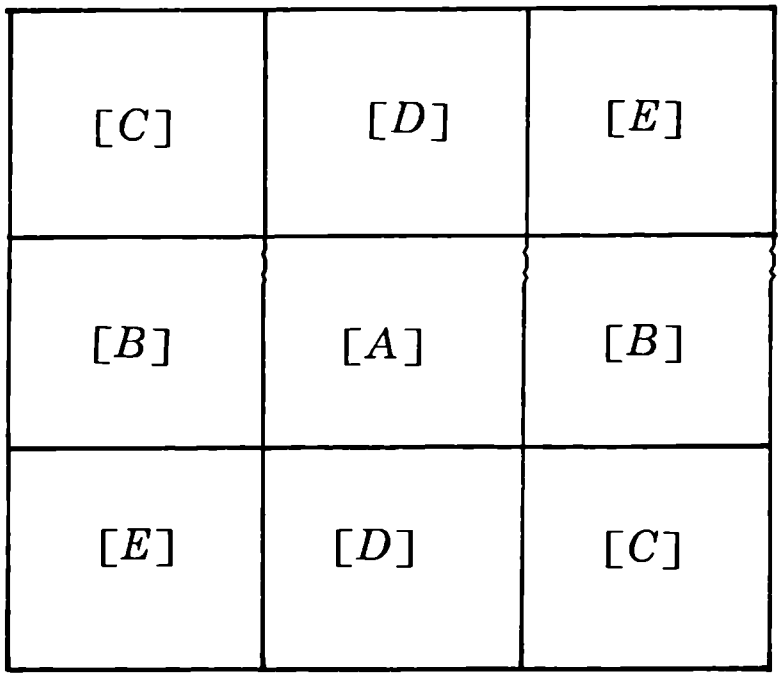

Figure (4.5) Multiple map method

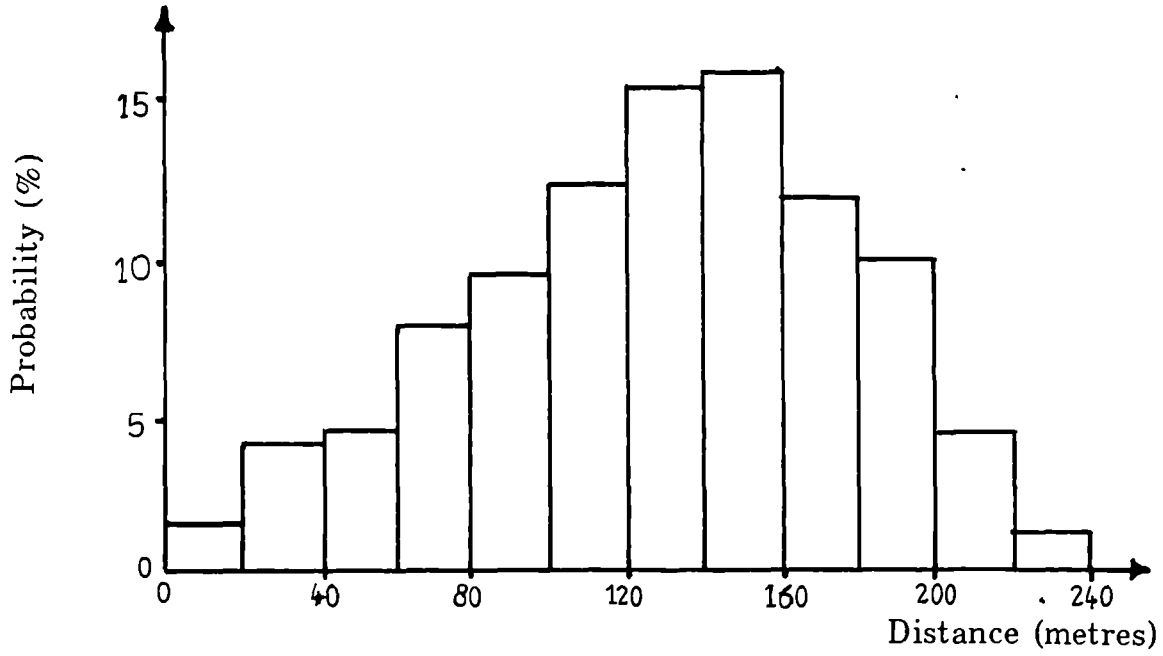

Figure (4.6a) Scatterer location distribution for single map.

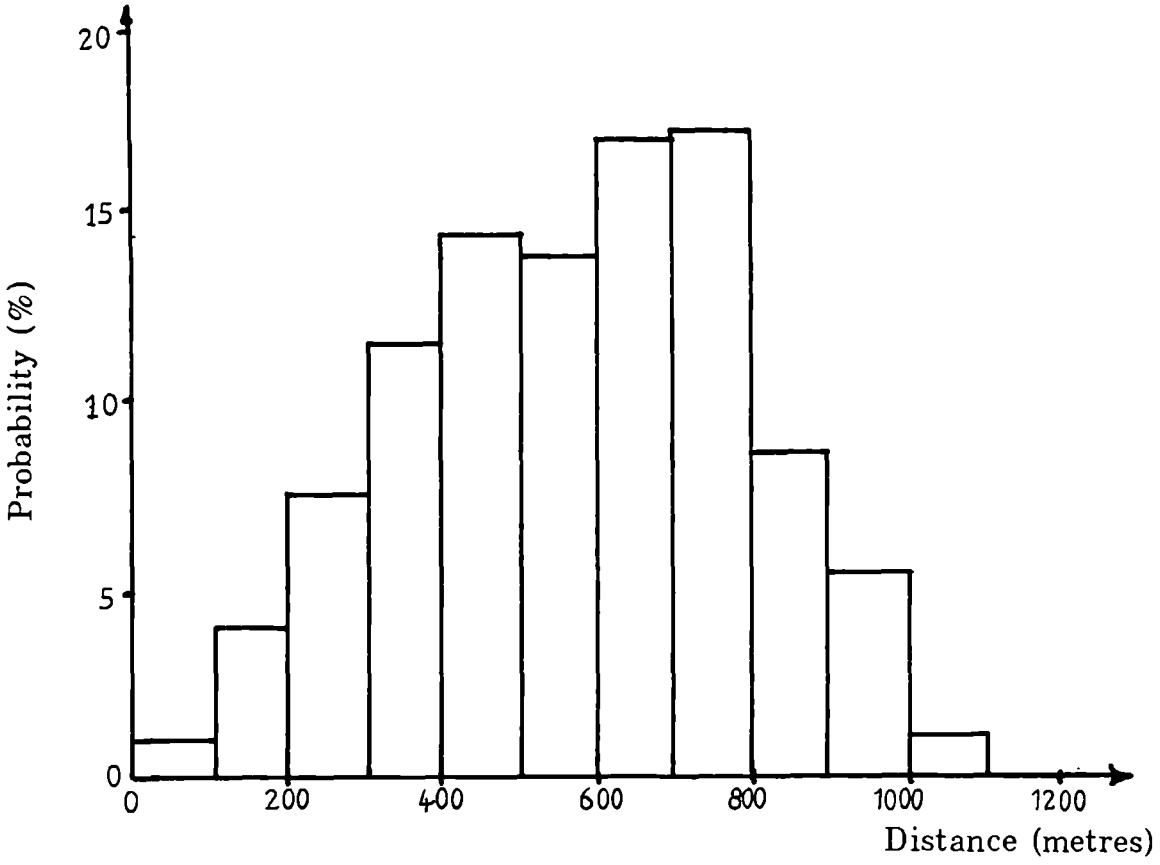

Figure (4.6b) Scatterer location distribution for multiple map.

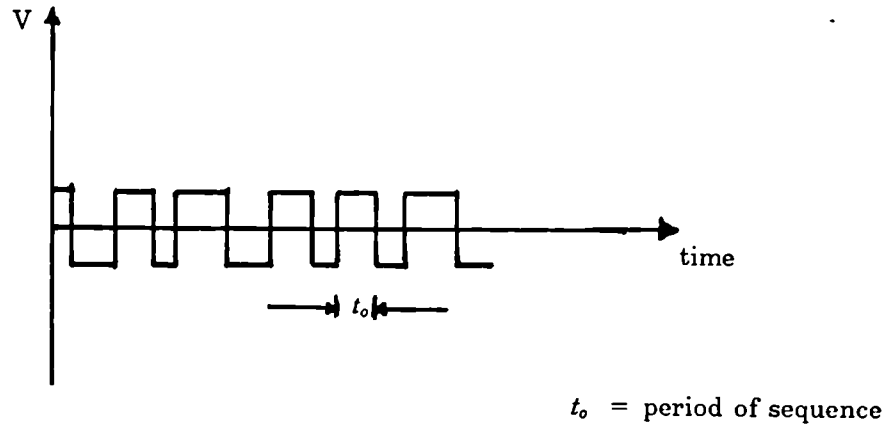

Figure (4.7a) Segment of a pseudo-random sequence.

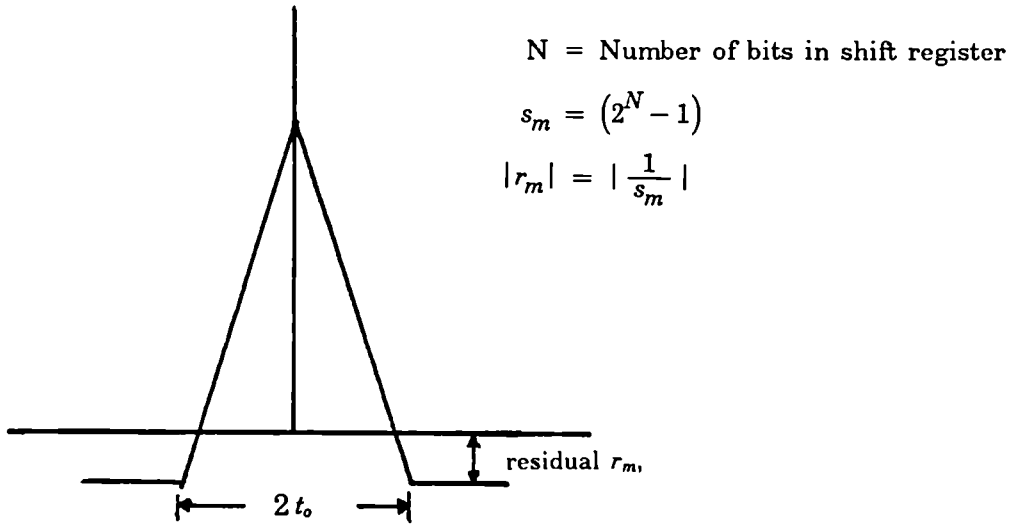

Figure (4.7b) Correlation function of pseudo-random sequence.

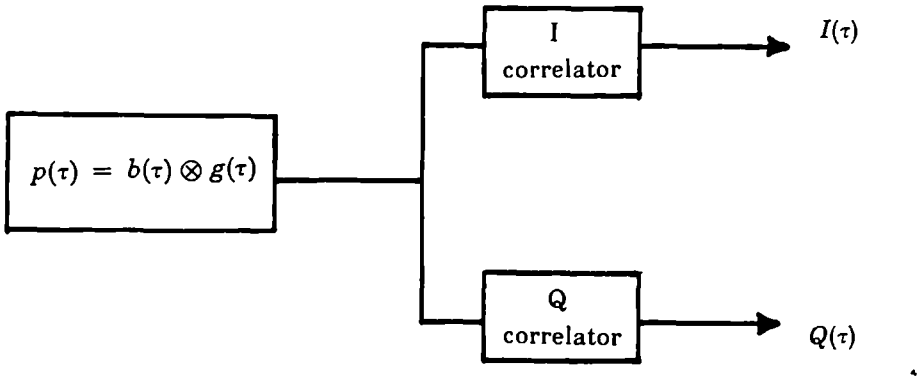

Figure (4.8) Linear system representation of measuring equipment.

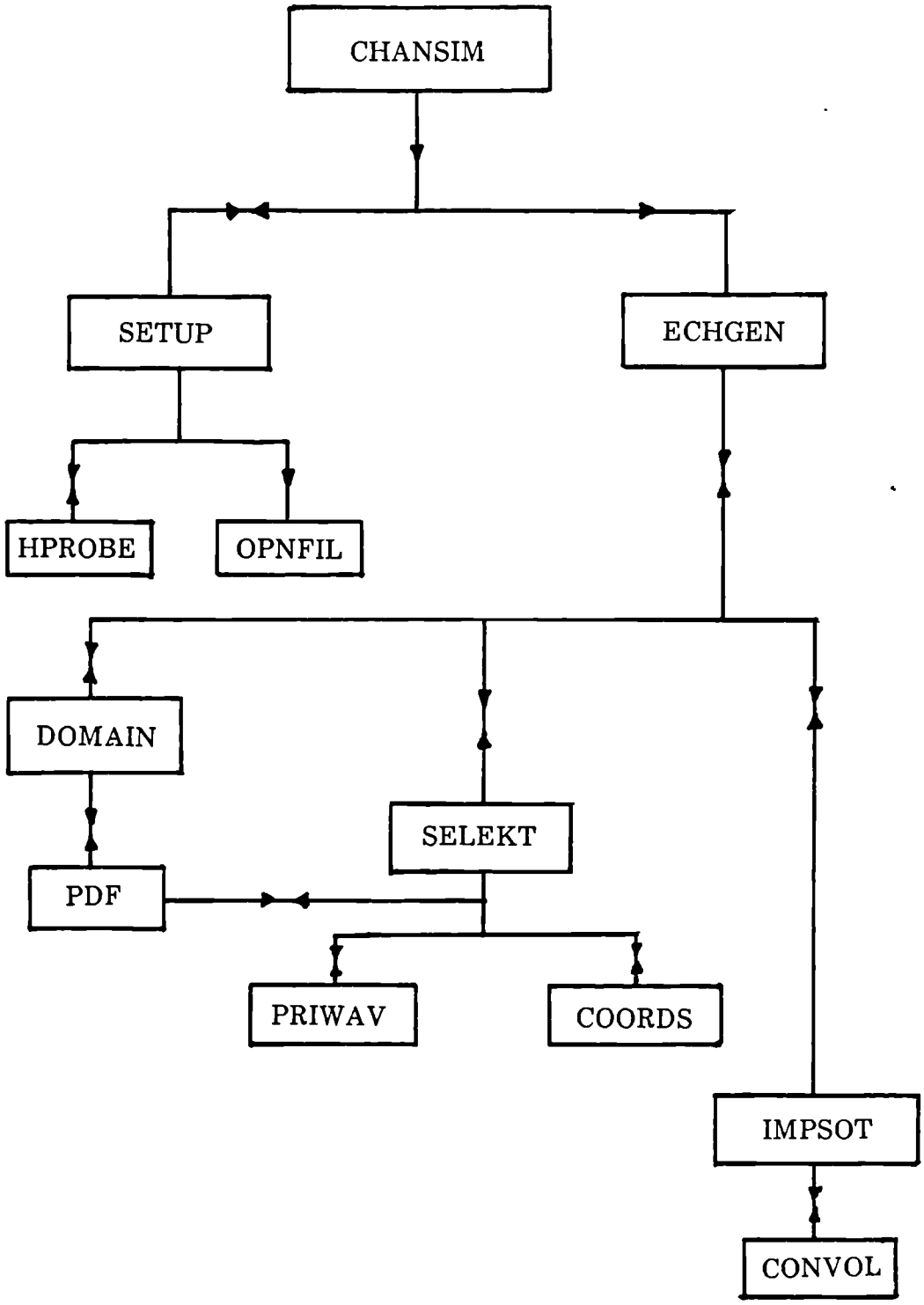

Figure (4.9) Module linkage chart for simulation package.

CHAPTER FIVE

5. CLASSIFICATION OF THE MOBILE RADIO ENVIRONMENT

And God said,"Let the waters under the heavens be gathered into one place, and let the dry land appear". And it was so. And God called the dry land Earth.
Genesis 1:9,10

5.1 The Classification Problem.

The propagation of radio waves in built up areas has been shown to be strongly influenced by the nature of the environment, such as the size and density of buildings. Generally, in propagation studies for MR links, a qualitative description of the environment, with terms such as rural, urban and suburban, is often employed. The urban area is defined as dominated by tall buildings, office blocks and other commercial buildings while the suburban area comprises residential houses, parks and gardens. The rural term defines open farmland with sparse buildings, woodland and forests. These qualitative descriptions are not precise and are open to different specific interpretations by different users. For example, an area described as urban in Liverpool could be termed suburban in New York and this leads to doubts as to whether measurements or simulations made in one city are applicable in another. There is, therefore, an obvious need to describe the environment quantitatively to surmount the current unavoidable ambiguity embodied in the qualitative definitions which might arise from cultural differencies and subjective judgement.

5.2 A Classification Approach.

In numerous situations of interest, the environment can be regarded as composed of many different mutually independent scatterer classes or types and different number of scatterers given any one particular type. Owing to various environmental interactions, be they ecological, geographical or cultural, terrain features such as buildings and trees, commonly aggregate around many population centres which are themselves dispersed in space. From this perspective, the terrain landscape is viewed as a conglomerate of numerous clustered objects. For example, a town appears as a random collection

of buildings, each building being a scatterer. Likewise a forest appears as a random collection of trees, each tree being regarded as a scatterer. If the statistical properties of groups or clusters of individual scatterers are known, as well as the scatterer population per group, then it is possible to derive quantitative descriptions of the environment using these statistics [28].

The environment classification proposed in this study is based on the approach described above. Any given mobile radio service area can be viewed as a mixture of composite environments (e.g mixture of rural and suburban type localities). The term 'composite' thus refers to a set of locally homogeneous landcover (e.g buildings of a particular type). Following Ordnance Survey descriptions, we divide the service area into square cells A_o, of dimension 500 metres x 500 metres. Any given test cell is then regarded as a sample of an ensemble of composite environments with the ensembles described by different terrain type and landcover. Although, sample cells in an ensemble are not identical, they are sufficiently similar to allow a meaningful statistical description. In order to circumvent the need for a detailed description, the scattering environment is represented by an equivalent set of randomly dispersed elementary scatterers. Similar approaches have been used to study the statistics of atmospheric noise and reverberation [86-88].

Considering the relevance and effects of the environment on radio propagation, it is seen that the following characteristics could be used in classifying the land cover types:

(a) building density: percentage of area covered by buildings
(b) building size : area covered by a building
(c) building height
(d) building location
(e) vegetation density

(f) terrain undulations

Using some of these characteristics, some workers have devised classifications for the environments in which they carried out their experiments [29,30]. We now examine some of these classifications.

5.3 Review of Previous Classifications.

Kozono and Watanabe [29] working in Tokyo in 1977 attempted to quantitatively classify the urban environment in their investigation of the influence of buildings on received mean field strength. They proposed four parameters which were termed :

(1) area factor of occupied buildings, α.

(2) extended area factor of occupied buildings, α'.

(3) building volume over a sampled area, β.

(4) building volume over an extended area, β'.

A sampled area, based on the Japanese Community map, is a circle of 250 metres radius. The extended area extends the sampled area towards the base station by a 500m x 500m area along the straight line joining the base station to the sampled area, consequently having a total area of 500 x 1000 square metres. In their study of the influence of buildings on the mean received signal strength, they concluded that, although β often correlated better with the median received signal, α was more suitable since it is easier to extract from the maps.

Ibrahim and Parsons [30], characterising the test areas for their experiments in inner London, introduced two parameters, Land Usage factor L and Degree of Urbanisation factor U.

Land usage factor L is defined as the percentage of the test square, dimensioned 500m x 500m, that is covered by buildings, regardless of their height. This factor, essentially the same as the α defined in [29], defines what is colloquially known as 'bricks on the ground'. A good correlation was observed between path loss value and L.

Degree of Urbanisation factor U is defined as the percentage of building site area, within the test square, occupied by buildings having four or more floors. U may vary between zero and 100%, a value approaching zero indicates a suburb while a value approaching 100% indicates a highly developed urban area.

British Telecom [31] proposed a ten point land cover categorisation based on qualitative descriptions. This scale is shown in Table 5.1. These categories, though comprehensive, can be interpreted differently by other service providers. Table 5.2 shows how the BT categories compare to those employed by other organisations [32,33,34,35].

The comparisons in Table 5.2 clearly indicates the fallibility of employing mainly qualitative descriptions in classifying land use within the mobile radio service areas. In Germany, built-up areas are classified under one category, while in Britain and Japan, they come under three broad classes : suburban, urban and dense urban. Experiments have shown however that these three categories do not cause the same level of signal distortion and it would therefore be inappropriate to compare results obtained in built-up areas in Germany with those collected in UK. A more detailed description of land use in Germany would be required, and this would be more expensive in terms of cost and time. The need for a more accurate and universal standard of categorisation is therefore very apparent, more so now that the Pan European Mobile Radio System is being adopted.

Until recently, the derivation of land cover data, which is essential for classifying land-use, involved manual, costly and time consuming procedures. Now, with the availability of geographic information systems (GIS) which use digital database technology to enable the storage and retrieval of geographic information indexed to some coordinate system [36], land cover data will ultimately be available in machine readable form. The Ordnance Survey is currently intensifying the process of digitising terrain and community maps for the whole of the UK. The digitised community maps are available for 500m x 500m grid areas while terrain contour maps are available for much larger areas. It is, therefore, most appropriate to adopt some standard categories of land use which relate to the standards employed in a GIS and are applicable not only in the UK but also worldwide. To achieve this objective, we first identify the relevant land-cover parameters obtainable from conventional OS map sources. The statistical properties of, and possible relationships between them are obtained and employed in creating standard parameters which are then used, singly or in combinations, to classify the environment.

5.4 Identification of Available Land Use Parameters.

The type of map employed in this study is the standard OS community map dimensioned 500 x 500 square metres. The map scale is 1:1250 metres and measurements can be made to an accuracy of 0.1 metre. A section of one such map is shown in Figure (5.1). As can be observed, buildings and other local terrain features such as trees etc, are clearly defined : the building walls as a series of continous lines and the areas with vegetation with tree symbols. The terrain height information is given as spot heights rather than contour lines while building heights are not given. The house numbers are given in most cases. The map identification number is derived from the National Grid

(NG) two-coordinate reference of the southwest (SW) corner of the map. The method of identification will be discussed fully in section 5.7.

The spatial location of a point on the map is referenced east(E) and north(N) from the SW corner, for convenience and uniformity. Using this reference method, coordinates of any feature on the map can be obtained. The following land cover parameters can thus be extracted:

(1) building location

(2) building size or base area

(3) total building occupied area

(4) number of buildings in the grid

(5) terrain spot height

(6) parks and/or areas with trees and vegetation

It is possible in some cases to extract some building height information from the house numbers. For example, a building marked 1-4 would imply a 4-storey structure. By making a number of site visits to various locations, this hypothesis was confirmed to hold for residential areas but not for commercial or city centres.

5.5 Development of Proposed Classification Parameters.

Having established the relevance of the environment to the mode of propagation, and identified the relevant land use parameters available from local sources, great care must be taken in defining parameters which will be considered as 'standard' for use in classifying the scattering environment. First we consider parameters which describe man-made land cover, namely building size and total building occupied area, building height and location.

5.5.1 Building Size Distribution, BSD.

- The building size s_b is defined as the ground area, in square metres, covered by the building and it is independent of the location of the building within the test cell A_{os}. The cell A_{os} contains a collection of buildings of different sizes and it can be observed that there are a different number of buildings given any particular size. Due to the size variations, it is more appropriate to represent the parameter as a density distribution. We thus define the Building Size Distribution, BSD which is completely described by its mean (or expected value) μ_s and standard deviation ε_s. Mean μ_s indicates the type of use to which the land has been put, e.g for residential or commercial purposes. The latter tends to have a larger value than the former. The standard deviation ε_s is an indicator of the homogeneity, a small value of spread indicating a relatively homogeneous set of structures and a large value implying a diverse range.

If the area under the probability curve is designated A_{bs}, then it is possible to define A_{bs} as the summation of all the building sizes, that is:

$$A_{bs} = \sum_{i=1}^{Nb} s_{bi} \tag{5.1}$$

where Nb is the total number of buildings in A_{os}.

5.5.2 Building Area Index, BAI.

A_{bs} is a useful measure of the extent of land development if referenced to A_{os}. We thus define the Building Area Index BAI, as the percentage of the cell A_{os} that is occupied by buildings irrespective of type or height, that is

$$BAI = \left[\frac{A_{bs}}{A_{os}} \right] \times 100 \qquad (5.2)$$

This factor is similar to α defined by Kozono and Watanabe [29], and the L defined by Ibrahim and Parsons [30]. It varies between 0% (in areas with no development, e.g open fields, forests or mountianous regions) and 60% (in highly developed cities).

The propagation of radiowaves in a built-up area is influenced not only by the building density, but also by the building height. This parameter is considered next.

5.5.3 Building Height Distribution, BHD.

The building height is defined in terms of the number of storeys above ground level. This information is not usually included in community maps, but in some central city areas, building height is available in the form of a storey index, SI defined as the total floor area of a building divided by the building base area or size which we have defined in 5.5.1. SI has been found to underestimate the actual building heights. In this study, the height information has been obtained by visual inspection of the test sites. It is envisaged that in the future, this vital information will be included in all community maps. We define the Building Height Distribution, BHD as the probability density distribution of the heights of all the buildings within the cell A_{os} . The mean of the distribution μ_h represents the average building height while the standard deviation ε_h gives an indication of the spread in the heights. The last aspect of the building to be considered is its location.

5.5.4 Building Location Distribution, BLD.

The collection of buildings in the cell A_{os} are not only of various sizes and heights, but are also spatially diverse. The location of each building can be obtained indexed to any point on the map, chosen in this case to be the centre of the test cell. From discussions in section 3.4.1, the location can be described by the polar coordinates (R,ϕ) where R is the range and ϕ the azimuth. R and ϕ are independent, therefore we define the Building Location Distribution BLD, as the probability density distribution of all buildings in A_{os} irrespective of type, size or height.

$$BLD = p(R, \phi) = p(R)p(\phi) \tag{5.3}$$

The range location distribution is described by its mean μ_R which gives the average distance at which a building is likely to be located, and its standard deviation ε_R which shows spatial diversity of the locations.
The azimuth location distribution is a good indicator of the clustering centres, if any, in the cell area and is described by its mean μ_ϕ and standard deviation ε_ϕ. The building location distribution defines the probability density distribution of the locations of the buildings within the test square indexed to the coordinates of the centre of the square. The mean of the distribution gives the average distance at which a building is likely to be found while the standard deviation shows the spread or clustering of the buildings about the chosen reference.

Next, we examine natural landcover, in the form of trees and other vegetation.

5.5.5 Vegetation Index, VI.

Patches of vegetation can be found in some parts of the service area. This could be in the form of public parks and gardens, woods or forests, or just a few tree decorations around a property. It is well known that vegetation causes attenuation of radiowaves, hence its inclusion in the proposed set of standard classification parameters. If A_v is the area covered by vegetation in a test cell, then the Vegetation Index, VI is defined as:

$$VI = \left[\frac{A_v}{A_{os}} \right] \times 100 \qquad (5.4)$$

This parameter varies from 0% in densely built-up urban areas (colloquially known as concrete jungles) to 100% in woodlands and forests.
Finally, the variability of the height of natural terrain is examined.

5.5.6 Terrain Index, TI.

On maps, terrain heights are given relative to the sea level, either in the form of terrain contours, or spot heights. In order to obtain an accurate assessment, it would be necessary to examine the terrain on a global basis within the proposed service area, rather than on the basis of individual cells A_{os}. The sample areas chosen for our site survey are relatively flat, hence there is no data to support the parameter. The terrain index would define the level of irregularities in the terrain.

These parameters have been selected on the basis of their proven relevance to the propagation mechanism in built up areas and their effects on the path loss characteristics. In addition, they are simple to use and can be extracted from Ordnance Survey maps or other land use data sources, with perhaps BHD being the exception in the meantime, requiring more detailed and manual

procedures for its extraction. Having obtained the relevant standard environmental parameters, it is now possible to quantitatively classify the environment.

5.6 The Environmental Classification.

Three main classes of environments are proposed based on the qualitative descriptions of rural, suburban and urban, which are presently in use. Each class can be further divided into sub-classes to give a more precise characterisation.

5.6.1 Class 1 Environment.

This class defines areas which are generally undeveloped or with very little development in terms of buildings etc.. It comprises of farmlands, woodlands or forests, hilly and mountainous regions. There is insufficient data to enable a thorough classification of this type of environment. It can however be broadly divided into three subclasses as follows:

(A) Flat rural area

(B) Hilly rural area

(C) Mountainous rural area

The level of development is indicated by BAI while the vegetation cover can be obtained from VI. The level of terrain irregularity is shown by TI.

5.6.2 Class 2 Environment.

This class defines the suburban areas, characterised by residential dwellings. These buildings are of different types, but mainly bungalows, 2-storey detached and semi-detached houses *, terraced buildings, and high rise blocks of flats such as is found in council estates. These residential dwellings are sometimes interspersed with large public buildings such as clinics or hospitals, schools, utility halls or churches.

In areas with predominantly semis and detached houses, there is a fair amount of open space as the houses usually have gardens attached. The building heights are fairly uniform, but the base areas may vary from one locality to another. It is expected that the building density will be low, that there will be some vegetation cover and the average building height will be 2 storeys.

Another distinct building type, the terraced house, is a characteristic feature of suburban residential localities. These are usually found in the areas surrounding the central urban core of the city. These buildings, with uniform height of 2-3 storeys, are laid out in parallel rows on both sides of the street and very often do not have attached gardens. Where gardens exist, they are very small patches of land indeed. The building density in this type of locality is expected to be higher than the former, and with very little or no vegetation cover. A terraced structure can be viewed as a cluster of individual buildings with sizes comparable to those of the semis and detached houses.

The third distinct type of building is the high rise block of flats, a predominant feature in council housing estates. These structures are sometimes interspersed with open spaces for recreational purposes and car parking

---

* The semi-detached house will be referred to as semis forconvenience.

facilities. The vegetation cover is minimal while the average building height is expected to be at least 4 storeys.

On the basis of these distinct building types, this class of environment is further divided into three subclasses as follows :

(A) Residential (semis and detached) with some open spaces.

(B) Residential (terrace-type) with little or no open spaces.

(C) High rise residential areas (e.g council estates) with some open spaces.

It is seen that a combination of the standard parameters is required to uniquely describe these subclasses, the set comprising BSD, BAI, BHD, and VI. BLD is useful in determining if the buildings are uniformly located within the test cell A_{os} or if they are clustered in a particular area. There is ofcourse some degree of overlap between these subclasses, but they can be said to represent the best, middle of the road, and worst cases respectively, of the class 2 environment. It is worth noting that building density in class 2C may be comparable to that in class 2A, and the distinguishing factor will be the building height distribution and associated descriptors. While the BHD and its descriptors are expected to be similar for class 2A and 2B, the BAI and VI will enable a distinction of type to be made.

5.6.3 Class 3 Environment.

This class describes the urban / dense urban type environments which comprise of mixtures of buildings used for office, shopping, commercial and industrial purposes. These areas are densely built up with the minimum of open spaces between buildings. In large cities such as Liverpool, a demarcation of the area on the basis of land use type can be observed. Shopping precincts are located in the centre of the city, with office blocks surrounding them,

interspersed with commercial buildings. The industrial sections are located on the outer fringes of the city.

The shopping area comprises of buildings, at least 4 storeys high, built like terraced structures, with no space between individual shops. This implies that the BAI is high and VI is very low. The average building size is also expected to be large.

The commercial area includes large office blocks, hotels, warehouses and large buildings used for other commercial purposes. Like the shopping precinct, the BAI is high and VI is low as the buildings are built close in together. The industrial category, which in Liverpool is found in the North-West area of the city and in the docklands, comprises of very large buildings used as factories and warehouses etc. The buildings are generally 2-4 storeys high and with open spaces in some cases. The average building size is expected to be much larger than that of the shopping and commercial areas, but BAI should be large. These areas are not clearly defined, but there exists transition regions so that a degree of overlap is unavoidable. The class 3 environment is, on the basis of land cover, further divided into 3 subclasses as follows:

(A) Shopping with commercial area

(B) Commercial area

(C) Industrial area

A full description of each subclass is achieved using the parameter set BSD, BAI, BHD and VI. In all three subclasses, VI is expected to be low but with BSD very similar indeed. However, BHD for classes 3A and 3C will be instrumental in distinguishing one from the other.

In order to derive the quantitative values for the parameters for each class of environment, a large amount of land use data is required. The method of extracting the data used in this study is now examined.

5.7 Methods of Extraction of Land Use Data.

Land use data was extracted from Ordnance Survey (OS) community maps for use in the channel simulation and environmental classification. These maps are available in the conventional paper form and increasingly in digital form. A brief description of the National Grid Index Plan employed by the OS is given below.

5.7.1 Large scale National Grid (NG) index plan.

Great Britain is divided into 100 kilometer squares each of which is identified by two letters. Each 100 km square is divided into smaller squares by grid lines set at 10 kilometer intervals. These are numbered 0 - 9 in an easterly and northerly direction from the southwest corner of each 100 km square. The 10 km squares are further subdivided by lighter grid lines set 1 km apart also numbered 0 - 9 in an easterly and northerly direction from the southwest corner of each 10 km square, but prefixed by the number of the respective 10 km square. Finally, the 1 km squares are divided into 500 metre squares, identified by the southwest corner coordinate of the 1 km square and the compass notations SW(southwest), SE(southeast), NW(northwest) and NE(northeast). This index method is illustrated in Figure 5.2 for Liverpool. The 100 km prefix is SJ and the areas of interest lie in the 10 km squares SJ38 and SJ39. The enlargement of square SJ38 shows the division into 1 km squares. The shaded map area A is identified as SJ3589 with unique 6 digit

east and north NG coordinates (335000, 389000) while map area B is uniquely identified as SJ3589NE with NG coordinates (335500, 389500).

The three basic scales of survey employed by the OS are 1:1250, 1:2500 and 1:10000 as illustrated in Figure (5.2). The shaded area B is covered by one 1:1250 NG plan while the shaded area A is covered by one 1:2500 plan or four 1:1250 scale plans. The 1:10000 scale map would cover an area of 4 km x 4 km. The most suitable scale for use in this study is the 1:1250 scale map on which the building features are clearly defined. Hence, several such maps of areas in Liverpool were thus purchased for use in the study. The bulk of the data was extracted from the paper maps while a digital map was purchased in order to assess the feasibility of its use in the automated channel simulation procedure. Following is a brief assessment of the usability of both maps.

5.7.2 Use of Conventional Ordnance Survey Map.

The manual extraction of data from the conventional map is tedious, time consuming and requires much judgement. The use of a digitising table would have made the process less difficult, but in the absence of that, another method of extraction was devised. With the SW corner of the map as reference, the scaled location of the four or more points representing the corners of a building were measured and input into the computer. They were then converted into actual physical values using the source map scale in a simple conversion program. An area with vegetation is obtained as a series of points representing the boundary containing this feature and a street as a series of points measured along its length on both sides. Each feature is marked with a unique serial number.

This method does not lend itself to the extraction of vast amounts of data but the availability of digital maps offer a hugely attractive alternative method.

5.7.3 Use of Digital Ordnance Survey Map.

A digital map may be defined as the representation of conventional map detail (line, point, text) in a form suitable for manipulation by computer. The map detail is recorded as strings of coordinates on storage media eg. magnetic tape. Once recorded, this map information can be redrawn using a plotter [89]. Digital OS maps are becoming increasingly available and offer the possibility of an automated approach to the data collection without recourse to tedious extraction methods.

The OS digital map data is held on magnetic media and is produced primarily for the purpose of making plots or producing displays.The data is Fortran readable and held as fixed length 8-character records in blocks of 1800 or 2048 characters. It is organised so that all the feature details required to produce a map of an area appropriate to the source map scale is held in one logical unit. A feature is a point,line or series of lines forming a coherent object. Every feature has a unique identifier, the feature serial number (FSN) and only one primary attribute record described by a 3-digit feature code (FC). A feature can be selected either by its FSN or FC. For compact storage, a 3-level method of referencing the coordinates is employed:

Level 1 : National Grid (NG) coordinates of south west corner of the map, held once per map.

Level 2 : Basic grid square reference ,held once at the start of each feature and once for each change of grid square. The map area is divided up for reference purposes into 100 equal squares of the size given in the sheet heading, these squares are referenced from (0,0) at the SW corner of the map.

Level 3 : Reference within the basic grid square, held for each point. The point is referenced east(E) and north(N) from the SW corner of its basic grid square to an accuracy of 0.001 of the basic grid square dimension.

The digital data is supplied together with a map plotting program D09. Written in standard FORTRAN and, when compiled with the users own plotter routines and in conjunction with OS map data and the user-written parametres, D09 enables the user to create an output file which contains suitable plot instructions to drive the user's plotter. It was found necessary to reformat the data for use with the D09 software.

In order to extract coordinates of the features required for the channel simulation study, a new set of software was developed using the D09 program as a reference. It was absolutely essential to understand the data structure before any meaningful software could be developed, but once this was achieved, the process speeded up. For convenience, a transformation was applied to the 3-level coordinate reference system of the OS to produce a single level system with the SW corner of the map as reference. This proved to be a more useful approach for our use, simple to manipulate and similar to the reference system employed for the conventional map.

Although digital maps are easy to use in derivation of land use data, the cost for each map unit is high, thus putting it out of reach of small users although large service providers, the target group most interested in this item, are able to afford it. However, with improving database technology and increased use of the digital map, it is envisaged that the unit cost will reduce substantially. Another factor which precluded the use of the digital map in this study was the non-availability for locations of interest in and around Liverpool. According to OS sources, these should be available by 1992.

For our present purposes, a set of conventional maps of residential locations in Southampton and built-up areas in Liverpool, were purchased, manually digitised and processed to obtain values for our standard classification parametres.

5.7.3 Processing of Map Derived Land Use Data.

Three programs were developed to process the land use data extracted from the maps. Each test cell A_{os} is processed separately. The functions of each program are stated briefly below :

Program SJD09 reads the D09-formatted data, converts the scaled values into real data, and calculates the following building attributes:

(1) building location (R,ϕ) with reference to the coordinates (CX,CY) of the centre of test cell A_{os}. R is the distance between (CX,CY) and (SX,SY), the coordinates of the centre of the building. Azimuth ϕ is measured anticlockwise from the x-axis direction as illustrated in Figure (5.3).

(2) building size s_b. This was obtained by considering the building as a polygon with sides (n-1), where n is the number of feature coordinates and calculating the area accordingly [38].

SJD09 also formats the data in a form suitable for use by the simulation program.

Program SJPROC calculates the density distributions BSD, BHD, BLD and the corresponding statistical descriptors, that is mean and standard deviations. It also calculates BAI and VI.

Program SJDRAW plots the density distributions obtained by *SJPROC.*

The results from all test cells were then collated and boundary values for parametres classifying the categories discussed in section 5.6 déduced. The parametre values of the sample test squares, considered as typical for the different environmental classes, are presented in Table (5.3). The final results are presented in the discussions of the next section.

5.8 Classification Results

During the data extraction process, it was observed that the preliminary qualitative class structure proposed in sections 5.6.2 and 5.6.3 were well supported by the available data. As expected, there was a degree of overlap in the classes, however, the main characteristics of each class were sufficiently predominant to enable correct classification. We now look at the results in detail.

5.8.1 Class 2 Environment

For this category, man made land cover in the form of buildings occupies 12 % to 30 % of the test square A_{os}. One interesting feature highlighted in this survey is that the fraction of A_{os} occupied by roads and pavements is in some cases comparable to the area occupied by buildings. This observation led to the definition of a Road Index, RI. If A_R is the area covered by roads and pavements in a test cell, then the Road Index, RI is defined as:

$$RI = \left[\frac{A_R}{A_{os}} \right] \times 100 \qquad (5.5)$$

Its value was observed to vary from 12% to 25%, averaging about 17%.

Generally, it was found that man made and natural landcover occupies up to 60% of A_{os}, while the remaining 40% is open space, either between buildings, or simply undeveloped land.

Preliminary studies showed that the maximum building size varied from one sample cell to the next. While the limit in some was 700 m^2, others had buildings (e.g clinics, schools and other public buildings) with base areas as large as 2000 m^2. These large-based buildings tend to contribute a strong bias in the calculations of the mean and standard deviation of the BSD, giving erroneous statistics for the ensemble of squares. It was thus considered necessary to set a maximum limit on the size values employed in deriving the distribution. Careful observations showed that in over 95% of test squares examined, the sizes for 90% or more of the buildings were below 500m^2. This value was thus chosen as the maximum limit. Buildings with sizes in excess of 500m^2 are few in number and can be described by a sparse distribution, as will be shown.

It was also observed that in areas with predominantly detached and semis, up to 200 one-storey buildings with sizes less than 20m^2 could be identified. These are generally, green houses, garden sheds etc. located behind the main houses. It is thus intuitively evident that the contributions of these structures to the scattering process is negligible, if not non-existent. In addition, they occupy less than 1% of the test square, hence they have been neglected in the classification process. The following discussions describe the observed characteristics for four sample squares representative of this class of environment.

Map SU4315SW

The BSD, BHD, and BLD for this sample square are shown in Figure (5.4). With about 99% of the building sizes within the set limit, the mean μ, and standard deviation ε, are 103.11 m^2 and 57.26 m^2. The buildings are relatively homogeneous, as shown by p(s) in Fig (5.4a) and p(H) in Fig (5.4b). 97% of the buildings are two-storey structures. BAI is 16.28% , RI is 14% while the vegatation cover VI is 5.06%. The building location distributions of Fig (5.4c) and (5.4d) show that the buildings are located approximatly uniformly around the centre of the square at a mean distance of 188.40 metres. This test square is typical of the class 2A category. It contained only one building in excess of the limit and this occupies 0.27% of the total area.

Map SU4214NE

The distributions for this square are presented in Figure (5.5). These show close similarity to those of map SU4315SW, with the exception of the BSD, which has mean and standard deviation values of 112.13 m^2 and 64.72 m^2 respectively, both larger than those of the previous map. This suggests that, although the areas covered by these two maps support landcover of the same type, the structures in SU4214NE are generally larger than those in SU4315SW, as was observed on inspection of the maps. There are three buildings with sizes in excess of the limit and these occupy 0.81% of the square. The BAI is 15.66%, RI is 13.13% and VI is 2.97%.

Map SJ3589NE

The distributions for this map are shown in Figure (5.6). For this square, the mean of the BSD with a value of 112.42m² is comparable to that of map SU4214NE although the value of spread at 88.53m² is larger than the latter two examined. This reflects the large variation in sizes evident in the density distribution. This sample square is typical of the class 2B category. The terraced buildings have been divided into individual blocks whose sizes are comparable to that of the semis and detached houses examined earlier. BAI is 30.98% and with RI 24.93%. There is 2.45% vegetation cover. The BHD shows that 70 % of the buildings are three storey structures. Hence, μ_h is 3 and ε_h is 1. The location distribution shows that on average, a building is located at a distance of 195.12 metres form the centre of the test square. The $p(\phi)$ distribution suggests a concentration of buildings in the NW and SW quadrants of the square. Further examinations revealed that the terraces are mainly located in these quadrants. The subdivision into individual blocks accounts for the clustering effect.

Thirty-three buildings have sizes in excess of the limit, occupying 11.17% of the square. These buildings are sparsely uniformly distributed with mean 849.24 m² and standard deviation 446.54 m² as shown in Figure (5.6e).

Map SJ3591NE

The distributions for the map are shown in Figure (5.7). Within this test square are a few high-rise residential buildings, up to 10 storeys. The BSD and its associated μ_s and ε_s of 106.74 m² and 60.68 m² are comparable with those examined previously.

However, considering buildings with sizes in excess of the allowable limit, it is seen that the sparse distributions of Figures (5.7e) and (5.7f) are adequately descriptive of the building set. These buildings occupy 2.76% of the square while the smaller ones occupy 12.55%. The corresponding mean height is 4 storeys and the standard deviation is also 4 storeys. This data suggests descriptive statistics for a sample square with predominantly high rise buildings.

The BLD highlights one feature of the square. Located in the centre of this map is a large open field with the buildings located around it. This feature is evident in both p(R) and $p(\phi)$. A close look at the distributions shows that buildings are located on average at a distance of 210 metres from the centre of the square and are concentrated in the NW and SW quadrants. RI for this sample square is 17.52 while VI is 0.57%.

Based on the observed statistics of the extracted data, parametre values for BAI, VI, RI, μ_s, ε_s, μ_h and ε_h have been proposed for the three subclasses in the Class 2 Environment and are shown in Table 5.4.

5.8.2 Class 3 Environment

The areas classified under this category are highly built-up and the studies have shown that man made land cover occupies up to 80% of the area. As expected, there are more roads in this tupe of environment, and as such values of RI observed ranged between 20% and 30%, averaging 25% or more in over 50% of the test squares examined. BAI values were observed to be higher than those of class 2 with values as large as 52% occuring in the shopping districts. Building sizes up to 5000 m^2 were recorded with different maximum values occuring in the various sample squares. Similar to the method employed in the processing of data for the class 2 environment, the sizes considered for the derivation of the BSD were limited to 1000 m^2, having noted that in over

95% of squares, 90% or more building sizes were below this limit. A small degree of overlap of building types was observed and this is mentioned where applicable in the following discussions of three sample squares that are representative of this category of environment.

Map SU3490SE

The BSD, BHD and BLD for this square are shown in Figure (5.8a) to (5.8f). The area covered by this map is used for shopping purposes and is located in the city centre. Not suprisingly, the BSD shows a large range of building sizes with a mean of 248.78m^2 and a spread of 197.65m^2. The buildings in shopping areas tend to vary from the small service stores to large departmental stores, and this characteristic is clearly seen in Fig (5.8a). Twenty four of the buildings sizes recorded for this map were in excess of the limit, occupying 25.67% of the square. Fig (5.8e) shows the sparse distribution for these buildings and (5.8f) the corresponding height distribution. The BAI is 52.30%, the highest observed in this category, while the RI is 27.29% and VI is 0%.

Over 60% or more of the buildings are three or more storeys high, giving a mean height of 4 storeys for this locality. The BLD illustrates that buildings are located approximately uniformly at an average distance of 201.14 metres from the centre of the square. A small degree of overlap between shopping and commercial buildings was observed, but this square typifies the dense shopping areas often encountered in cities, which is here defined as the class 3A environment.

Map SJ3489NE

This map is of a commercial locality, bodering on the shopping area described above. The BSD of Figure (5.9a) indicates that about 37% of building sizes are between 50m^2 and 100m^2. Some of these are residential type buildings which have been converted for commercial use, while some are still employed for residential purposes. The distribution has a mean of 176.58m^2 and an almost equal standard deviation value. Figure (5.9b) shows the corresponding height distribution, with a mean height of 3 storeys. A few building sizes were observed to be in excess of the set limit, occupying 6.43% of the square and distributed as shown in Fig (5.9e). The correponding height distribution is shown in Fig (5.9f). The BAI for this square is 35.07%, larger than values for class 2 but smaller than that observed in shopping areas. There is no vegetation cover, however, the RI is 23.95%. The p(R) and p(ϕ) location distributions show no appreciable deviation from the Gaussian and Uniform distributions respectively. This is a typical class 3B environment.

Map SJ3489SE

This map is of an industrial area, categorised as class 3C. This map area is characterised by large warehouse-type buildings of two to three storeys. In the course of this study, it has been observed that industrial centres are often located near residential locations on the outer fringes of the city where space is available for the construction to the large building structures required. Some degree of overlap with residential dwellings is therefore unavoidable. The BSD illustrated in Figure (5.10a) shows a large range of building sizes. Some of the 24% of buildings with sizes below 100m^2 are used for residential purposes. The mean size is 294.73m^2 and the spread is 246.38m^2, reflecting the diverse range of sizes. The BHD of Fig (5.10b) shows that the average

height is 3 storeys. The BAI is 43.74%, high as expected with RI of 29.26% and a vegetation cover of 0.83%. The p(R) location distribution best fits the uniform distribution, a depature from previous recorded distributions. The large sizes imply that the buildings are fewer in number than is obtained in either class 3A or 3B and are therefore spread out more evenly around the square, giving rise to the uniform distribution. The p(ϕ) distribution shows that fewer buildings are located in the NW and SW quadrants of the square. A 6-lane dual carriageway is located in these two quadrants, giving rise to the observed characteristic. Based on the observed statistics of the extracted data, parametre values for BAI, VI, RI, μ_s, ε_s, μ_h and ε_h have been proposed for the three subclasses in the Class 3 Environment and are shown in Table 5.5.

5.8.3 Conclusions.

Classification parametres for use in categorising the various types of environments encountered within a mobile radio service area have been developed. The Building Size Distribution is particularly useful in determining the type of use to which the land has been put, as has been shown. The Building Location Distributions are useful in identifying any unusual landcover characteristics in the service area. Site visits can then be made to clarify the situation. These parametres have been used to classify land use in Liverpool, and can be used in other parts of the country to give a universal quantitative description of the environment.

The proposed classes of environments have been derived using the well known qualitative Urban and Suburban descriptions. Therefore, the use of these categories in systems planning is enhanced as designers will have as a tool, precise quantitative definitons, rather than the often subjective qualitative terms hitherto employed.

Category	Description
0	Rivers, lakes and seas
1	Open rural areas; eg. fields and heathlands with few trees
2	Rural areas, similar to the above, but with some wooded areas eg. parkland
3	Wooded or forested rural areas
4	Hilly or mountainous rural areas
5	Suburban areas, low density dwellings and modern industrial estates
6	Suburban areas, higher density dwellings eg. council estates
7	Urban areas with buildings of up to four storeys, but with some open space between
8	Higher density urban areas in which some buildings have more than four storeys
9	Dense urban areas in most of the buildings have more than four storeys and some can be classed as 'skyscrapers'. This category is restricted to the centre of a few large cities.

Table 5.1 British Telecom Land use categories

BT(UK)	Germany	BBC(UK)	Denmark	Okumura (Japan)
0	4	-	-	Land/sea
1	2	1	0/2	-
2	3	1	1/2	-
3	2	1	4	-
4	2/3	1	-	Undulating
5	1	2	3	Suburban
6	1	2	6	Suburban
7	1	3	7	Urban
8	1	3	8	Urban
9	1	4	9	Urban

Table 5.2 Comparisons of BT and other land use categories

MAP INDEX	BAI (%)	BSD		BLD (R)		BLD (ϕ)		BHD		VI (%)	RI (%)
		$\mu_s(m^2)$	$\varepsilon_s(m^2)$	$\mu_R(m)$	$\varepsilon_R(m)$	$\mu_\phi(deg)$	$\varepsilon_\phi(deg)$	μ_H (storey)	ε_H (storey)		
SU4315SW	16.28	103.1	57.26	188.40	75.18	181.98	105.47	2	1	5.06	13.56
SU4214NE	15.66	112.13	64.72	195.00	72.53	177.46	109.49	2	1	2.97	13.13
SJ3589NE	30.98	112.42	88.53	195.12	63.28	223.44	90.92	3	1	2.45	24.93
SJ3591NE	12.55	106.74	60.68	212.07	52.49	170.27	117.85	2	1	0.57	17.52
SJ3490SE	52.30	248.78	197.65	201.14	68.61	185.31	111.16	4	1	0	27.29
SJ3489NE	35.07	176.58	176.11	181.00	73.70	153.91	101.93	3	1	0	23.95
SJ3489SE	43.74	294.73	246.38	189.29	83.10	169.05	134.10	3	1	0.83	29.26

Table 5.3 Statistical descriptors for sample test squares.

Class	BAI (%)	BSD, (m^2)		BHD, (no. storeys)		VI (%)
		μ_s	ε_s	μ_H	ε_H	
2A	12 - 20	95 - 115	55 - 70	2	1	≥ 2.5
2B	20 - 30	100 - 120	70 - 90	2 - 3	1	< 5
2C	≥ 12	≥ 500	> 90	≥ 4	1	≤ 2

Table 5.4 Descriptive parameter values for Class 2 Environment.

Class	BAI (%)	BSD, (m^2)		BHD, (no. storeys)		VI (%)
		μ_s	ε_s	μ_H	ε_H	
3A	≥ 45	200 - 250	≥ 180	≥ 4	1	0
3B	30 - 40	150 - 200	≥ 160	3	1	0
3C	35 - 45	≥ 250	≥ 200	2 - 3	1	≤ 1

Table 5.5 Descriptive parameter values for Class 3 Environment.

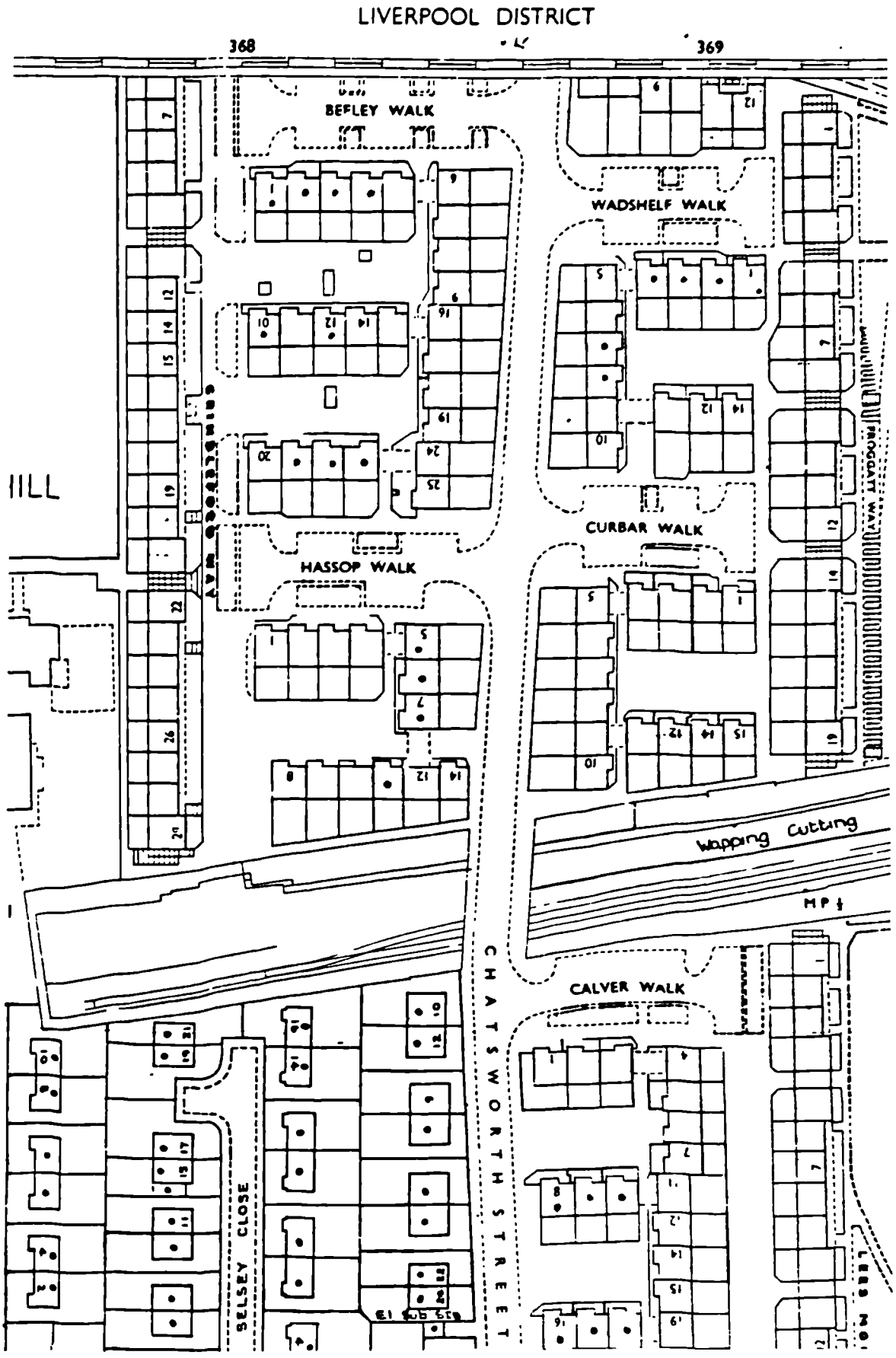

Figure (5.1) A section of an Ordnance Survey map; scale 1:1250

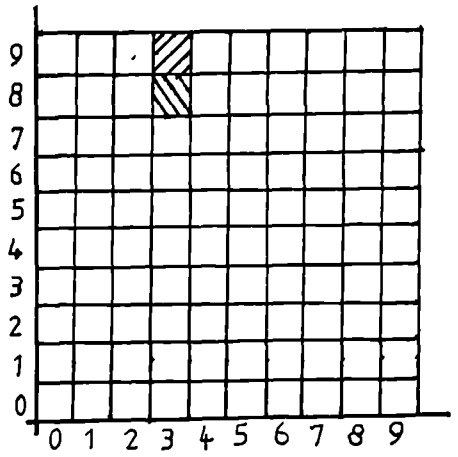

(a) 100 Km square SJ

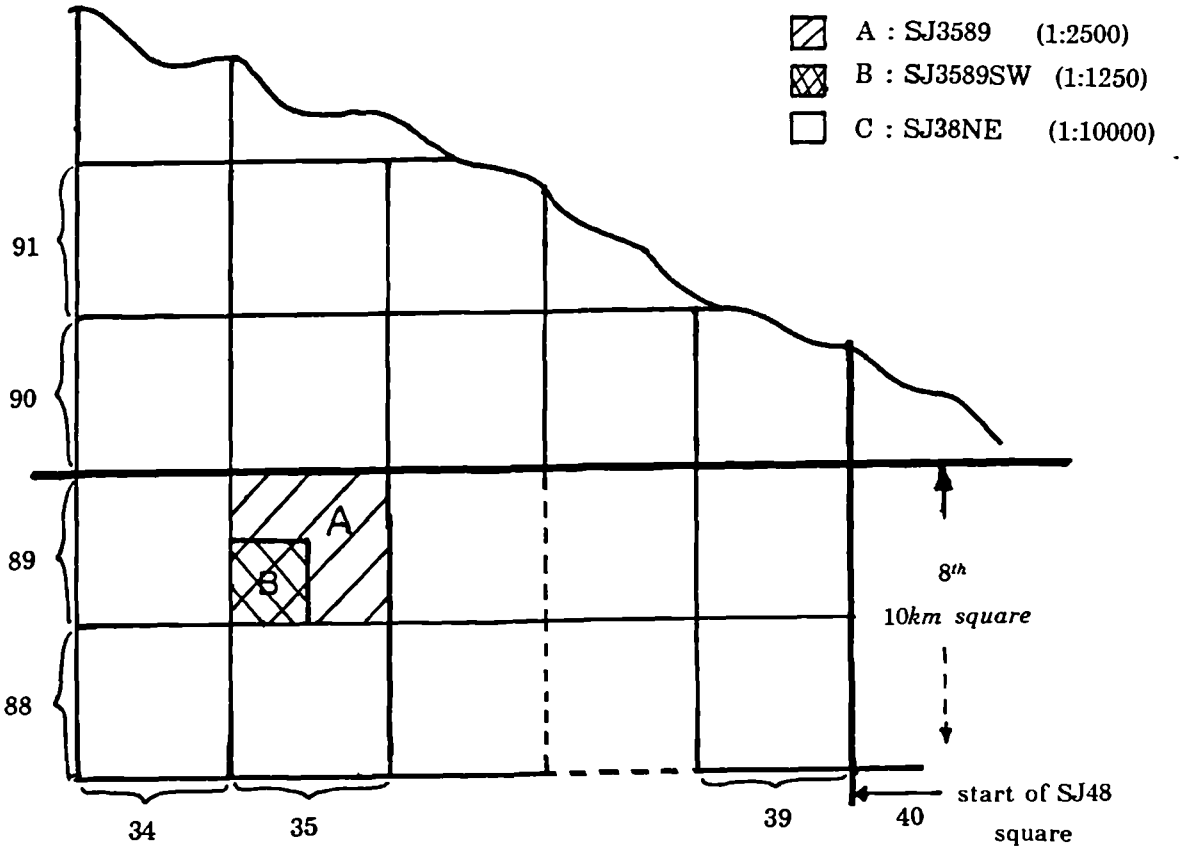

(b) Enlargement of part of SJ38 and SJ39 squares

Figure (5.2) Ordnance Survey NG index plan for Liverpool area.

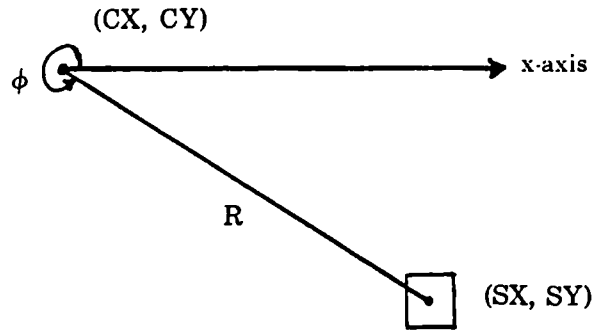

Figure (5.3) Measurement of scatterer location (R, ϕ).

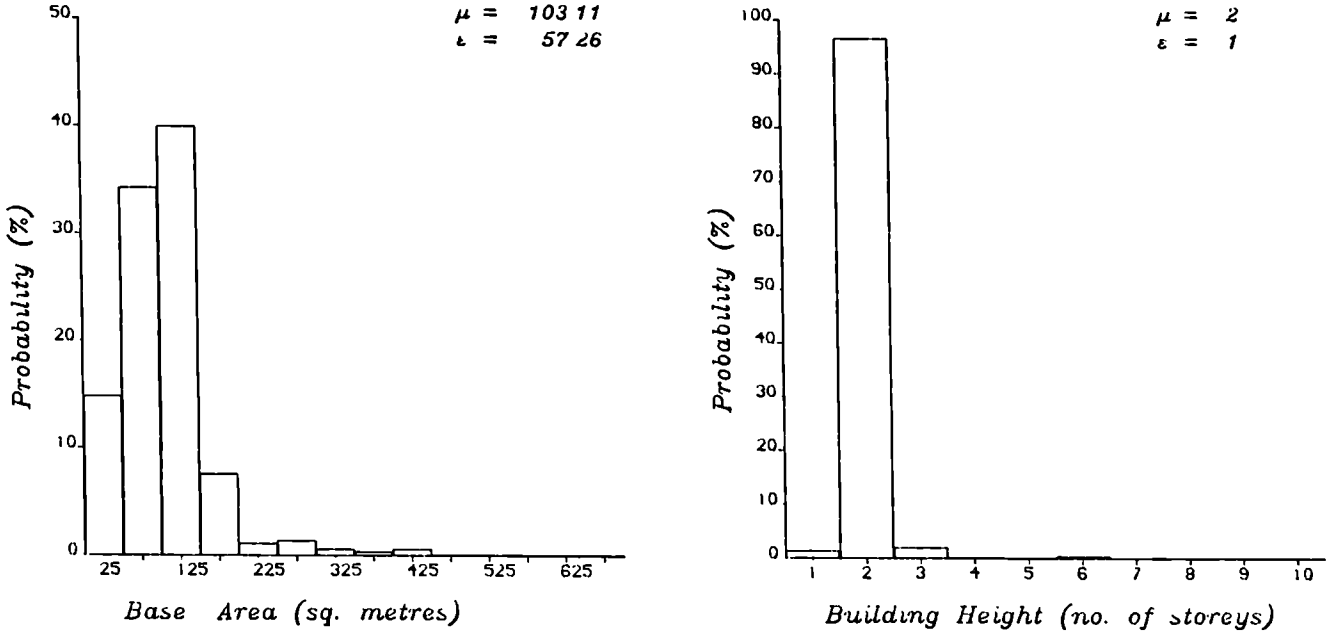

(a) (b)

Figure (5.4) Descriptive distributions for map SU4315SW.

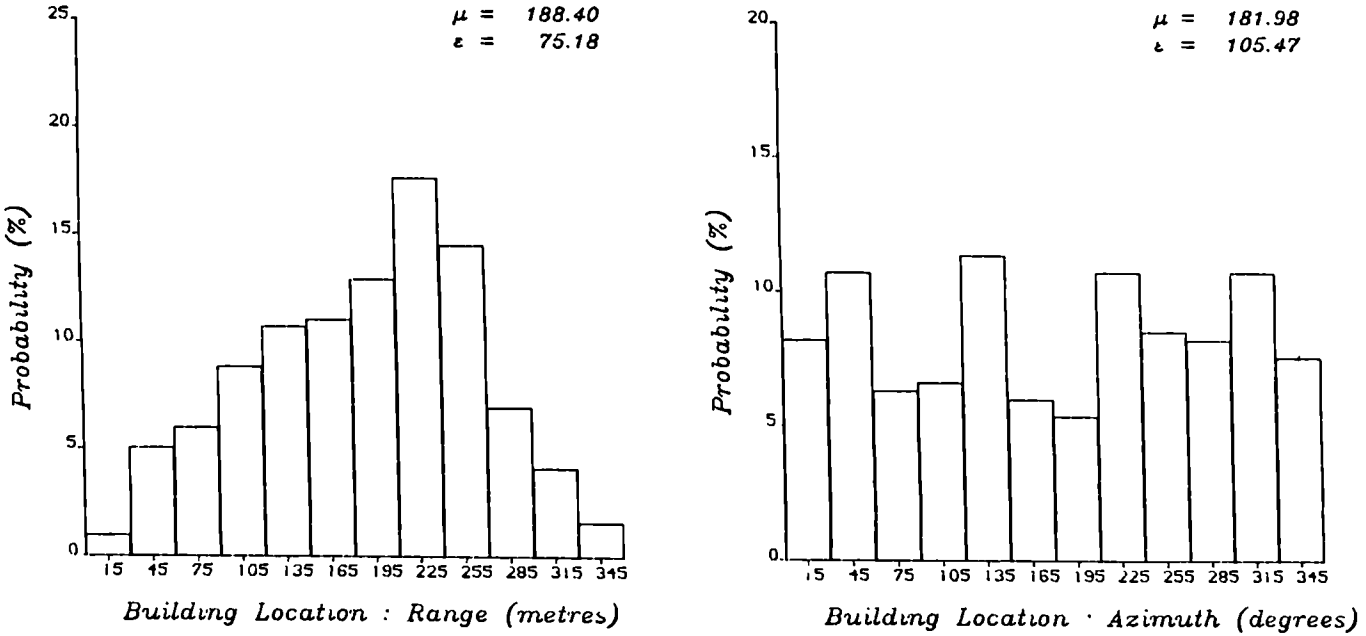

Figure (5.4) Descriptive distributions for map SU4315SW.

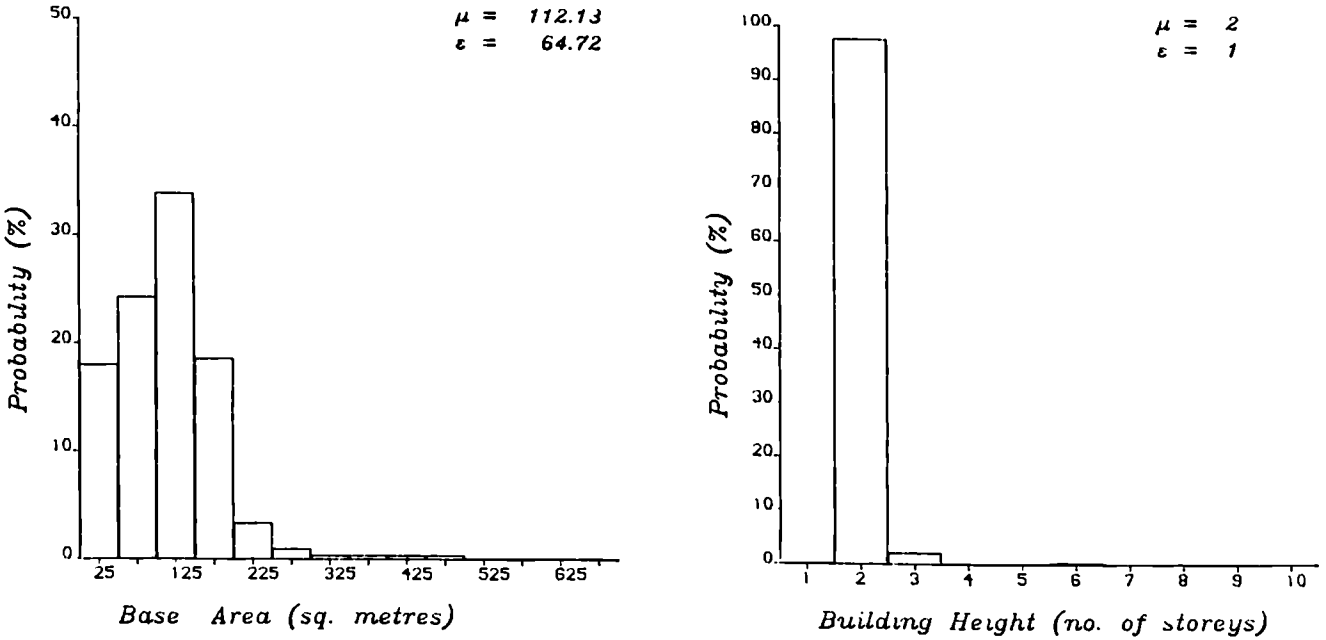

Figure (5.5) Descriptive distributions for map SU4214NE.

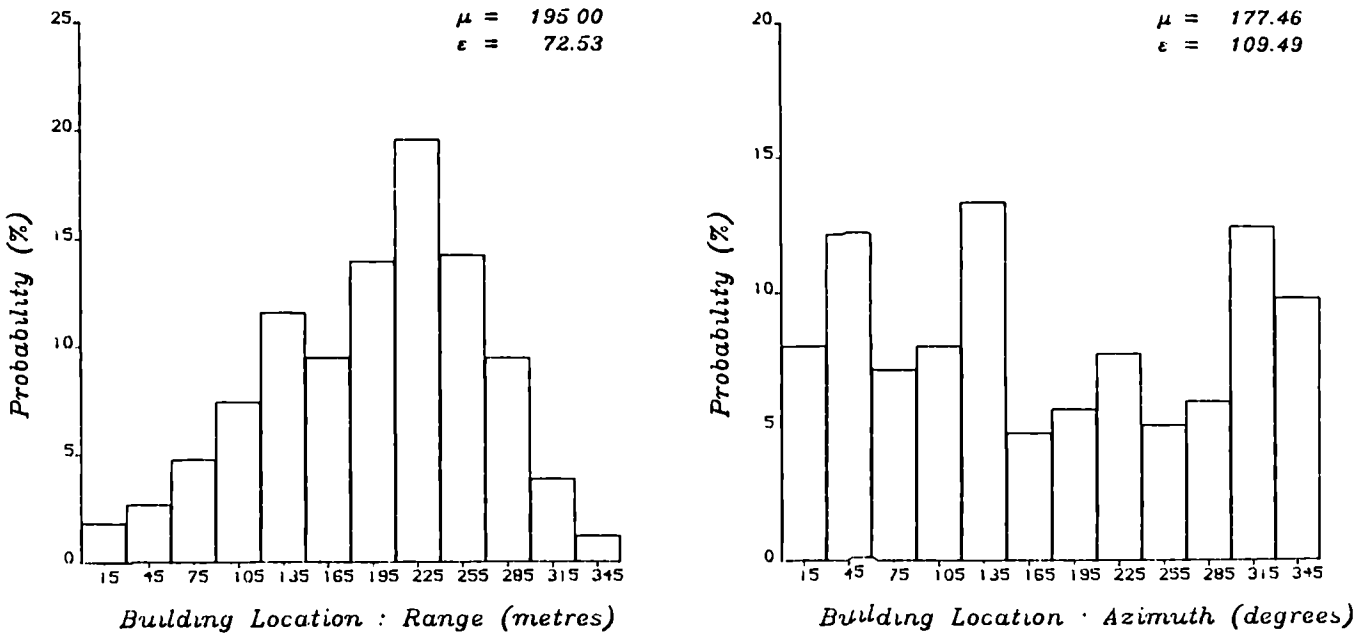

(c) (d)

Figure (5.5) Descriptive distributions for map SU4214NF

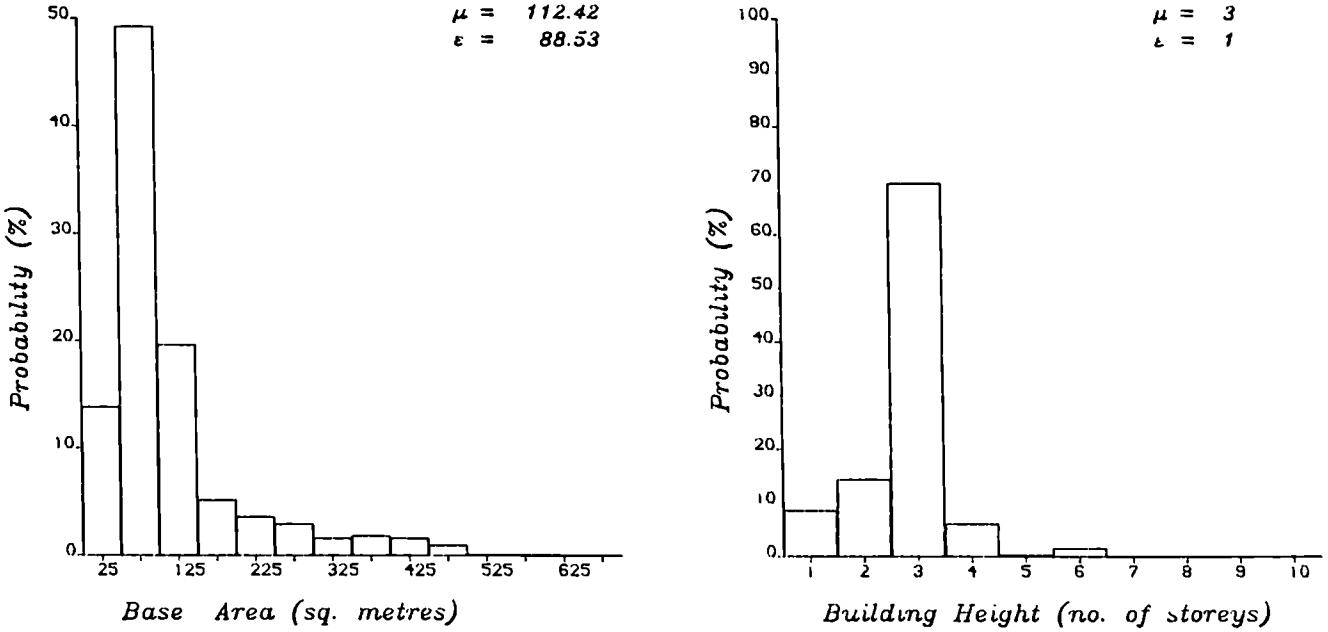

Figure (5.6) Descriptive distributions for map SJ3589NE.

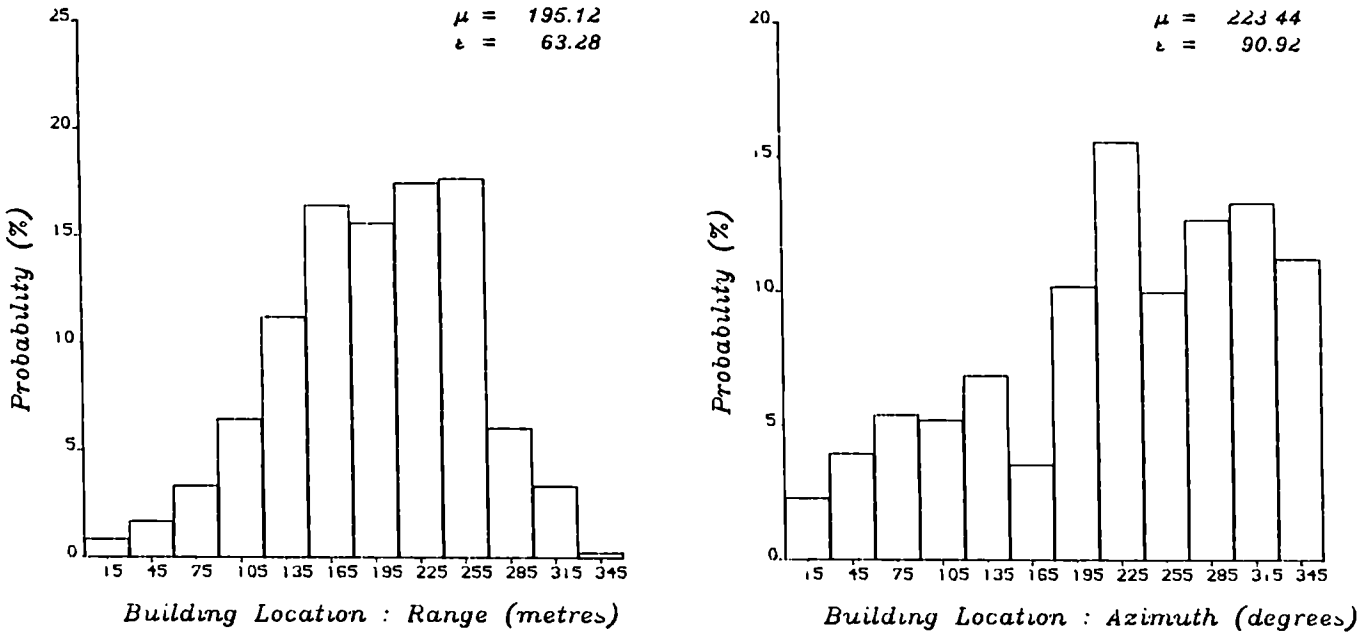

(c) (d)

Figure (5.6) Descriptive distributions for map SJ3589NE

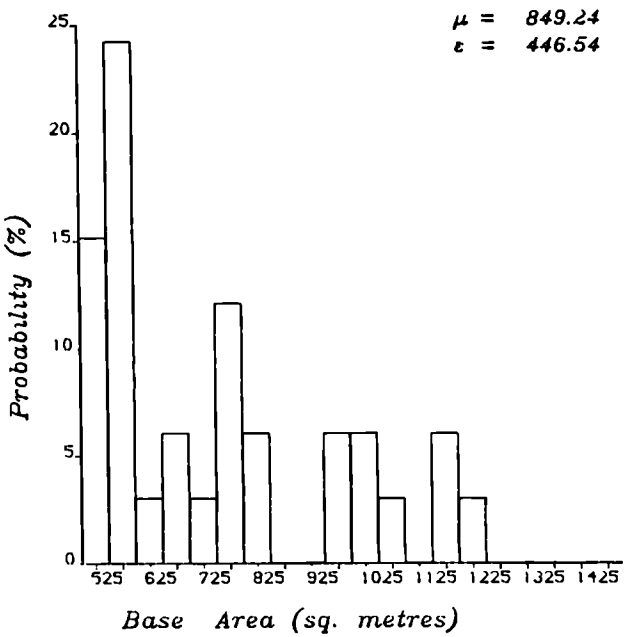

(e)

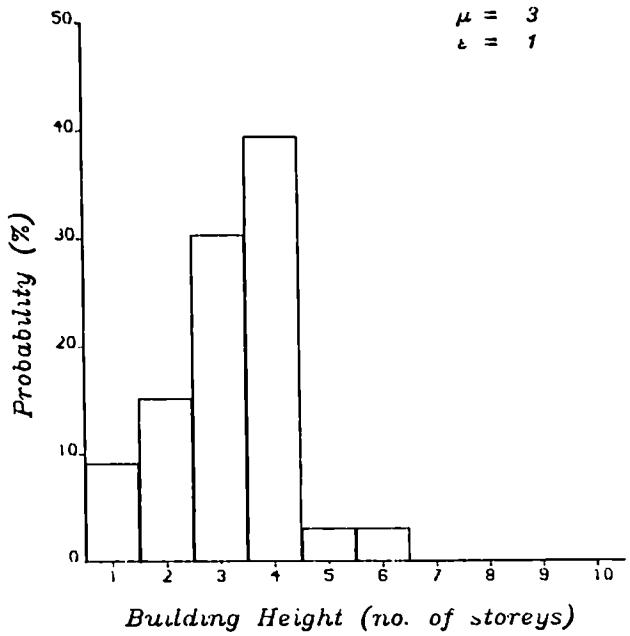

(f)

Figure (5.6) Descriptive distributions for map SJ3589NE.

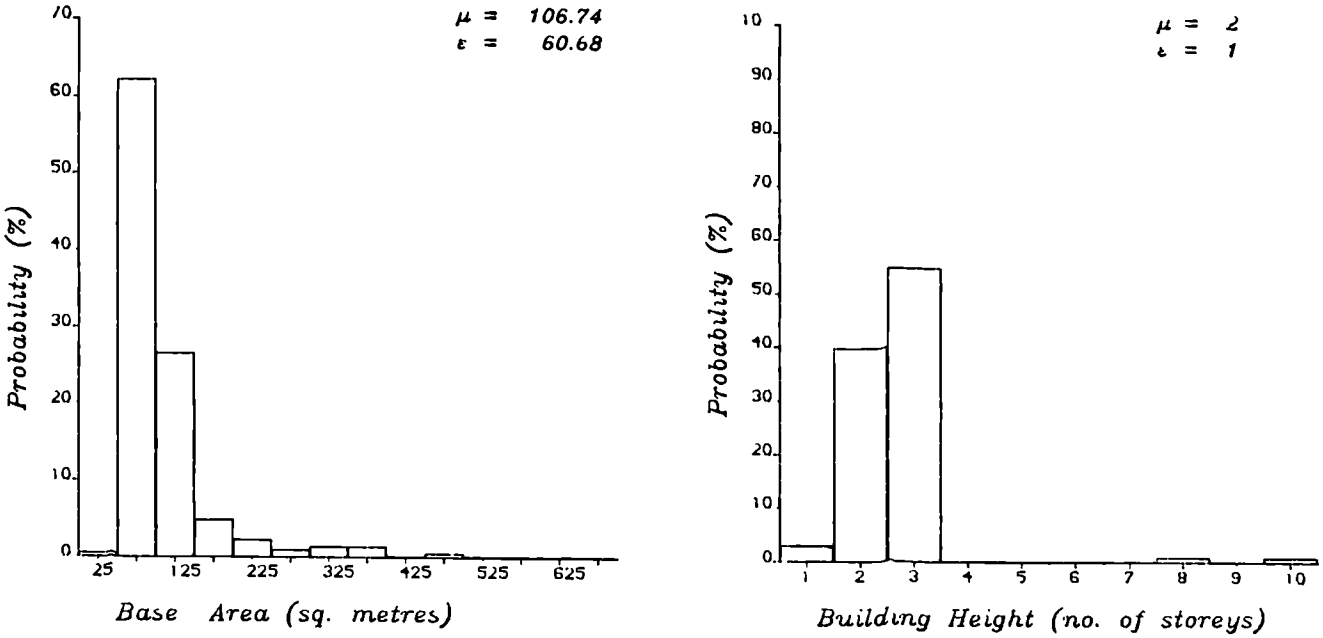

Figure (5.7) Descriptive distributions for map SJ3591NE.

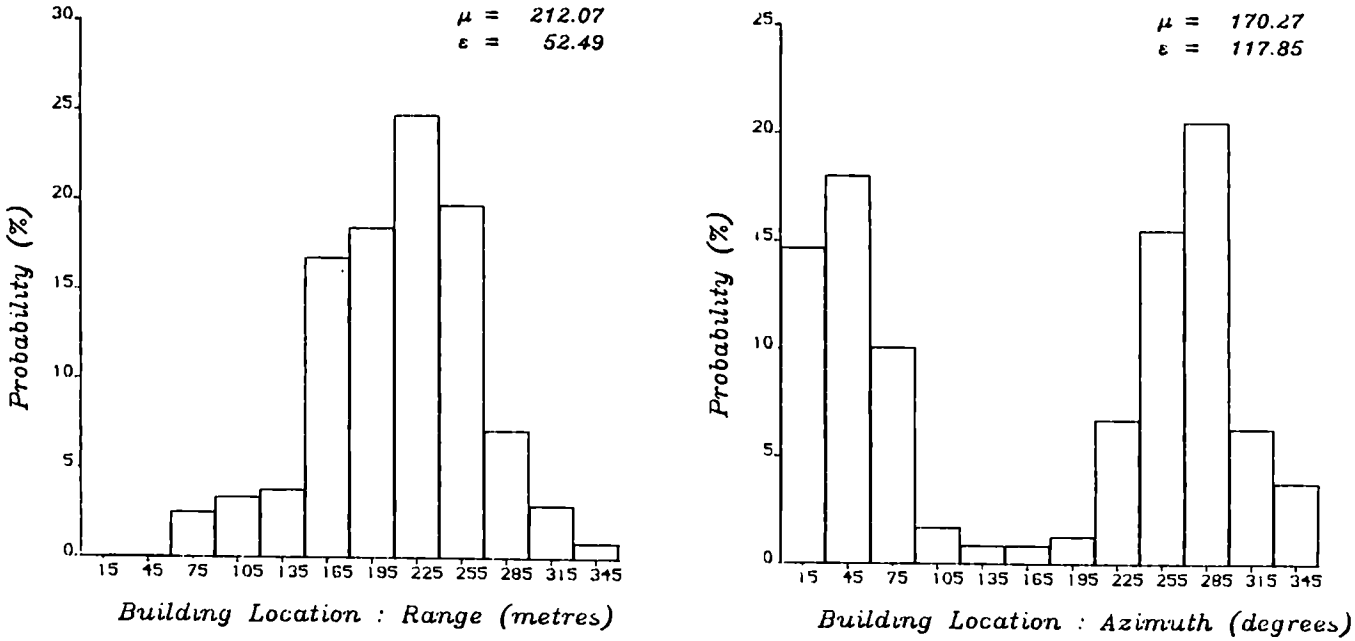

Figure (5.7) Descriptive distributions for map SJ3591NE.

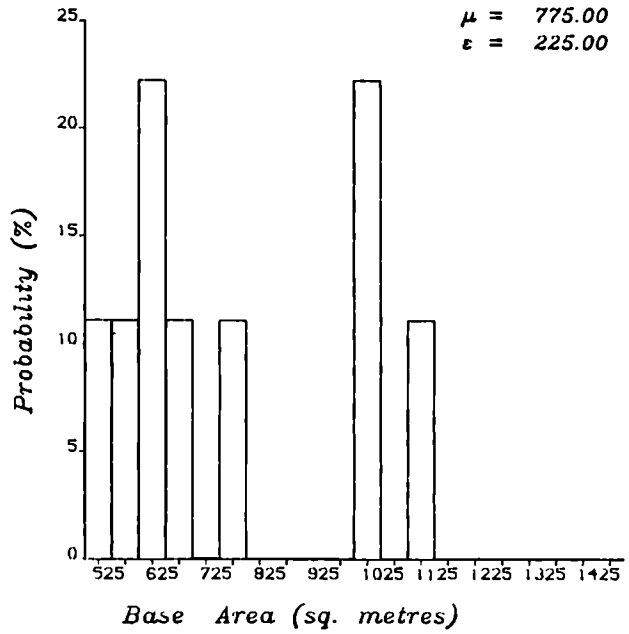

(e)

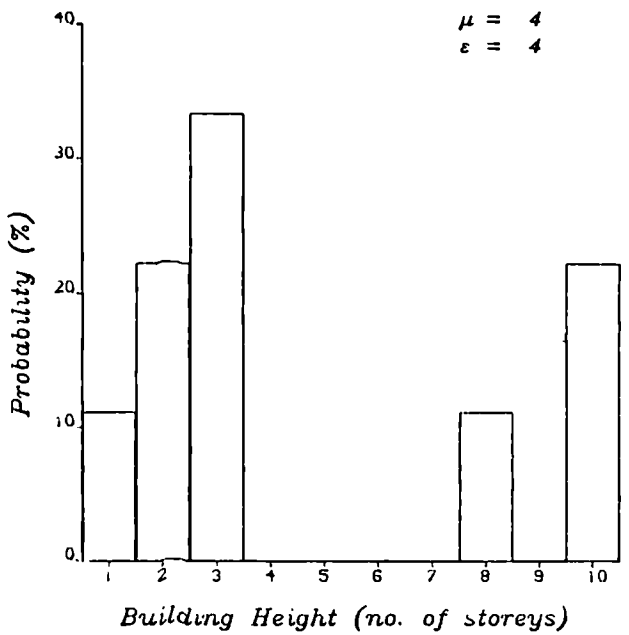

(f)

Figure (5.7) Descriptive distributions for map SJ3591NE.

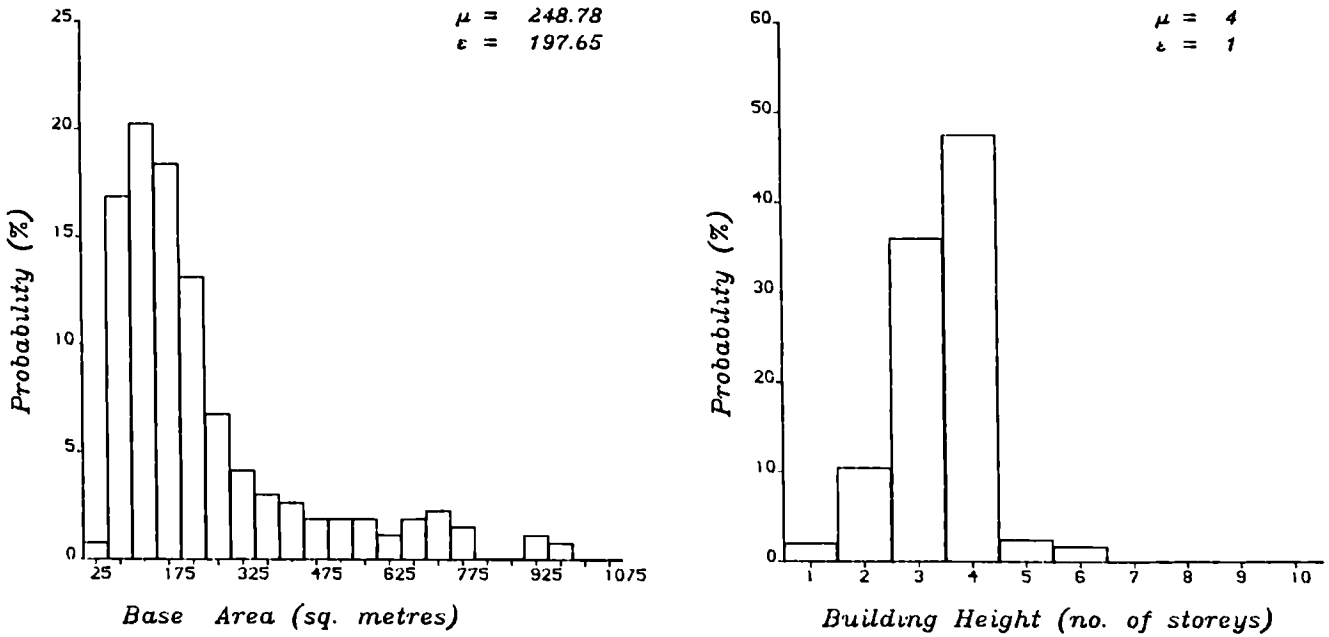

(a) (b)

Figure (5.8) Descriptive distributions for map SJ3490SE.

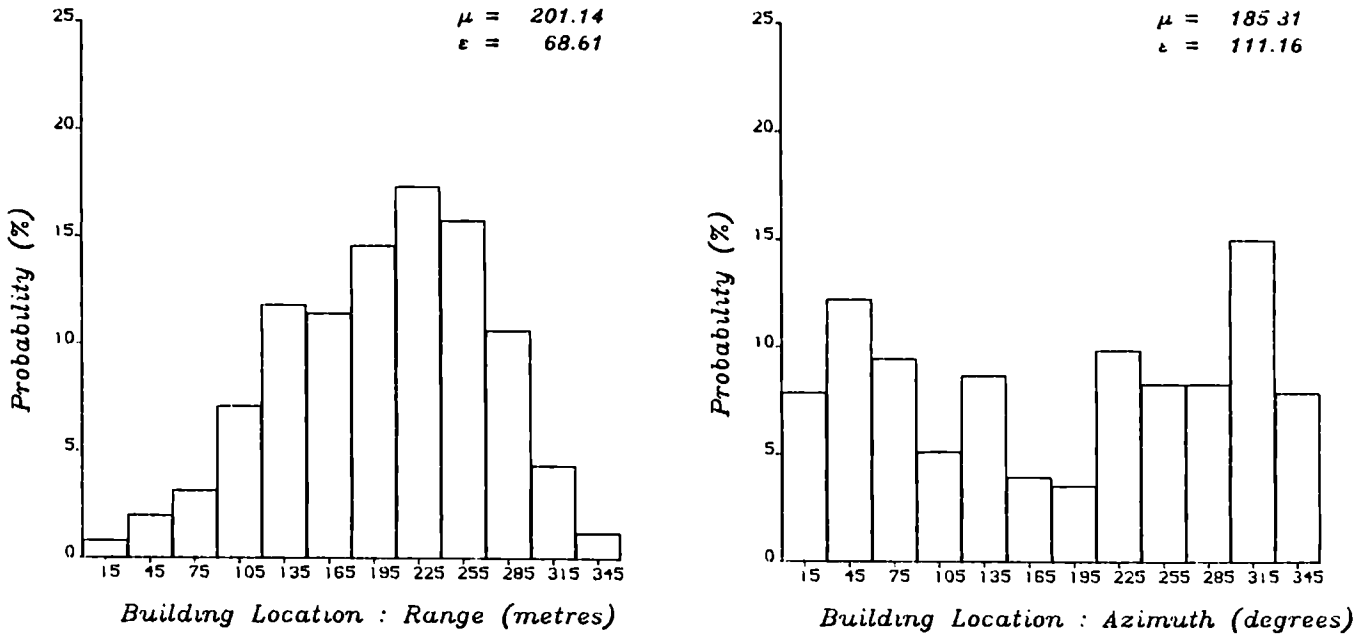

Figure (5.8) Descriptive distributions for map SJ3490SE.

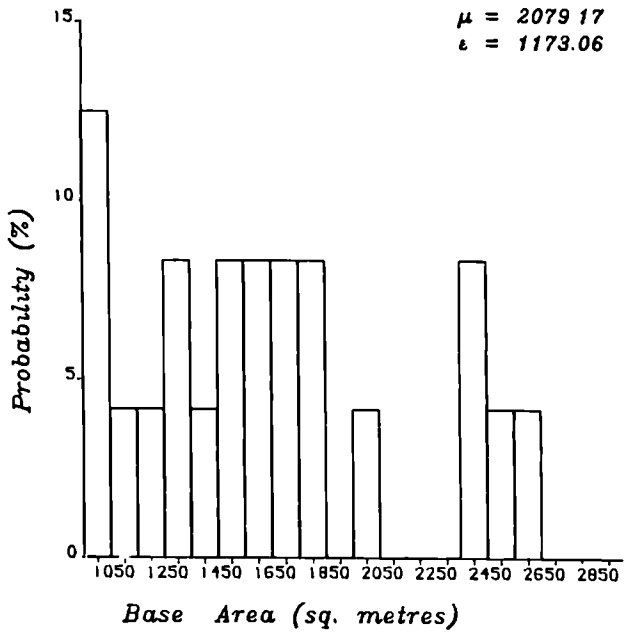

(e)

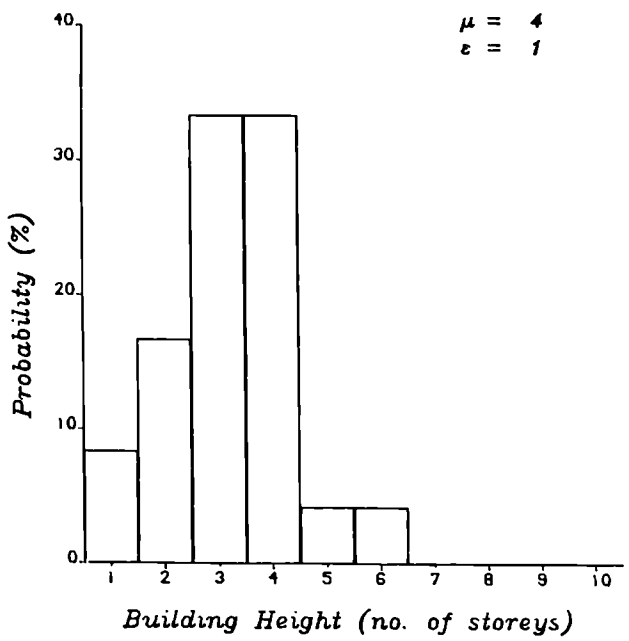

(f)

Figure (5.8) Descriptive distributions for map SJ3490SE.

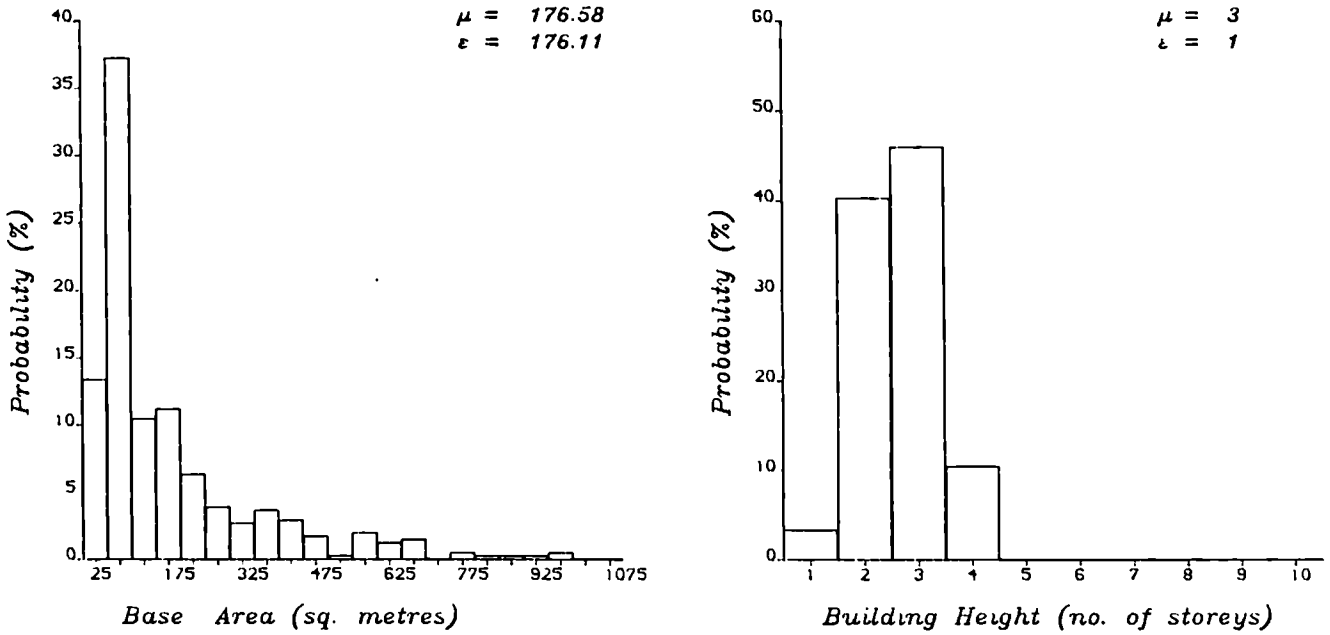

Figure (5.9) Descriptive distributions for map SJ3489NE.

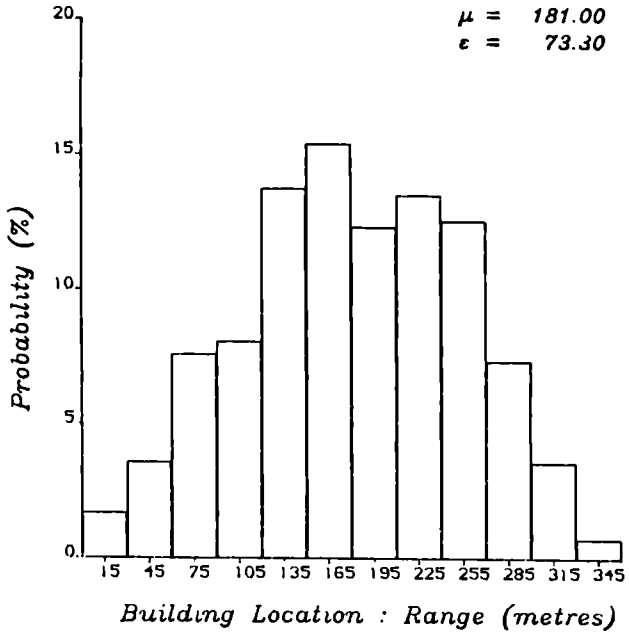

(c)

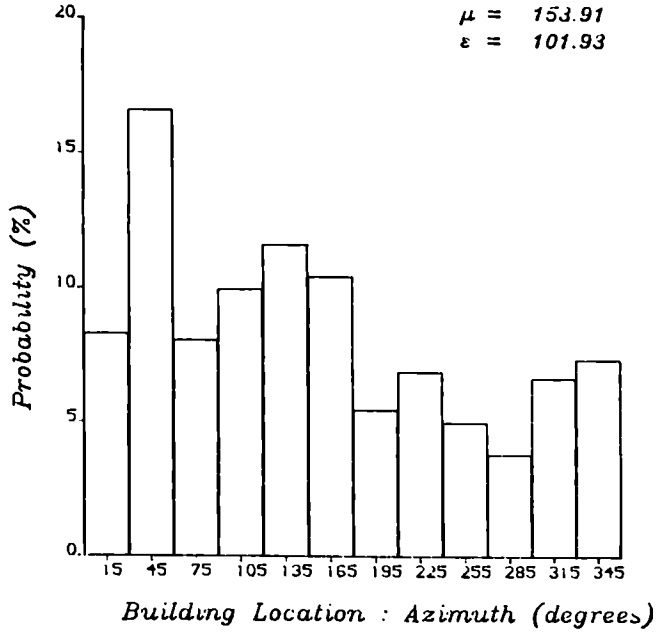

(d)

Figure (5.9) Descriptive distributions for map SJ3489NE.

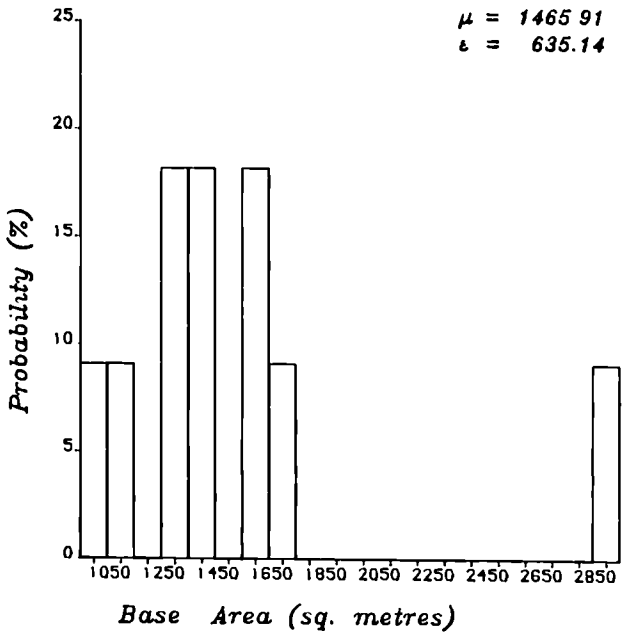

(e)

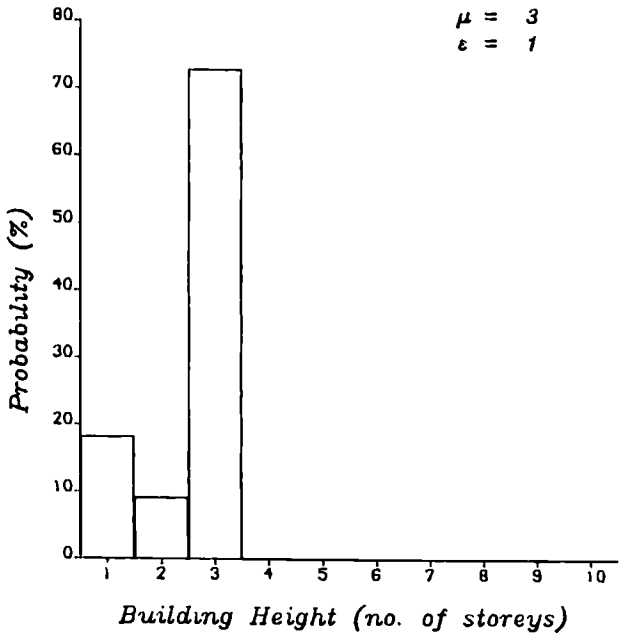

(f)

Figure (5.9) Descriptive distributions for map SJ3489NE.

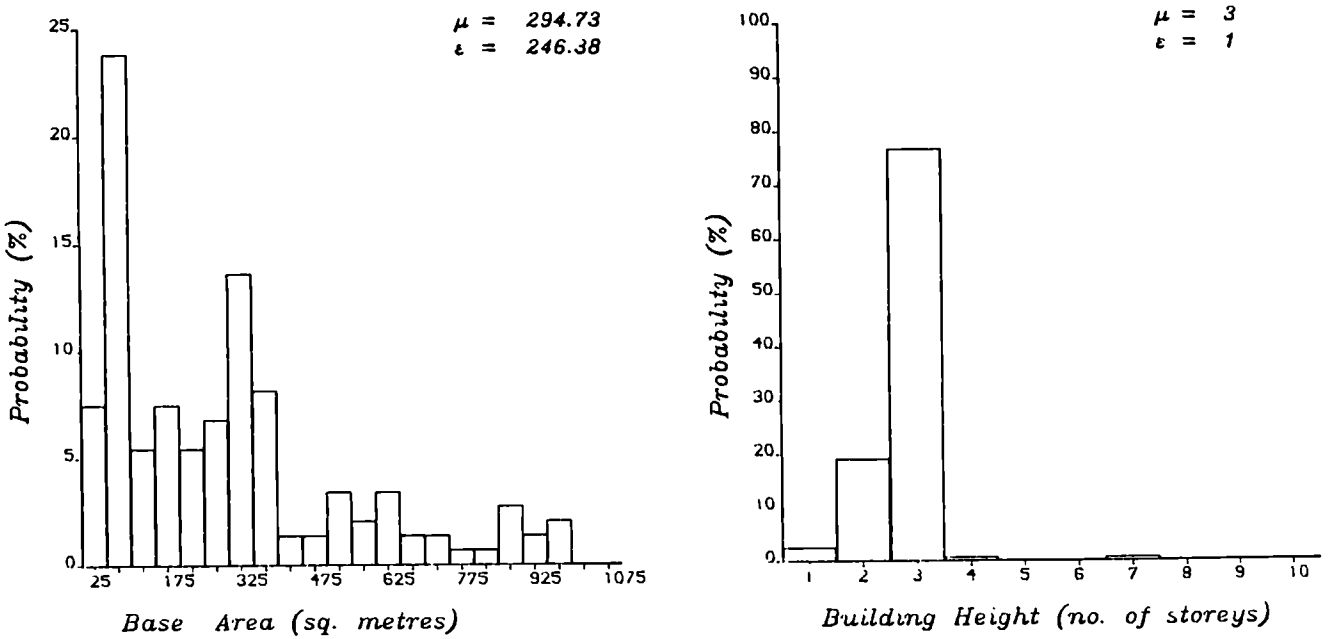

Figure (5.10) Descriptive distributions for map SJ3489SE.

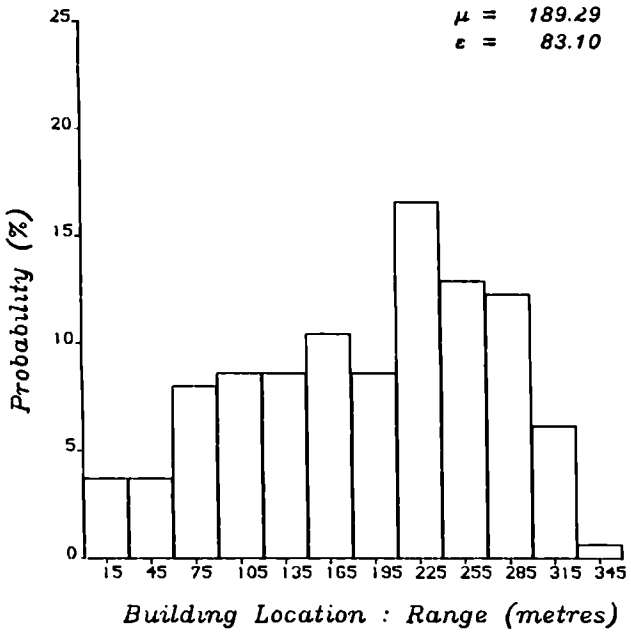

(c)

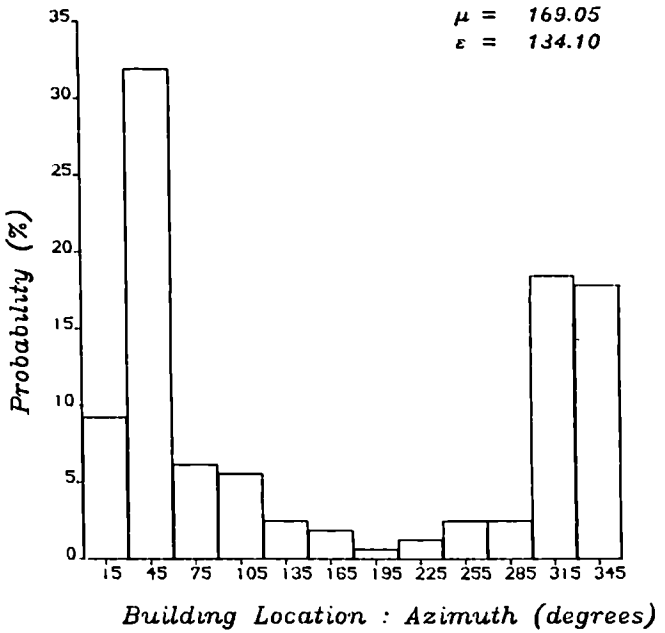

(d)

Figure (5.10) Descriptive distributions for map SJ3489SE.

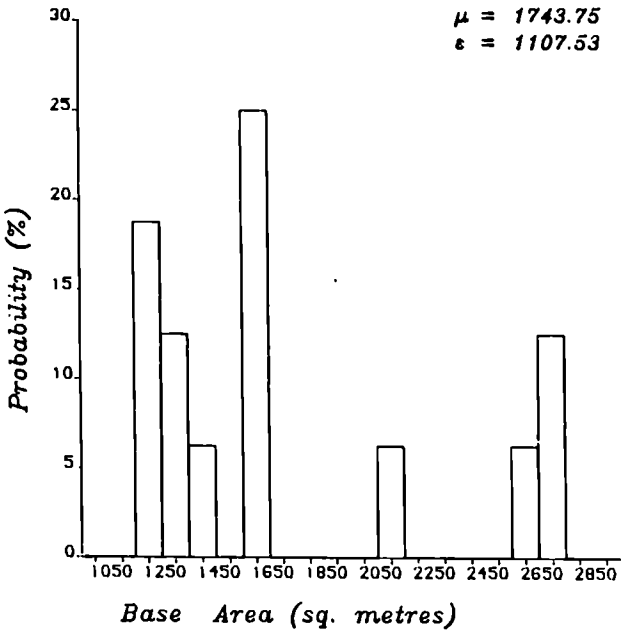

(e)

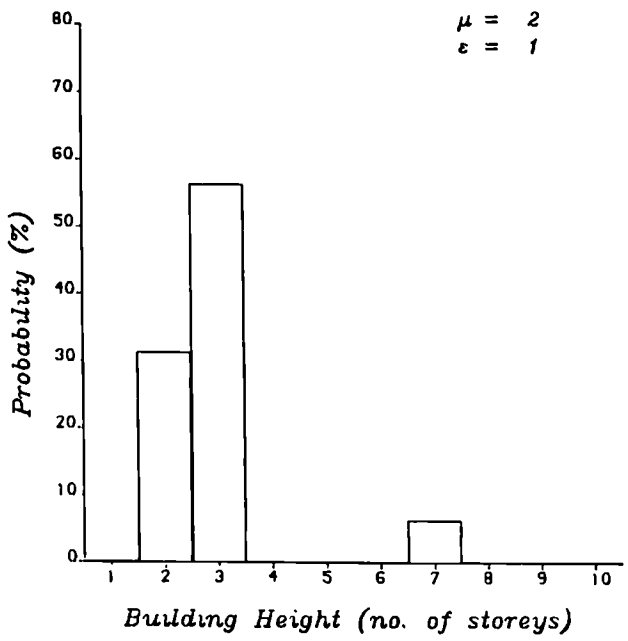

(f)

Figure (5.10) Descriptive distributions for map SJ3489SE.

CHAPTER SIX

6. THE SIMULATED CHANNEL CHARACTERISTICS

Every good tree bears good fruit, but a bad tree bears bad fruit.
...thus, by their fruit you will recognize them.
Matthew 7:17,20b

The results of the radio channel simulation at 900 MHz using the model presented in chapter 3 in conjunction with the techniques outlined in chapter 4 are presented in this chapter. The data describes both small and large scale behaviour of the channel in some of the categories of environments defined in chapter 5, with emphasis on the effect of the landcover surrounding the mobile. Some measured data has been provided for use in validating the model*. Some of the results presented have been chosen for locations for which measured data is available. For each location, the discussion includes the general description of the test square in which the street is located and of the street itself. The sources of the echos evident in the average power profiles are identified with the aid of the time-delay/Doppler shift scattering functions and the OS map of the square. The characterising distributions of these contributory scatterers are also discussed. The simulation-generated profiles are then compared with the measured profiles. The global path occupancy distributions, and cumulative amplitude distributions at fixed delays are also presented.

6.1 Melville Place.

Melville Place is a minor road situated in the square defined by map SJ3689NW, in a class 2B type environment located on the edge of the university campus. The buildings are mainly 3-4 storey blocks of flats and terraces. The road is situated adjacent to Munster Court, a 4-storey block of flats about 120 metres long. With the mobile travelling in a northerly direction, Munster

* The data was provided by D.A Demery, of the Department of Electrical Engineering, University of Liverpool from channel sounding measurements carried out in some parts of Liverpool city.

Court is on the farside[#] while on the nearside is an open space about 40 metres wide. Some large university buildings are located in the NW section of the map and separated from Munster court by the open space. The road is at an angle of 35 degrees to the direction of a radial from the transmitter. The mobile is at an average distance of 600 metres from the transmitter for the simulation run.

6.1.1 Small scale characteristics

Figure (6.1a) shows the average power delay profile for a 6 metre section of the road received with the mobile situated about midpoint of Munster Court. The profile shows a small degree of dispersion, with most of the energy arriving within 1 μs delay. There are three identifiable echo paths in this profile. The average excess time delay and delay spread values are 0.15μs and 0.10 μs respectively. The smooth variation in the frequency correlation function of Figure (6.1b) and the corresponding large value of 0.5 correlation bandwidth is a result of the small dispersion exhibited by the channel. From Figure (6.2), the scattering function for this section of the channel, it is seen that scattering occurs from almost all possible angles. For delays up to 0.4μs, most of the energy arrives from ahead of the vehicle (+ Doppler shift), while most of the energy from 0.5μs comes from behind the vehicle (- Doppler shift). This is consistent with the landcover surrounding the mobile. More precise identification of the scatterers can be obtained by examining the Doppler spectra at some fixed delays. Figure (6.3a) is the Doppler spectra at fixed excess delay of 0.2μs and (6.3b) at 0.4μs. The lower horizontal scale of Fig.(6.3a) is the frequency offset (Doppler shift) from the centre frequency. Since the Doppler frequency shift is proportional to the cosine of the angle of arrival

---

Farside indicates the right hand side of the road farthest from the mobile and nearside refers to the opposite left hand side.

of the incoming wave referred to the direction of vehicle travel, the frequency scale can be converted to an angle of arrival scale, which is the upper horizontal scale on the figure. The approximate maximum plus and minus shifts are indicated by the vertical dashed lines. Although the description provided by the angle of arrival conversion in Fig (6.3) allows the distinction between scatterers ahead and behind the mobile, the left-right ambiguity can often be resolved by careful consideration of the range location of the scatterers. In Fig (6.3a), the strong echos arriving from ahead are due to scattering by the university buildings on the nearside, while the weaker echos are from sections of Munster Court which lie behind the mobile. In Figure (6.3b), the scattering centre giving rise to the spectrum around 0 Hz is primarily a large university building opposite the mobile on the nearside. The negative Doppler shifts are caused by a community centre and church building located between 60 to 100 metres behind and on the nearside of the mobile. Two consecutive small-scale profiles of this section of the channel are illustrated in Figure (6.4). It is observed that the profile characteristics are very similar, indicating that the channel exhibits wide sense stationarity as previously assumed.

In Figure (6.5), the simulated profiles are compared with a set of measured profiles along the same section. The average power profiles are seen to compare very well, with the simulated profile (solid line) displaying the main characteristics of the measured profile (dashed lines). The amplitudes of the weaker echoes are slightly underestimated in the simulation, resulting in the difference in average delay and delay spread values. However, this has not affected the frequency correlation functions which are seen to correlate very well, resulting in coherence bandwidth values which are very similar. For example, for the small section described by Fig (6.5), the 0.5 coherence bandwidth values are 2.217 MHz and 2.131 MHz for the simulated and measured profiles respectively. This location has produced a response close to a LOS

situation because of its accessibility to the transmitter. This scenario does not always exist therefore, a more extreme case is considered.

Figure (6.6) shows the profiles at a location 50 metres from that for Fig (6.1). Munster Court is now behind the mobile and the LOS path is blocked by the university buildings. The strongest echo is seen to arrive $0.4\mu s$ after the first echo. The scattering function of Figure (6.7) shows the distribution of echos, with the strong echos arriving from ahead of the mobile as expected and the weaker ones from the residential flats behind it. The average delay and delay spread values are larger along this section of the channel, with values of $0.235\mu s$ and $0.160\mu s$ respectively for the profile shown. The first two echoes are within 2 dB of each other, giving rise to the oscillatory behaviour of the frequency correlation function and corresponding small value of 828 KHz for the 0.5 coherence bandwidth. This illustrates the non stationarity of the channel over large distances. The parameters which describe the sets of average profiles obtained over a 36 metre section of the channel illustrated by previous profiles are tabulated in Table 6.1

6.1.2 Large scale characteristics

The gross features of the channel over a large area are now presented. First, the scatterer location and size distributions are discussed.

6.1.2.1 Scatterer Distributions

The details of the location and size distributions descriptive parameters for buildings within the occupational domain and the significant scatterers are given in Tables 6.2 and 6.3 respectively. Each row in the table represents data for a 10 metre mobile movement as explained in section 4.5.1. These figures illustrate the gross changes in the scattering environment which occur as the

mobile moves along the street. The significant scatterers comprise only 14% - 16% of the buildings within the domain and occupy up to 4.86% of the total area. The range location distribution p(R) of Figure (6.8a) indicates that 51% of these significant scatterers are situated within 120 metres of the mobile, further confirming the observations that scattering is predominantly local. The p(ϕ) distribution of Fig (6.8b) shows that most of the scattering centres are on the farside of the mobile. Munster Court is a major scatterer, and the block has been divided into smaller equal sized structures, hence the observed concentration of scattering centres.

6.1.2.2 Echo Path Occupancy Distribution.

Figure (6.9) shows the echo path occupancy distribution over a large distance of about 100 meters. This distribution has been obtained by considering profiles from different small-scale sections within the square, including the sections described by the profiles in Figure (6.1) and (6.6). It is seen that echos with excess delays up to 0.7μs are very stable with at least 70% probability of occurrence. Echos with excess delays greater than 1 μs are however much less stable, having a maximum probability of occurence of 20%, a factor of three less than the early arrival paths. It can be said therefore that scattering is very much localised in this section of the channel.

6.1.2.3 Cumulative Amplitude Distributions at Fixed Delays.

Figure (6.10a) shows samples of the amplitude distributions at fixed excess delays of 0.1μs, 0.4μs and 0.5μs marked (1), (2) and (3) respectively. Figure (6.10b) shows samples of the amplitude distributions of fixed excess delays of 0.6μs, 0.7μs and 0.8μs marked (4), (5) and (6) respectively. These distributions are plotted on Rayleigh coordinates. A Rayleigh distribution appears as a

straight line with a specific slope. The distribution marked (1) deviates from Rayleigh at low signal values, indicating extremely low probability of receiving low signal levels. On the other hand, line (3) for 0.5μs shows that 1% of the time, signal levels below -30dB are received, compared to 0.1% for a truly Rayleigh distributed signal. Graph (2) for 0.4μs closely follows the Rayleigh slope, suggesting that a number of scatter paths with independent RF phases contribute to the overall signal received at this delay. The amplitude distributions of the early arrival paths show Rayleigh characteristics while longer path amplitudes tend to be lognormally distributed.

6.2 Netherfield Road

Netherfield Road is a major road situated in the square defined by map SJ3591NE. The area is a class 2A type environment, but with some high rise 8-10 storey blocks of flats which are clearly visible from most parts of the square. There is a large open space about 100 metres wide and 150 metres long, located mainly in the NW quadrant of the map. Netherfield Road runs through the NW/SW quadrants and two 8-storey buildings are situated about the halfway point of the road. The square is 1.5km away from the transmitter site which is on the university campus and the direction of vehicle travel is towards the transmitter.

6.2.1 Small scale characteristics

Figure (6.11a) is the average power delay profile of a 6m section of the road. At this position, the eight-storey blocks are on the nearside and behind the mobile at distances of 120m and 200 m respectively while 2-3 storey residential buildings can be found on the farside. The open space is on the nearside and houses situated on its fringes are visible to the mobile. This profile shows

a large degree of dispersion, with echoes arriving at excess delays up to 1.8 μs. The average delay and delay spread values of 0.184μs and 0.348μs are large, as expected. Up to five distinct echo paths can be identified - arriving at 0.1, 0.2, 0.4, 0.9 and 1.5μs excess delay. Figure (6.12) is the scattering function for this section of the road, while Figure (6.13) shows the Doppler spectra at fixed excess delays of 0.2, 0.4, 0.9 and 1.5μs respectively. The sources of the echos at 0.9 and 1.5μs are identified as originating from behind the mobile, and the delays correspond to the locations of the high rise buildings. The echos at 0.4μs are caused by a public house and a 3-storey building on the farside and behind the mobile while the echos at 0.2μs are from the buildings both on the near and farside of the mobile but located ahead of it. The scattering function shows that early arrival paths with excess delays up to 0.4μs are from ahead of the mobile while paths with longer delays are from scattering sources behind. This observation is consistent with the direction of vehicle travel and relative location of buildings around the mobile. In Figure (6.14), the profiles for two consecutive small-scale locations are seen to exhibit very similar characteristics. This illustrates the wide sense stationarity of the channel over small distances. The frequency correlation function of figure (6.11b) exhibits some oscillatory behaviour caused by the echo at 1.5μs which is 12 dB below the main echo. This has resulted in the 0.5 and 0.9 correlation bandwidth values of 1.53 MHz and 155kHz respectively.

In Figure (6.15), the simulated profiles are compared with some measured profiles along the same section of road. The measured profiles show echos at delays greater than 2μs but for the purpose of the comparisons, these have not been considered. The main characteristics of the measured profiles are exhibited by the simulated profiles. In (6.15a), the echo at 0.9μs has been overestimated and arrives one microsecond earlier than that measured. This has led to the noticeable difference in average delay values, with the measured profile having a larger value then the simulated profile. However, the delay

spread values compare very well, 0.348μs for the simulated profile and 0.377 for the measured profile. The frequency correlation functions of (6.15b) exhibit the same characteristics, and the 0.5 and 0.9 correlation bandwidth values are seen to compare very well also. The small scale parameters for a 24 metre section of the channel are given in Table 6.4.

6.2.2 Large scale characteristics

6.2.2.1 Scatterer Distributions

The details of the location and size distributions descriptive parameters for buildings within the occupational domain and the significant scatterers are given in Tables 6.5 and 6.6 respectively. The occupational domain at this location overlaps into adjacent map areas because the road is situated toward the edge of the test square. There are over 390 buildings in each domain giving a Building Area Index of up to 21%, with an average of 16% of this fraction occupied by buildings with base areas up to 500 sq. metres. The significant scatterers comprise only 10% - 13% of the buildings within the domain and occupy up to 3.64% of the total area. The distributions of Figure (6.16) are for scatterers which contribute to the multipath illustrated by the profiles discussed in section 6.2.1. The p(R) distribution shows that local scatterers within 120 metres of the mobile constitute 31% of the total while non local scatterers located between 200 and 270 metres constitute 32%. The p(ϕ) distribution of Fig (6.16b) indicates some clustering of scattering centres. These are the 2-storey housing estates. It was observed that 88% of the contributory scatterers had base areas less than 500 sq.metres.

6.2.2.2 Echo Path Occupancy Distribution.

Figure (6.17) shows the echo path occupancy distribution obtained over several small-scale sections within the test square. It is seen that echos with excess delays up to 1.0μs have at least a 50% probability of occurence. The excess delay around 0.9μs occurs consistently over a large area, while that at 1.5 μs is not as frequent. The tower blocks account for this observation, although it would appear that the contributions from one of them falls below the set threshold.

6.2.2.3 Cumulative Amplitude Distributions at Fixed Delays.

Figure (6.18) shows samples of the amplitude distributions at excess delays between 0.0μs and 0.5μs. The distributions for the first 0.3μs follow the Rayleigh statistics closely while the other two spend more time at higher signal values than the Rayleigh signal. The longer path amplitudes tend to be lognormally distributed.

6.3 Heyworth Street.

Heyworth Street is a major road which is also located in the area defined by map SJ3591NE. It runs parallel to Netherfield road such that the open space mentioned in section 6.2 is enclosed by the two roads. Travelling away from the transmitter, 2 and 3-storey houses are situated on the farside of the mobile right along the length of the road, while ahead and on the nearside are 2-storey semi-detached houses. The two tower blocks are also visible from this road as are some other large buildings along the road behind the mobile.

6.3.1 Small scale characteristics

Figure (6.19) shows the average power delay profile and frequency correlation function for a small scale area on this road. The concentration of power within the first 0.5μs is a result of scattering from the 2-storey residential buildings along the road. Echos arrive with excess delays up to 2.2μs Figure (6.20) is the scattering function for this section of the channel. It shows most of the major echos arriving from ahead of the mobile. At this location, the two tower blocks are between 180 meters and 250 metres ahead of the mobile and would account for the echos at delays of about 1.2μs and 1.8μs. The similarity between the two consecutive profiles of Figure (6.21) illustrates the wide sense stationarity of the channel. In Table 6.7, the small scale parameters for a 24-metre section of the channel are given

In Figures (6.22) and (6.23), the simulated profiles are compared with measured results. Here again, the comparison between simulation and measurement results are seen to be very good. In the power profiles of Fig (6.22), although the main characteristics of the measured profile are exhibited by the simulated profile, there exist some differences in the amplitudes of the peaks. In particular, the overestimation of the echo amplitude at 1.7μs results in the larger simulated delay spread value. The frequency correlation functions are also very similar, and this is reflected in the coherence bandwidth values. The power profiles of Fig (6.23) infact compare more closely than those of (6.22). The main difference being the amplitude of the echo around 0.5μs which has been underestimated in the simulation. The effect of this is the smaller value of average delay, although the delay spread values compare very closely. The frequency correlation functions in figure (b) also compare well with almost identical $B_{0.9}$ values. The difference in the $B_{0.5}$ can be attributed to the underestimation in the power profile mentioned above.

6.3.2 Large scale characteristics

6.3.2.1 Scatterer Distributions

The details of the location and size distributions descriptive parameters for buildings within the occupational domain and the significant scatterers are given in Tables 6.8 and 6.9 respectively. The occupational domain at these locations extend into adjacent map areas because the road is situated toward the edge of the test square. Between 250 and 280 buildings can be found in the domains, with a BAI of up to 15%. Buildings having base areas up to 500 sq. metres occupy 11% of the domain. The significant scatterers comprise between 13% - 14% of the buildings within the domain and occupy on average, 3.64% of the total area. The distributions of Figure (6.24) illustrate scatterer location characteristics for significant scatterers in one domain. The p(R) distribution shows that 51% of these scatterers are located within 60 to 150 meters of the mobile, and can be regarded as local. The p(ϕ) distribution of Fig (6.24b) indicates some clustering of scattering centres, these being houses in the estates located along the road.

6.3.2.2 Echo Path Occupancy Distribution.

The echo path occupancy distribution of Figure (6.25) exhibits some interesting features. The first four paths have a very high probability of occurence of at least 90%. Then the distribution shows peaks around 0.5-0.8 μs, 0.9-1.4μs and 1.7-1.9μs. The common feature of these peaks is that they are very stable, having probability of occurence of at least 50%. This implies that scattering within this area is caused by both local and non local with almost equal intensity.

6.3.2.3 Cumulative Amplitude Distributions at Fixed Delays.

The distribution of echo amplitudes at the early delays and shown in Figure (6.26) conforms with previous observations, exhibiting Rayleigh characteristics for early arrival paths and lognormal characteristics for longer delay paths.

6.4 Duke Street.

This road is situated in the square defined by map SJ3489NE, in a class 3B type of environment (commercial district of Liverpool). The characteristics of the buildings in this square have been described previously in section 5.8.2. Buildings are situated on both sides of the road, with little or no space between adjacent structures. The experimental location is 1.5km from the transmitter site and the direction of vehicle motion is away from the transmitter.

6.4.1 Small scale characteristics

In Figure (6.27), the average power delay profile and frequency correlation function for a 6m section are shown. This profile of (6.27a) exhibits a large degree of delay dispersion, with average delay and delay spread values of 0.170 μs and 0.231μs respectively. It is seen that the echo at 0.1μs is slightly stronger than the first arrival path. Most of the received power is concentrated within the first 1μs although echos are seen to arrive with delays up to 2μs. This has resulted in the rapidly decaying correlation function of Fig (6.27b) and corresponding small values of 238kHz and 824kHz for the $B_{0.9}$ and $B_{0.5}$ respectively. This concentration of power can be attributed to the fact that there are many more scatterers closer in to the mobile than are encountered in a class 2 environment. Six distinct echo paths can be identified in this profile, occuring at 0.1, 0.4, 0.6, 0.9, 1.4 and 1.9μs respectively.

The scattering function for a 24 metre section of the channel is shown in Figure (6.28). It shows that scattering occurs from all around the mobile for small delays, while the longer echos are seen to arrive from ahead of the mobile. The Doppler spectra at 0.2 and 0.3μs are shown in Figure (6.29). It is seen from these figures that a significant amount of power is spread out over a large frequency range.

The channel exhibits WSS behaviour as shown by the two consecutive profiles of Figure (6.30). The small scale parameters for the 24 metre section are given in Table 6.10.

6.4.2 Large scale characteristics

6.4.2.1 Scatterer Distributions

The location and size distribution parameters for this locality are given in Tables 6.11 and 6.12. As expected the BAI within the domain is high, in all cases greater than 32%. The buildings with base areas less than 1000 sq.meteres occupy 21% of the domain. The number of buildings that contribute to the scattering phenomenom varies from 26 to 36 in different sections of the channel. These constitute between 6% - 10% of the total number of scatterers within the domain. Although these significant scatterers occupy between 2.4% and 3.5% of the total area, they occupy up to 11% of the developed area.

Figure (6.31) shows the p(R) and p(ϕ) distributions for scatterers contributing to the multipath in the channel section analysed in the previous section. The probability of finding a scatterer between 120m and 150m of the mobile

is 38% while p(ϕ) shows a that up to 60% of the scattering centres are located in the NW quadrant of the occupational domain.

6.4.2.2 Echo Path Occupancy Distribution.

The path occupancy distribution is shown in Figure (6.32). The probability of occurence of echos is at least 50% for the first five delay bins. This further confirms that local scattering is predominant in this type of environment. Echos from 0.5μs to 1.0μs are relatively stable, with a probability *of occurence* of at least 30%.

6.4.2.3 Cumulative Amplitude Distributions at Fixed Delays.

The distribution of echo amplitudes at the early delays shown in Figure (6.33) conforms with previous observations, exhibiting Rayleigh characteristics for early arrival paths and lognormal characteristics for longer delay paths.
is 38% while p(ϕ) shows a that up to 60% of the scattering centres are located in the NW quadrant of the occupational domain.

6.4.2.2 Echo Path Occupancy Distribution.

The path occupancy distribution is shown in Figure (6.32). The probability of occurence of echos is at least 50% for the first five delay bins. This further confirms that local scattering is predominant in this type of environment. Echos from 0.5μs to 1.0μs are relatively stable, with a probability of occurence of at least 30%.

6.4.2.3 Cumulative Amplitude Distributions at Fixed Delays.

The distribution of echo amplitudes at the early delays shown in Figure (6.33) conforms with previous observations, exhibiting Rayleigh characteristics for early arrival paths and lognormal characteristics for longer delay paths.

6.5 Discussion

The results presented in this chapter have shown the that it is possible to employ an environment-based simulation in the characterisation of the radio channel. By using ray optics techniques, it has been possible to produce impulse response profiles which compare very well to measured data. Although in some cases, the amplitudes of the echos are underestimated or overestimated, the effect on average delay and delay spread values has not been pronounced. The simulated profiles exhibit the same characteristics of the measured profiles, illustrating that the simulation method is capable of accurately predicting the effects of the landcover around a mobile.

It was observed that only a fraction of the buildings around a mobile contribute to the scattering phenomenom. For instance, for Melville Place, a maximum of 16% of the buildings within the occupational domain acted as scatterers. The figure for Netherfield Road is 13%, comparable to 14% for Heyworth street. The lowest figure of 10% was recorded for Duke Street. The fraction of the test square occupied by these contributory reflectors ranges from 2.4% on Duke Street to 5% on Melville Place. In Table 6.3, the BAI values for significant scatterers on for Melville Place are between 4.26% to 4.86%. The few large university buildings identified as valid scatterers would account for these values which are large compared with those obtained on the other routes. The values of spread for the BSD confirm the diversity in building sizes in this test square. The average distance of these scatterers from the mobile is 124 meters , while the ε_R values show a moderate spread in the location distribution.

Comparing the parameter values for Melville Place with those obtained for Netherfield Road in Table 6.6, some significant differences can be observed, notably the spread parameters ε_s and ε_R. On Netherfield Road, ε_s ranges from 44 to 86 m^2, values which are a fraction of two or more smaller that those observed for Melville Place. The road is situated in a class 2A type environment and the figures in the table are consistent with those for this class. The mean μ_R values range from 180 to 207 meters and the spread ε_R between 94 and 109 metres, indicating that the buildings are on average situated at longer distances than was obtained for Melville Place. An examination of the OS map confirmed this observation, as the buildings on this square are located around a large open space as described in section 6.2. This feature also accounts for the large values of ε_R. Although the number of contributory scatterers in both cases are comparable, the building sizes for Netherfield Road are smaller, hence the smaller values of BAI.

The landcover for Heyworth Street is similar to that for Netherfield Road as the figures in Table 6.9 indicate. μ_R values are larger than obtained along Melville Place but smaller than for Netherfield Road, while the ε_R values are smaller than those for the other two. At this location, there are more buildings around and closer to the mobile and this is reflected in the μ_R and ε_R values. For the BSD, the μ_s and ε_s values indicate a greater diversity in building sizes than those obtained for Netherfield Road but less than for Melville Place.

The effect of non local scattering is observed by considering the power profiles obtained on these routes. On Melville Place, there is a near line of sight situation, resulting in small delay times as shown in Figure (6.1). The multi-storey buildings on map SJ3591NE, as discussed in sections 6.2 and 6.3 contribute the echoes at longer delays shown in Figures (6.11) and (6.19) for Netherfield and Heyworth respectively. In (6.19a), the power concentration at delays less than 1 μ_s are due to the local scatterers, and is similar in characteristics to that of (6.1a).

Duke Street is in a class 3B type environment and the descriptive parameters for the significant scatterers are shown in Table 6.12. This is a high density area, with buildings having little or no space in between them unlike the cases considered earlier. The μ_s values are larger than the previous sets as expected, while the μ_R values show that the contributory scatterers are on average, located closer to the mobile than in the previous cases. The ε_R values are comparable to those for Melville Place. The BAI for this case range from 2.5% to 3.5%, small values for a high density area. The fact that buildings are very closely located means that those situated at long distances from the mobile will be screened by the ones located nearer and therefore will not contribute by way of single scattering. This accounts for the smaller number of scatterers and BAI values for this route. The power delay profile of Figure (6.28) shows a

high concentration of power within the first microsecond excess delay and is consistent with the landcover around the mobile.

These observations in addition to the fact that the simulation-generated data compares very well with the measured data confirms that scattering in built-up areas is predominantly local. Non local scattering does occur as has been illustrated. Its effect is to increase the average delay and delay spread values significantly as can be seen when the values of these parameters for Melville Place given in Table 6.1, and Heyworth Street given in Table 6.7 are compared. The coherence bandwidth values are also much reduced . It is seen that the channel parameters are directly affected by the type of landcover surrounding the mobile.

The occupational domain around the mobile can be increased to take into account scattering from distant sources, for example terrain features such as hills which may be on the outskirts of the town, but perhaps visible to the mobile.

The profiles which have been selected for presentation are samples of the results obtained in this study.

Average Profile	Average Delay,μs	Delay Spread,μs	0.5 Coherence Band-width,Mhz	0.9 Coherence Band-width,Mhz
1	0.193	0.168	2.153	0.317
2	0.151	0.101	2.217	0.562
3	0.150	0.117	2.027	0.465
4	0.147	0.119	1.782	0.452
5	0.121	0.201	0.774	0.260
6	0.207	0.182	0.730	0.284
7	0.235	0.235	0.828	0.323
8	0.195	0.195	0.674	0.264

Table 6.1 Small scale characteristics in different sections on Melville Place

Set	Number of scats	BAI (%)	BSD, (m^2)		BLD (R m)		BLD (ϕ °)	
			μ_s	ε_s	μ_R	ε_R	μ_ϕ	ε_ϕ
1	270	15.46	91.41	74.65	190.44	74.72	212.44	110.35
2	255	14.95	92.01	76.36	187.35	73.06	213.94	111.42
3	252	14.83	92.01	76.66	190.12	73.93	218.33	109.79
4	246	14.59	91.81	77.52	192.56	74.63	226.95	106.39
5	222	13.80	93.25	81.28	192.16	71.26	231.49	106.13

Table 6.2 Distribution parameters for scatterers in occupational domain for Melville Place.

Set	Number of scats	BAI (%)	BSD, (m^2)		BLD (R m)		BLD (ϕ °)	
			μ_s	ε_s	μ_R	ε_R	μ_ϕ	ε_ϕ
1	39	4.26	111.36	113.38	125.77	81.77	211.15	107.69
2	40	4.46	120.59	128.73	122.25	70.24	225.00	104.14
3	39	4.43	111.94	132.14	121.92	71.79	225.00	105.51
4	35	4.32	126.72	139.18	121.29	73.97	225.86	101.73
5	37	4.86	140.00	135.92	130.14	60.21	229.86	102.84

Table 6.3 Distribution parameters for significant scatterers for Melville Place.

Average Profile	Average Delay,μs	Delay Spread,μs	0.5 Coherence Band-width,Mhz	0.9 Coherence Band-width,Mhz
1	0.145	0.273	1.573	0.201
2	0.286	0.456	0.368	0.114
3	0.127	0.223	1.591	0.255
4	0.139	0.219	1.611	0.283
5	0.184	0.348	1.527	0.155
6	0.058	0.152	2.216	0.536

Table 6.4 Small scale characteristics in different sections on Netherfield Road.

Set	Number of scats	BAI (%)	BSD, (m^2)		BLD (R m)		BLD (ϕ °)	
			μ_s	ε_s	μ_R	ε_R	μ_ϕ	ε_ϕ
1	394	16.30	108.42	59.67	262.39	105.36	205.89	106.31
2	397	16.42	109.22	60.77	261.69	104.29	206.73	106.94
3	394	16.44	108.89	60.74	259.87	103.45	205.58	107.88
4	394	16.43	108.99	60.63	258.05	101.45	207.18	108.99

Table 6.5 Distribution parameters for scatterers in occupational domain for Netherfield Road.

Set	Number of scats	BAI (%)	BSD, (m^2)		BLD (R m)		BLD (ϕ °)	
			μ_s	ε_s	μ_R	ε_R	μ_ϕ	ε_ϕ
1	50	3.58	118.33	67.92	207.00	103.75	136.20	104.09
2	41	2.89	115.54	57.54	197.93	109.37	159.15	97.95
3	36	2.68	120.31	44.61	180.00	98.46	216.67	94.22
4	39	3.64	143.18	86.44	195.77	94.74	232.69	105.89

Table 6.6 Distribution parameters for significant scatterers for Netherfield Road.

Average Profile	Average Delay,μs	Delay Spread,μs	0.5 Coherence Band-width,Mhz	0.9 Coherence Band-width,Mhz
1	0.204	0.408	1.104	0.133
2	0.277	0.440	0.769	0.122
3	0.261	0.466	0.794	0.114
4	0.297	0.489	0.720	0.108

Table 6.7 Small scale characteristics in different sections on Heyworth Street.

Set	Number of scats	BAI (%)	BSD, (m^2)		BLD (R m)		BLD (ϕ °)	
			μ_s	ε_s	μ_R	ε_R	μ_ϕ	ε_ϕ
1	276	14.73	104.36	60.10	198.37	60.37	193.91	99.31
2	257	14.14	104.57	60.60	196.79	59.75	194.33	100.42
3	264	14.01	105.24	60.95	199.32	59.90	190.00	101.77
4	254	13.61	105.86	60.08	197.24	61.45	184.61	104.12

Table 6.8 Distribution parameters for scatterers in occupational domain for Heyworth Road.

Set	Number of scats	BAI (%)	BSD, (m^2)		BLD (R m)		BLD (ϕ °)	
			μ_s	ε_s	μ_R	ε_R	μ_ϕ	ε_ϕ
1	38	3.11	146.21	94.40	149.21	67.89	184.74	99.93
2	36	2.89	137.90	95.71	154.17	69.21	198.33	94.81
3	37	2.95	137.50	90.70	162.57	63.00	209.59	96.34
4	36	2.94	128.23	90.31	165.00	63.74	221.67	85.39

Table 6.9 Distribution parameters for significant scatterers for Heyworth Road.

Average Profile	Average Delay,μs	Delay Spread,μs	0.5 Coherence Band-width,Mhz	0.9 Coherence Band-width,Mhz
1	0.170	0.231	0.825	0.239
2	0.217	0.255	0.682	0.210
3	0.150	0.229	0.204	0.600
4	0.269	0.257	0.236	0.762

Table 6.10 Small scale characteristics in different sections on Duke Street.

Set	Number of scats	BAI (%)	BSD, (m^2)		BLD (R m)		BLD (ϕ °)	
			μ_s	ε_s	μ_R	ε_R	μ_ϕ	ε_ϕ
1	394	32.48	152.13	109.56	169.34	64.22	167.66	91.42
2	394	32.57	152.27	111.06	168.27	63.35	170.25	92.46
3	394	32.44	150.55	111.66	167.66	63.99	175.81	92.56
4	394	32.88	152.42	112.96	166.90	62.68	176.27	94.85

Table 6.11 Distribution parameters for scatterers in occupational domain for Duke Street.

Set	Number of scats	BAI (%)	BSD, (m^2)		BLD (R m)		BLD (ϕ °)	
			μ_s	ε_s	μ_R	ε_R	μ_ϕ	ε_ϕ
1	26	2.48	219.00	99.29	118.85	68.53	176.54	96.03
2	29	2.85	221.30	103.71	120.52	73.76	173.28	98.16
3	31	3.12	228.45	104.31	115.65	70.80	172.74	93.90
4	36	3.49	212.88	101.57	120.00	68.97	180.00	90.85

Table 6.12 Distribution parameters for significant scatterers for Duke Street.

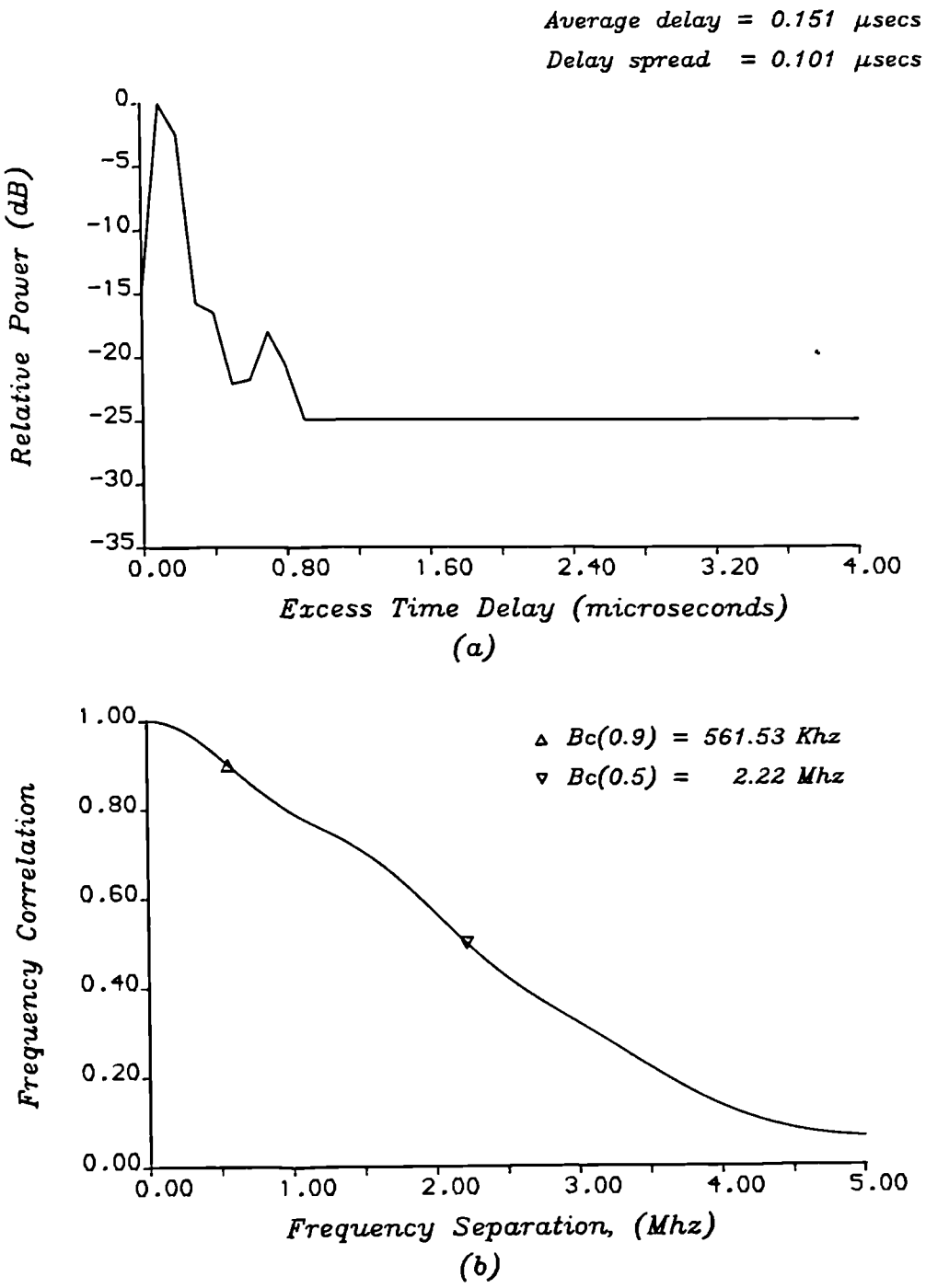

Figure (6.1) Small scale characteristics of Melville Place.

(a) Average power delay profile.

(b) Frequency correlation function.

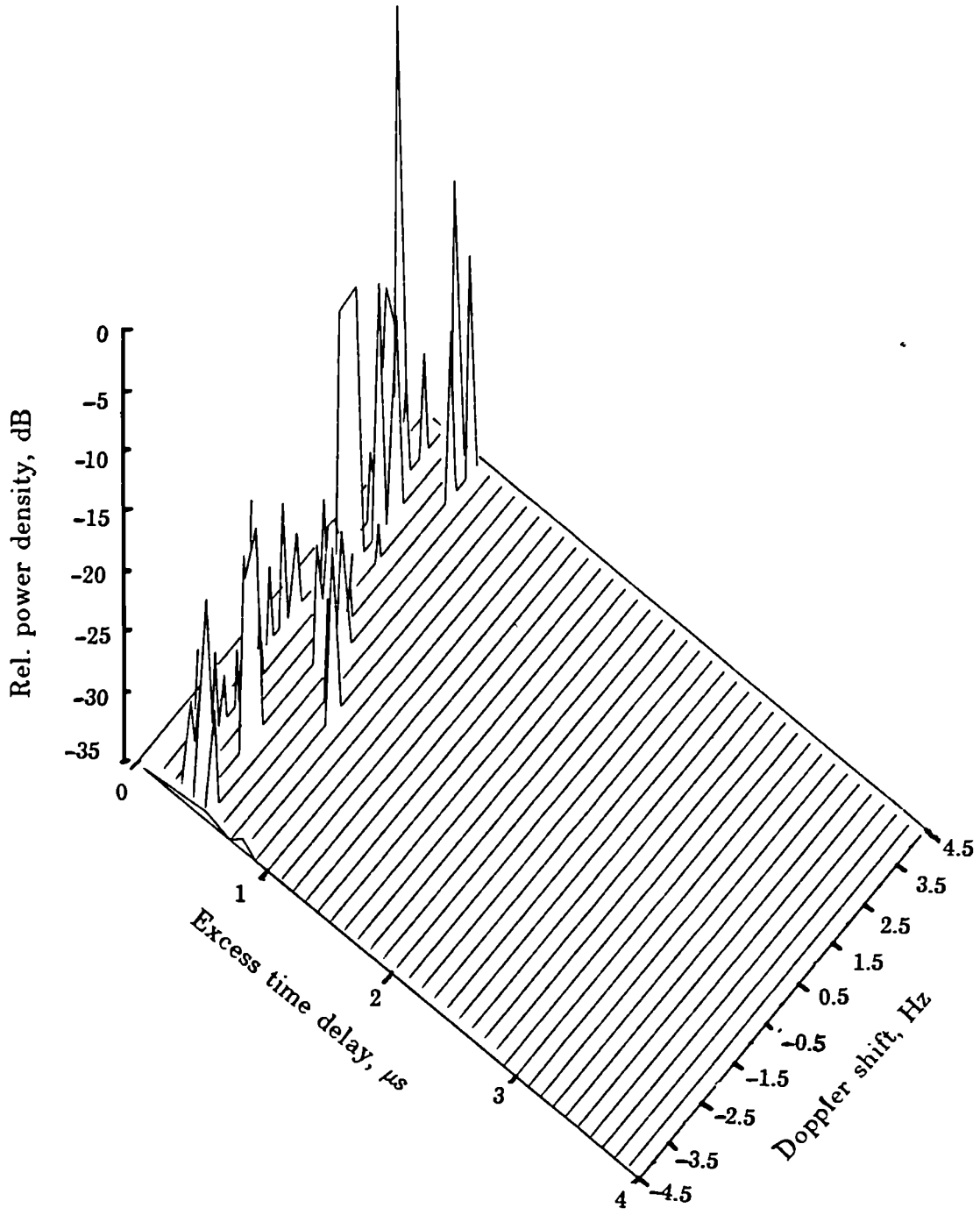

Figure (6.2) Scattering function for Melville Place : Simulation.

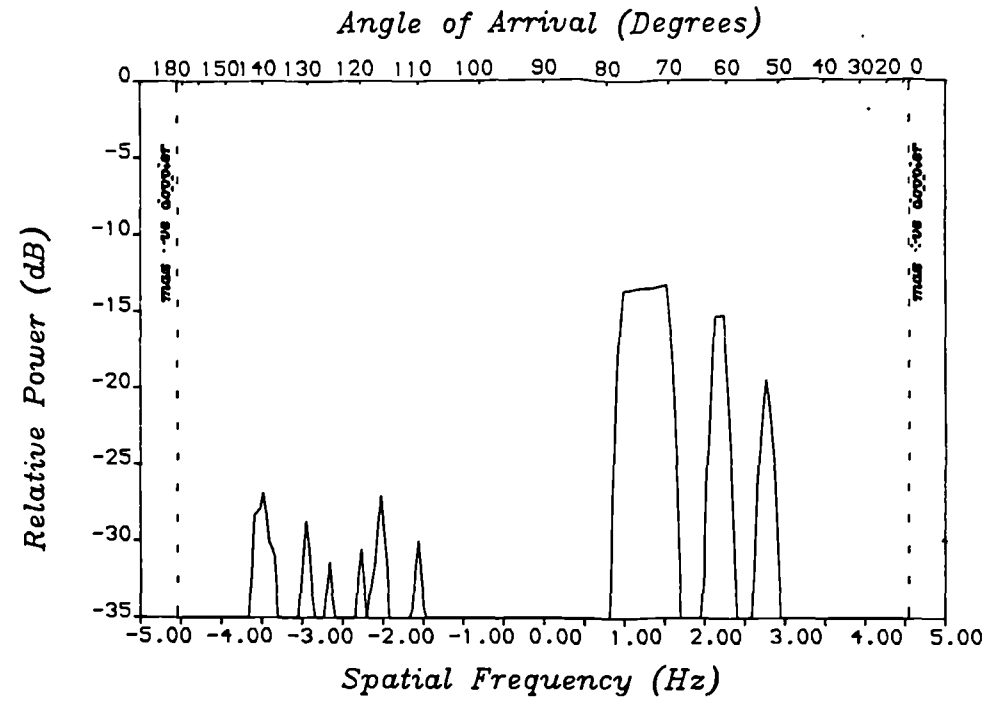

Figure (6.3a) Doppler spectrum at 0.2μs excess delay on Melville Place.

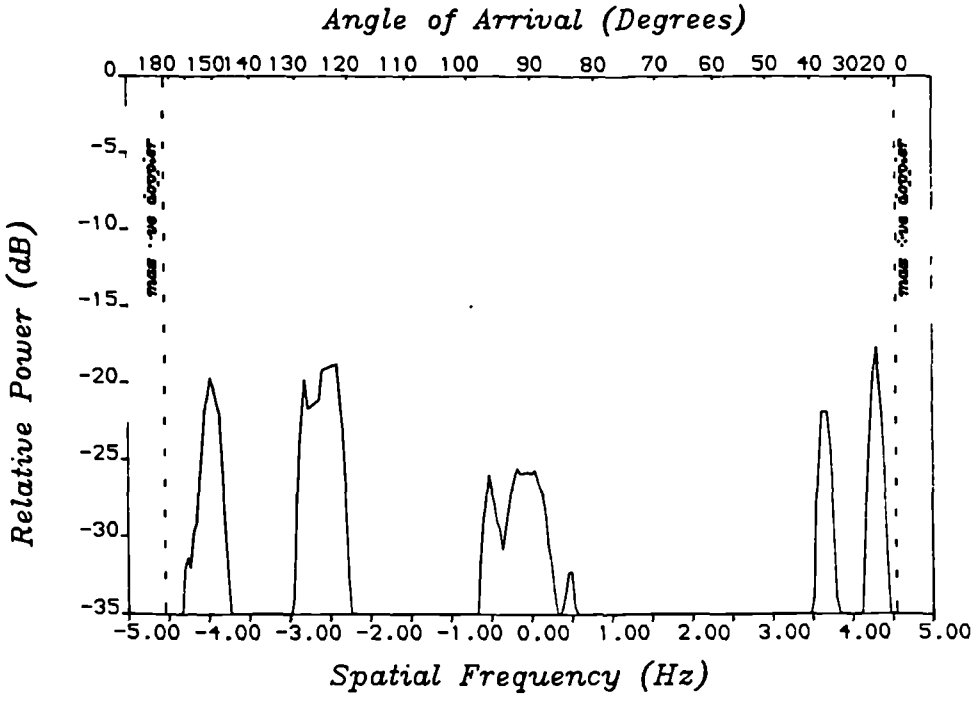

Figure (6.3b) Doppler spectrum at 0.4μs excess delay on Melville Place.

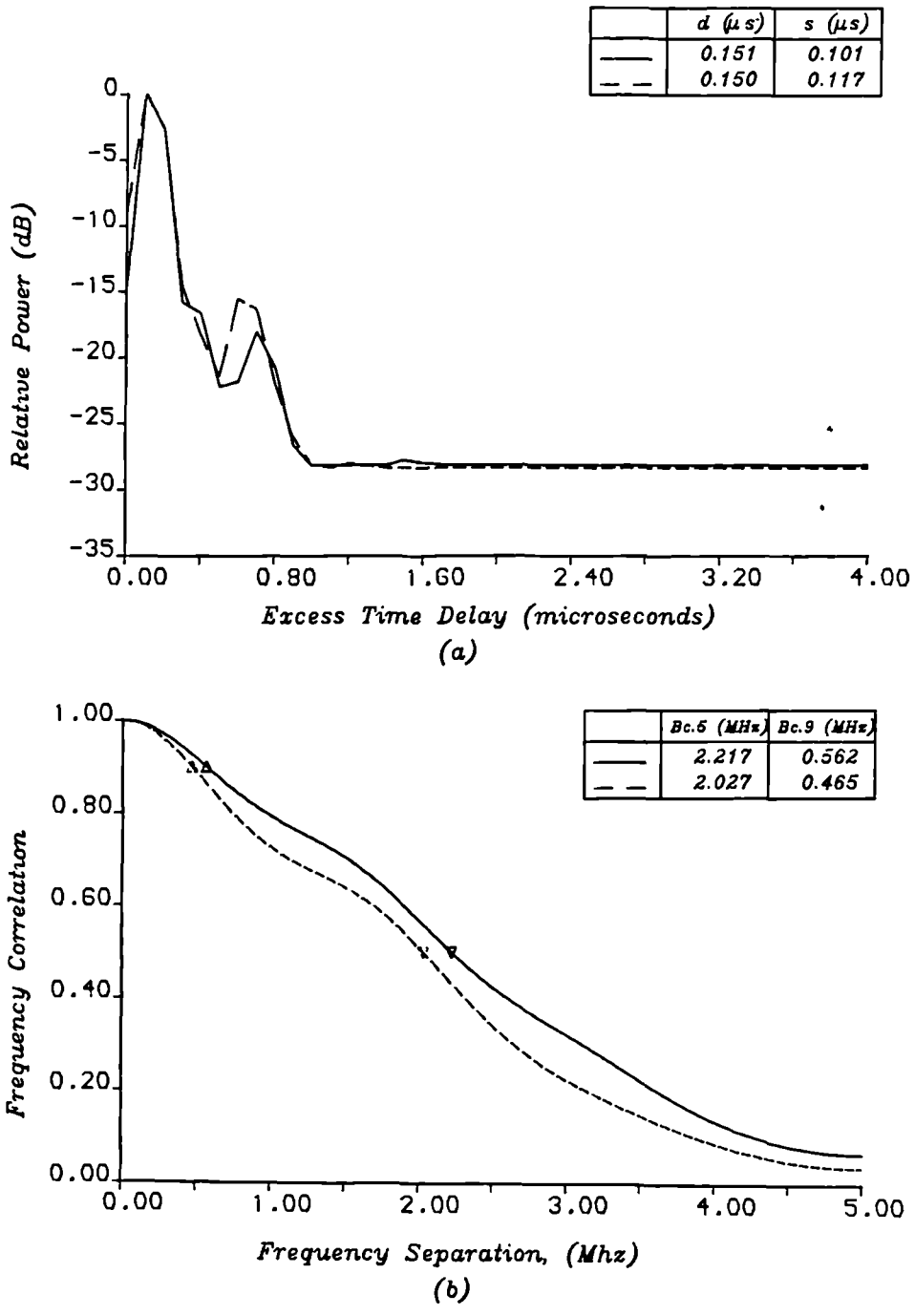

Figure (6.4) Small scale characteristics of Melville Place showing WSS behaviour of channel.
(two consecutive simulated average profiles)

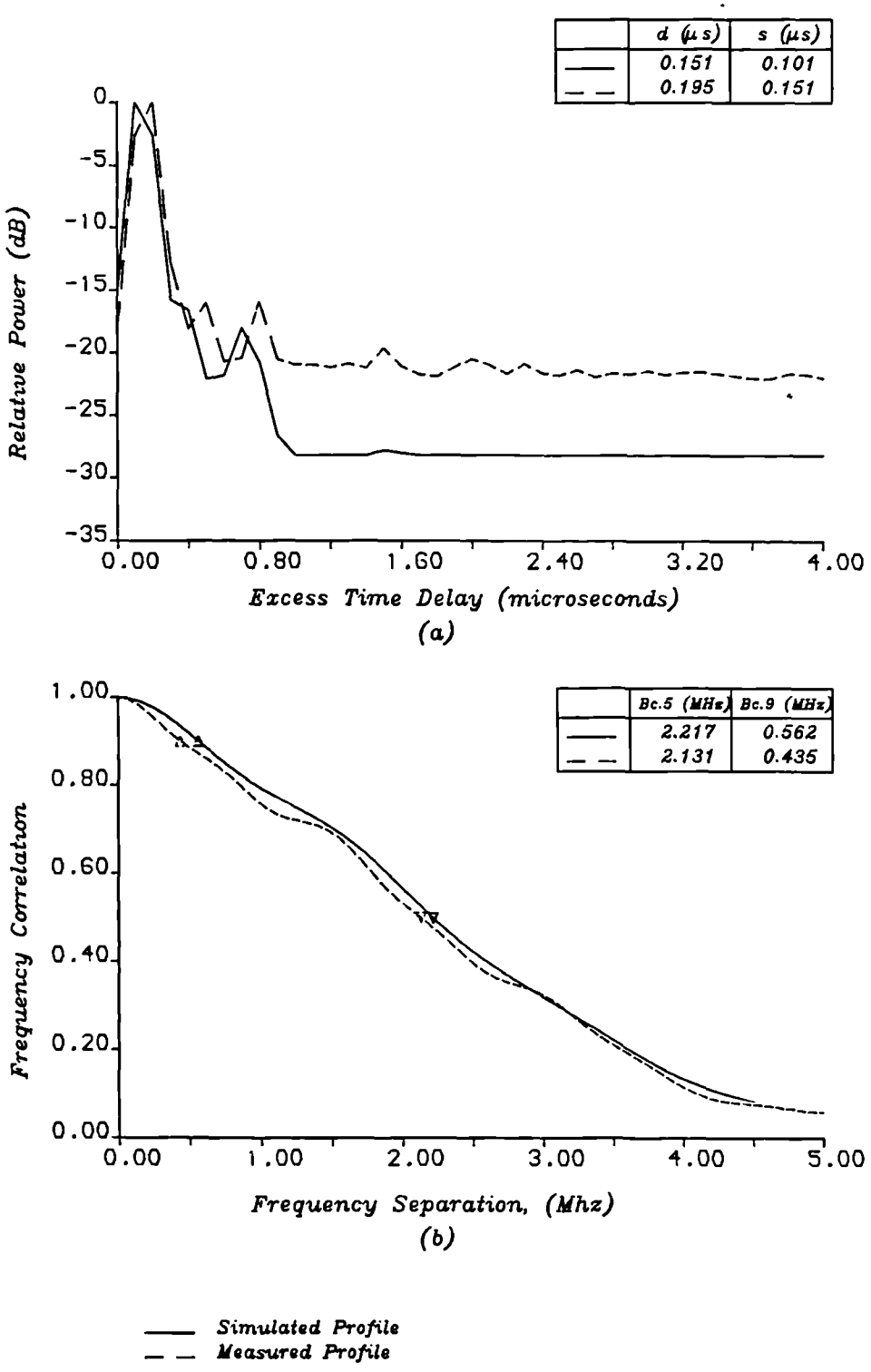

Figure (6.5) Small scale characteristics of Melville Place : simulation vs measured.

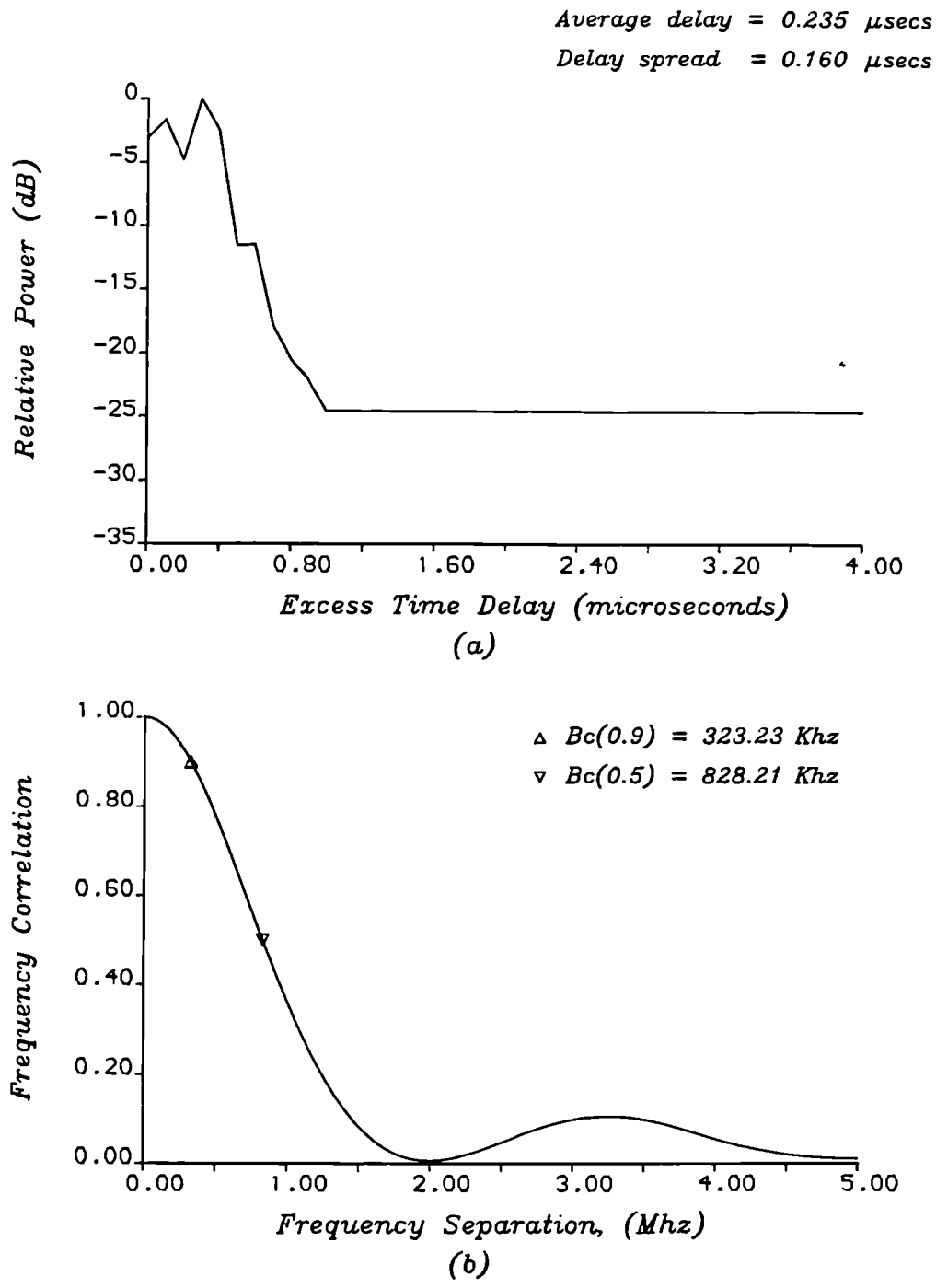

Figure (6.6) Small scale characteristics of Melville Place with no LOS.

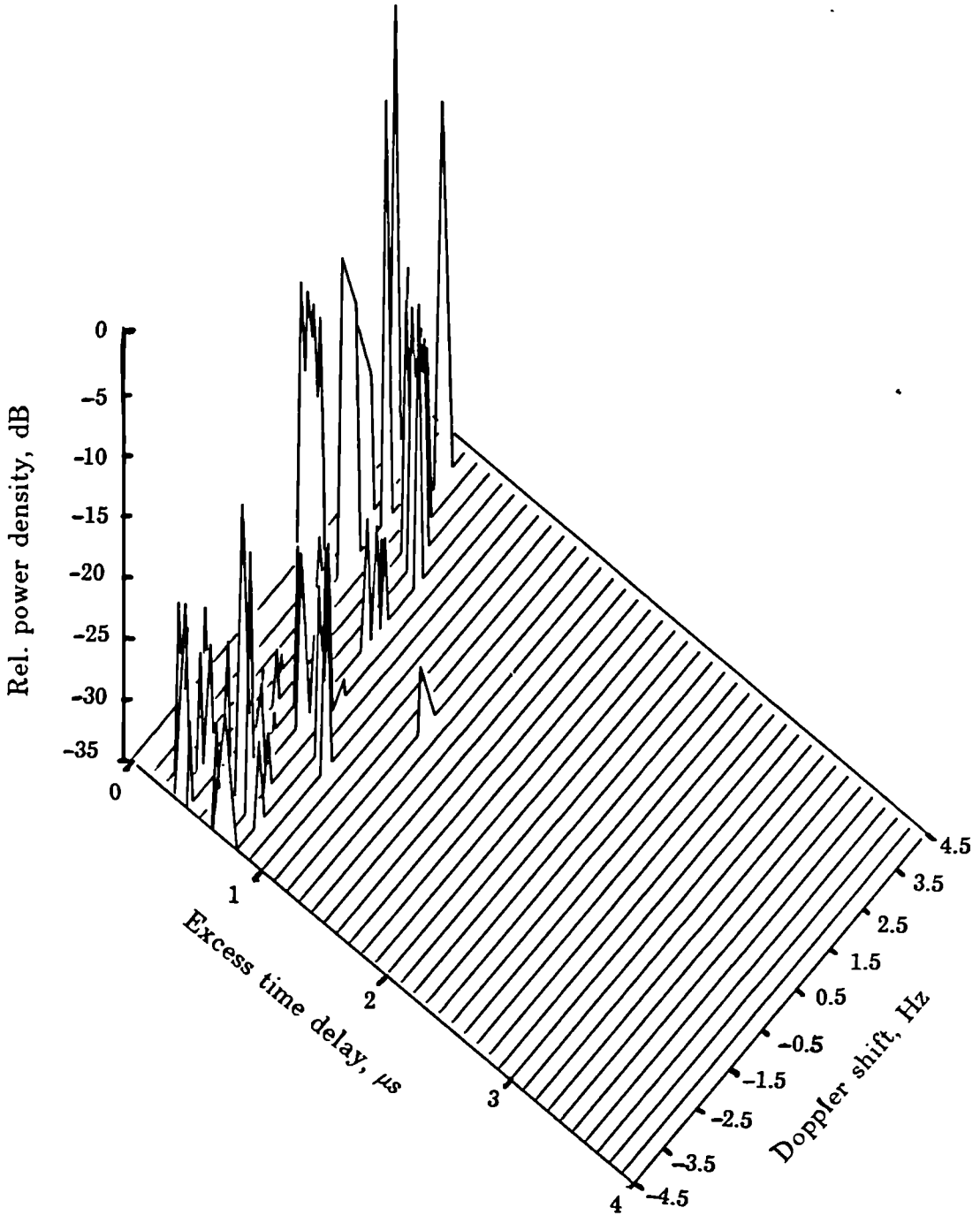

Figure (6.7) Scattering function for Melville Place : simulation, no LOS.

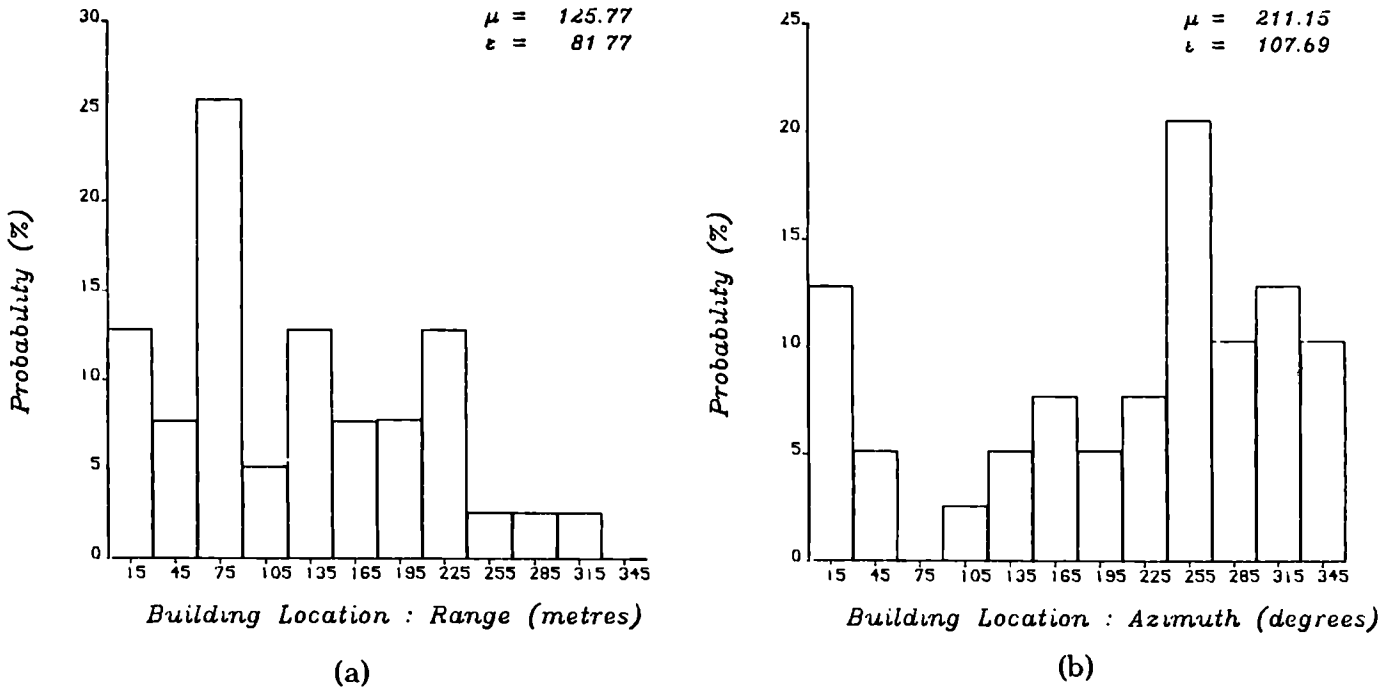

Figure (6.8) Location distributions for significant scatterers on Melville Place.

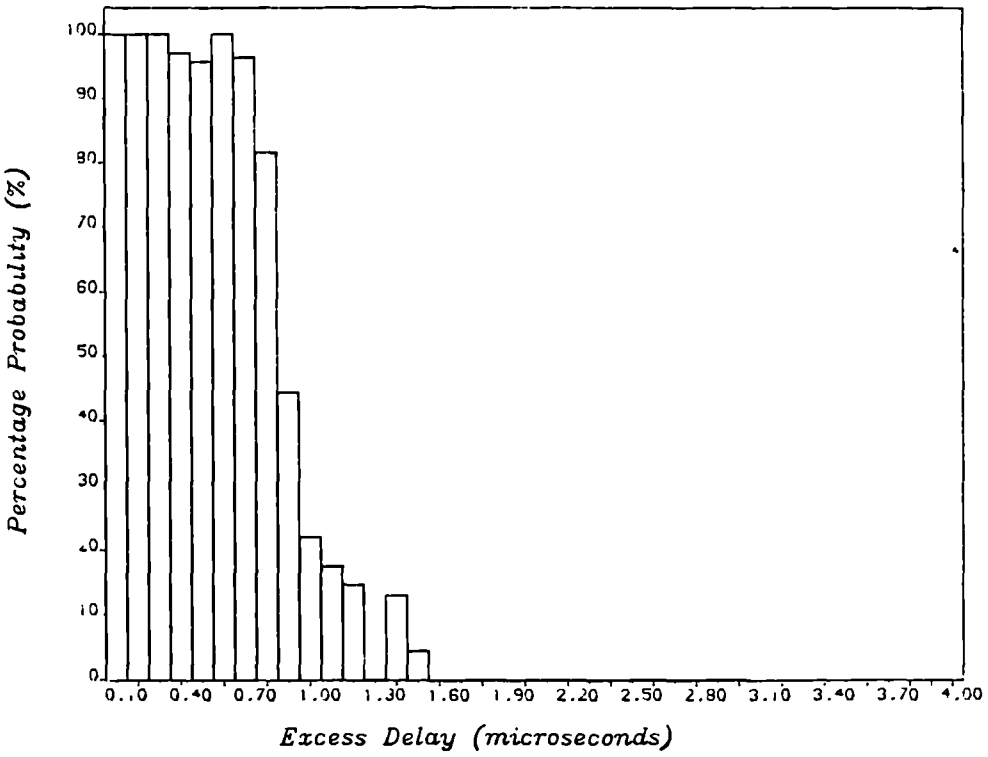

Figure (6.9) Echo path occupancy distribution for Melville Place.

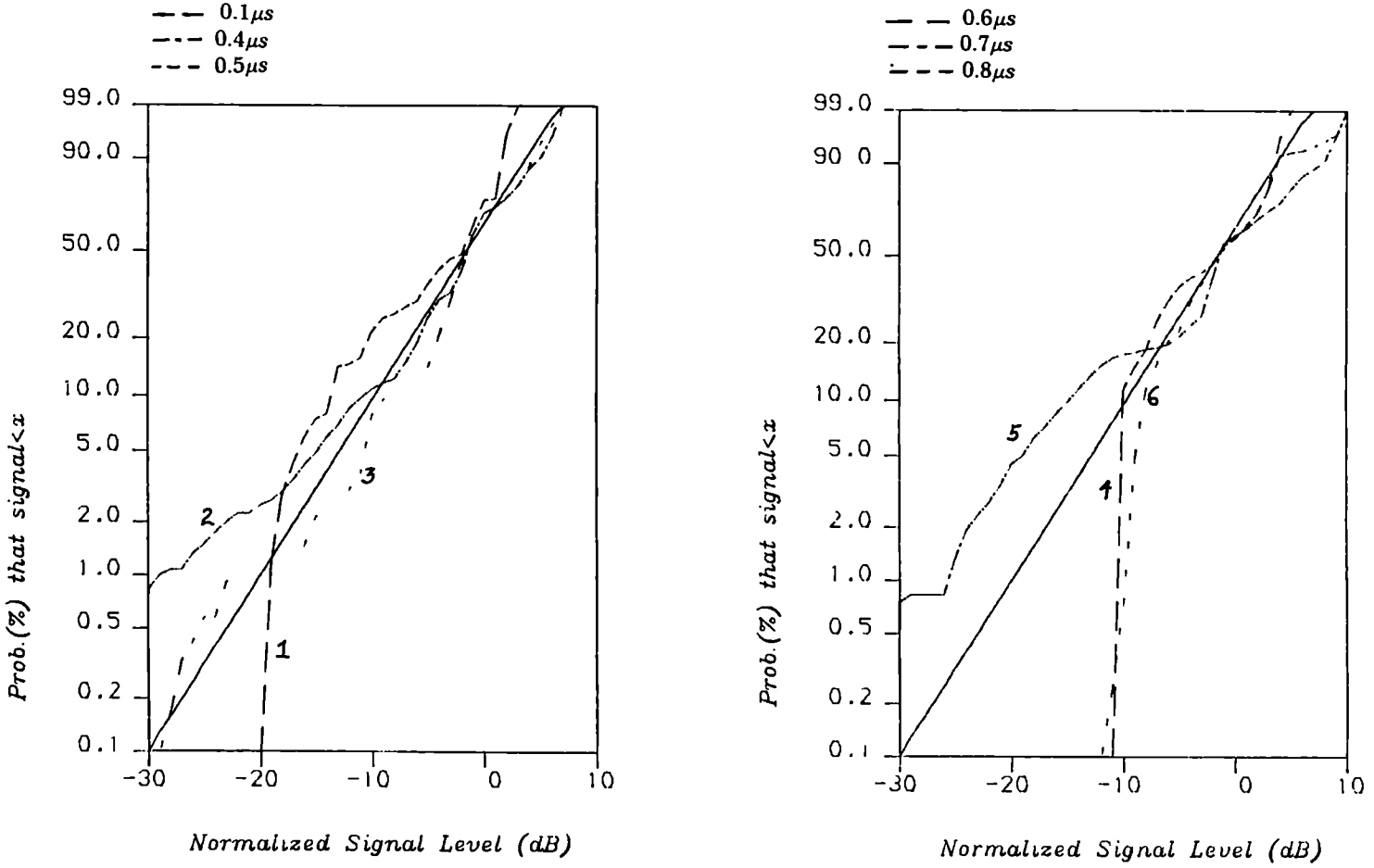

Figure (6.10) Amplitude distributions at fixed excess delays for for Melville Place.

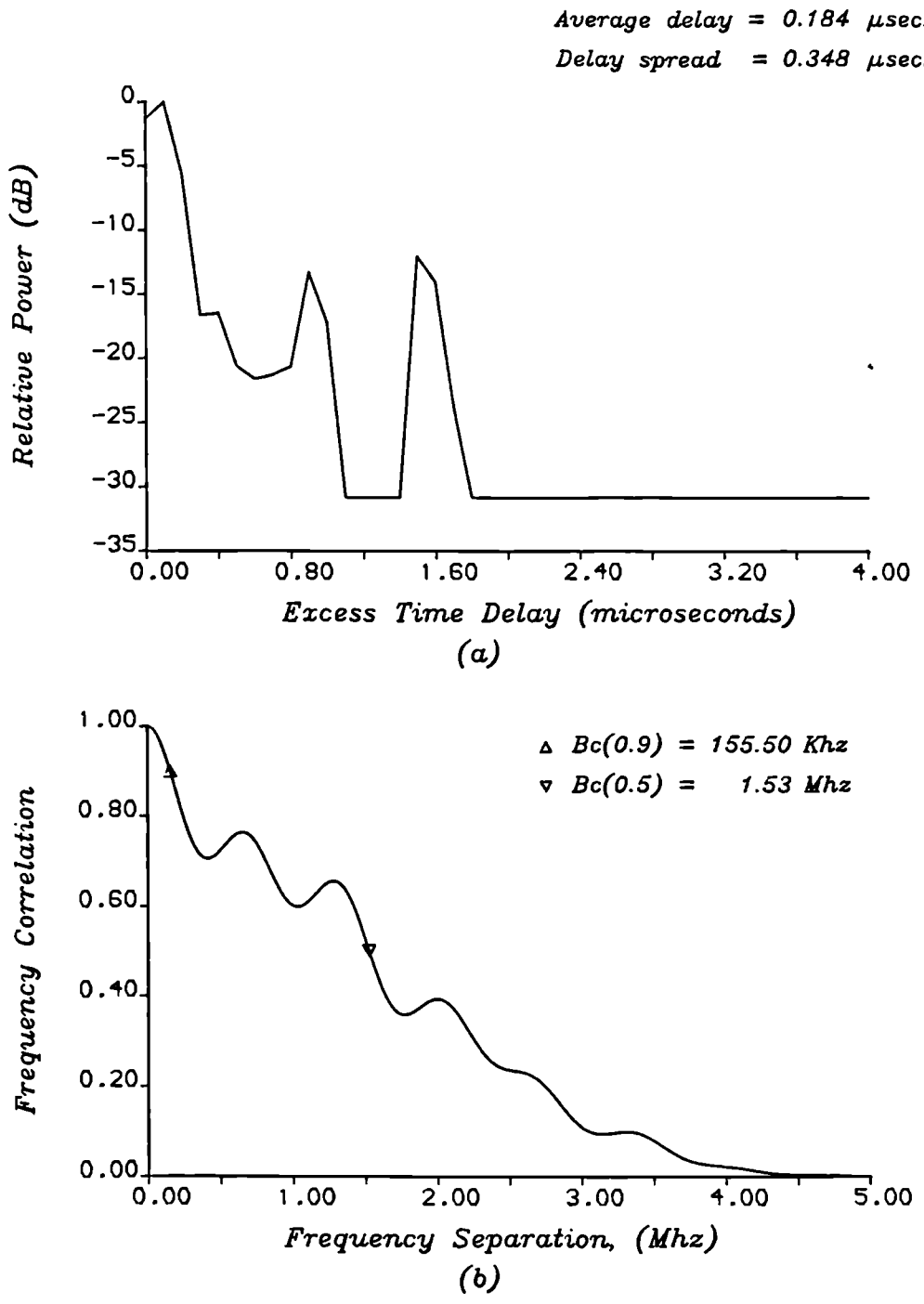

Figure (6.11) Small scale characteristics of Netherfield Road.

(a) Average power delay profile.

(b) Frequency correlation function.

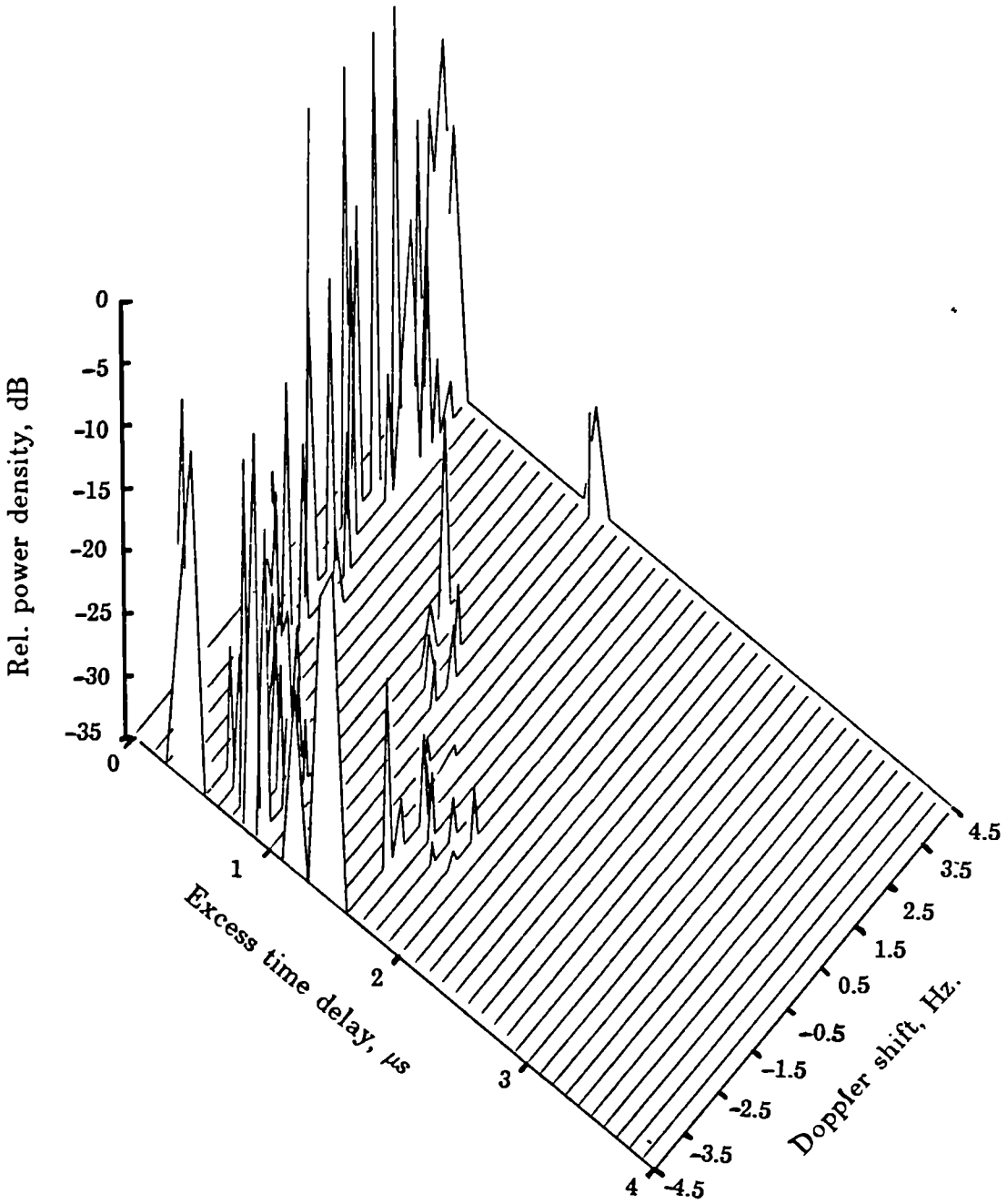

Figure (6.12) Scattering function for Netherfield Road : Simulation.

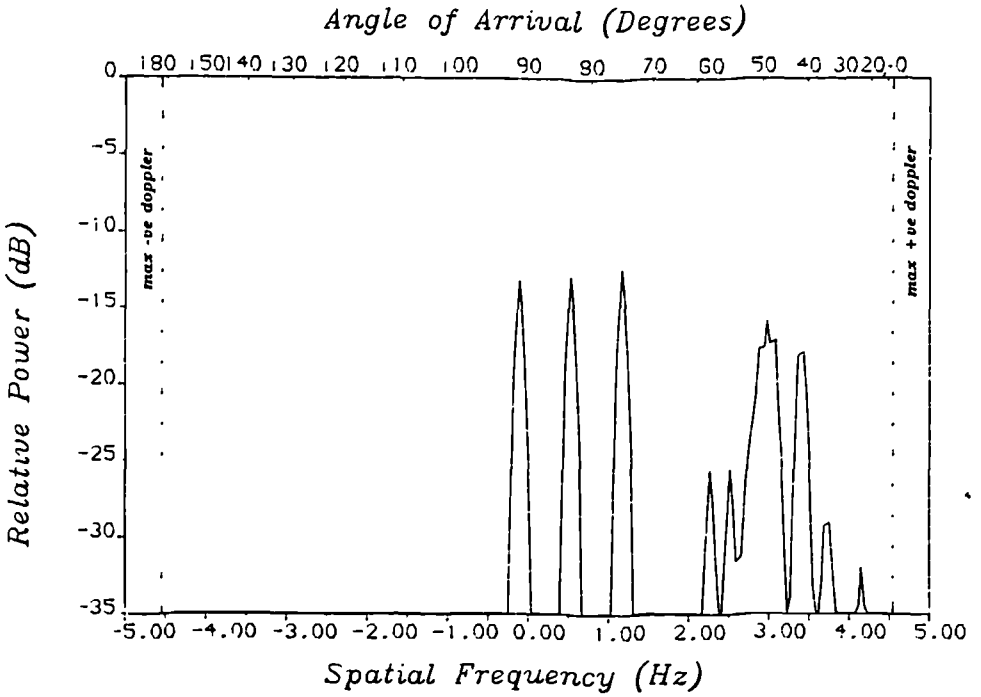

Figure (6.13a) Doppler spectrum at 0.2 μs excess delay on Netherfield Road.

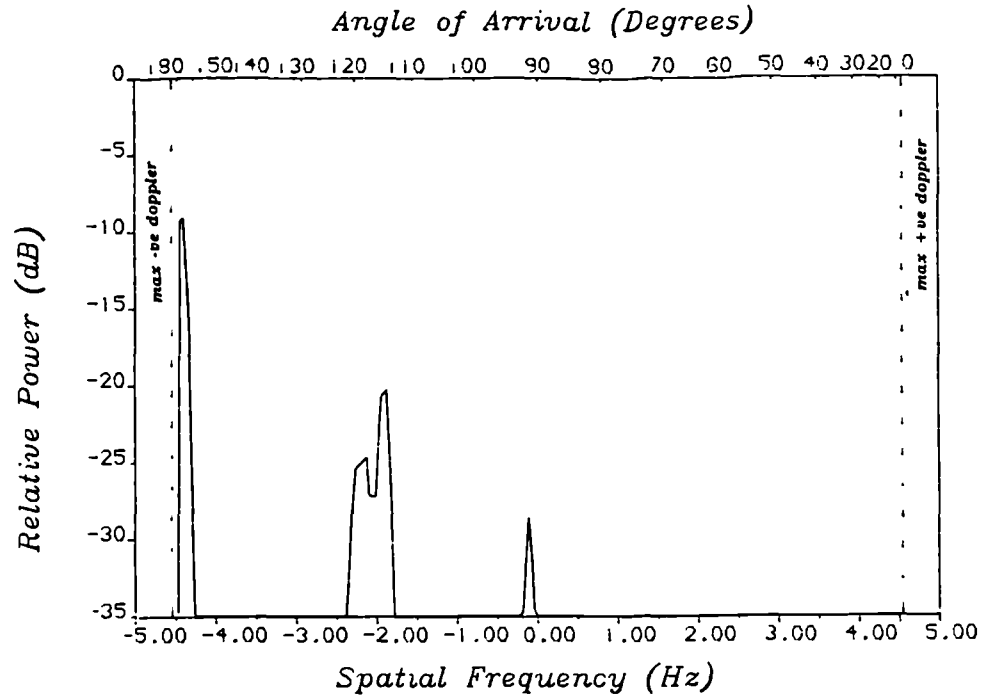

Figure (6.13b) Doppler spectrum at 0.4 μs excess delay on Netherfield Road.

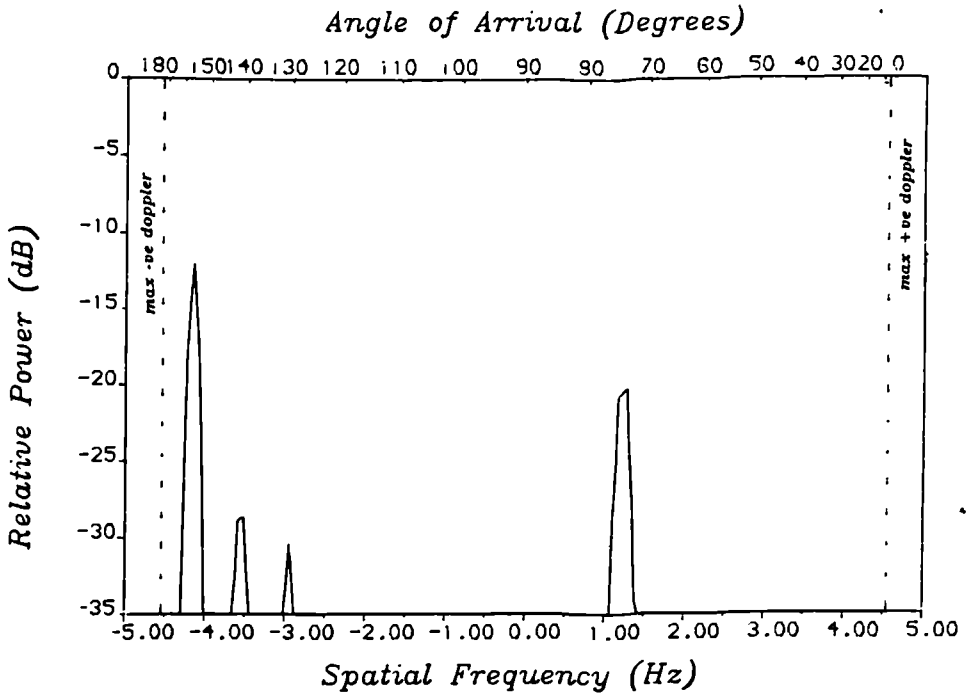

Figure (6.13c) Doppler spectrum at 0.9 μs excess delay on Netherfield Road.

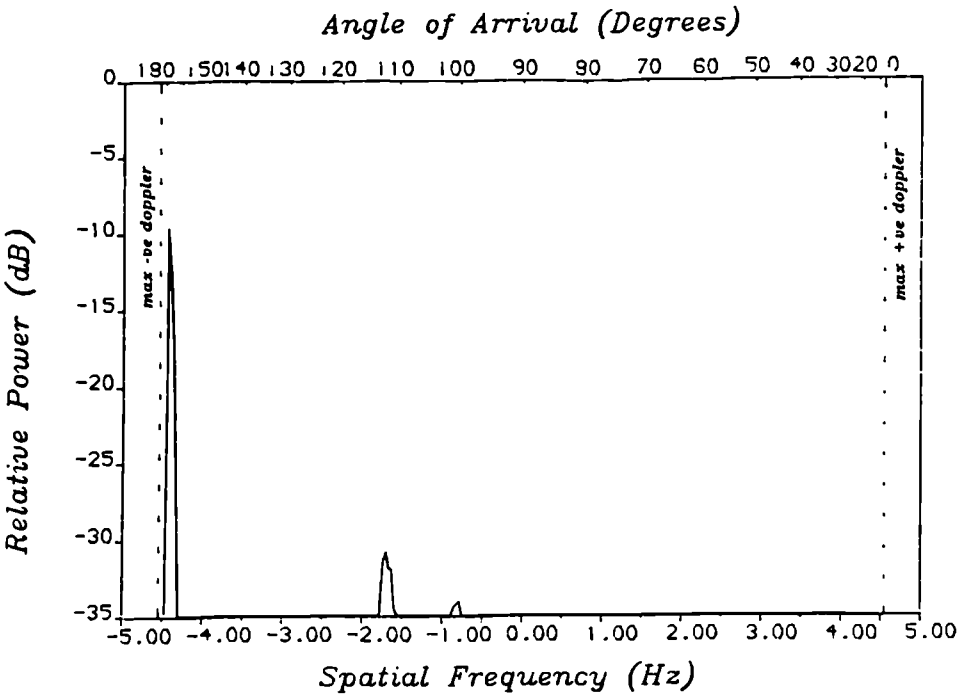

Figure (6.13d) Doppler spectrum at 1.5 μs excess delay on Netherfield Road.

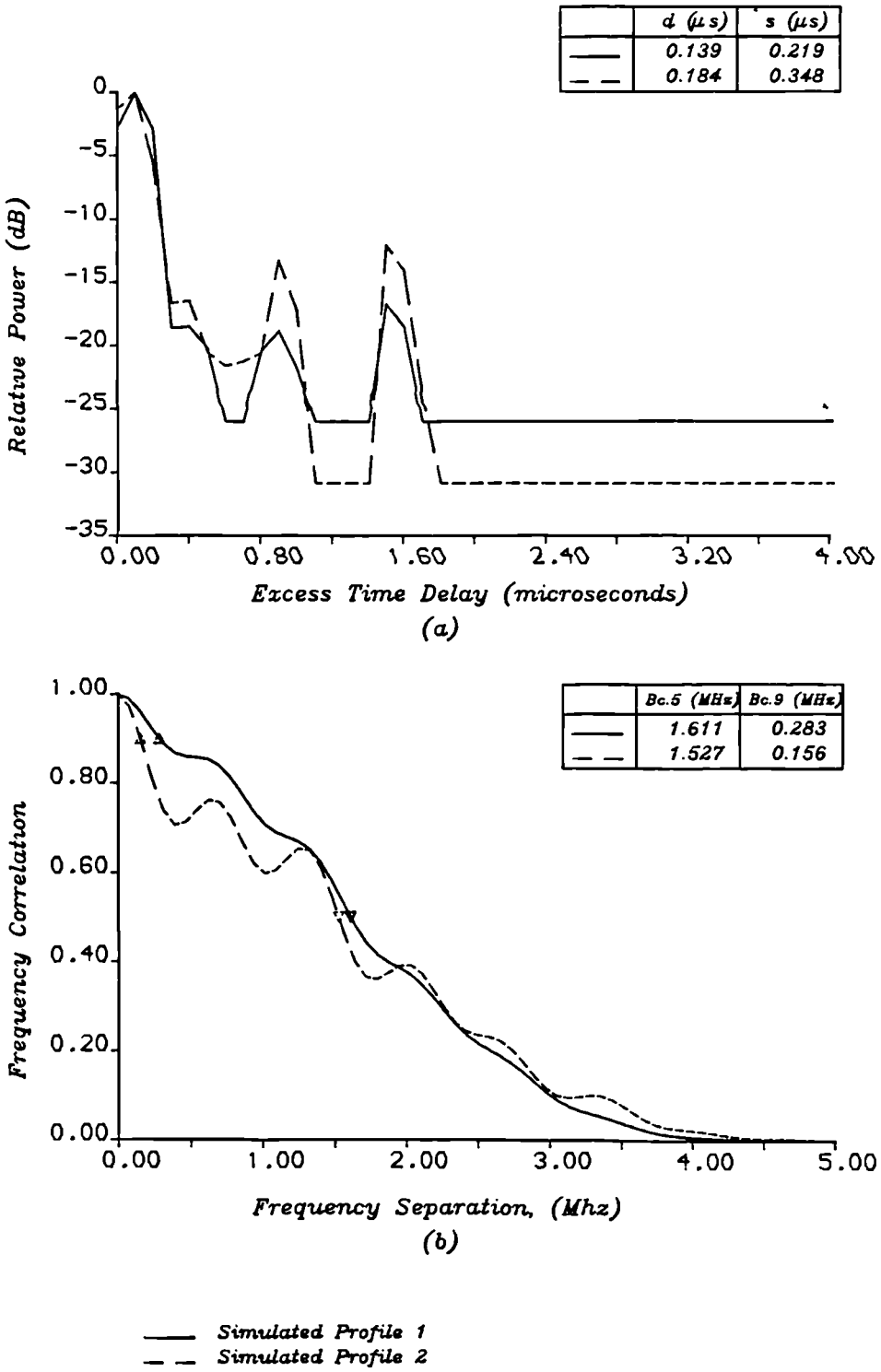

Figure (6.14) Small scale characteristics of Netherfield Road showing WSS behaviour of channel.
(two consecutive simulated average profiles)

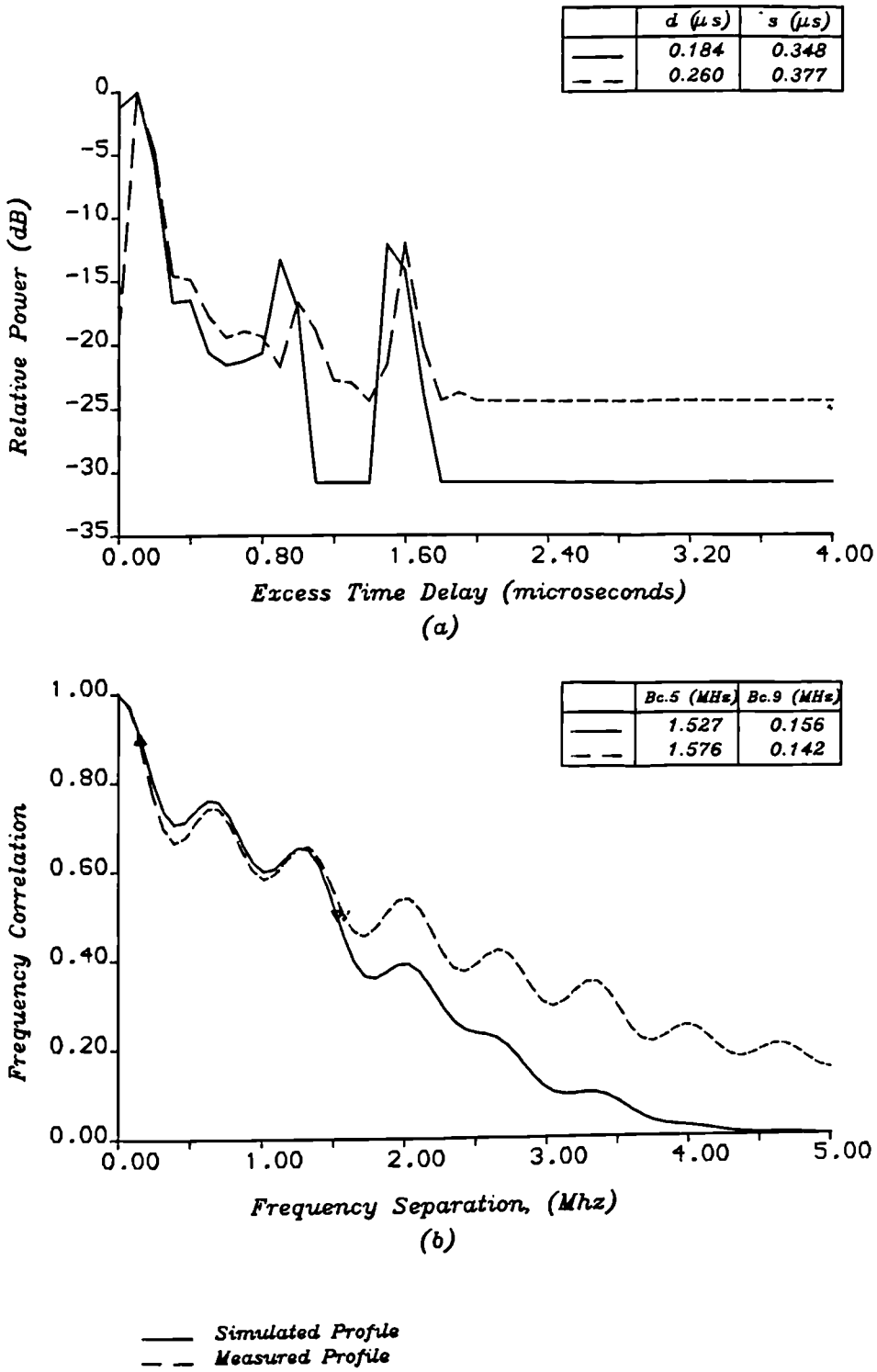

Figure (6.15) Small scale characteristics of Netherfield Road : simulation vs measured

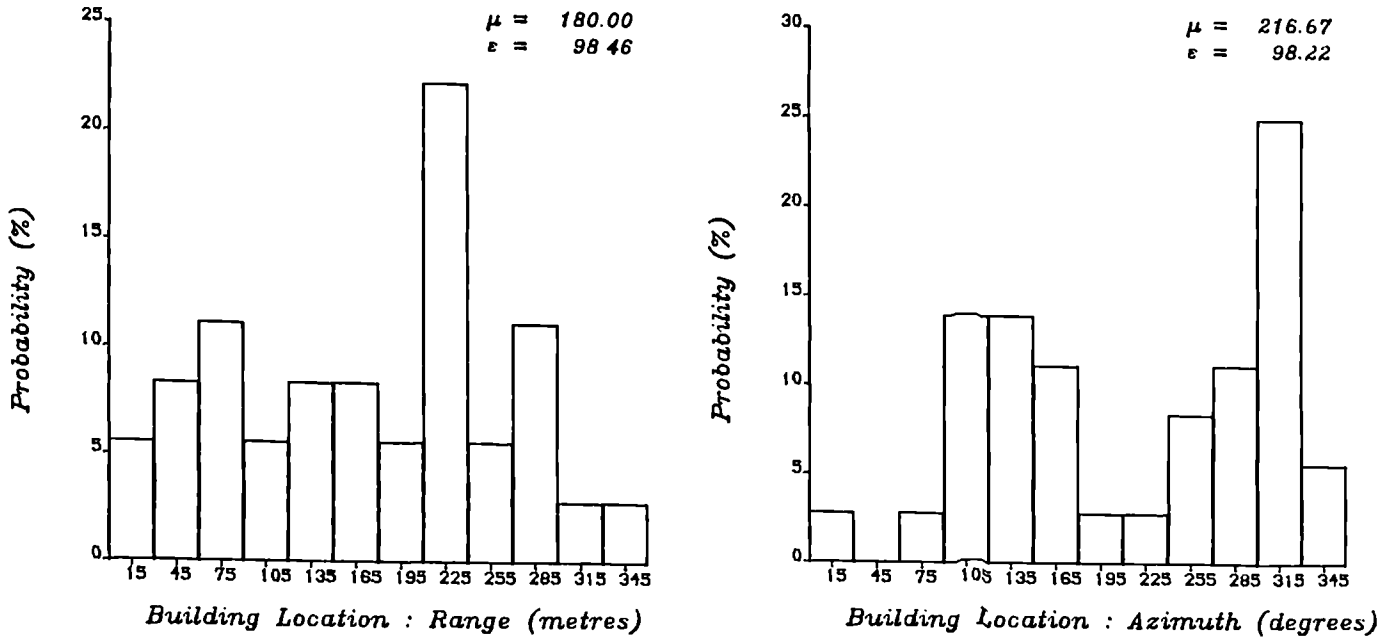

(6.16) Location distributions for significant scatterers on Netherfield Road.

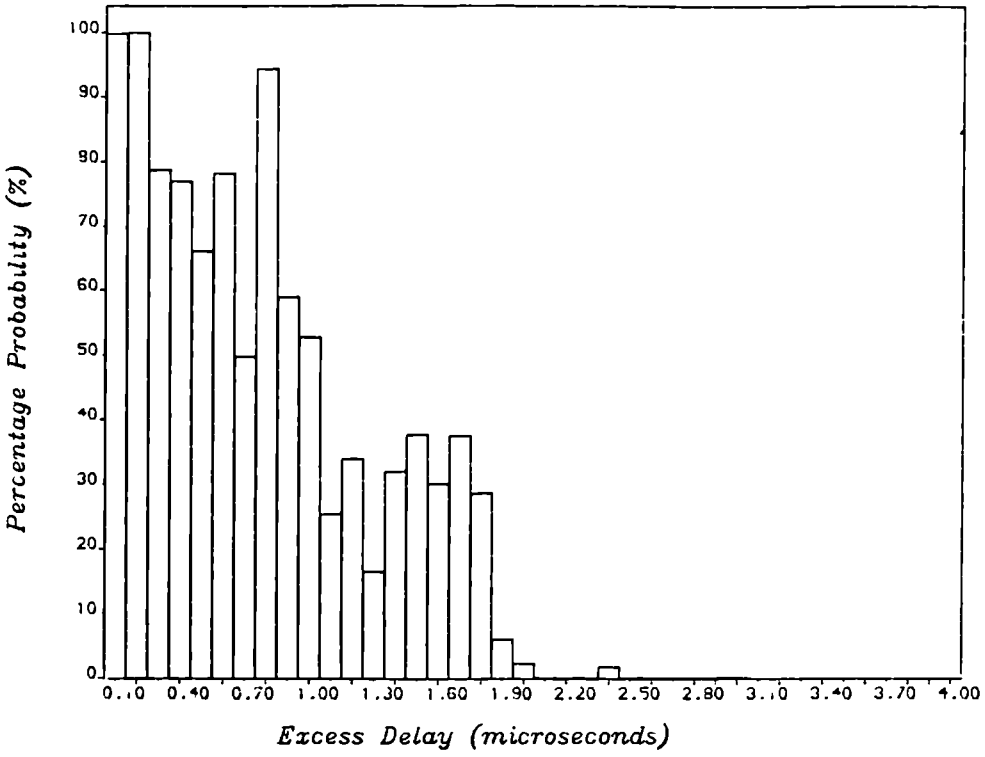

Figure (6.17) Echo path occupancy distribution for Netherfield Road.

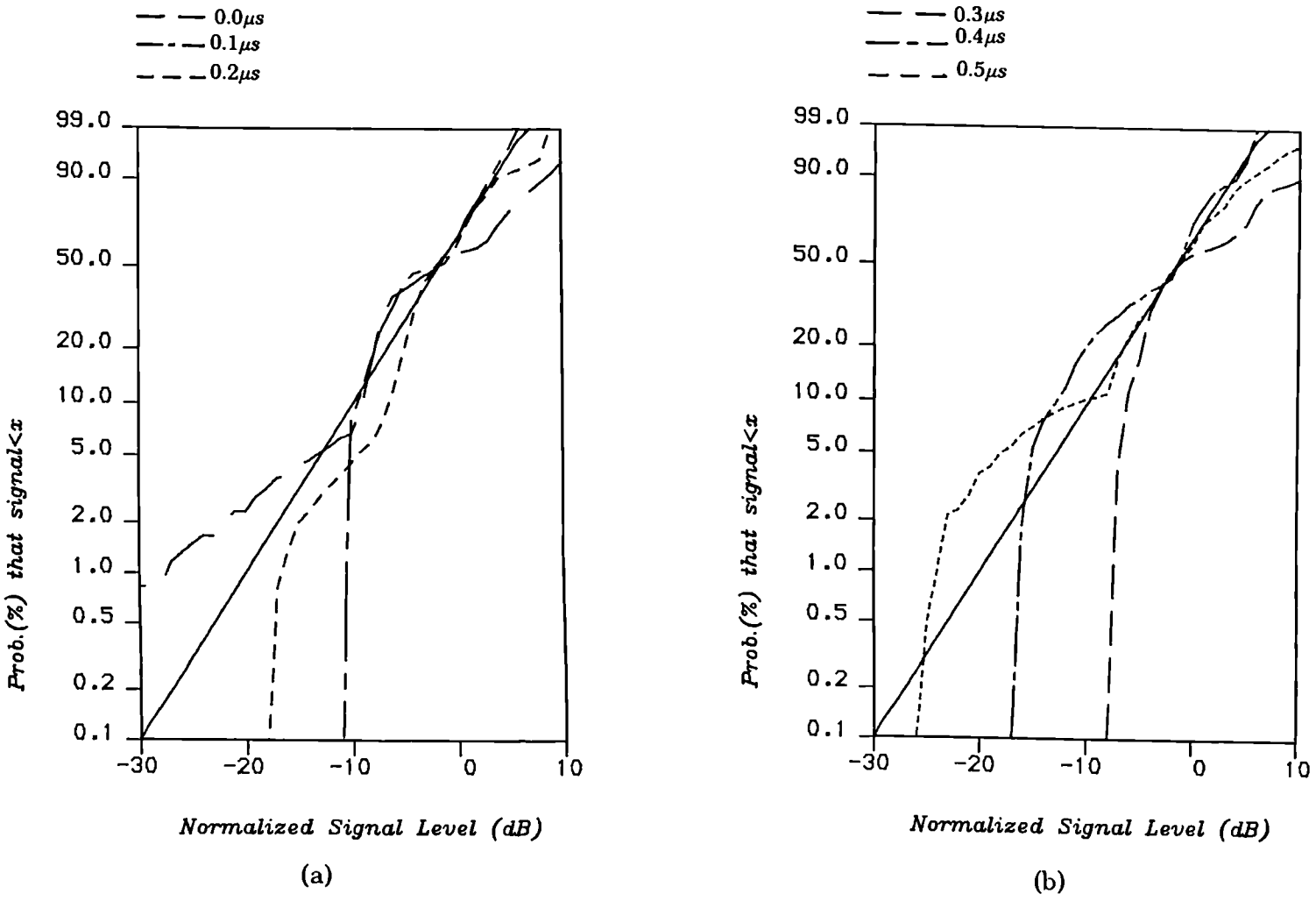

Figure (6.18) Amplitude distributions at fixed excess delays for Netherfield Road.

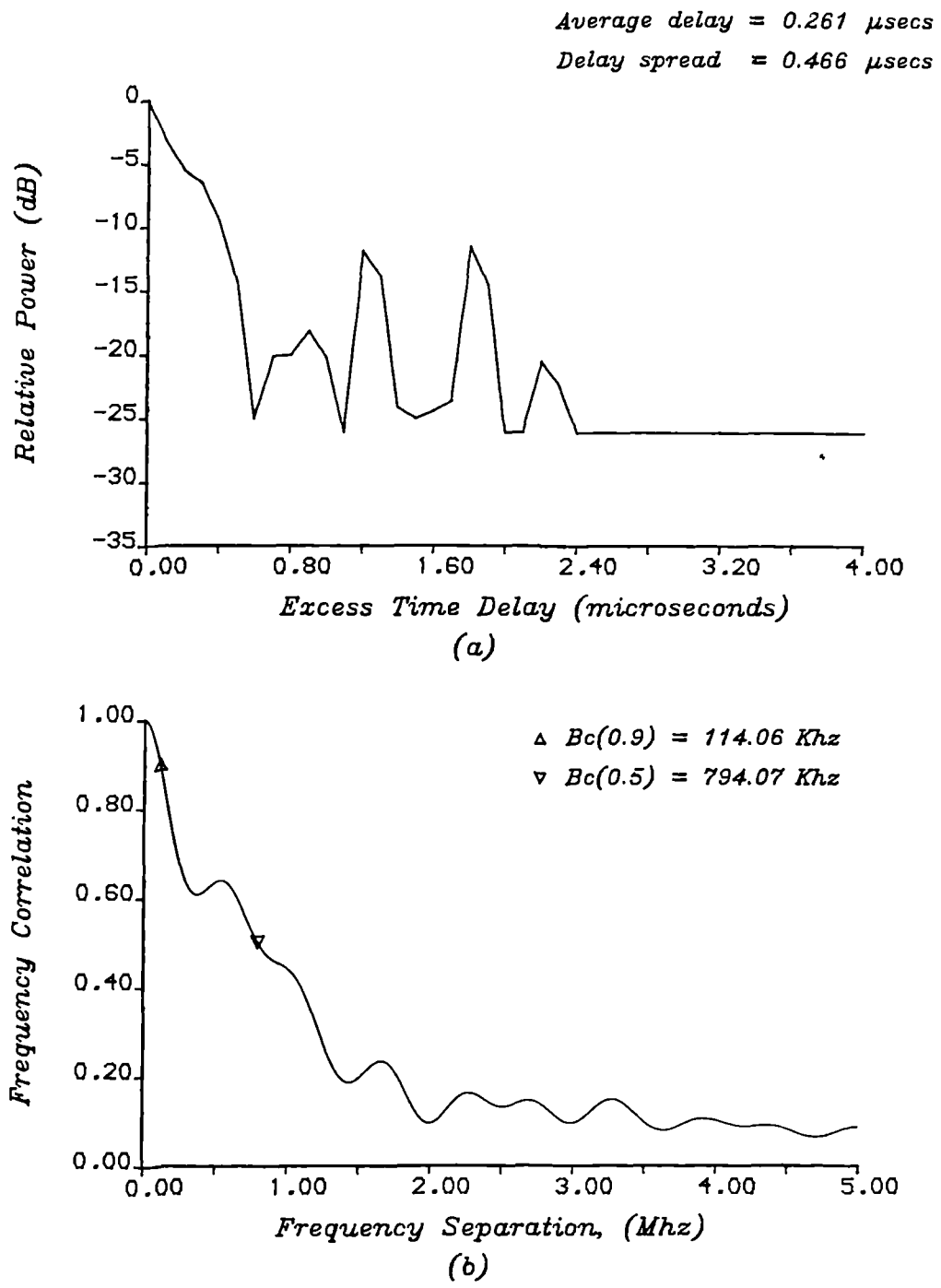

Figure (6.19) Small scale characteristics of Heyworth Street.

(a) Average power delay profile.

(b) Frequency correlation function.

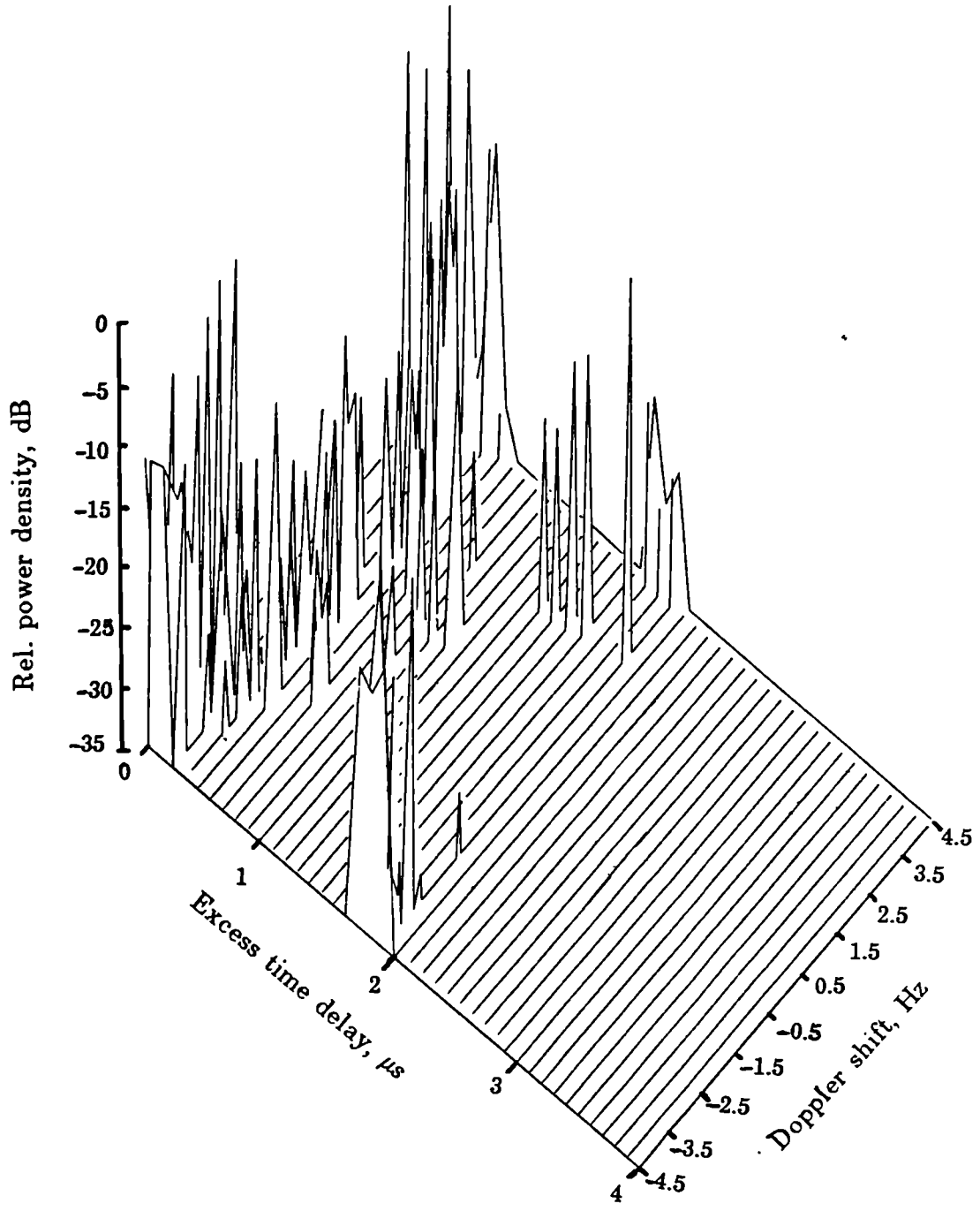

Figure (6.20) Scattering function for Heyworth Street : Simulation.

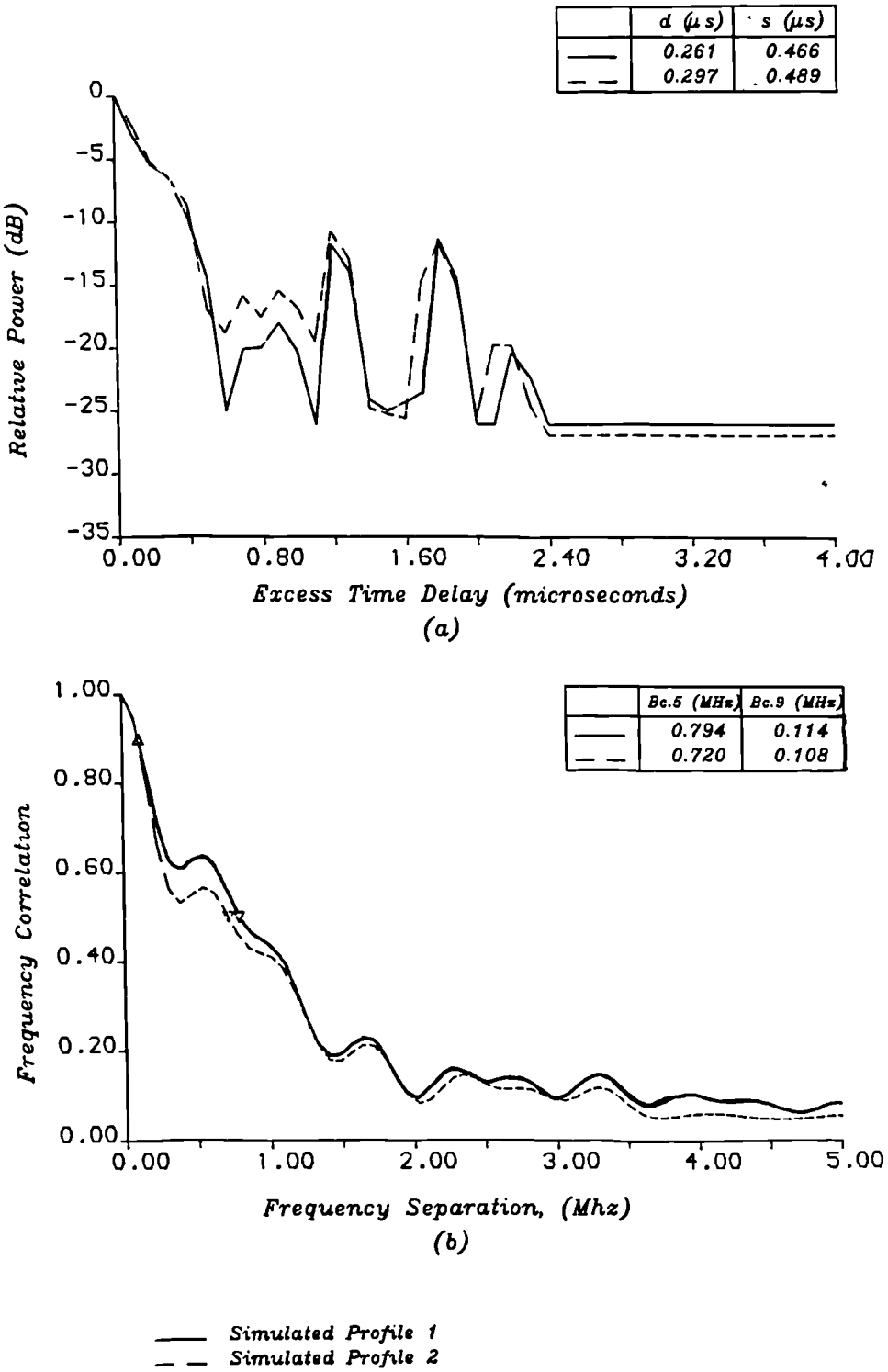

Figure (6.21) Small scale characteristics of Heyworth Street showing WSS behaviour of channel.
(two consecutive simulated average profiles)

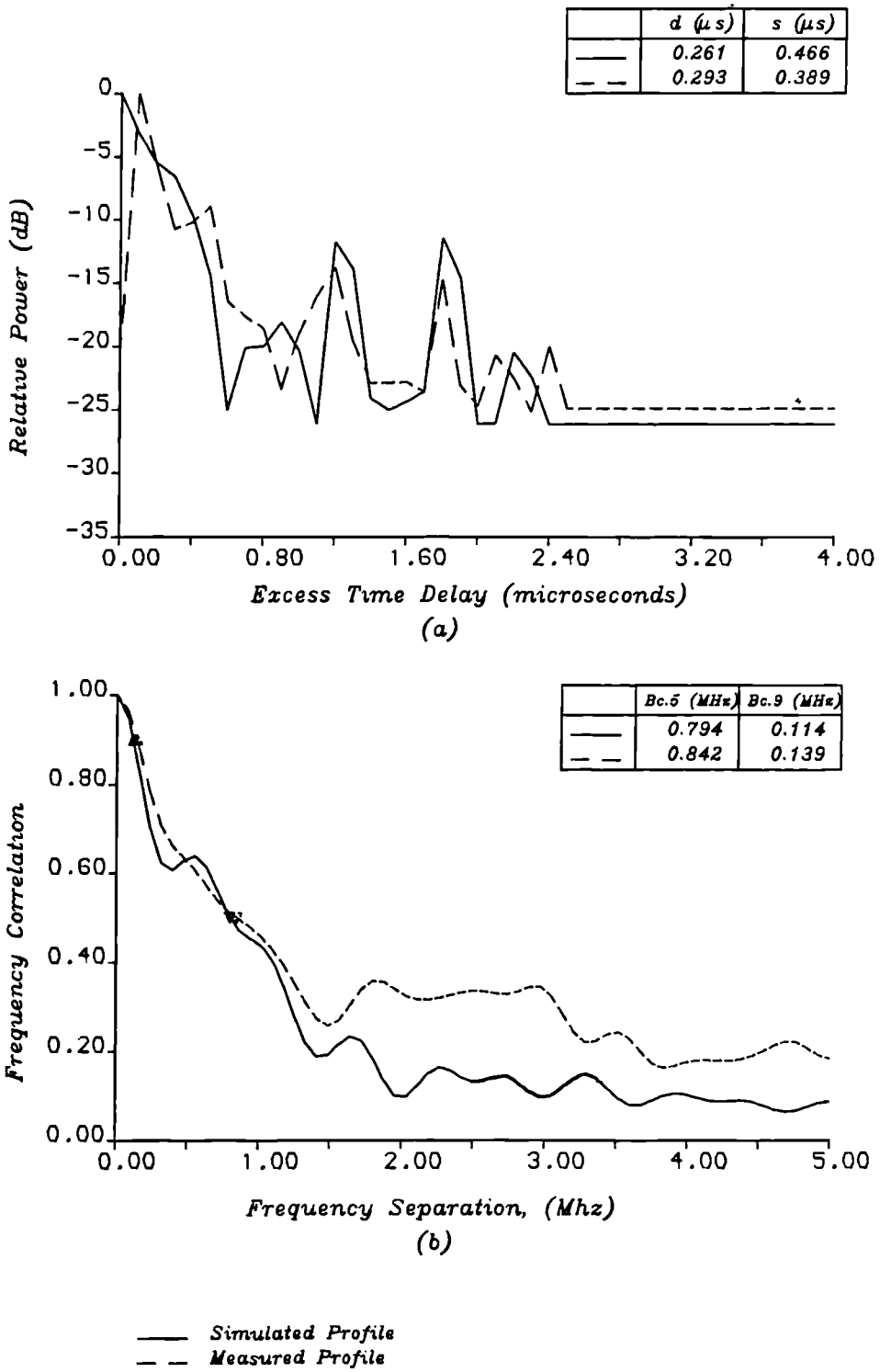

Figure (6.22) Small scale characteristics of Heyworth Street : simulation vs measured.

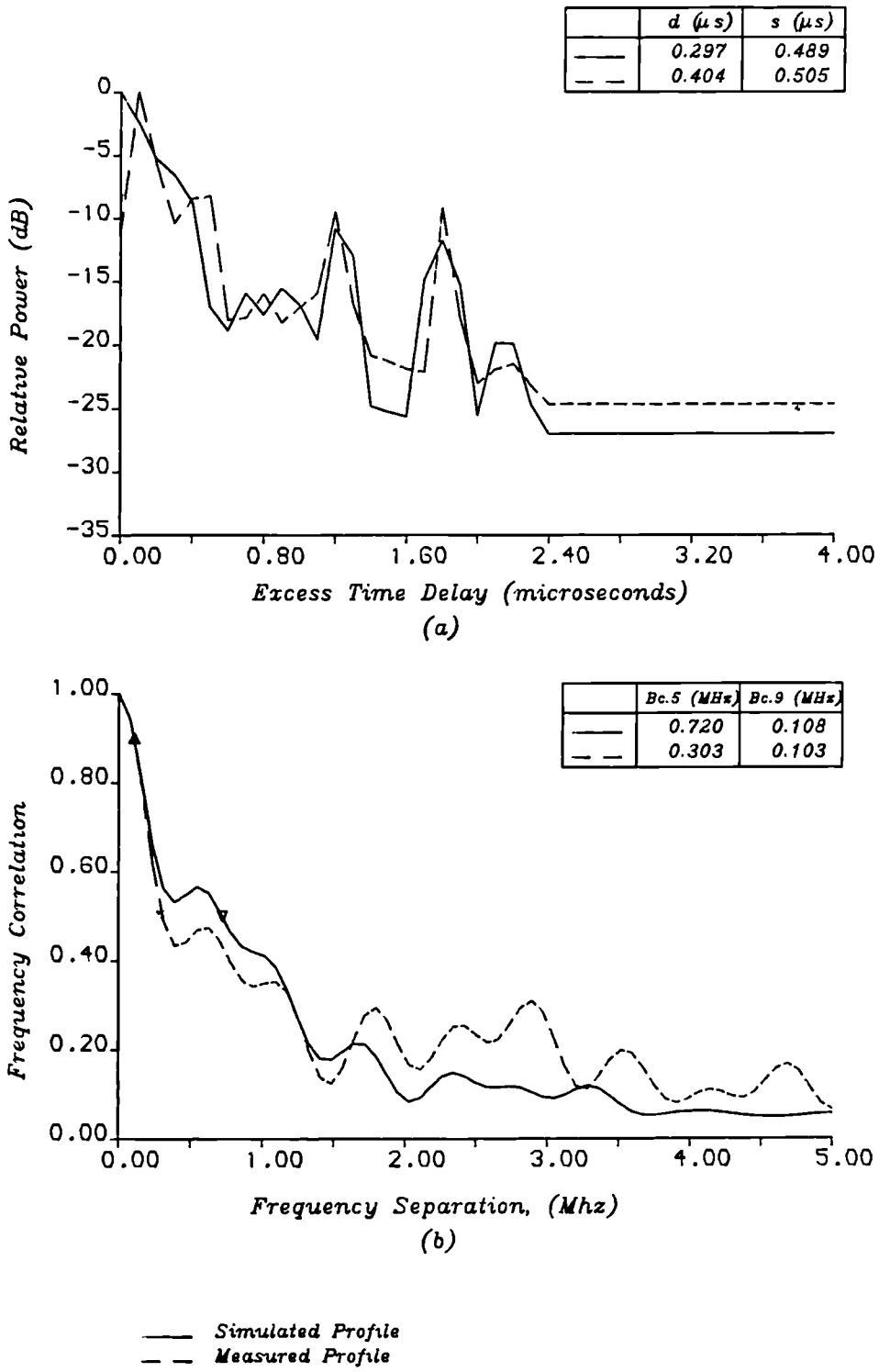

Figure (6.23) Small scale characteristics of Heyworth Street : simulation vs measured.

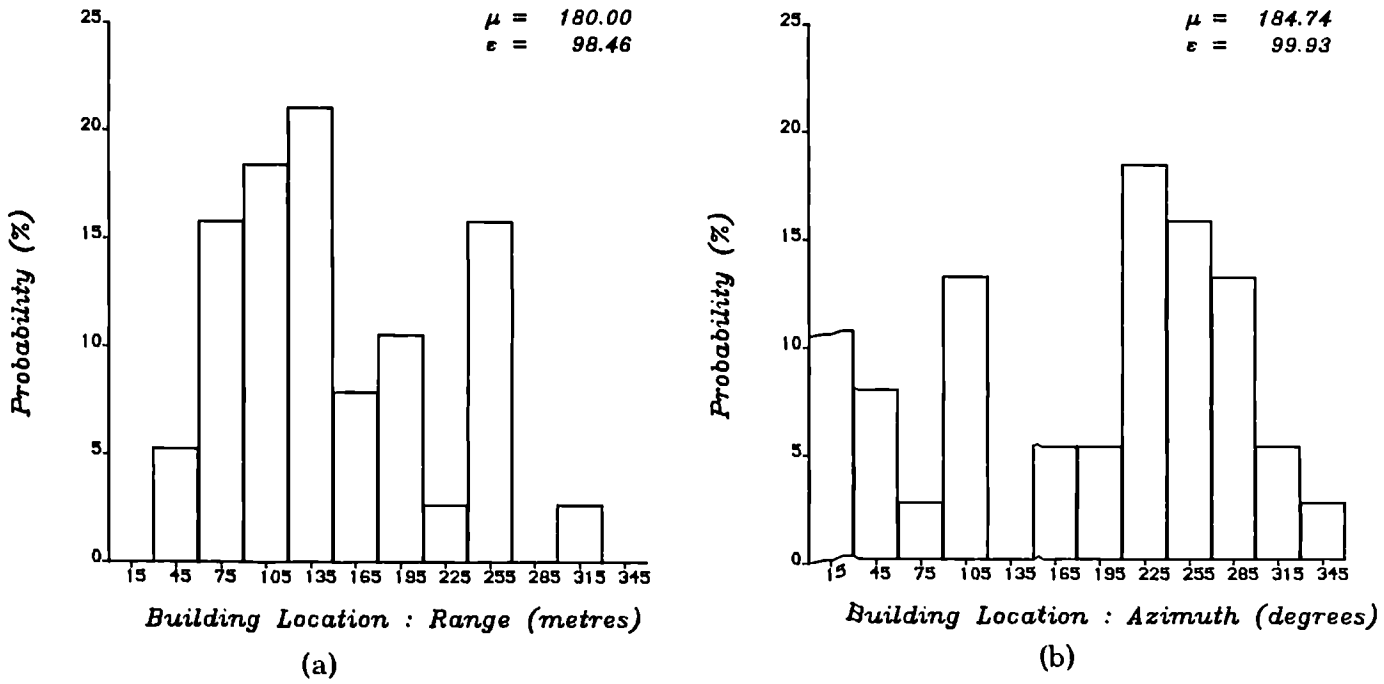

Figure (6.24) Location distributions for significant scatterers on Heyworth Street.

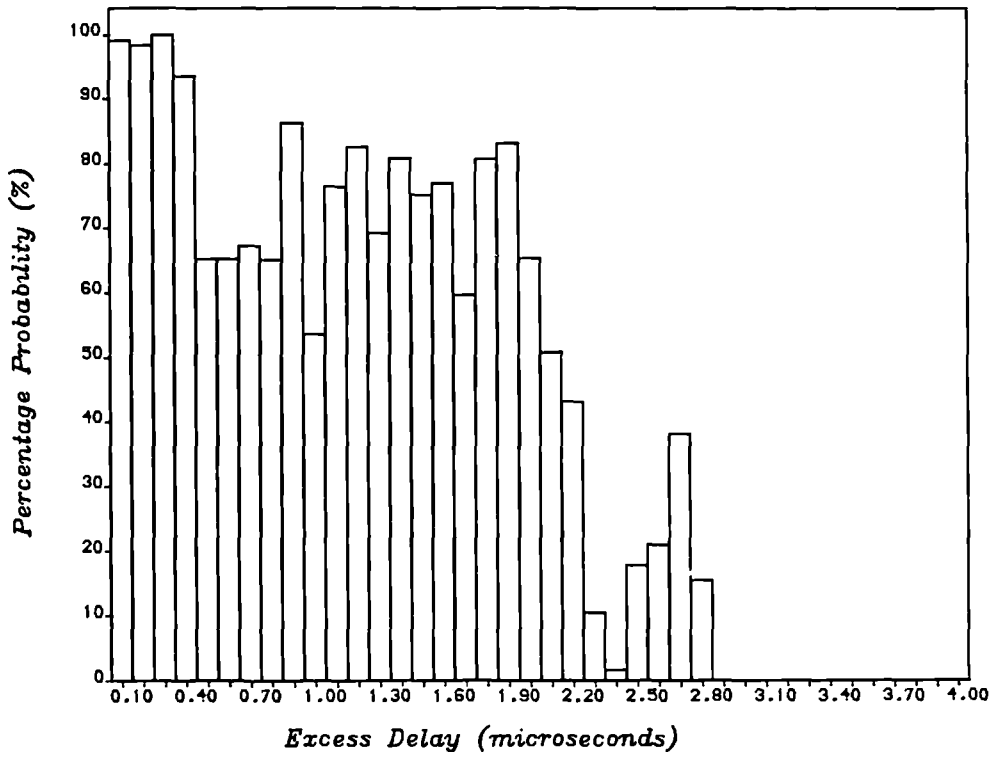

Figure (6.25) Echo path occupancy distribution for Heyworth Street.

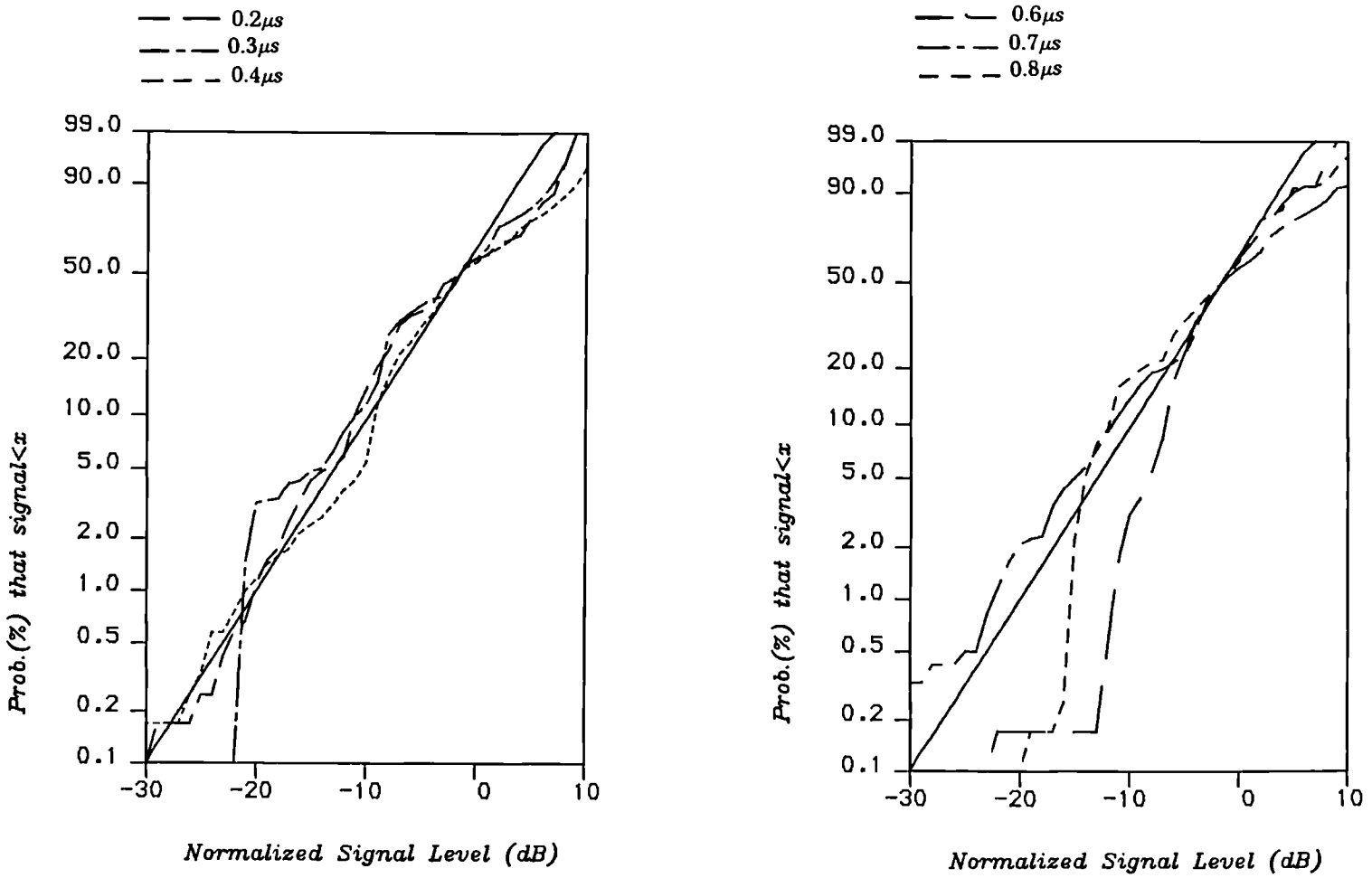

Figure (6.26) Amplitude distributions at fixed excess delays for Heyworth Street.

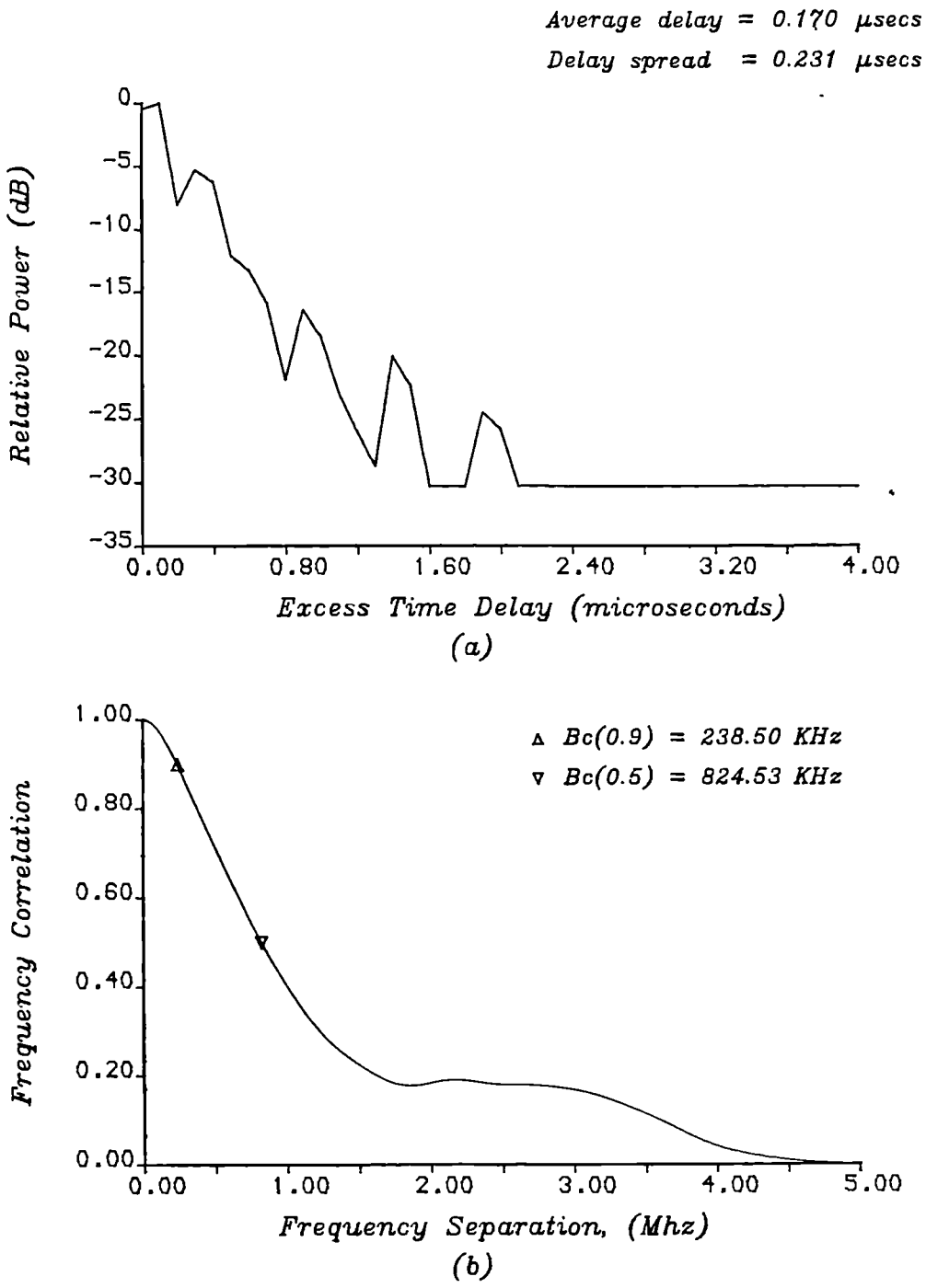

Figure (6.27) Small scale characteristics of Duke Street.

(a) Average power delay profile.

(b) Frequency correlation function.

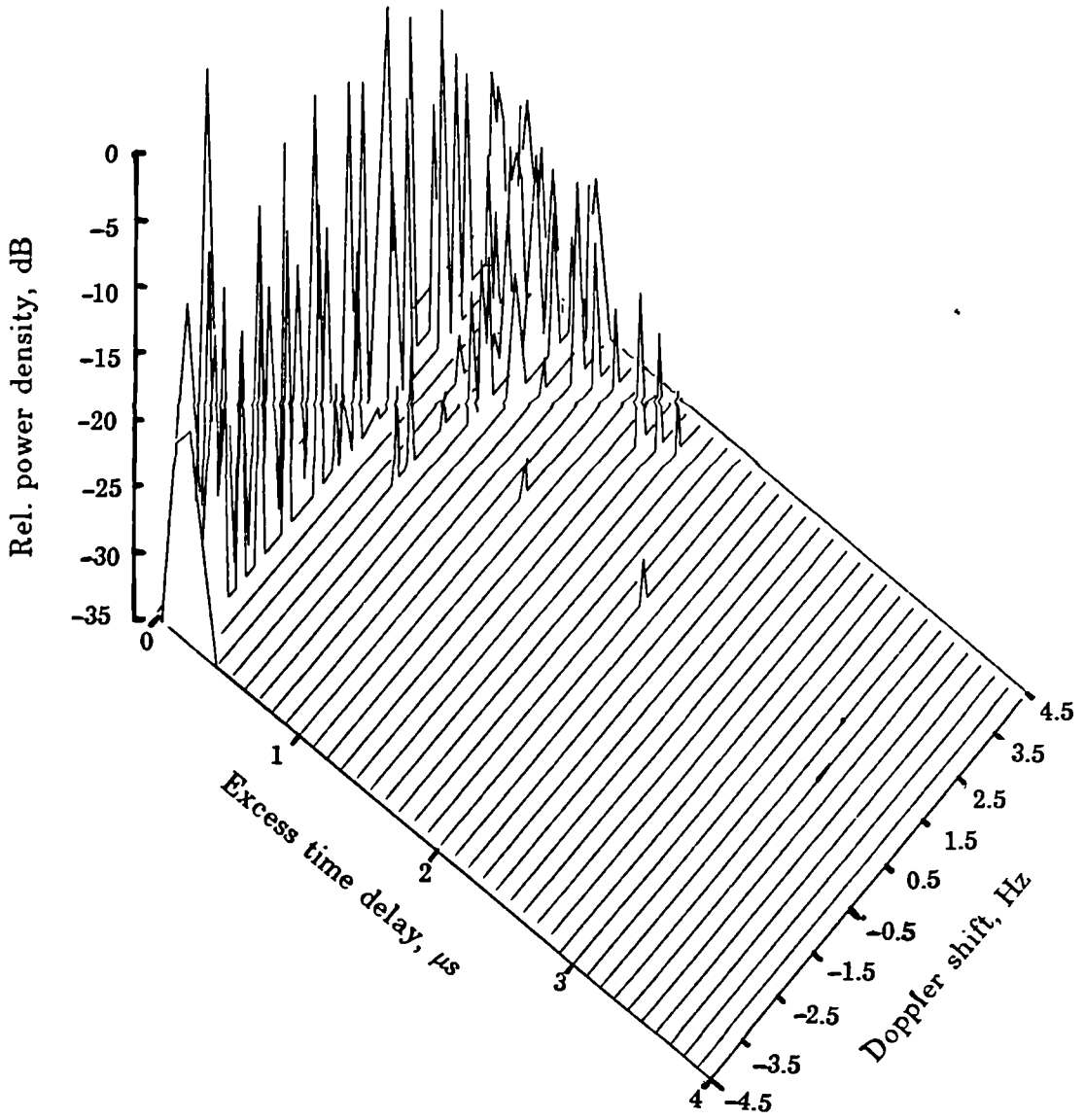

Figure (6.28) Scattering function for Duke Street : Simulation.

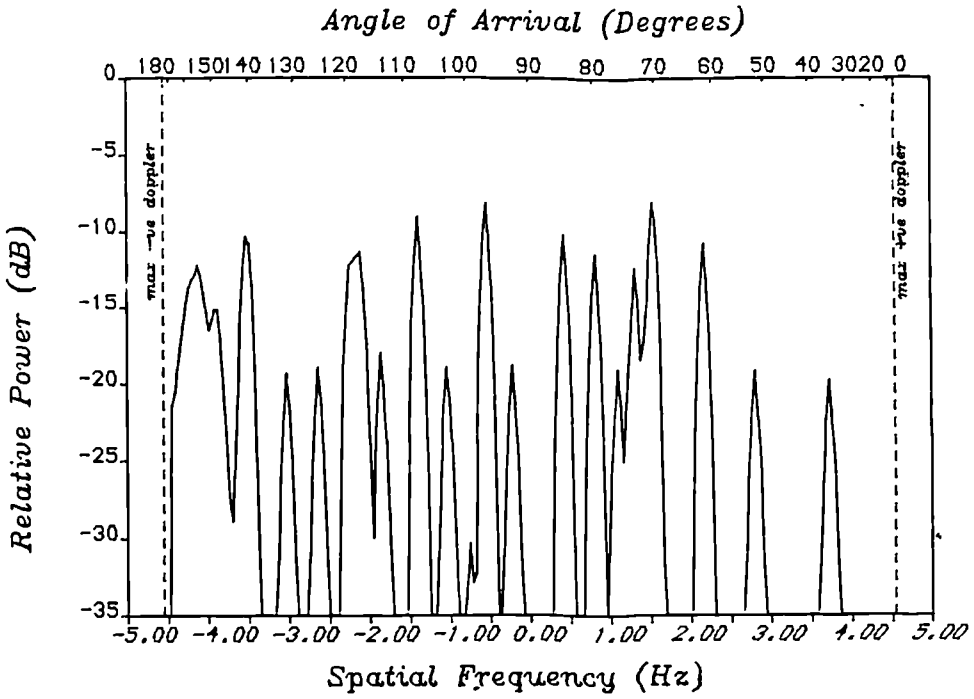

Figure (6.29a) Doppler spectrum at 0.2 μs excess delay on Duke Street.

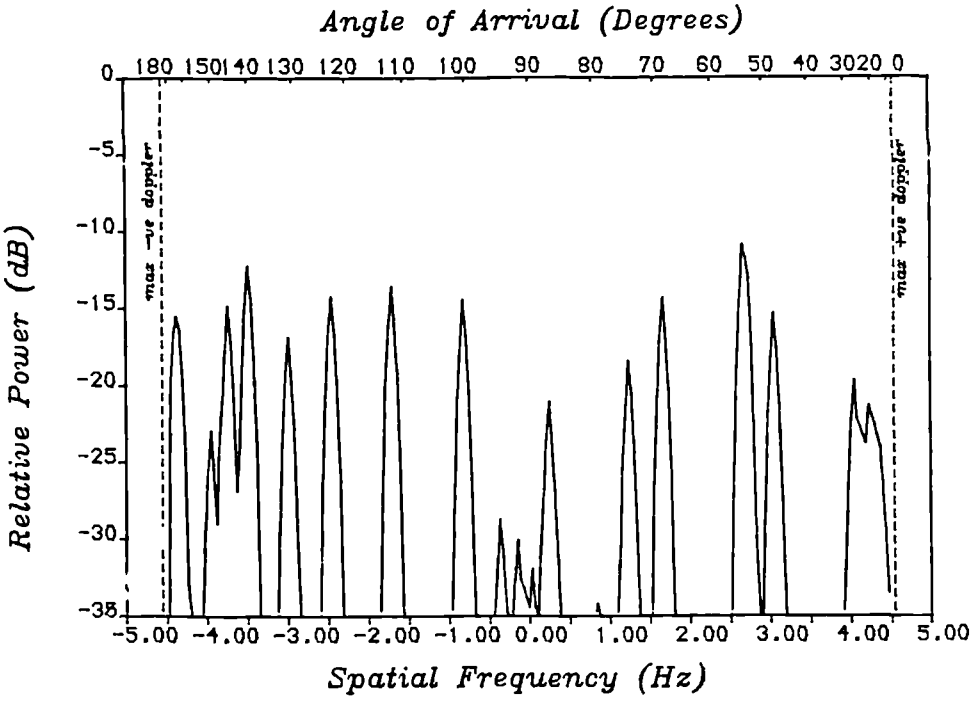

Figure (6.29b) Doppler spectrum at 0.3 μs excess delay on Duke Street.

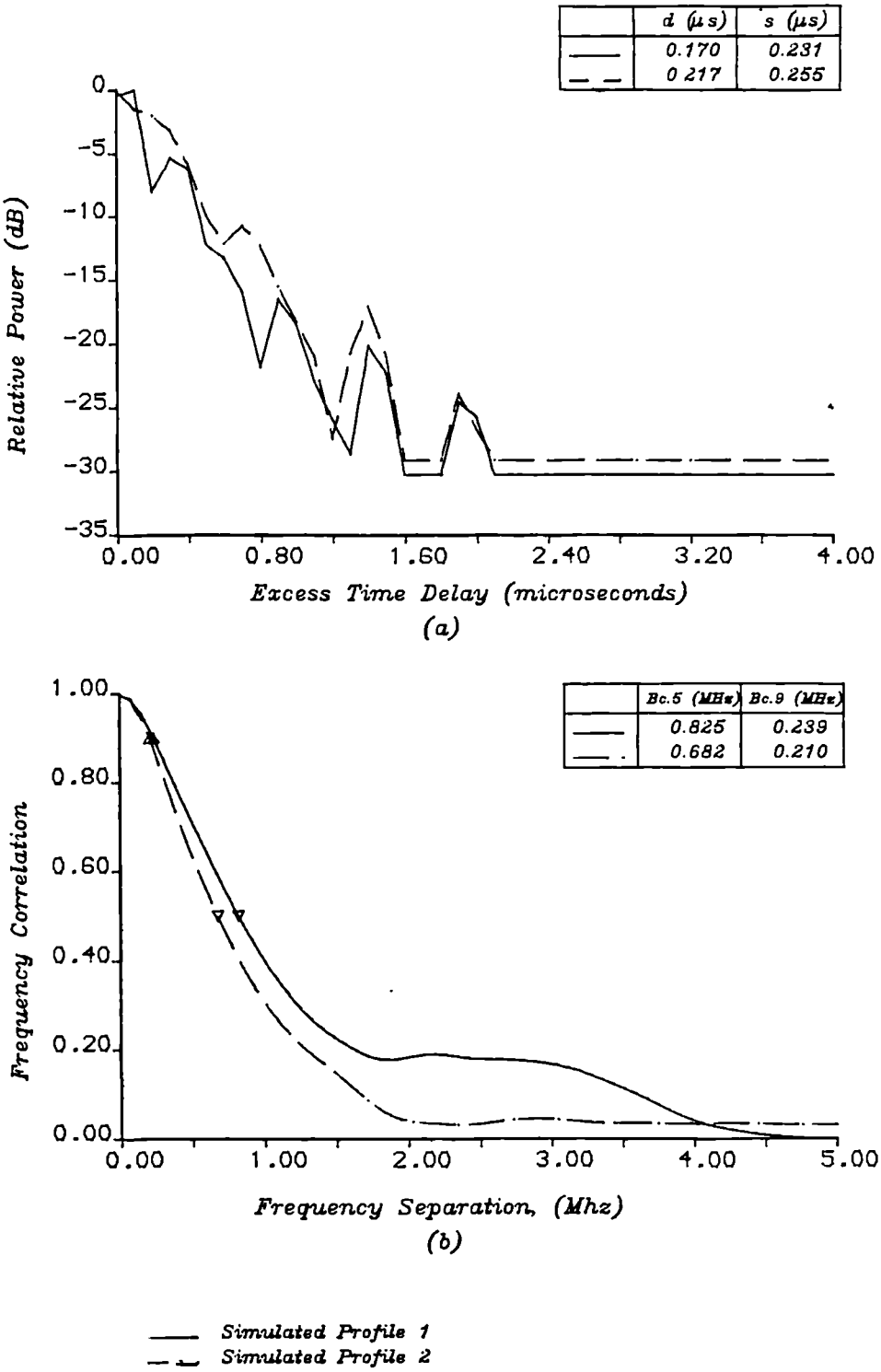

Figure (6.30) Small scale characteristics of Duke Street showing WSS behaviour of channel.
(two consecutive simulated average profiles)

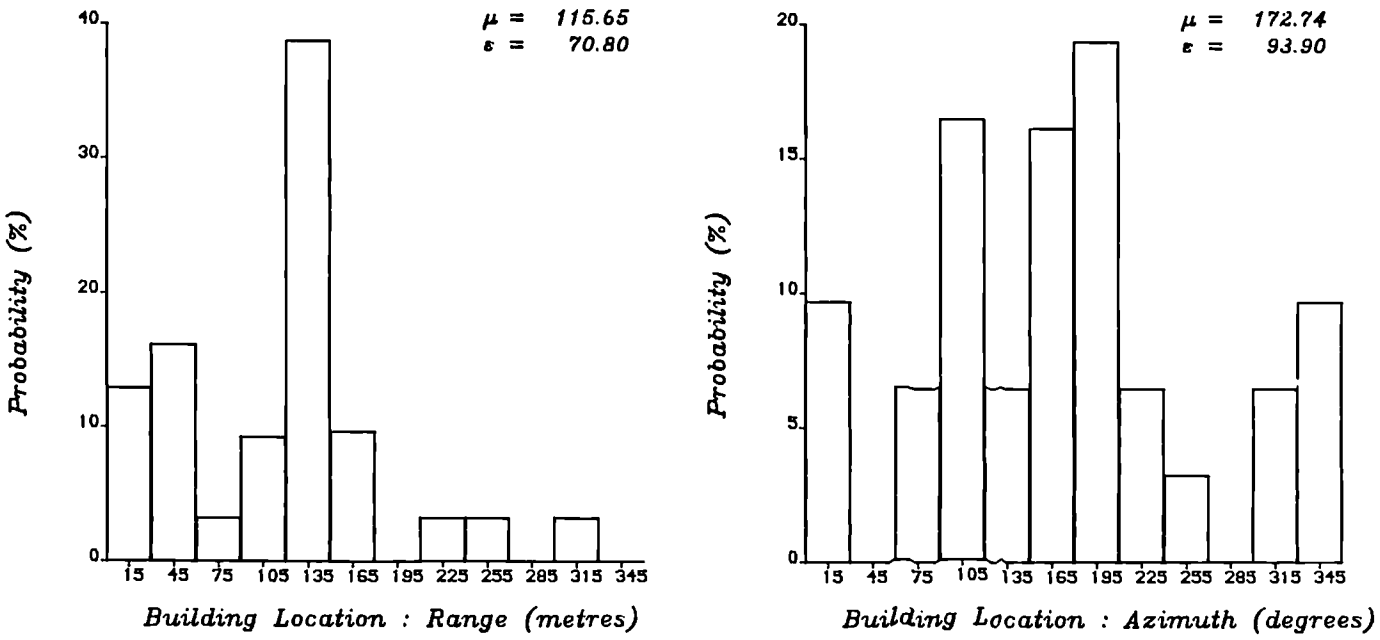

Figure (6.31) Location distributions for significant scatterers on Duke Street.

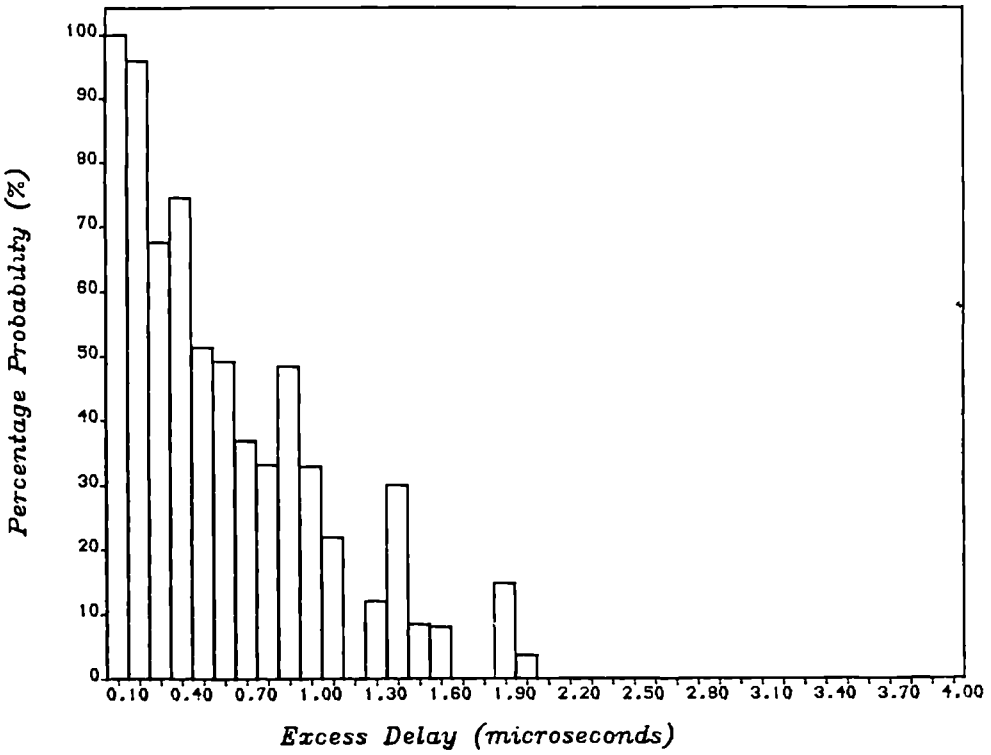

Figure (6.32) Echo path occupancy distribution for Duke Street.

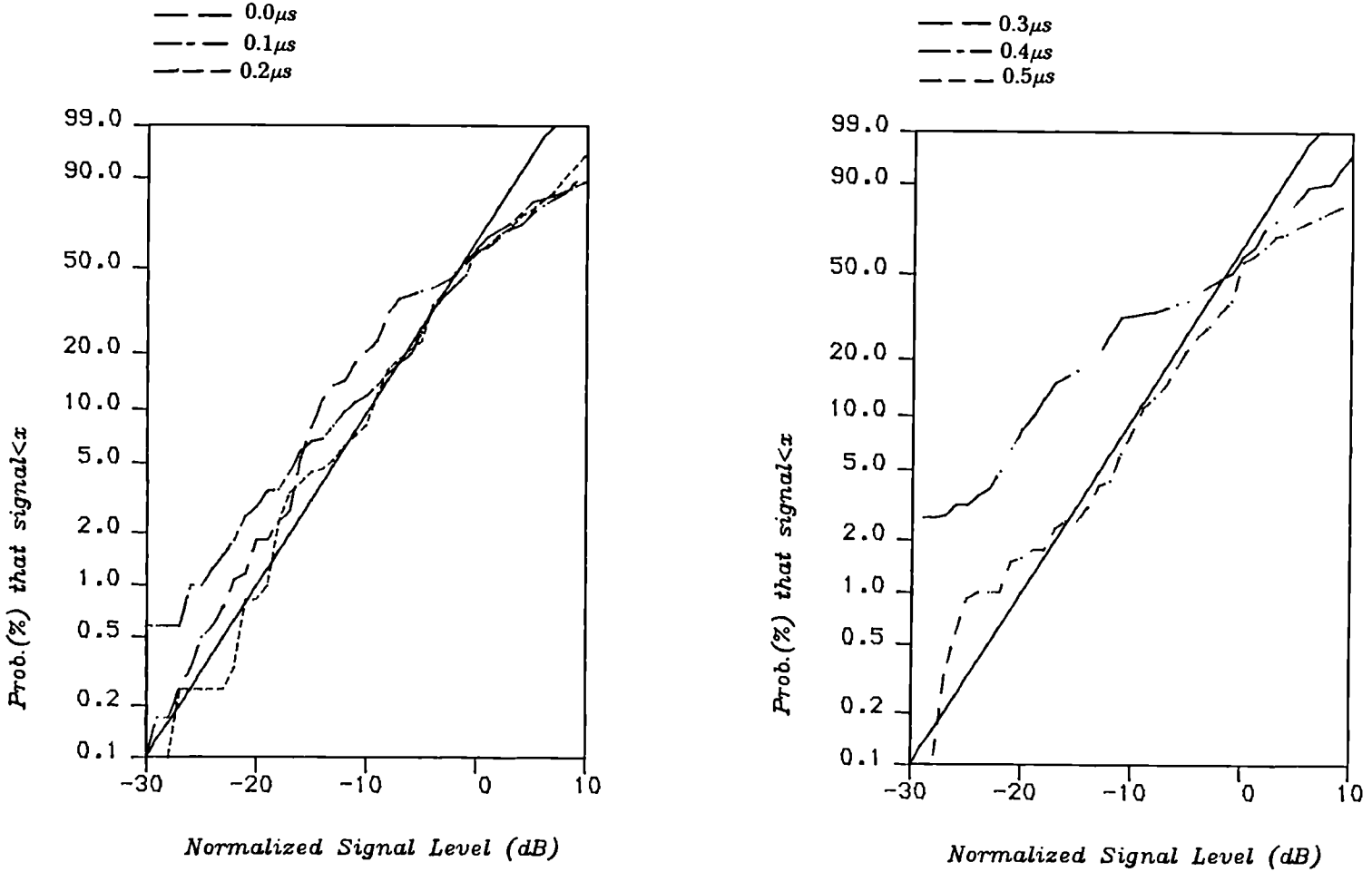

Figure (6.33) Amplitude distributions at fixed excess delays for Duke Street.

CHAPTER SEVEN

7. CONCLUSIONS

And on the seventh day ....., God rested from all his work which he had done in creation.
Genesis 2:2,3

A statistical multipath model for the echo time delays, amplitudes and carrier phase shifts caused by multipath propagation in a mobile radio channel has been derived. This model, based on a scattering approach, is simple and suitable for use in a software simulation of the channel as has been shown in this work. The model is directly dependent on the type of environment encountered in a mobile radio service area and its parameters include the location and size of the scatterers in the area.

The echo amplitude at the receiver is a function of the reflective property of the scatterer and its location with respect to the mobile. The reflection coefficient ρ, the measure of the reradiating capability of the scatterer, has been derived using the building size. In order to include the distance dependent wave intensity variations of em waves, recourse was made to geometric wave optics. The amplitude of the scattered wave was then shown to vary as the inverse of the distance between the scatterer and mobile. The inclusion of the reflection coefficient and distance-dependent factor ensures that the contributions of the scatterers are weighted in accordance with their physical properties. In addition, this approach is more representative of the situation in a physical channel as the simulation results have shown. This contrasts with Clarkes model of horizontally travelling, equal amplitude plane waves, a model which has always been widely used regardless of the fact that it is well known that the physical situation is otherwise.

The principal mode of propagation in this model is single scattering. The simulation results have been shown to compare very well with measured data and this would suggest that single scattering is a primary mode of propagation while multiple scattering is a secondary phenomenon. Although the model predicts very well the propagation characteristics for channels having excess delays up to 2 μs, it does not cope well with longer delays. It is thus primarily a local model.

By empowering the mobile to move in the simulation, and with the knowledge of the scatterer azimuth location, it has been possible to include the Doppler induced carrier phase shifts, a factor hitherto omitted from previous simulation models. The time delay-Doppler shift scattering function has been shown to give a good insight into radio channel propagation. It enables the identification of the significant propagation paths as has been illustrated in chapter 6.

Results have shown that the characteristics of the received signal is directly dependent on the type of landcover around the mobile. Only a fraction of the buildings within 250 metre radius of the mobile contribute to the scattering phenomenon, the values obtained in this work ranging from 10% to 16%.

A new classification of the types of environments encountered in a mobile radio service area has been developed. This classification provides precise quantitative definitions rather than the ambiguous and often subjective qualitative terms hitherto employed.

An extension of this study should include the effect of terrain features within the service area. The propagation characteristics in a town with hilly characteristics would differ from that on flat terrain. In addition, propagation over a mixed land and sea path could be studied and modelled. A means of incorporating some multiple scattering should be investigated bearing in mind that a limit will need to be set on the allowable number of reflections, as to do otherwise might lead to a model too complex to handle by its intended users.

The results of this channel simulation show that the model developed in this work can, with some confidence, predict the propagation characteristics in a wideband mobile radio channel in built-up areas.

REFERENCES

[1] JAKES,W.C ,Ed.:' Microwave Mobile Communications', J.Wiley & Sons, 1974.

[2] GRIFFITHS,J.:' Radio Wave Propagation and Antennas', Prentice-Hall, U.K, 1987.

[3] TURIN,G.L ,CLAPP,F.D ,JOHNSTON,T.L ,FINE,S.B ,LAVRY, D.:' A Statistical Model of Urban Multipath Propagation', IEEE Trans., Vol. VT-21, No.1, Feb. 1972, pp 1 - 9.

[4] COX,D.C :' Delay Doppler Characteristics of Multipath Propagation at 910 MHz in a Suburban Mobile Radio Environment', IEEE Trans., Vol. AP-20, No.5, Sept. 1972, pp 625-635.

[5] CLARKE,R.H :' A Statistical Theory of Mobile Radio Reception', Bell Syst. Tech. Jnl., Vol. 47, July 1968, pp 957-1000.

[6] GILBERT,E.N :' Energy Reception for Mobile Radio', Bell Syst. Tech. Jnl., Vol. 44, Oct 1965, pp 1779-1803.

[7] OSSANNA,J.F :' A Model for Mobile Radio Fading Due to Building Reflections: Theoretical and Experimental Fading Waveform Power Spectra', Bell Syst. Tech. Jnl., Vol. 43, Nov. 1964, pp 2935-2971.

[8] SUZUKI,H. :' A Statistical Model for Urban Radio Propagation', IEEE Trans., Vol. COM-25, No. 7, July 1977, pp 673-680.

[9] BAJWA,A.S :' Wideband Characterisation of UHF Mobile Radio Propagation in Urban and Suburban Areas', Ph.D Thesis, Department of Electronic and Electrical Engineering, University of Birmingham, UK, 1979.

[10] IEEE Transactions on Vehicular Technology, Special Issue on Mobile Radio Propagation, Vol. VT-37, No. 1, Feb. 1988.

[11] IKEGAMI,F. and YOSHIDA,S. :' Analysis of Multipath Propagation Structure in Urban Mobile Radio Environments', IEEE Trans., Vol. AP-28, No. 4, Jul. 1980, pp 531-537.

[12] BERTONI,H.L and WALFISCH,J. :' A Diffraction Based Theoretical Model for Prediction of UHF Path Loss in Cities', Proc. AGARD Conf., Terrestrial Prop. Characts. in Modern Systems, Ottawa, 1986, pp 8-1 - 1-9.

[13] BULLINGTON,K. :' Radio Propagation for Vehicular Communications', IEEE Trans., Vol. VT-26, No.4, Nov. 1977, pp295-308.

[14] BORN,M. and WOLF,E.: ' Principles of Optics ', Pergamon Press, Lon., 1965.

[15] FELSEN,L.B and MARCUVITZ,N. :' Radiation and Scattering of Waves', Prentice-Hall, Englewood Cliffs-N.J, 1973.

[16] LEE,W.C.Y :' Mobile Communications Engineering', McGraw-Hill, New York, 1982.

[17] HOLBECHE,R.J ,Ed.:' Land Mobile Radio Systems', IEEE Telecomms series 14, Peter Peregrinus ltd., Lon., 1985.

[18] SHEPHERD,N.H :' UHF Radio Wave Propagation in Dallas, Texas Base to Mobile Stations for Vertical Polarisation', Gen. Elec. Tech. Inf. Series, R75-MRD-1, Mar. 1975.

[19] HASHEMI,H. :' Simulation of the Urban Radio Propagation Channel', IEEE Trans., Vol. VT-28, No.3, Aug. 1979, pp 213-225.

[20] BELLO,P.A :' Characterisation of Randomly Time Variant Linear Channels', IEEE Trans.on Comm. Syst., Vol. CS-11, Dec. 1963, pp 360-393.

[21] KAILATH,T. :' Sampling Models for Linear Time Variant Filters', M.I.T Research Lab. of Electronics, Cambridge Mass., Rept No 352, May 1959.

[22] KENNEDY,R.S :' Fading Dispersive Communication Channels', J.Wiley, New York, 1969.

[23] HATA,M. :' Empirical Formula for Propagation Loss in Land Mobile Radio Services', IEEE Trans., Vol. VT-29, No.3, Aug. 1980, pp 317-325.

[24] ZADEH,L.A :' Frequency Analysis of Variable Networks', Proc. IRE, Vol. 38, Mar. 1950, pp 291-299.

[25] ZANDER,J. :' A Stochastical Model of the Urban UHF Radio Channel', IEEE Trans., Vol. VT-30, No.4, Nov. 1981, pp 145-155.

[26] COX,D.C :' 910 MHz Urban Mobile Radio Propagation Multipath Characteristics in New York City', IEEE Trans., Vol. COM-21, No.11, Nov. 1973, pp 1188-1194.

[27] BAJWA,A.S and PARSONS,J.D :' Small Area Characterisation of UHF Urban and Suburban Mobile Radio Propagation', IEE Proc., Pt.F, No.2, Apr. 1982, pp 102-109.

[28] JAO,J.K :' Amplitude Distribution of Composite Terrain Radar Clutter and the K-Distribution', IEEE Trans., Vol. AP-32, No.10, Oct.1984, pp 1049-1062.

[29] KOZONO,S. and WATANABE,K. :' Influence of Environmental Buildings on UHF Land Mobile Radio Propagation', IEEE Trans., Vol. COM-25, No.10, Oct.1977, pp 1133-1143. (Correction in COM-26, Jan.1978, pp 199-200)

[30] IBRAHIM,M.F and PARSONS,J.D :' Signal Strength Prediction in Built Up Areas. Part 1: Median Sitnal Strength ', IEE Proc., Vol. 130, Pt.F, No.5, Aug.1983, pp 377-384.

[31] HUISH,P.W and GURDENLI,E. :' Radio Channel Measurement and Prediction for Future Mobile Radio Systems', Br.Telecom.Tech.Jnl, Vol. 6, No.1, Jan. 1988, pp 43-53.

[32] OKUMURA,Y., OHMORI,E., KAWANO,T. and FUKUDA,K. :' Field Strength and Its Variability in VHF and UHF Land Mobile Radio Service',Review of the Electrical Communication Laboratory, Vol. 16, No.9-10, Sept-Oct 1968, pp 825-873.

[33] KING,R.W and CAUSEBROOK,J.H :' Computer Programs For UHF Co-channel Interference Prediction Using a Terrain Data Bank ', BBC Research Report, BBC RD 1974/6.

[34] LORENZ,R.W :' Field Strength Prediction Program DBPR1, COST 207 Technical Document', COST 207 TD(86)#02, 1986.

[35] JUUL-NYHOLM,G. :' Land Usage Figures For Use in Field Strength Prediction as Measured in Denmark',COST 207 Technical Document, COST 207 TD(86)#28, 1986.

[36] Lord CHORLEY (Chairman) : 'Handling Geographic Information', HMSO, London, 1987.

[37] KAFARU,O.O, BAJWA,A.S and PARSONS,J.D :'An Environment- Dependent Approach to Wideband UHF Multipath Propagation Modelling', IERE Fourth International Conference on Land Mobile Radio, University of Warwick, Dec. 1987, pp 121-127.

[38] HAUSNER,M. :' A Vector Space Approach to Geometry', Prentice Hall, N.J, 1965, pp 169-190.

[39] BELLO,P.A :' Time - Frequency Duality ', IEEE Trans.Inf.Theory, Vol. IT-10, Jan. 1964, pp 18-33.

[40] BELLO,P.A and NELIN,B.D :' The Effect of Frequency Selective Fading on the Binary Error Probabilities of Incoherent and Differentially Coherent Matched Filter Receivers ' IEEE Trans.on Comm. Syst., Jun. 1963, pp 170-186.

[41] PAPOULIS,A,:' The Fourier Integral And Its Applications', McGraw-Hill, New York, 1962.

[42] PRICE,R. and GREEN,P.E :' Communication Technique for Multipath Channels', Proc. IRE, Mar.1958, pp 555-570.

[43] NIELSON,D,L :' Microwave Propagation Measurements for Mobile Digital Radio Application ', IEEE Trans. Veh. Tech., Vol VT-27, No.3, Aug.1978, pp 117-132.

[44] RICE,S.O :' Statistical Properties of a Sine Wave plus Random Noise', Bell Sys.Tech.Jnl, Vol 27, Jan.1948, pp 109-157.

[45] SLACK,M :' The Probability Distributions of Sinusoidal Oscillations Combined in Random Phase', Jnl. IEEE, Vol 93, 1946, pp 76-86.

[46] BENNETT,W.R :' Distribution of the Sum of Randomly Phased Components', Quart.Appl.Maths, Vol 5, Jan.1948, No.4, pp 385-393.

[47] SMITH,J.I :' A Computer Generated Multipath Fading Simulation for Mobile Radio', IEEE Trans.Veh.Tech., Vol VT-24, No.3, Aug.1975, pp 39-40.

[48] ARNOLD,H.W and BODTMAN,W.F :' A Hybrid Multichannel Hardware Simulator for Frequency Selective Mobile Radio Paths', IEEE Trans. Comm., Vol COM-31, No.3, Mar.1983, pp 370-377.

[49] CAPLES,E.L, MASSAD,K.E and MINOR,T.R :' A UHF Channel Simulator for Mobile Radio', IEEE Trans.Veh.Tech., Vol VT-29, No.2, May 1980, pp 281-289.

[50] ARREDONDO,G.A, WILLIAM,H.C and WALKER,E.H :' A Multipath Fading Simulator for Mobile Radio ',IEEE Trans.Comm., Vol COM-21, No.11, Nov.1973, pp 1325-1328.

[51] GLADSTONE,K.J and MCGEEHAN,J.P :' Computer Simulation of Multipath Fading in the Land Mobile Radio Environment', IEE Proc., Vol.127, Pt.G, No.6, Dec.1980, pp 323-326.

[52] TURIN,G.L :' Introduction to Spread Spectrum Antimultipath Techniques and their Application to Urban Digital Radio', Proc. IEEE, Vol.68, No.3, Mar.1980, pp 328-353.

[53] MENTZER,J.R :' Scattering and Diffracton of Radio Waves', Pergamon Press, New York, 1955.

[54] MARION,J.B :' Classical Electromagnetic Radiation', 2nd edition, Academic Press, New York, 1980.

[55] KLINE,M and KAY,I.W :' Electromagnetic Theory and Geometrical Optics', Krieger Pub. Co., New York, 1979.

[56] KELLER,J.B, LEWIS,R.M, and SECKLER,B.D :' Asymptotic Solution of Some Diffraction Problems, Comm. Pure & App.Maths', vol.9, 1956, pp 207 - 265.

[57] STRATTON,J.A :' Electromagnetic Theory', McGraw-Hill Inc., 1941.

[58] LONGHURST,R.S :'Geometrical and Physical Optics ', Longmans 1957

[59] SCHWARTZ,M., BENNETT,W.R. and STEIN,S. :' Communication Systems and Techniques', McGraw-Hill, N.Y., 1966

[60] BANKS,J. and CARSON II,J.S :' Discrete-Event System Simulation ', Prentice-Hall, N.J, 1984.

[61] SHANNON,R.E :' Systems Simulation: the art and science', Prentice- Hall, N.J, 1975.

[62] GOLOMB,S.W Ed. :' Digital Communications With Space Applications ', Prentice-Hall, N.J, 1964.

[63] COX,D.C :' Time and Frequency Domain Characterisation of Multipath Propagation at 910 MHz in a Suburban Mobile Radio Environment', Radio Science, Vol.7, No.12, Dec.1972, pp 1069-1077.

[64] IKEGAMI,F., and YOSHIDA,S.:' Feasibility of Predicting Mean Field Strength for Urban Mobile Radio by Aid of Building Data Bases', IEEE Int. Conf. Comms., Mass., June 1983, Vol.1, pp 68 - 71.

[65] IKEGAMI,F., YOSHIDA,S., TAKEUCHI,T. and UMEHIRA,M. : 'Propagation Factors Controlling Mean Field Strength on Urban Streets', IEEE Trans. Ant.& Prop., Vol. AP-32, No.8, Aug.1984, pp 822 - 829.

[66] BAJWA,A.S and PARSONS,J.D.:' Small-area Characterisation of UHF Urban and Suburban Mobile Radio Propagation', IEE Proc, Pt.F, Vol.129, No.2, Apr.1982, pp 102-109.

[67] BAJWA,A.S and PARSONS,J.D.:' Large-area Characterisation of UHF Urban Multipath Propagation and Its Relevance to the Performance bounds of Mobile Radio Systems', IEE Proc, Pt.F, Vol.132, No.2, Apr.1985, pp 99-106.

[68] PARSONS,J.D and BAJWA,A.S.:' Wideband Characterisation of Fading Mobile Radio Channels', IEE Proc, Pt.F, Vol.129, No.2, Apr.1982, pp 95-101.

[69] BAJWA,A.S.:' UHF Wideband Statistical Model and Simulation of Mobile Radio Multipath Propagation Effects', IEE Proc, Pt.F, Vol.132, No.5, Aug.1985, pp 327-333.

[70] DAVIES,W.S.:' Physical Optics Estimation of Urban Mobile Radio Channel Delay-Doppler Responses', Arch. Electron Uebertrag. Tech. (West Germany), Band 41, Heft 6, Nov-Dec.1987, pp 341-346.

[71] TERMAN,F.E.:' Electronic and Radio Engineering', McGraw-Hill, New York, 1955, Chap.22

[72] MIDDLETON,D.:' Statistical - Physical Models of Urban Radio Noise Environments. Part I: Foundations ', IEEE Trans. Elec.Comp., Vol EMC-14, No.2, May 1972, pp 38-56.

[73] MIDDLETON,D.:' Man-made Noise in Urban Environments and Transportation Systems : Models and Measurements', IEEE Trans.Coms., Vol COM-21, No.11, Nov 1973, pp 1232-1241.

[74] LEE,W.C.Y.:' Estimate of Local Average Power of a Mobile Radio Signal', IEEE Trans.Veh.Tech., Vol.VT-34, No.1, Feb.1985, pp 22-27.

[75] ALLESBROOK,K. and PARSONS,J.D.:' Mobile Radio Propagation in British Cities at Frequencies in the VHF and UHF Bands', IEEE Trans.Veh.Tech., Vol VT-26, No.4, Nov.1977, pp 313-323.

[76] DELISLE,G.Y., LEFEVRE,J.P., LECOURS,M. and CHOUINARD,J.Y.: 'Propagation Loss Prediction: A Comparative Study with Application to the Mobile Radio Channel', IEEE Trans.Veh.Tech., Vol.VT-34, No.2, May 1985, pp 86-96.

[77] DADSON,C.E, DURKIN,J. and MARTIN,R.E.:' Computer Prediction of Field Strength in the Planning of Radio Systems', IEEE Trans.Veh. Tech., Vol.VT-24, No.1, Feb.1975, pp 1-8.

[78] FRENCH,R.C.:' The Effect of Fading and Shadowing on Channel Reuse in Mobile Radio', IEEE Trans.Veh.Tech., Vol.VT-28, No.3, Aug.1979, pp 171-181.

[79] COX,D.C. and LECK,R.P.:' Correlation Bandwidth and Delay Spread Multipath Propagation Statistics for 910 MHz Urban Mobile Radio Channels', IEEE Trans.Comm., Vol.COM-23, No.11, Nov.1975, pp 1271 - 1280.

[80] COX,D.C. and LECK,R.P.:' Distribution of Multipath Delay Spread and Average Excess Delay for 910 MHz Urban Mobile Radio Paths ', IEEE Trans.Ant.& Prop., Vol.AP-23, No.2, Mar.1975, pp 206-213.

[81] REES,J.V.:' Measurements of the Wideband Radio Channel Characteristifs for Rural, Residential and Suburban Areas', IEEE Trans.Veh.Tech., Vol.VT-36, No.1, Feb.1987, pp 1-6.

[82] KERR,D.E.,Ed.:' Propagation of Short Radio Waves', P. Peregrinus Ltd., Lon., 1987.

[83] PICQUENARD,A.:' Radio Wave Propagation', Macmillan, Lon., 1974.

[84] BAKER,B.B and COPSON,E.T.:' The Mathematical Theory of Huygen's Principle', Oxford Press, 1939.

[85] JORDAN,E.C and BALMAIN,K.G..:' Electromagnetic Waves and Radiating Systems, 2nd ed., Prentice-Hall, Englewood Cliffs, N.J, 1968.

[86] MIDDLETON,D.:' A Statistical Theory of Reverberation and similar First Order Scattered Fields, Part I, Waveforms and the General Process', IEEE Trans.Inform.Theory, Vol IT-13, No.3, Jul.1967, pp 372-392.

[87] MIDDLETON,D.:' Statistical - Physical Models of Electromagnetic Interference', IEEE Trans. Elec.Comp., Vol EMC-19, No. , 1977, pp 106-127

[88] GIORDANO,A.A and HABER,F.:' Modelling of Atmospheric Noise', Radio Science, Vol.7, No. , 1972, pp 1011-1023.

[89] Ordnance Survey Information :' Digital Mapping', Leaflet No.48, OS, Southampton, April 1986.

[90] RALPHS,J.D and SLADEN,F.M.E.:' An H.F Channel Simulator Using a New Rayleigh Fading Method', The Radio and Electronic Engineer, Vol.46, No.12, Dec. 1976, pp 579 - 587.

[91] LAW,H.B., LEE,F.J., LOOSER,R.C and LEVETT,F.A.W.:' An Improved Fading Machine', Proc. Inst. Electr. Engnrs., Vol.104, Part B, 1952, pp 117-147.

[92] BECK,D. and BETTS,J.A.:' Fading Machine For the Simulation of the ionosphere', Electron. Engng, Vol.37, Feb.1965, pp 74-79.

[93] YOUNG,W.R. and LACY,L.Y :' Echos in Transmission at 450 Megacycles From Land-to-Car Radio Units', Proc. IRE, Vol.38, Mar.1950, pp 255-258.

[94] BAILEY,C.C :' Characterisation of Tropospheric Scatter Channels by Impulse Response Measurements', AGARD 16th Symposium, Aug-Sept 1970, Dusseldorf, Part II, pp 39-1 to 39-11.

[95] MAYNARD,J. :'Modular Programming ', Auerbach Publishers, Princeton, N.J, 1972.

APPENDIX A

The Multipath Geometric Relationships.

To obtain d_s, consider the triangle of T, S_i and (0,0) of Figure (A1). It is seen that

$$a = d_s \cos\alpha \tag{A.1}$$

and

$$b = R_i \cos\beta \tag{A.2}$$

so that

$$Z = a + b = d_s \cos\alpha + R_i \cos\beta \tag{A.3}$$

From equation (A.3)

$$d_s \cos\alpha = Z - R_i \cos(180 - \phi) \tag{A.4}$$

For $Z >> R_i$, α is very small, hence $\cos\alpha \simeq 1$.

Hence, using the relationship $\cos(\pi - x) = -\cos x$, equation (A.4) becomes

$$d_s = Z + R_i \cos\phi \tag{A.5}$$

Similarly to obtain r_i, consider the triangle of S_i, M and (0,0) of Figure (A2).

$$c = r_i \cos\psi \tag{A.6}$$

and

$$d = m \cos \gamma \tag{A.7}$$

so that

$$R_i = c + d = r_i \cos \psi + m \cos \gamma \tag{A.8}$$

From equation (A.8)

$$r_i \cos \psi = R_i - m \cos(\phi - \eta) \tag{A.9}$$

For $R_i > > m$, ψ is very small, hence $\cos \psi \simeq 1$.

Therefore equation (A.9) becomes

$$r_i = R_i - m \cos(\phi - \eta) \tag{A.10}$$

The distance from T to M via S_i is d_i and is given by

$$\begin{aligned} d_i &= d_s + r_i \\ &= Z + R_i(1 + \cos \phi) - m \cos(\phi - \eta) \end{aligned} \tag{A.11}$$

The propagation delay time τ_i for scatterer i is related to the distance d_i traversed by the relationship

$$\tau_i = \frac{d_i}{c} \tag{A.12}$$

where c = velocity of light.

Hence from equations (A.11) and (A.12), we obtain τ_i, the propagation delay for the echo caused by scatterer i as

$$\tau_i = \frac{1}{c}[Z + R_i(1 + \cos \phi) - m \cos(\phi - \eta)] \tag{A.13}$$

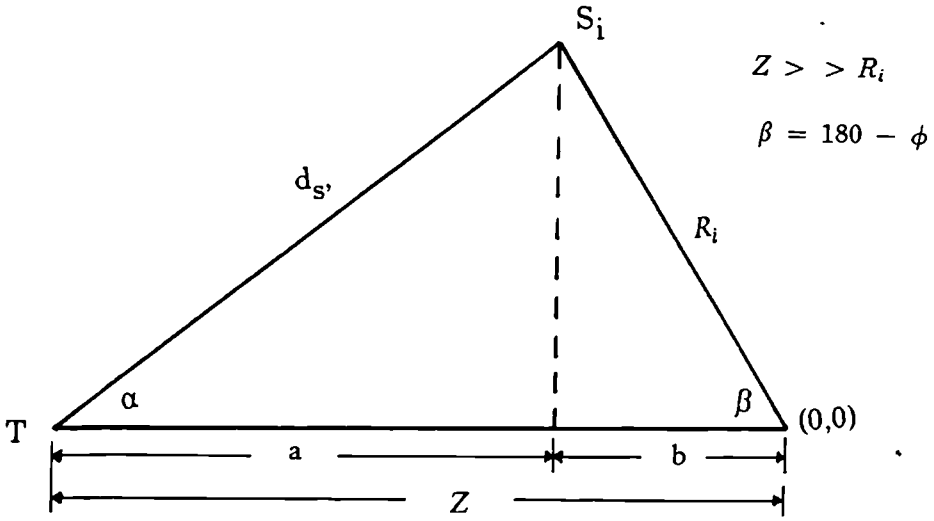

Figure A1. Derivation of d_s.

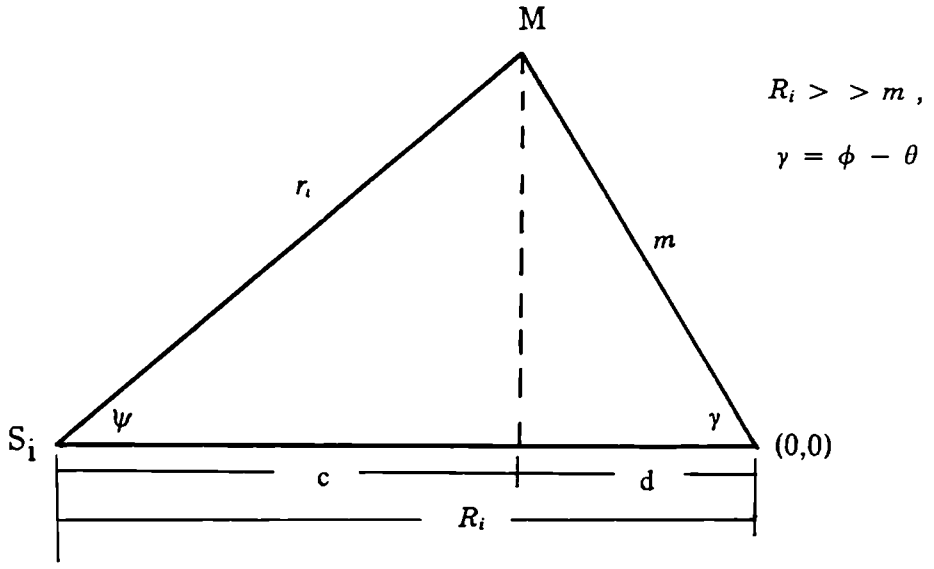

Figure A2. Derivation of r_i.

APPENDIX B

The Geometric Wave Optics Method.

The geometric wave optics approach, first introduced by Luneberg, is here applied to the derivation of the amplitude of the scattered wave component. From Maxwell's equations in a source-free isotropic, homogeneous medium, the electric field satisfies the Helmholtz equation [56]

$$\nabla^2\hat{E} + k^2\hat{E} = 0 \qquad (B.1)$$

subject to the condition that

$$\nabla.\hat{E} = 0 \qquad (B.2)$$

where

k = phase constant $\left(\frac{2\pi}{\lambda}\right) = \frac{\omega}{c}$

ω = angular frequency of the source

λ = wavelength of the source

c = speed of light

The asymptotic expansion of the electric field for k, apart from the time factor $\exp(j\omega t)$ is of the form

$$\hat{E}(x,y,z) \sim \exp(-jk\psi)\sum_n (jk)^{-n}\hat{E}_n(x,y,z) \qquad (B.3)$$

Inserting (B.3) in (B.1) and equating to zero the coefficients of each power of k, we obtain

$$(\nabla.\psi)^2 = 1 \qquad (B.4)$$

$$2\nabla.\hat{E}_n\nabla.\psi + \hat{E}_n\nabla^2\psi = -\nabla^2\hat{E}_{n-1} \quad n = 0, 1, ..., \infty, \ \hat{E}_{-1} = 0 \qquad (B.5)$$

Equation (B.4) is the eiconal equation of geometrical optics and determines the phase function ψ. Equations (B.5) are a recursive system which can be used for determining the $\hat{E}_n$ successively.

$\hat{E}_n\nabla.\psi = \frac{d\hat{E}_n}{ds}$ where s denotes the arc length along a ray (i.e the curve orthogonal to the wavefronts ψ = constant). The solution of (B.5) along a ray is

$$\hat{E}_n(s) = \hat{E}_n(s_o)\left[\frac{G(s)}{G(s_o)}\right]^{\frac{1}{2}} - \sqrt{G}\,(s)\int\sqrt{G}\,(p)\,\nabla^2.\hat{E}_{n-1}(p)dp \qquad (B.6)$$

where

G(s) = the curvature of the wavefront at the point s on a ray
(or the Gaussian curvature)

s_o = the reference point.

For n = 0, the integral on the right hand side of equation (B.6) vanishes and we obtain the high frequency limit of interest given by

$$\hat{E}_o(s) = \hat{E}_n(s_o)\left[\frac{G(s)}{G(s_o)}\right]^{\frac{1}{2}} \qquad (B.7)$$

Inserting (B.7) in (B.3) gives

$$\begin{aligned}\hat{E} \sim & \exp\{-jk\psi(s)\}\hat{E}_o(s) \\ \sim & \exp\{-jk\psi(s)\}\hat{E}_n(s_o)\left[\frac{G(s)}{G(s_o)}\right]^{\frac{1}{2}}\end{aligned} \qquad (B.8)$$

This solution is seen to contain the factor $\exp(-jk\psi)$. G(s) is the expansion coefficient along a ray of the cross-section of the wavefront cut out by an infinitesimal tube of rays. For convenience, the scatterers are assumed to be spherical and the incident waves are plane e.m waves. The geometrical law of reflection implies that the reflected wavefronts will be spherical. This is in agreement with the Huygen's principle stated previously.

For the incident plane wave, the wavefronts are parallel planes and therefore $G(s) = 0$. If these waves are parallel to the x-axis, then from (B.4)

$$\psi = \pm x + constant \qquad (B.9)$$

The constant may be set to zero without loss of generality, then

$$\nabla^2\psi = 0 \qquad (B.10)$$

Since $\hat{E}$ is independent of x, the solution of (B.6) for n = 0 is

$$\hat{E}_o(x, y, z) = \hat{E}_o(x_o, y, z) = \hat{E}_o(y, z) \qquad (B.11)$$

Inserting (B.11) in (B.3) gives

$$\hat{E}(x, y, z) \sim \exp\{-jk\psi(x)\}\hat{E}_o(y, z) \qquad (B.12)$$

The plane wave has precisely the geometrical optics term for its asymptotic expansion.

Using the spherical coordinate system, the reflected wavefront at anytime t is given by

$$\psi(r, \theta, \phi) = ct \tag{B.13}$$

where ψ satisfies the eiconal equation.

If the time coordinate is selected such that the secondary wavefront appears to have its beginning at the point r = 0 at t = 0 , then

$$\psi(r, \theta, \phi) \equiv r \tag{B.14}$$

The wavefronts r = ct represent a spherical wave propagating outward from r = 0. Now following the work of Kline and Kay [55],

$$\frac{G(s)}{G(s_o)} = \frac{ds(s_o)}{ds(s)} \tag{B.15}$$

$ds(s)$ and $ds(s_o)$ are infinitesimal surface elements on the wave front at s and s_o.

For a spherical wave,

$$ds = r^2 \sin\theta d\theta d\phi \tag{B.16}$$

$$G(r) = \frac{1}{r^2} \tag{B.17}$$

Substituting equations (B.16) and (B.17) in (B.15), we obtain

$$\frac{G(r)}{G(r_o)} = \frac{r_o^{\,2}}{r^2} \tag{B.18}$$

From (B.7) and (B.18) we obtain

$$\hat{E}_o^{\,r}(r, \theta, \phi) = \frac{g_o^{\,r}(\theta, \phi)}{r} \tag{B.19}$$

where

$$g_o^{\,r}(\theta, \phi) = r_o(\theta, \phi)\, \hat{E}_o^{\,r}[r_o(\theta, \phi), \theta, \phi] \tag{B.20}$$

is a vector given by the initial value of $\hat{E}_o^r$ on the surface whose equation can be expressed in the form

$$\rho = r_o(\theta, \phi) \tag{B.21}$$

This surface can be described as the scatterer surface which reflects the incident wave and can be represented by ρ, the reflection coefficient. The field observation point is r.

Since $\hat{E}_o^r[r_o(\theta, \phi), \theta, \phi]$ is the incident wave, we have from (B.12)

$$\hat{E}_o^{\,r}[r_o(\theta, \phi), \theta, \phi] = \hat{E}_o^{\,i}(r_o) \exp\{-jk\psi(r_o)\} \tag{B.22}$$

Then (B.19) becomes

$$\hat{E}_o^{\,r}(r) = \frac{\rho \hat{E}_o^{\,i}(r_o)}{r} \exp\{-jk\psi(r_o)\} \tag{B.23}$$

and from (B.8)

$$\hat{E}^r(r) = \frac{\rho \hat{E}_o^{\,i}(r_o)}{r} \exp\{-jk(\psi(r_o) + \psi(r))\} \tag{B.24}$$

Equation (B.24) gives the field strength of the reflected wave at a distance r from the surface of the scatterer and r_o the reference point is at the scatterer surface. The field at r is thus specified in terms of a known field at r_o. If the reference phase $\exp\{-jk\psi(r_o)\}$ is supressed, the equation becomes

$$\hat{E}^r(r) = \frac{\rho \hat{E}_o^{\,i}(r_o)}{r} \exp\{-jk\psi(r)\} \tag{B.25}$$

Equation (B.25) contains the phase factor $\exp\{-jk\psi(r)\}$ and the factor $\frac{1}{r}$, which account for the polarisation and wave nature respectively of the e.m field.

It can be seen that both equations (3.17) and (B.25) are identical. Therefore, the field strength of the wave reflected from the scatterer can be said to vary as the inverse of the distance r between the scatterer and the mobile. The reflection coefficient ρ accounts for the reradiating characteristics of the scatterer. Hence the echo amplitude is given by

$$c_i = \frac{\rho_i E_i}{r_i} \qquad (B.26)$$

where E_i is the field incident on the scatterer.

APPENDIX C

Probability Density Function of the Reflection Coefficient.

Having assumed that the density function of the reflection coefficient follows a cosine law, and referring to the relationship between ρ and the building size given in equation (3.49), we postulate that the size s is sinusoidally distributed as shown in Figure (C1). Then,

$$p(s) = A \sin\left(\frac{\pi s}{2s_{av}}\right) \quad 0 < s < 2s_{av} \qquad (C.1)$$

To obtain the distribution for ρ, we use the transformation

$$p(\rho)d\rho = p(s)ds \qquad (C.2)$$

from which

$$p(\rho) = p(s)\frac{ds}{d\rho} \qquad (C.3)$$

from (3.49)

$$\rho = ks \quad 0 < \rho \leq 1$$

therefore

$$\frac{ds}{d\rho} = \frac{1}{k} \qquad (C.4)$$

substituting (C.1) and (C.4) in (C.3) gives

$$p(\rho) = \frac{A}{k}\sin\left(\frac{\pi\rho}{2ks_{av}}\right) \qquad (C.5)$$

To obtain the value of A, integrate equation (C.1)

$$\int_0^{2s_{av}} p(s)ds = \int_0^{2s_{av}} A \sin\left(\frac{\pi\rho}{2ks_{av}}\right)ds \qquad (C.6)$$

Since the area under the probability curve is 1, the integration results in

$$A = \frac{\pi}{4s_{av}} \qquad (C.7)$$

Subsituting (C.7) in (C.5) gives

$$p(s) = \left(\frac{\pi}{4s_{av}}\right)\sin\left(\frac{\pi s}{2s_{av}}\right) \qquad (C.8)$$

and (C.8) in (C.5) gives

$$p(\rho) = \left(\frac{\pi}{4ks_{av}}\right)\sin\left(\frac{\pi\rho}{2ks_{av}}\right) \qquad (C.9)$$

To obtain the value of k in (C.9), we integrate as follows

$$\int_0^1 p(\rho)d\rho = \frac{\pi}{4ks_{av}}\int_0^1 \sin\left(\frac{\pi\rho}{2ks_{av}}\right)d\rho = 1 \qquad (C.10)$$

From (C.10)

$$k = \frac{1}{2s_{av}} \qquad (C.11)$$

Subsituting (C.11) in (C.9) gives

$$p(\rho) = \left(\frac{\pi}{2}\right)\sin(\pi\rho) \quad 0 < \rho \leq 1 \qquad (C.12)$$

which is the desired density function.

Transformation : Uniform to Sinusoidal

In order to generate random values of sinusoidally distributed ρ from equation (C.12), it is necessary to make a transformation using a similar distribution available in the NAG library. We consider a uniform distribution p(x) as in Figure (C2)

$$p(x) = \frac{1}{\alpha} \tag{C.13}$$

Equating the incremental probabilities and integrating

$$\int p(x)dx = \int p(\rho)d\rho \tag{C.14}$$

Substituting for $p(x)$ and $p(\rho)$ in (C.14) and integrating

$$\frac{x}{\alpha} = \frac{\pi}{2}\int \sin(\pi\rho)\, d\rho = -(\frac{1}{2})\cos(\pi\rho) \tag{C.15}$$

rearranging and noting that

$$\cos(x + \pi) = -\cos x \tag{C.16}$$

then

$$x = \left(\frac{\alpha}{2}\right)\cos[\pi(\rho + 1)] \tag{C.17}$$

rearranging to obtain an expression for ρ in terms of x,

$$\rho = \left| (\frac{1}{\pi})\cos^{-1}(\frac{2x}{\alpha}) - 1 \right| \tag{C.18}$$

which is the transformation desired.

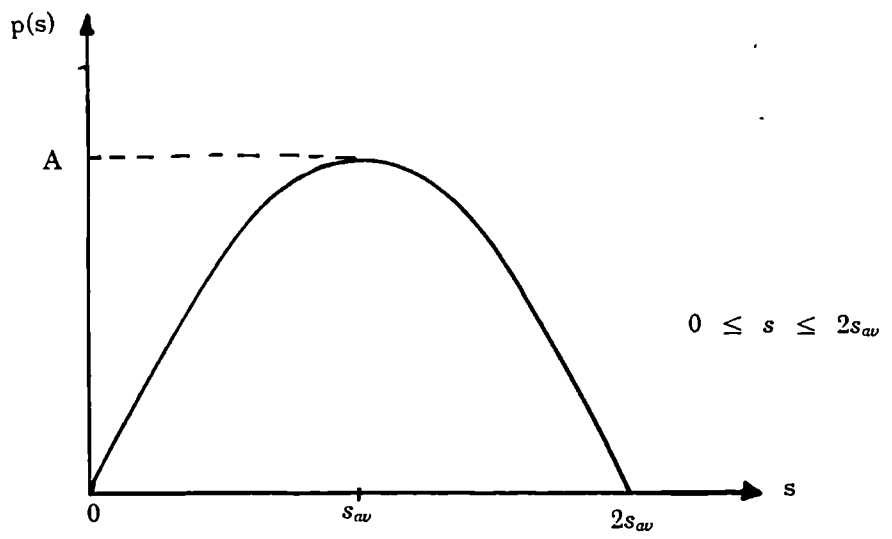

Figure (C1) Probability density function of size s.

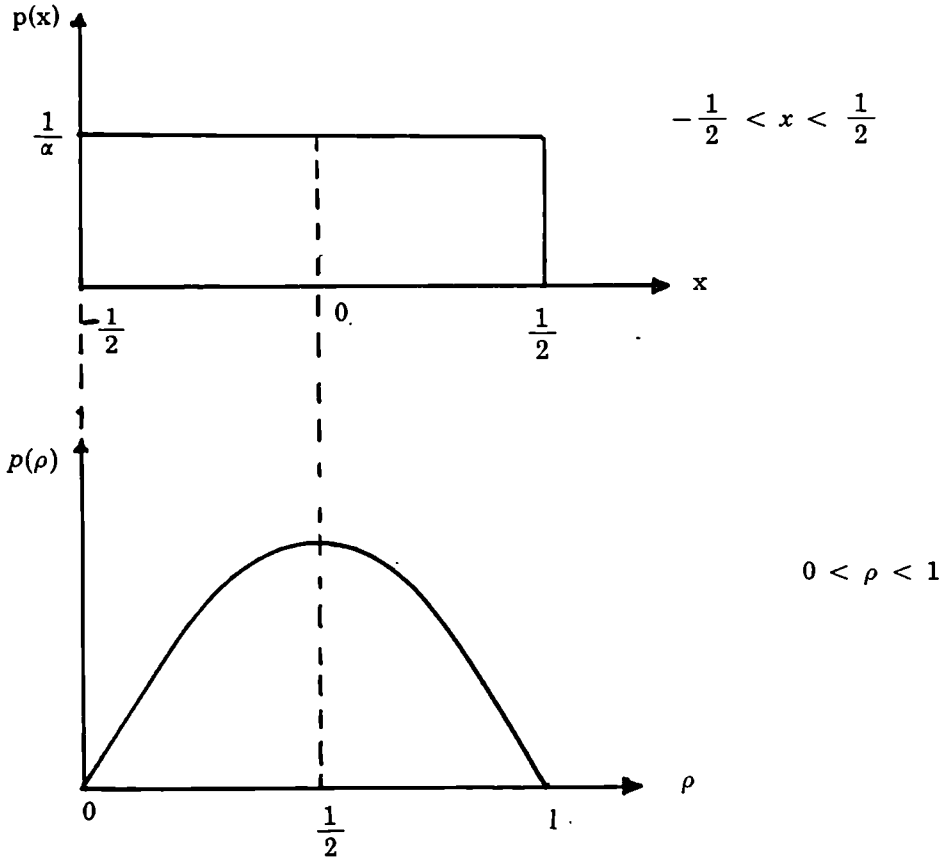

Figure (C2) Uniform to Sinusoidal distribution transformation.

APPENDIX D

Autocorrelation Function of the Transfer Function

The autocorrelation function of $T(f,\bar{x})$ is defined as

$$R_T(f_1,f_2;\ \bar{x}_1,\bar{x}_2) \equiv < T(f_1,\bar{x})\ T^*(f_2\ \bar{x}_2) > \tag{D.1}$$

where

$$T^*(f,\bar{x}) = \text{complex conjugate of } T(f,\bar{x}) \tag{D.2}$$

If

$$T(f_1,\bar{x}_1) = E_i\int_0^{2\pi} \frac{\rho(\phi)\ \exp[-\ j\frac{2\pi f_1}{c}\ \{R(\phi)(1+\cos\phi) - m_1\cos(\phi-\eta_1)\}]}{R(\phi) - m_1\cos(\phi-\eta_1)}\ d\phi \tag{D.3}$$

Then

$$T(f_2,\bar{x}_2) = E_i\int_0^{2\pi} \frac{\rho(\psi)\ \exp[-\ j\frac{2\pi f_2}{c}\ \{R(\phi)(1+\cos\psi) - m_2\cos(\psi-\eta_1)\}]}{R(\psi) - m_2\cos(\psi-\eta_2)}\ d\psi \tag{D.4}$$

From (D.1), (D.3) and (D.4)

$$R_T = <\Big[E_i^2\int_0^{2\pi}\int_0^{2\pi} \frac{\rho(\phi)\ \rho(\psi)}{[R(\phi) - m_1\cos(\phi-\eta_1)][R(\psi) - m_2\cos(\psi-\eta_2)]}$$

$$\times \exp\{j\frac{2\pi}{c}[f_2R_2(\psi)(1+\cos\psi) - f_1R_1(\phi)(1+\cos\phi) + f_1m_1\cos(\phi-\eta_1) - f_2m_2\cos(\psi-\eta_2)]\}\ d\phi\ d\psi\Big] > \tag{D.5}$$

Taking the expectation inside the integral and noting equation (3.46), (D.5) becomes

$$R_T = E_i^2K^2\int_0^{2\pi} <\Big[\frac{\exp\{j\frac{2\pi}{c}[f_1m_1\cos(\phi-\eta_1) - f_2m_2\cos(\phi-\eta_2) - (f_1-f_2)R(\phi)(1+\cos\phi)]\}}{[R(\phi) - m_1\cos(\phi-\eta_1)]\ [R(\phi) - m_2\cos(\phi-\eta_2)}\ d\phi\Big] > \tag{D.6}$$

over very short distances of the order of magnitude less than a few wavelengths, the denominator term in (D.6) simplifies under the assumption that

$$m_1 = m_2 = m$$
$$\eta_1 = \eta_2 = \eta \tag{D.7}$$

This simplification is however not applicable to the phase factor term in the numerator because the phase changes are path length related. If we let the ratios $(m_1:\lambda_c)$ and $(m_2:\lambda_c)$ be described by

$$z_1 = \frac{f_1 m_1}{c} \tag{D.8a}$$

$$z_2 = \frac{f_2 m_2}{c} \tag{D.8b}$$

and if $\Delta f = f_2 - f_1$ (D.8c)

then (D.6) becomes

$$R_T = E_i^2 K^2 \int_0^{2\pi} < \left[\frac{\exp\{j2\pi[z_1 \cos(\phi-\eta_1) - z_2 \cos(\phi-\eta_2) + \frac{\Delta f}{c} R(\phi)(1+\cos\phi)]\}}{[R(\phi) - m\cos(\phi - \eta)]^2} \right] > d\phi \tag{D.9}$$

Taking the stochastic part outside the equation

$$R_T = E_i^2 K^2 \int_0^{2\pi} \exp\{j2\pi[z_1 \cos(\phi - \eta_1) - z_2 \cos(\phi - \eta_2)]\} \; x < \left[\frac{\exp[j2\pi \frac{\Delta f}{c} \{R(\phi)(1 + \cos\phi)\}]}{[R(\phi) - m\cos(\phi - \eta)]^2} \right] > d\phi \tag{D.10}$$

Evaluation of the expectation in (D.10) requires the pdf of R which is given in equation (3.43). Since

$$< y > = \int_{-\infty}^{\infty} y\, f(y)\, dy \tag{D.11}$$

where f(y) is the pdf of y, it follows that the expectation $<[\cdot]>$ in

(D.10) is

$$\langle[\cdot]\rangle = \frac{1}{D}\int_{W/2D}^{\infty} \exp\left(\frac{W}{2D}\right)\exp\left(-\frac{R}{D}\right)\frac{\exp[j2\pi\,\Delta f/c\;R(1+\cos\phi)\,]}{[R - m\cos(\phi-\eta)]^2}\,dR \qquad (D.12)$$

$$\langle[\cdot]\rangle = \frac{\exp(w/2D)}{D}\int_{W/2D}^{\infty}\frac{\exp[\,R\,\{-1/D + j\,2\pi\,\Delta f/c\,(1+\cos\phi)\}]}{[\,R - m\cos(\phi-\eta)]^2}\,dR \qquad (D.13)$$

Let $$\Phi = \frac{1}{D} - j\,2\pi\,\frac{\Delta f}{c}(1+\cos\phi) \qquad (D.14a)$$

and $$\Delta m = m\cos(\phi-\eta) \qquad (D.14b)$$

Then

$$\langle[\cdot]\rangle = \frac{\exp(w/2D)}{D}\int_{W/2D}^{\infty}\frac{\exp[-\alpha R]}{(R-\Delta m)^2}\,dR \qquad (D.15)$$

Integrating by parts

$$\langle[\cdot]\rangle = \frac{\exp(w/2D)}{D}\left[\frac{\exp(-\Phi w/2))}{(W/2-\Delta m)} + \int_{W/2D}^{\infty}\frac{\exp(-\Phi R)}{(R-\Delta m)}\,dR\right] \qquad (D.16)$$

Let $u = (R - \Delta m)\Phi$

then (D.16) becomes

$$\langle[\cdot]\rangle = \frac{\exp(W/2D)}{D}\left[\frac{\exp(-\Phi W/2)}{(W/2-\Delta m)} + \Phi\exp(-\Phi\Delta m)\int_{\Phi(W/2-\Delta m)}^{\infty}\frac{\exp(-u)}{u}\,du\right] \qquad (D.17)$$

but $$\int_{v}^{\infty}\frac{\exp(-u)}{u}\,du = E_x(z) \qquad (D.18)$$

is the exponential function, therefore

$$\int_{\Phi(W/2-\Delta m)}^{\infty}\frac{\exp(-u)}{u}\,du = E_x\left[\Phi\frac{W}{2} - \Delta m\right] \qquad (D.19)$$

Equation (D.19) is a complex exponential function because Φ in (D.14a)

is complex valued. For simplification purposes if the mobile is at the origin, i.e. m = 0 in (D.14b), then $\Delta m = 0$ and (D.17) can be written as

$$\langle[\cdot]\rangle = \frac{\exp(W/2D)}{D}\left[\frac{\exp(-\Phi W/2)}{W/2} + \Phi\, E_x(\Phi\, W/2)\right] \tag{D.20}$$

substituting (D.14a) in (D.20)

$$\langle[\cdot]\rangle = \frac{\exp(W/2D)}{D}\left[\exp\left\{-\frac{W}{2D}\left[1 - j2\pi\frac{\Delta f}{c}D(1+\cos\phi)\right]\right\}\right.$$

$$\left. + \left[\frac{1}{D} - j2\pi\frac{\Delta f}{c}(1+\cos\phi)\right] \cdot E_x\left[\frac{W}{2}\left[\frac{1}{D} - j2\pi\frac{\Delta f}{c}(1+\cos\phi)\right]\right]\right] \tag{D.21}$$

Substituting (D.21) in (D.10) gives

$$R_T = E_i^2 K^2 \int_0^{2\pi} \exp\{j2\pi[z_1\cos(\phi - \eta_1) - z_2\cos(\phi - \eta_2)]\}$$

$$\times \frac{\exp(W/2D)}{D}\left[\exp\left\{-\frac{W}{2D}\left[1 - j2\pi\frac{\Delta f}{c}D(1+\cos\phi)\right]\right\}\right.$$

$$\left. + \left[\frac{1}{D} - j2\pi\frac{\Delta f}{c}(1+\cos\phi)\right] \cdot E_x\left[\frac{W}{2}\left\{\frac{1}{D} - j2\pi\frac{\Delta f}{c}(1+\cos\phi)\right\}\right]\right] d\phi \tag{D.22}$$

Equation (D.22) is the expression for the autocorrelation function of the low pass transfer function $T(f,\bar{x})$ of the mobile radio channel given the pdf of parameter R as in equation (3.43).

APPENDIX E

Linear System Representation of the Propagation Measurement.

The channel sounder equipment makes use of the correlation properties of pseudo-random binary sequences (prbs) which produce low data recording bandwidths for high resolution time delay measurements. An N-bit shift register is clocked at f_o MHz to produce a prbs sequence s(t) of + and - transitions (see Figure 4.7a). s(t) is upconverted (phase reversal modulated) on a suitable carrier to produce

$$s_T(t) = A\, s(t) \cos \omega_o t \otimes a(t) \qquad (E.1)$$

where

A = amplitude constant

a(t) = impulse response of amplifiers

$\otimes$ = convolution

s(t) repeats itself exactly after time interval $T = (2^N - 1)t_o$, where t_o is the clock period and $t_o = \frac{1}{f_o}$. The time autocorrelation function $R_s(\tau)$ of $s(t)$ is

$$R_s(\tau) = \frac{1}{T}\int_0^T s(t)s(t - \tau)dt \qquad (E.2)$$

and is a triangle of base width $2t_o$ with period T as shown in Figure (4.7b). The nearly zero portion of $R_s(\tau)$ is a residual or bias r_m of magnitude $\frac{1}{(2^N - 1)}$.

Since the entire mobile radio communication system is linear, all the transmitter and receiver filters can be lumped together as filters in cascade.

The measuring system can be modelled by a linear system as shown in Figure (E1). z(t) is the input to the receiver correlators and is given by

$$z(t) = g(\tau) \otimes b(\tau) \otimes s_T(t) \tag{E.3}$$

Let

$$f(\tau) = g(\tau) \otimes b(\tau) = \int_{-\infty}^{\infty} g(u)b(v - u)du \tag{E.4}$$

Then substituting (E.4) in (E.3)

$$z(t) = f(\tau) \otimes s_T(t) = \int_{-\infty}^{\infty}\left[\int_{-\infty}^{\infty} g(u)b(v - u)du\right]s_T(t - v)dv \tag{E.5}$$

Rearranging (E.5)

$$z(t) = \int_{-\infty}^{\infty}\int_{-\infty}^{\infty} g(u)b(v - u)s_T(t - v)dudv \tag{E.6}$$

The filters are bandlimited about the center frequency f_o, thus a bandpass representation is appropriate for $b(\tau)$ and $g(\tau)$:

$$\begin{aligned} b(\tau) &= 2Re[b_l^{\times}(\tau)\exp(j\omega_o\tau)] \\ &= 2b_{lx}(\tau)\cos\omega_o\tau + 2b_{ly}(\tau)\sin\omega_o\tau \end{aligned} \tag{E.7}$$

$$\begin{aligned} b(\tau) &= 2Re[b_l^{\times}(\tau)\exp(j\omega_o\tau)] \\ &= 2b_{lx}(\tau)\cos\omega_o\tau + 2b_{ly}(\tau)\sin\omega_o\tau \end{aligned} \tag{E.8}$$

where

$$b_l(\tau) = b_{lx}(\tau) + jb_{ly}(\tau) \tag{E.9}$$

$$g_l(\tau) = g_{lx}(\tau) + jg_{ly}(\tau) \qquad (E.10)$$

are the equivalent lowpass filter representations.

The correlator output will be

$$I(\tau) = Re[z(t) \otimes s(t)] = \frac{1}{T}\int_0^T z(t)s(t - \tau)\cos\omega_o t dt \qquad (E.11a)$$

$$Q(\tau) = Im[z(t) \otimes s(t)] = \frac{1}{T}\int_0^T z(t)s(t - \tau)\sin\omega_o t dt \qquad (E.11b)$$

Substituting (E.6) in (E.11a)

$$I(\tau) = \frac{1}{T}\int_0^T \left[\int_{-\infty}^{\infty}\int_{-\infty}^{\infty} g(u)b(v - u)s_T(t - v)dudv\right] s(t - \tau)\cos\omega_o t dt \qquad (E.12)$$

Let

$$s_T(t - v) = s(t - v)\cos\omega_o(t - v) \qquad (E.13)$$

Substituting (E.13) in (E.12) and rearranging gives

$$\begin{aligned} I(\tau) = &\left\{\frac{1}{T}\int_0^T s(t - v)s(t - \tau)\cos\omega_o(t - v)\cos\omega_o t dt\right\} \\ &\times \left[\int_{-\infty}^{\infty}\int_{-\infty}^{\infty} b(v - u)g(u)dudv\right] \end{aligned} \qquad (E.14)$$

Now

$$\cos\omega_o(t - v)\cos\omega_o t = \frac{1}{2}\{\cos(2\omega_o t - \omega_o v) + \cos(-\omega_o v)\} \qquad (E.15)$$

Using the trigonometric relationship of equation (E.15) in the expression in braces { . } in equation (E.14), we obtain

$$\begin{aligned} \{.\} &= \frac{1}{T}\int_0^T s(t-v)s(t-\tau)\frac{1}{2}\cos(2\omega_o t - \omega_o v)dt \\ &= \frac{1}{T}\int_0^T s(t-v)s(t-\tau)\frac{1}{2}\cos\omega_o v dt \end{aligned} \qquad (E.16)$$

since $\cos(2\omega_o t)$ is zero, (E.16) reduces to

$$\{.\} = \frac{1}{2T}\int_0^T s(t-v)s(t-\tau)\cos\omega_o v dt \qquad (E.17)$$

using the variable substitutions

$t = t' + v$, $dt = dt'$, $t - \tau = t' + v - \tau$, (E.17) becomes

$$\{.\} = \frac{\cos\omega_o v}{2T}\int_0^T s(t')s(t'-(\tau-v))dt = \frac{1}{2}R_s(t-v)\cos\omega_o v \qquad (E.18)$$

where

$$R_s(t-v) = \frac{1}{T}\int_0^T s(t')s(t'-(\tau-v))dt \qquad (E.19)$$

From equations (E.14) and (E.18) we obtain

$$I(\tau) = \frac{1}{2}\int_{-\infty}^{\infty}\int_{-\infty}^{\infty} g(u)b(v-u)R_s(t-v)\cos\omega_o v du dv \qquad (E.20)$$

Similarly,

$$Q(\tau) = \frac{1}{2}\int_{-\infty}^{\infty}\int_{-\infty}^{\infty} g(u)b(v-u)R_s(t-v)\sin\omega_o v\,du\,dv \qquad (E.21)$$

Therefore

$$I(\tau) = Re[\, b(\tau) \otimes g(\tau) \otimes R_s(\tau)\,] \qquad (E.22)$$

and

$$Q(\tau) = Im[\, b(\tau) \otimes g(\tau) \otimes R_s(\tau)\,] \qquad (E.23)$$

It is convenient at this point to lump the effects of the probe and equipment filters

$$p(\tau) = b(\tau) \otimes R_s(t-\tau) = \int_{-\infty}^{\infty} b(\tau)R_s(t-\tau)d\tau \qquad (E.24)$$

$p(\tau)$ is the bandlimited approximation to an impulsive probing signal. Therefore (E.22) and (E.23) become

$$I(\tau) = Re[\, p(\tau) \otimes g(\tau)\,] \qquad (E.25)$$

and

$$Q(\tau) = Im[\, p(\tau) \otimes g(\tau)\,] \qquad (E.26)$$

The receiver correlator outputs $I(\tau)$ and $Q(\tau)$ are the quadrature components of the bandlimited complex bandpass impulse response envelope $h(\tau)$, ie. $h(\tau) = p(\tau) \otimes g(\tau)$ so that $I(\tau) = Re[h(\tau)]$ and $Q(\tau) = Im[h(\tau)]$.

That is

$$I(\tau) = Re\left[\int_{-\infty}^{\infty} g(x)p(\tau - x)dx\right] \qquad (E.27)$$

$$Q(\tau) = Im\left[\int_{-\infty}^{\infty} g(x)p(\tau - x)dx\right] \qquad (E.28)$$

Let $E^2(\tau)$ be the squared envelope of the impulse response (or the individual power delay profile) which is

$$\begin{aligned} E^2(\tau) &= I^2(\tau) + Q^2(\tau) = \left|\int_{-\infty}^{\infty} g(x)p(\tau - x)dx\right|^2 \\ &= |h(\tau)|^2. \end{aligned} \qquad (E.29)$$

A simplified linear system representation of the multipath propagation system is shown in Figure (E2), as a filter in cascade with the random medium. The average power delay profile is then obtained as

$$\begin{aligned} P(\tau) &= < |h(\tau)|^2 > = < |p(\tau) \otimes g(\tau)|^2 > \\ &= < I^2(\tau) + Q^2(\tau) > \end{aligned} \qquad (E.30)$$

$P(\tau)$ is the bandlimited estimate of the average impulse response envelope $< |g(\tau)|^2 >$ of the random medium. It is obtained by averaging over an ensemble of locations chosen uniformly along a street.

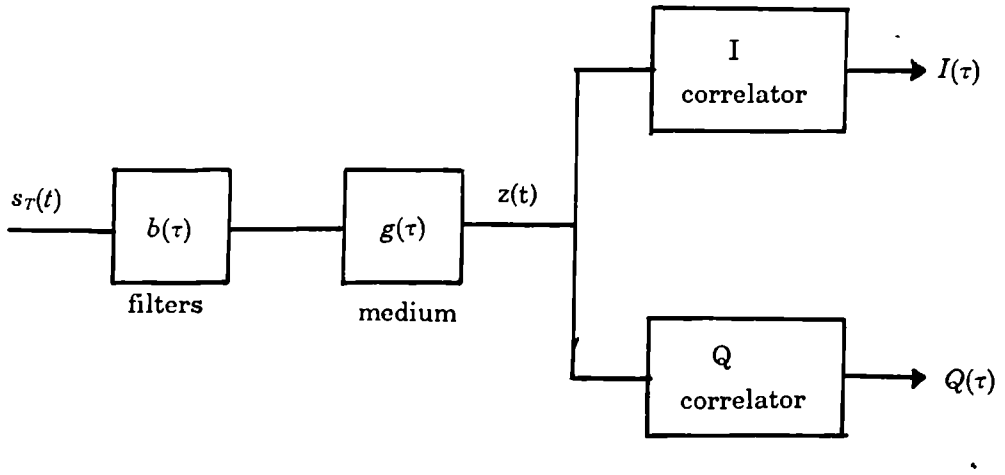

Figure (E1) Linear system representation of measuring system.

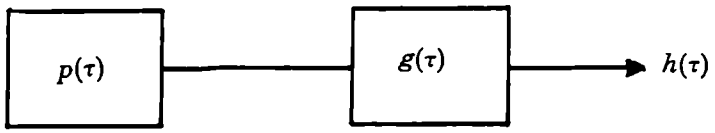

Figure (E2) Simplified linear-system representation of measuring system.

APPENDIX F

Flow Charts of Main Simulation Programs.

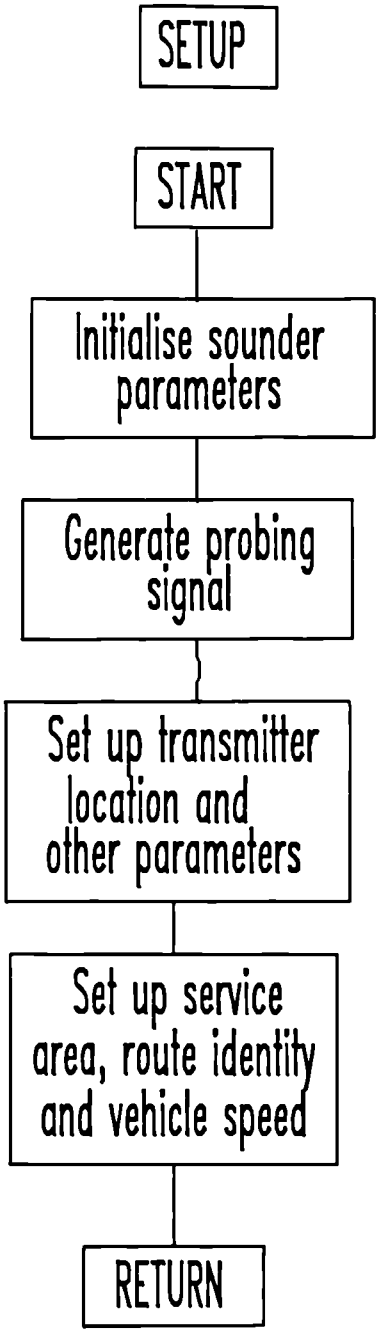

Figure F1 Flow diagram for SETUP

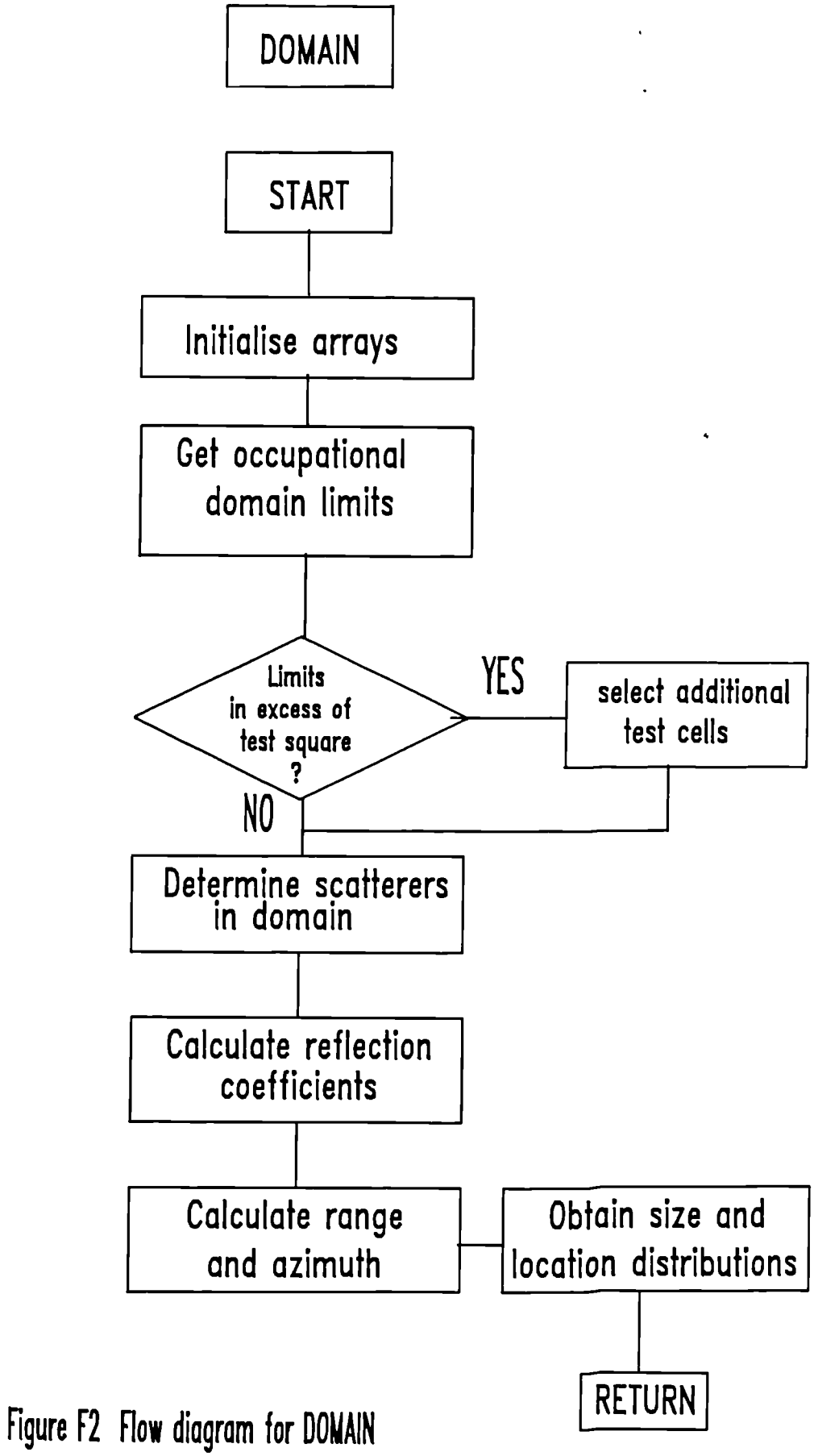

Figure F2 Flow diagram for DOMAIN

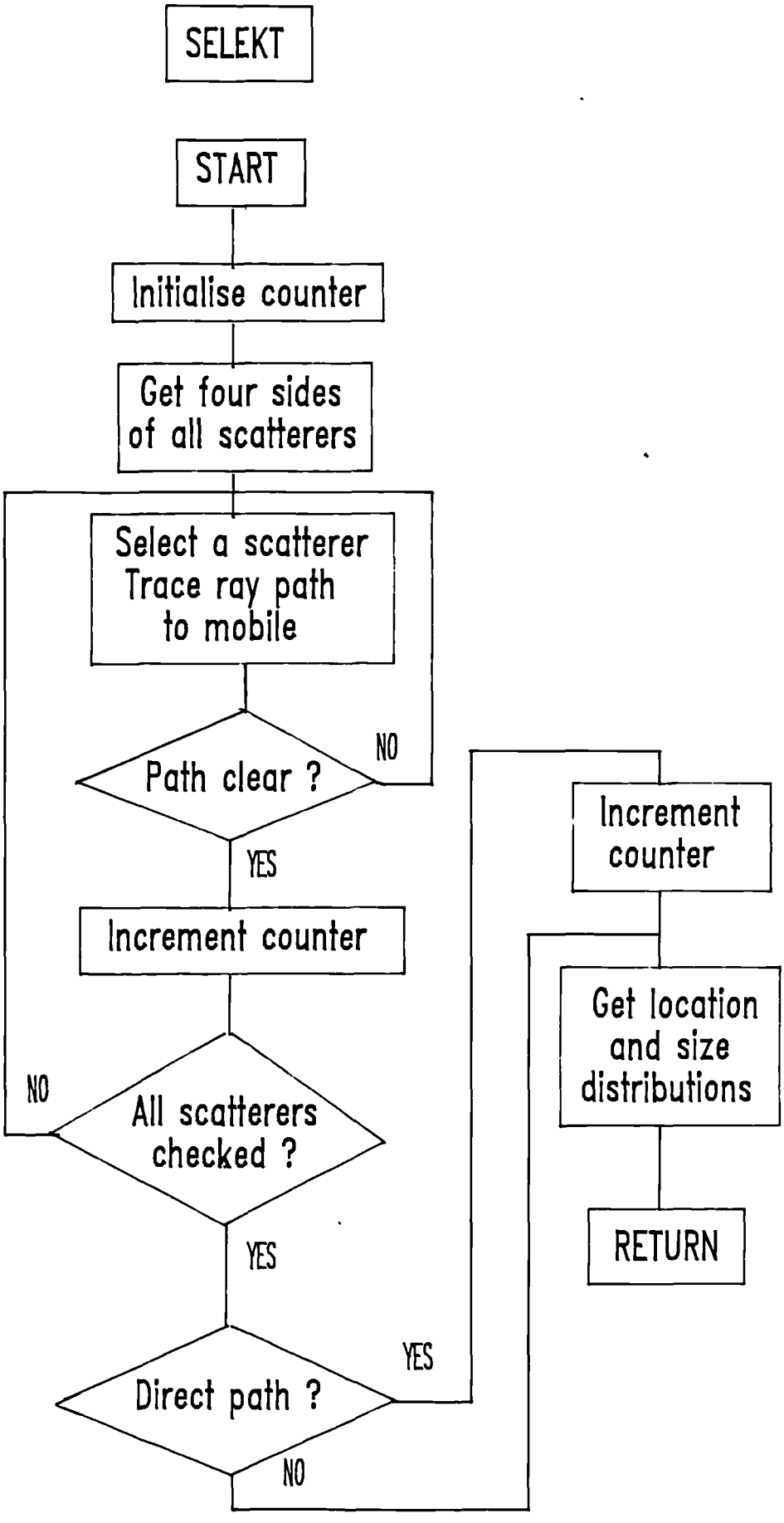

Figure F3 Flow diagram for SELEKT

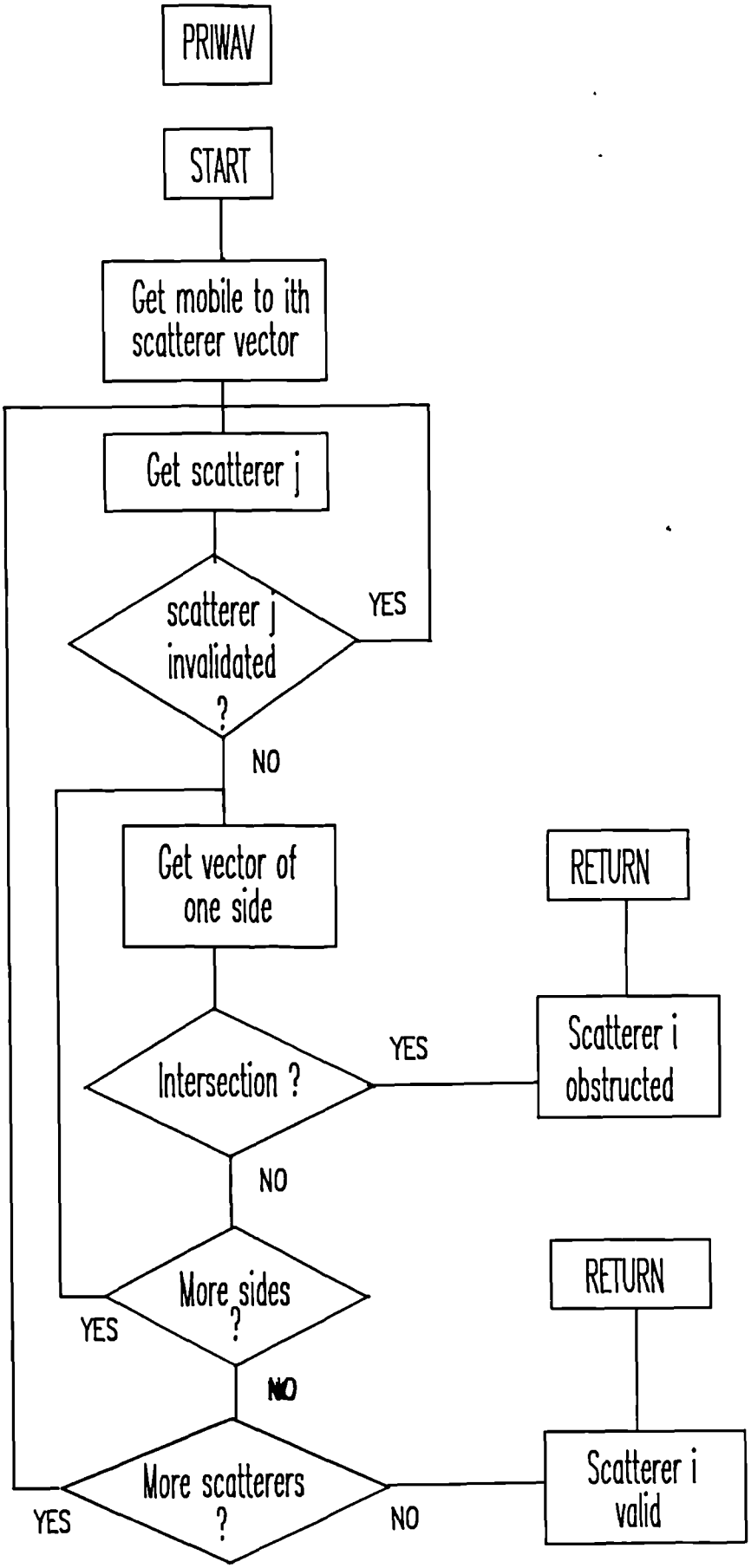

Figure F4 Flow diagram for PRIWAV

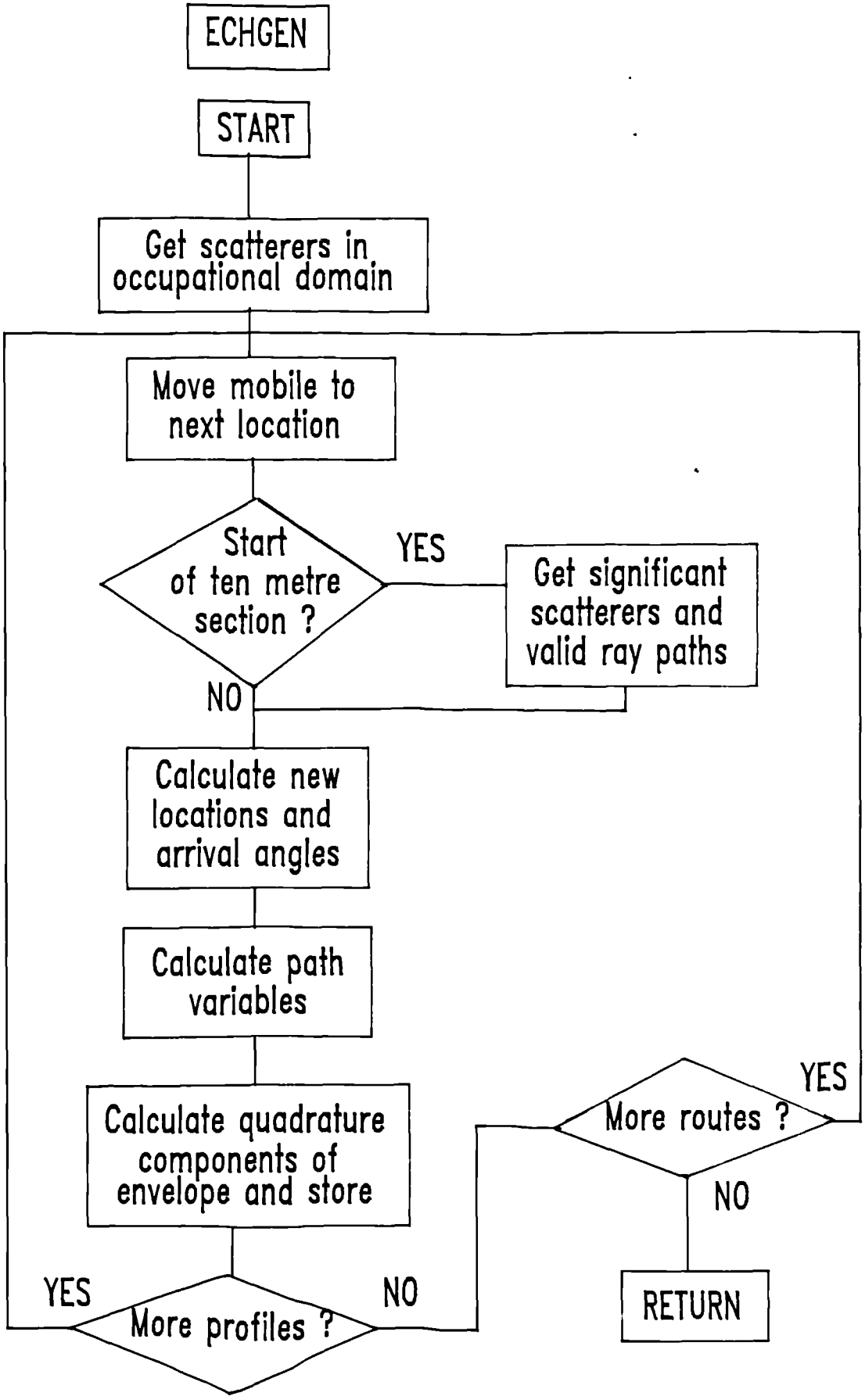

Figure F5 Flow diagram for ECHGEN

APPENDIX G

Technical Publications.

[1] Bajwa, A.S and Kafaru, O.O : 'A Simple Environment-Dependent Approach to Wideband Multipath Propagation Modelling', IEE Colloquium on Propagation in an Urban Environment, 3 April 1986, Savoy Place, London, pp 5/1 - 5/5.

[2] Bajwa, A.S and Kafaru, O.O : '900 MHz Wideband Multipath Propagation Measurements and Modelling', Second Nordic Seminar on Digital Land Mobile Radio Communication, Stockholm, 14-16 October 1986, pp 195 - 202.

[3] Kafaru, O.O, Bajwa, A.S and Parsons, J.D : 'An Environment-Dependent Approach to Wideband UHF Multipath Propagation Modelling', IERE Fourth International Conference on Land Mobile Radio, University of Warwick, Coventry, 15-17 December 1987, pp 121 - 127.

[4] Kafaru, O.O : 'Channel Modelling and Simulation for Wideband Systems', IEE Colloquium on Propagation Factors and Interference Modelling for Mobile Radio Systems, Savoy Place, London, 18 November 1988, pp 4/1 - 4/5.

A SIMPLE ENVIRONMENT-DEPENDENT APPROACH TO WIDEBAND MULTIPATH PROPAGATION MODELLING

A.S. Bajwa and Miss O.O. Kafaru

Introduction

Wideband transmission in any future digital cellular mobile radio system will be affected by the frequency-selective fading in the radio channel. Frequency-selective fading is a feature of the echo-path delays, caused by multipath propagation. Radio propagation in mobile environments is usually by way of scattering from buildings and other obstacles. These scattered radio-waves individually have different strengths and path delays dependent on the re-radiating characteristics of the scatterers. Thus the nature of scattering is environment dependent. We propose a simple stochastic model to include the features of the environment directly. These features may be extracted easily from digitised ordnance survey maps. Various statistical models have appeared in the literature for a narrowband channel [Refs 1,2] and wideband channels [Refs 3,4,5]. The model proposed by Turin et al [Ref 3] has been widely used in simulations despite the fact that the model is derived from sparse observations of the echo envelope at fixed locations. All these models, except Ref 5, ignore environmental characterisation.

Multipath model

The principal mode of scattering in the proposed simple model is single reflection. Each scatterer, randomly placed, behaves as an 'omnidirectional' secondary source of radiowaves. The reflection coefficients ρ, attributed to each scatterer, are also independently randomly distributed and depend on the scatterer sizes, regardless of location. In this simple model the two-dimensional geometry presumes equal scatterer heights. This may be relaxed in a more elaborate 3-dimensional model. Over distances less than a few hundred wavelengths in a homogeneous locality, the number of scatterers, ρ, and the location of scatterers remains unchanged.

The general situation for scatter k is depicted in Fig. 1. A number of equivalent 'point' scatterers surround the mobile located at the origin. Thus, the vectors $\bar{R}_k$; k = 1,2,3... N represent distances from the mobile to the N scatterers. Each scatterer has a reflection coefficient ρ_k; k = 1,2,3... N that is a complex constant over 200 wavelengths. The scatterer geometry is conveniently described in the (R_k, θ_k) polar form for scatterer k. In the multipath model R and Θ are environment-dependent stochastic processes.

The echo delay statistics are of interest in the transversal-filter type wideband simulators. We curtail the discussion here to this aspect only. To derive the time-delay τ_k in the depicted scatterer geometry we use the relationship.

$$\tau_k = \frac{d_T + R_k\,(1 + \cos\theta_k)}{c} \quad ; \quad d_T >> R_k \qquad (1)$$

where c is the velocity of the radiowave and d_T is the line of sight distance.

A.S. Bajwa and O.O. Kafaru are with the Department of Electronics, Computer Science and Information Engineering, University of Southampton, U.K.

The echo delays τ_k may be obtained when the stochastic processes R and θ are known for a particular environment. Details of the simple stochastic model are presented in Ref 6. Briefly, the probability density function (p.d.f.) of the location p(R) is shown to have the form

$$p(R) = \frac{1}{D} \exp\left[W/2D - \frac{R}{D}\right] \qquad (2)$$

where the parameter D is the average separation between scatterers and W is the street width. In the early model a scatterer size p.d.f. p(s) was assumed and the p.d.f. of the reflection co-efficient derived from it in the form

$$p(|\rho|) = \frac{\pi}{2} \sin(\pi |\rho|) \quad ; \quad 0 < |\rho| < 1 \qquad (3)$$

Further simplications arose from the classification of the channel as a Wide Sense Stationary Uncorrelated Scattering (WSSUS) channel (Ref 6). The theoretical approach was developed using stochastic simulation. It was evident from early results that map-derived probability distributions for R and size s were relevant and easily obtained. These extracted distributions were then used in a stochastic simulation model instead.

Map-derived environmental statistics

Digitised ordnance survey maps are increasely becoming available. This offers the possibility of an automated approach to the channel model without recourse to tedious information extraction. The multipath model presented here requires essentially two distributions: p(R) and p(s). In order to assess the feasibility of the approach these distributions were manually extracted for the selected environments. The scatterer size distribution showed a consistent behaviour in a number of residential areas, each easily characterised by a single parameter related to the first central moment or mean. Two representative histograms are shown in Fig 2. The histograms exhibit a reasonable fit on the sinusoidal distribution for p(s) [Ref 6]. Observe that the average size of scatterers ranges between 100 and 120 m^2. In contrast, the location distributions have shown a poorer fit on eq. (2) in local surroundings. Data is limited and tedious to process and awaits the availability of digitised map processing.

Model Predictions

The time-varying impulse response of the channel $h(t,\tau)$ has embedded in it the effects of the path lengths, angles of arrival and intensity of each radiowave. Measurements of $h(t,\tau)$ are reported in Ref 4 in a form suitable for comparison with the model proposed here. Of interest is the probability of echo-path occupancy, defined as:

$$P_{oc} \triangleq \Pr[\text{at least one echo in the interval } \tau,\ \tau + d\tau]. \qquad (4)$$

Clearly, it is important to note the probability or relative occurrence of an echo of a certain delay that exceeds a threshold amplitude.

A stochastic simulation approach has been used to obtain P_{oc} for typical residential environments. The scatterer size and location distributions were extracted from the 1:1250 scale maps. The P_{oc} obtained from the simulations are shown in Fig 3. The simulated model predictions when compared with measured results show a remarkably good fit.

Conclusions

Randomly-located and randomly scintillating scatterers are used in a simple geometric optics scattering model to predict the wideband echo time delay statistics. The model is easily characterised by map derived environmental statistics. The probability of echo-path occupancy shows a good fit on experimental data in suburban residential environments. Map-derived statistics show that a common distribution appropriately models the scatterer sizes. Typically, an average scatterer size is $110m^2$. Scatterer locations are conveniently described by street width and the average scatterer separation. Further modelling work is in progress to consider a variety of locations and also include scatterer height statistics.

Acknowledgements

This work is supported by the SERC as part of a research grant GR/D/21714. Miss O.O. Kafaru is a recipient of a Commonwealth scholarship award.

References

[1] Ossana, J.F. Jr.: "A model for mobile radio fading due to building reflections: Theoretical and experimental fading waveform power spectra", B.S.T.J., 43, No.6, pp.2935-2971, 1964.

[2] Clarke, R.H.: "A statistical theory of mobile reception", B.S.T.J., 47, pp.957-1000, 1968.

[3] Turin, G.L., Clapp, F.D., Johnston, T.L., Fine, S.B., Lawry, D.: "A statistical model of urban multipath propagation", IEEE Trans., VT-21, No.1, pp.1-9, 1972.

[4] Bajwa, A.S.: "UHF wideband statistical model and simulation of mobile radio multipath propagation effects", IEE Proc., Part F, 132, No.5, pp.327-333, 1985.

[5] Zander, J.: "A stochastical model of the urban UHF radio channel", IEEE Trans., VT-30, No.4, pp.145-155, 1981.

[6] Bajwa, A.S.: "A simple stochastical approach to wideband modelling of multipath propagation in mobile radio environments", IERE International Conference on Land Mobile Radio, Cambridge, 10-13 December 1985.

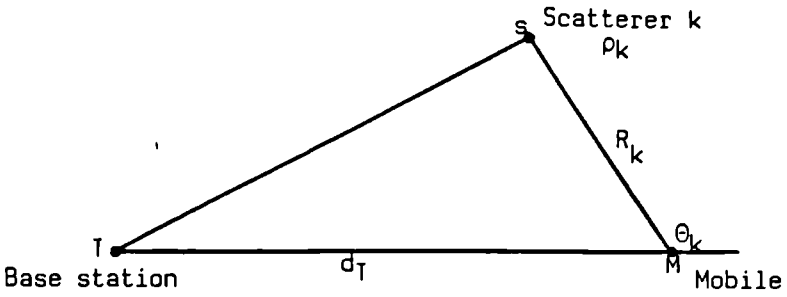

Figure 1: Model Geometry

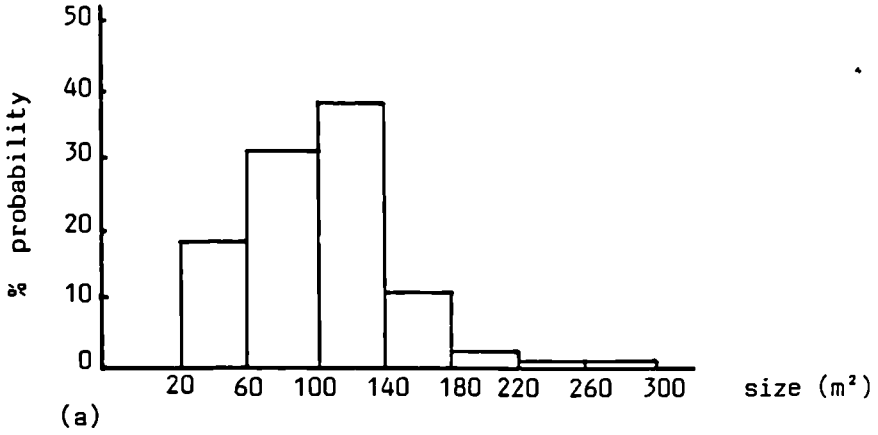

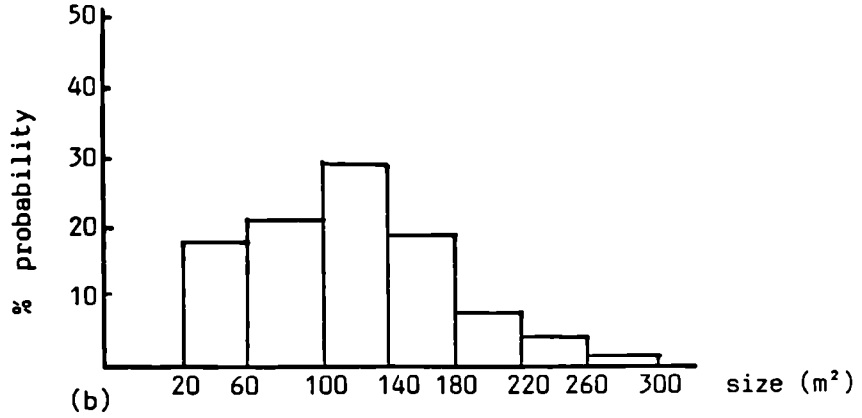

Figure 2: Scatterer size distributions obtained from ordnance survey maps.

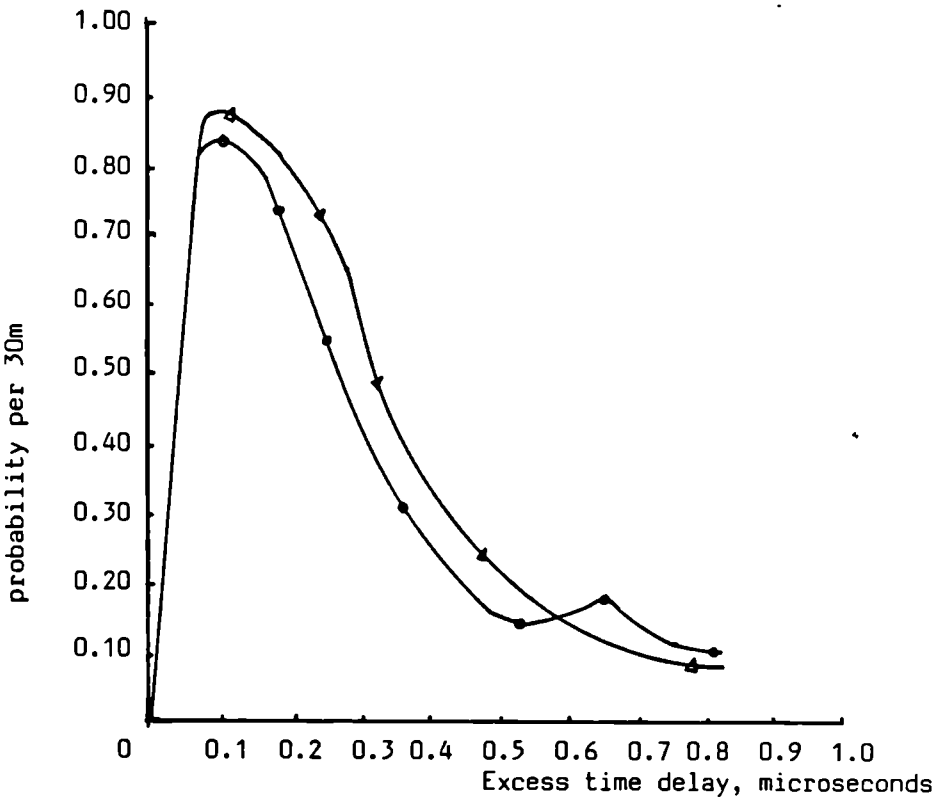

Figure 3: Probability of echo path occupancy in typical residential suburban environments

o——o Experimental

Δ——Δ Simulation

900 MHZ WIDEBAND MULTIPATH PROPAGATION MEASUREMENTS AND MODELLING

A.S. Bajwa,
Telecom Securicor Cellular Radio Ltd.,
Cellnet Centre, 142/148 Goswell Road,
London, EC1.

O.O. Kafaru,
Department of Electrical Eng. and Electronics,
University of Liverpool,
Liverpool, L69.

1. Introduction

The nature of the dynamic multipath propagation in urban, suburban and rural area results in space-selective fading in FDMA Cellular mobile radio systems. In addition, as the transmission is increased beyond the coherence bandwidth of the radio channel, the frequency-selective fading becomes apparent with significant impairment in transmission unless it is mitigated by added signal design and receiver processing. It can be viewed as a natural diversity provided by the channel, and perhaps harnessed, to improve the radio system's performance. The second generation digital cellular systems intend to exploit the channel characteristics and various proposals have now emerged (1). Some of the crucial aspects of these systems depend on a satisfactory understanding of the channel behaviour, especially over a wide bandwidth.

In mobile radio environments radio propagation is usually by way of scattering from buildings and natural obstacles either obstructing or surrounding the mobile. These scattered radiowaves individually travel different path lengths and exhibit strengths dependent on the scattering characteristics of reradiating obstacles etc. Thus a transmitted r.f. signal is received at the mobile randomly delayed, attenuated and phase-shifted for each propagation path. Various models have appeared in the literature, some develop the model from a scattering viewpoint (2), whilst others prefer to treat the signal fading as a stochastic process (3). Furthermore, these models view the characterisation as a narrowband random process. Few experimental results have been reported for a wideband radio channel (4, 5, 6). The characterisation views the channel as a linear randomly time-variant filter for the Wide-Sense Stationary Uncorrelated Scattering (WSSUS) class of channels (7). Two different approaches have been used to characterise the wideband channel; one treats the small-area echo impulse responses as WSSUS and derives the moments of the echo impulse response distributions while the other adopts a global statistical model of the echo strengths, delays and r.f. phases. Aside from the inadequacies in these approaches (4) both the narrowband and wideband approaches have a common deficiency. This lies in the omission of environments-dependent parameters to model the behaviour of the radio channel. Ossana (8) first proposed an approach based on deterministically placed, perfectly conducting, plane reflectors. Recently Zanders (9) proposed a simple geometric-optics approach based on randomly placed and randomly scintillating scatterers. The model extends the ray approach to include the path-length related wave phase-shifts but omits the wave intensity variations due to wave divergence. This leads to inconsistencies that are fortutiously not evident in the simple model proposed in Ref. 9. Nonetheless, an interesting environment-dependent parameter was derived in Ref. 9.

The model proposed in this paper allows for wave divergence in wave propagation and upon wave scattering. The latter phenomenon is introduced through the concept of Huygen's reradiation principle to discrete randomly-

placed and randomly scintillating sources. The model uses environment-dependent parameters extracted from digitised ordnance survey maps through an automated process. Thus for the first time a wideband channel model is available that is ideally suited for wideband simulators and, more importantly, depends on the physical characteristics of the environment. This model has been tested against measured channel statistics obtained from a purpose-built wideband channel sounder.

2. The Multipath Model

Single reflection is the principal mode of scattering in the simple model. Each scatterer, randomly placed, acts as a Huygens secondary source of radiowaves. The reflection coefficients attributed to each scatterer depend on the wave divergence and are independently randomly distributed in a locality, regardless of mobile location. In a two-dimensional model the scatterer height is ignored and the reradiation intensity of the scatterers is assumed to depend on the scatterer sizes. The model is local in the sense that it assumes a homogenesus environment and wide-sense stationarity. This is by no means a constraint upon the approach since the terrain or shadow effects may be modelled in the same manner over a large area with sparse scattering localities.

2.1 Geometric 'Wave' Optics

The geometric optics field is the leading term in the asymptotic high frequency solution of Maxwell's equations. The solution expressed in the Luneberg-Kline asymptotic expansion for the (vertically polarised) electric field has the form (10)

$$\bar{E} \sim \exp(-jk\psi) \sum_{m=0}^{\infty} \bar{E}m/(jw)^m \qquad (1)$$

where k is the wave number of the medium, w (rad/s) is the excitation frequency and the exp(jwt) term is suppressed. Substituting this into the vector Helmholtz wave equation for the electric field and integrating the resulting transport equation for the leading term, i.e., m=o, we obtain

$$\bar{E}(R) = \exp\left[jk\psi(s)\right] \bar{E}_o(R)$$

$$= \bar{E}_o(o)\exp\left[-jk\psi(o)\right] \cdot \left[r_1\, r_2/(r_1+R)(r_2+R)\right]^{\frac{1}{2}} \exp(-jkR) \qquad (2)$$

where R = O is taken as the reference on the ray path, and r_1, r_2 are the principal radii of curvature of the wavefront at R = O. This eikonal equation could have been deduced from Fermat's principle in classical geometric optics. However, classical optics ignores the polarisation and the wave nature of the electromagnetic fields. Observe, the leading term in the Luneberg-Kline asymptotic expansion contains this information. For a relatively smooth surface an incident electric field $\bar{E}^i$ on the scatterer results in a reflected field $\bar{E}^r(R)$ according to the boundary conditions as (10)

$$\bar{E}^r(R) = \bar{E}^i(R=R_o) \cdot \bar{R} \cdot \left[r_1^r r_2^r/(r_1^r+R)(r_2^r+R)\right]^{\frac{1}{2}} \exp(-jkR) \qquad (3)$$

where r_1^r, r_2^r the principal radii of the reflected wavefront may be obtained from principal radii of the incident wave fronts r_1^i, r_2^i respectively (10). $\bar{\bar{R}}$ is the dyadic reflection co-efficient determined by the polarisation and electrical characteristics of the reflector boundary. To simplify the mathematical treatment we assume that the divergence of the scattered radio waves of a known polarisation can be conveniently expressed in the scalar equivalent form

$$E^r(R) = E^i(R=R_o) \cdot (KS/R) \tag{4}$$

where the divergence depends on the reflector size s and the distance R from the secondary source for relatively smooth surfaces. This forms the basis of the approach adopted in this model.

2.2 Scatterer geometry

The general situation for scatterer is depicted in Fig. 1. A number of reradiating discrete scatterers surround the mobile located at the Cartesian coordinate origin (0,0). The vectors $\bar{R}_k$; $k= 1, 2, 3,...N$ represent the distances from the N scatterers to the mobile. Each scatterer has a reflection coefficient ρ_k^s where

$$\rho_k^s = KS \tag{5}$$

The scatterer geometry is more conveniently described in the polar (R_k, ϕ_k) form. We curtail the discussion in this paper to the echo time delay statistics, this being of prime interest here and also for the sake of brevity. To calculate the time-delay τ_k for a radiowave arriving from scatterer k, we use the path geometry, Fig. 1. In most practical situations, particularly in urban areas over flat terrain $d_T > R$. Then,

$$\tau_k = \left[d_T + R_k(1+\cos\phi_k)\right]/c \tag{6}$$

where c is the velocity of the radiowave and d_T is the separation between the base station and the mobile. Whenever the above approximation is invalid the exact relationship may be easily invoked.

2.3 The stochastic model

The echo time delays in equation (6) are obtained when the stochastic process R, ϕ, and s are known. The approach adopted in Ref. 9 models R as a stationary second-order stochastic process independent of ϕ and derived from a planar Poisson process for the location of the two-dimensional scatteres. In Ref. 11 we refined this model to account for street widths and showed that the probability density function (p.d.f) p(R) becomes

$$p(R) = (1/D)\ \exp\left[W/2D - R/D\right] \quad ; \quad R \geq W/2 \tag{7}$$

An important feature of our model is the explicit second-order process associated

with the reflection coefficient ρ^s. This has a significant bearing on the model predictions unlike the overly simplified results reported in Ref. 9. To understand this consider an assortment of randomly placed scatterers of randomly different sizes. The simplified model (9) does not distinguish between contributions from small and large scatterers at some distance R. Thus scatterers of the same size contribute equally whether close or distant from the mobile. Cognisant of this, we postulate a scatterer size pdf p(s) and account for wave divergence in propagation and scattering. In a practical situation the echo amplitude is only significant when it can cause noticeable distortion and it is important to discern between weak and strong echoes. By prescribing a scatterer size distribution, from which the average scatterer size and the spread in sizes is easily derived, it is possible to model the wideband echo characteristics more realistically. Both p(R) and p(s) are conveniently obtained from digitised survey maps. Further simplifications in the stochastic model are possible if a WSSUS class of channel behaviour is presumed (11).

3. Map-derived environmental statistics

Digitised ordnance survey (OS) maps are increasingly available and offer the possibility of an automated extraction of environmental statistics. These OS maps are stored on a magnetic tape for a 500m x 500m OS grid on a 1:1250 scale. The map features, i.e., point, line or series of lines forming a coherent object, are held as fixed-length character records in blocks of 1800 or 2048 characters. It is possible to extract:

1) scatterer size s for each building and hence p(s)
2) scatterer distance R from a chosen origin; p(R)
3) angular location for each scatter; p(Ø)
4) occupied area density; i.e., the fraction of the total area which is occupied by buildings.

The building heights are not included in the map so it will be necessary to find another means to obtain it for a 3 dimensional model.

3.1 Scatterer distributions

The scatterer distributions were derived after discarding very small-sized scatterers, typically less than $20m^2$ and occupying less than 1% of the map areas. These buildings are usually tool sheds, or garden sheds located behind the houses.

The scatterer size distributions for suburban Southampton (OS reference SU4214) are shown in Fig. 2. The average scatter size is typically $100m^2$ with a spread of $45m^2$. Not surprisingly, the scatterer location distribution, p(R), does not fit the distribution predicted by eqn. (7) or Ref. 9. Rather it is skewed with a mean that depends on the map area, Fig. 3. The angular distributions, p(Ø), give a reasonable fit to the uniform distribution and are not plotted here. The occupied area densities range between 17% and 22%, and may be employed as the locality classifier. Much further work is needed to establish the area classification and to systematically study the map-derived statistics. Nevertheless, the above distributions may be usefully deployed for the model predictions.

4. Time-domain characterisation

Wideband characterisation in the time-domain is conveniently derived from the time-varying complex impulse response of the channel (6, 7), $h(t,\tau)$. Effects of the path lengths, angles of arrival (Doppler shift) and echo intensity are embedded in the measurement of $h(t,\tau)$. A 900MHZ channel sounder has been specially designed to measure $h(t,\tau)$ in a variety of environments. In the interest of brevity we will consider only the echo amplitude and delay characteristics here. A convenient way to characterise this is to derive the probability that a 'significant' echo occupies a delay interval or bin (4,11,12).

4.1 Probability of echo-path occupancy

The probability of echopath occupancy is defined as

$$P_{oc} \triangleq \Pr\left[\text{at least one echo in the interval } (\tau,\ \tau+d\tau)\right] \tag{8}$$

To derive a relationship for P_{oc} we refer to eqn. (6) and Fig. 1. Additionally, we observe that the echo amplitudes from discrete scatterers at a range R_m and an angular placement relative to the mobile direction of motion ϕ_n has a p.d.f.

$$P_{mn}(\rho) = \frac{K}{R_m} A_R(R_m) A(\phi_n) \delta(R-R_m) \delta(\phi-\phi_n) \tag{9}$$

where K is a constant, $A_R(R_m)$ and $A(\phi_n)$ are the fractional intensities of the reradiated waves at a range R_m and angle ϕ_n. In eqn. (9) $A_R(R_m)$ and $A_\phi(\phi_n)$ are geometrically uniformly distributed along R and ϕ but depend on the scatterer sizes through the joint p.d.f's p(s,R) and $p(s,\phi)$ respectively. This allows the wave divergence to be introduced in eqn. (9) through the factor $\frac{K}{R}$ dependent on p(R). The probability that an echo originates from an annular ring R_1 to $R_2 = R_1 + dR$ and ϕ in the range ϕ_1 to $\phi_2 = \phi_1 + d\phi$ is then easily obtained from eqn. (9) by

$$P(\rho)_{R_1 \le R \le R_2\ ;\ \psi_1 \le \psi \le \psi_2} = k \sum_{R=R_1}^{R_2} \sum_{\psi=\psi_1}^{\psi_2} A_R(R_m) A_\phi(\psi_n) \delta(R-R_m) \delta(\psi-\psi_n) / R_m \tag{10}$$

Clearly, this is the probability that echoes from scatterers with a range of sizes s lie in a delay range $\frac{R_1}{C} \le \tau \le \frac{R_2}{C}$ and thus becomes the probability of echo path occupancy.

5. Results

Theoretical results were obtained from equation (10) by assuming an analytical form for p(s) given below

$$p(s) = (1/2S_o)\left[1 - \cos\left(\frac{\pi}{S_o} s\right)\right] \qquad 0 \le S \le 2S_o \tag{11}$$

$$= 0 \qquad s > 2S_o$$

This raised-cosine form is close in shape to the map-derived p(s) and convenient for the analytical derivation. In Fig.4 the result for two different p(R) are shown. The P_{oc} when a uniformly distributed p(R) is chosen has a lower probability of echo occupancy at the longer delays. At these delays presumably larger scatterers of significant sizes that contribute to these events are relatively few. The case where the map derived p(R) is chosen shows a greater occurrence even at longer delays. This is plausible when the p(s) is observed to have a skewed mean.

The simulated P_{oc} derived directly from the map-derived statistics (11) is shown in Fig.5. The 20dB relative threshold is set to discern between weak and strong echoes, the strong being only significant in the distortion analyses. The theoretical and simulated results show an expected trend when compared with available measured channel data (4,5,12). Further measurements are awaited, as well as data derived from digitised maps, to validate the model in a variety of environments.

6. Conclusions

A stochastic wideband channel model is proposed that includes environment dependent parameters. Map derived statistics have been obtained in an automated procedure and both this and the model are ideally suited for wideband channel simulation. Theoretical and simulated predictions are obtained for the probability of echo path occupancy. These predictions show an expected trend when compared with measurement deduced statistics. Further work to develop this model and the environment-dependent parameters is in progress.

7. References

1. Nordic Seminar on Digital Land Mobile Radio communication, Epsoo, Finland, Feb 1985.

2. R H Clarke, 'A statistical theory of mobile radio reception', B.S.T.J., Vol. 47, 1986, pp 957-1000.

3. W C Jakes, Ed., 'Microwave Mobile Communications', J Wiley & Sons, 1974.

4. G L Turin, F D Clapp, T L Johnston, S B Fine, D Lavry, 'A statistical model of urban multipath propagation', IEEE Trans, Vol. VT.21, No. 1, 1972, pp. 1-9.

5. D C Cox '910 MHZ urban mobile radio propagation: multipath characteristics in New York city', IEE Trans., COM-21, 1973, pp. 1188-1194.

6. A S Bajwa and J D Parsons, 'Small-area characterisation of UHF urban and suburban mobile radio propagation', IEE Proc., Vol. 129, PT.F, No. 2, April 1982, pp. 102-109.

7. J D Parsons, A S Bajwa, 'Wideband characterisation of fading mobile radio channels', ibid, pp. 95-101.

8. J F Cssana, Jnr., 'A model for mobile radio fading due to building reflections: Theoretical and experimental fading waveform power spectra', B.S.T.J., 43, No. 6, 1964, pp. 2935-2971

9. J Zanders, 'A stochastical model of the urban UHF radio channel', IEEE Trans., Vol. VT-30, No. 4, Nov. 1981, pp. 145-155.

10. R G Kouyournjian, 'The Geometrical Theory of Diffraction and its Applications', Numerical and Asymptotic Techniques in Electromagnetics, R Mittra, Ed., N.Y., Springer Verlag, 1975.

11. A S Bajwa, 'A simple stochastical approach to wideband modelling of multipath propagation in mobile radio environments', IERE International *Conf. on Land Mobile* Radio, Cambridge, 10-13 Dec. 1983.

12. A S Bajwa, 'UHF wideband statistical model and simulation of mobile radio multipath propagation effects', IEE Proc., Part F, 132, No. 5 1985, pp. 327-333.

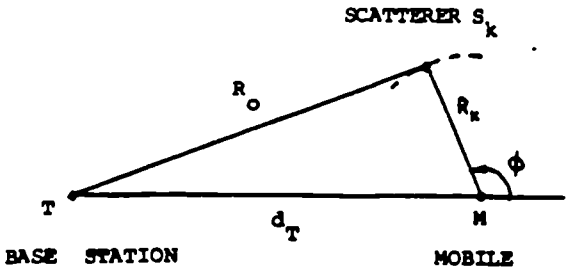

FIG. 1 SCATTERER GEOMETRY

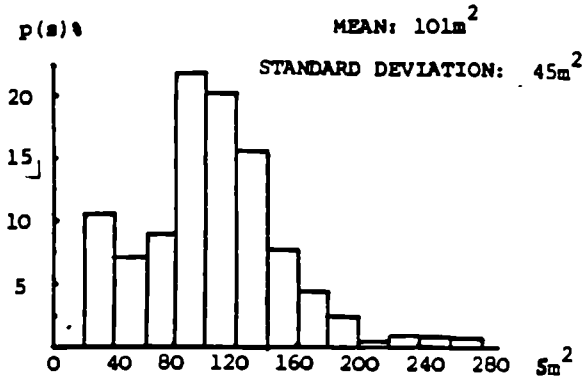

FIG. 2 SCATTERER SIZE DISTRIBUTION

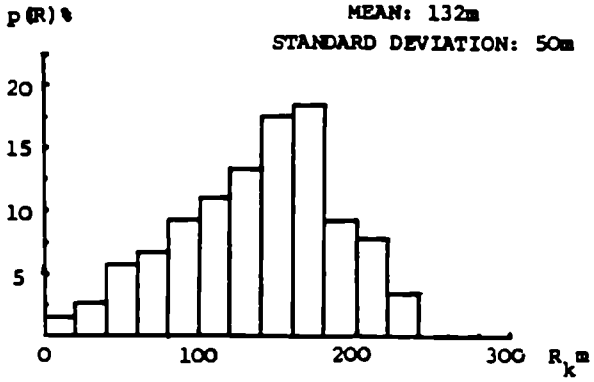

FIG. 3 DISTRIBUTION FOR SCATTERER LOCATION
MAP AREA 500 x 500m^2

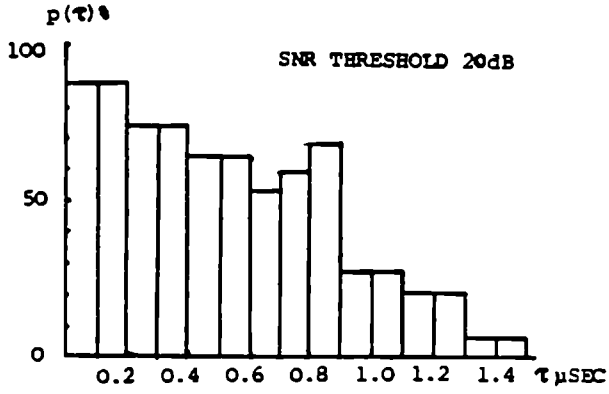

FIG. 5 PROBABILITY OF PATH OCCUPANCY

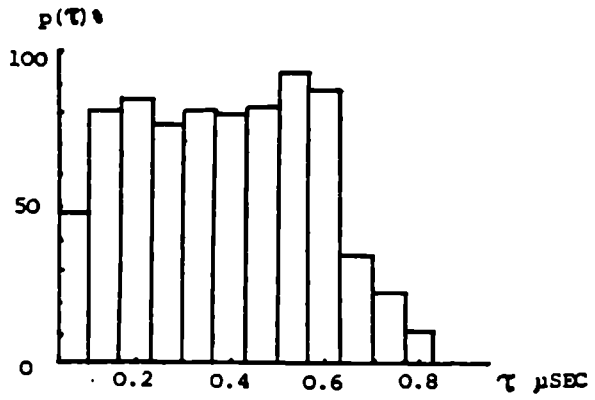

(a) MAP DERIVED P(R)

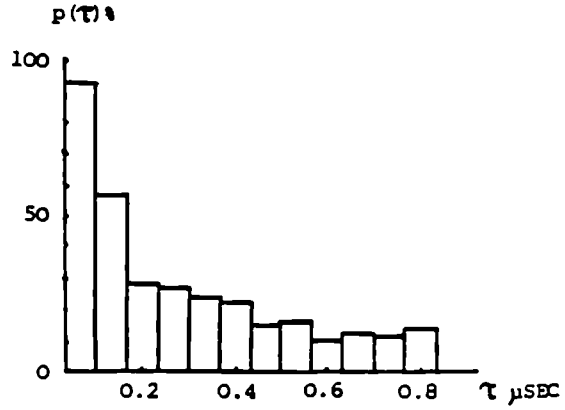

(b) UNIFORM P(R)

FIG. 4 PROBABILITY OF PATH OCCUPANCY
(THEORETICAL)

AN ENVIRONMENT-DEPENDENT APPROACH TO WIDEBAND UHF MULTIPATH PROPAGATION MODELLING

O.O. Kafaru*, A.S. Bajwa** and J.D. Parsons*

Summary

A simple multipath model with environment-dependent parameters has been developed for use in wideband propagation studies. The echo time delays and amplitudes are obtained as a function of the environment through which the mobile travels. The model has been simulated on a digital computer and used to predict signal statistics in the form of average power delay profiles, average delays, delay spreads and frequency correlation functions.

1 Introduction

The design of optimum performance wideband digital data transmission systems for use in a mobile radio environment depends largely on a satisfactory understanding of the channel behaviour over a wide bandwidth. If the medium is well characterised, the system can be designed to effectively reduce the effects of any disturbance, and in particular frequency selective fading which causes intersymbol interference.

Radio propagation in a mobile radio environment is by way of scattering from buildings and other obstacles surrounding the mobile. The received signal at the mobile is therefore the sum of scattered waves which are delayed, attenuated and phase-shifted replicas of the transmitted signal. The multipath nature of the channel is therefore environment-dependent, hence the necessity of including environmental parameters in the channel model. Some multipath propagation models have appeared in the literature [1, 2, 3, 4, 5] for both narrowband and wideband characterisation of the channel, but these omit the use of environment-dependent parameters. Zander [6] proposed a simple geometric optics approach based on randomly placed scatterers. Though the model includes path-length related phase differences, it omits wave intensity variations due to wave divergence.

The model presented in this paper, following the approach in [6], is based on the features of the local environment surrounding the mobile and includes the distance dependent intensity variations. The location R of the scatterer (with respect to a fixed origin) and the reflection coefficient ρ - a measure of the reradiating capability of the scatterer - are the two environmental parameters included in the model. The echo delays, amplitudes and phases are obtained based on the stochastic processes associated with R and ρ.

2. Channel Characterisation

The mobile radio channel can be described as a linear time varying filter [3, 5 7, 9] and modelled accordingly. A transmission of the form

$$s(t) = \mathrm{Re}\,[u(t)\exp(j\omega_c t)] \qquad (2.1)$$

is received as

$$y(t) = \mathrm{Re}\,[Z(t)\exp(j\omega_c t)] + n(t) \qquad (2.2)$$

where

$$Z(t) = \sum_{k=0}^{\infty} a_k u(t-\tau_k)\exp(-j\theta_k) \qquad (2.3)$$

and the lowpass complex impulse response of the channel is

$$h(t) = \sum_{k=0}^{\infty} a_k \delta(t-\tau_k)\exp(-j\theta_k) \qquad (2.4)$$

The k^{th} propagation path is characterised by its time delay τ_k, amplitude a_k and phase $\theta_k (=2\pi f_c \tau_k)$. The $n(t)$ is additive Gaussian noise.

In terms of the physical environment, if the scatterers are located randomly around the mobile, then the k^{th} echo path received within the time interval $(\tau_k, \tau_k + d\tau)$, the delay resolution of the receiver, is the superposition of i = 1, ... N subpaths reflected from the N scatterers. Therefore

$$a_k(\tau_k) = \sum_{i=1}^{N} c_i(\tau_i)\exp(-j\gamma_i) \qquad (2.5)$$

$$= X + jY$$

* The University of Liverpool
** Telecom Securicor Cellular Radio, London.

where

$$X = \sum_{i=1}^{N} c_i(\tau_i)\cos\gamma_i \qquad (2.6)$$

$$Y = \sum_{i=1}^{N} c_i(\tau_i)\sin\gamma_i \qquad (2.7)$$

and

$$\theta_k = \tan^{-1}\frac{Y}{X} \qquad (2.8)$$

The variables τ_i, c_i, γ_i, the time delay, amplitude and phase of the subpath due to scatterer i describe the effect of the scatterer on the received echo at the mobile.

Though the channel is time variant, its statistical properties remain stationary over a distance of a few hundred wavelengths [7], leading to its classification as a Wide Sense Stationary Uncorrelated Scattering channel. Small scale statistics obtained over the stationary sections can be combined to produce the global characteristics of the channel.

3. Environment Characterisation

In propagation studies for mobile radio links generally, a qualitative description of the environment is used - with terms like urban, suburban and rural. These definitions are not precise and are vague in a quantifying sense. In general, a service area may encompass all these areas and different classes of environments must be used in the system planning procedure to accommodate that variety. There is therefore an obvious need to describe the environment quantitatively to surmount the current unavoidable ambiguity embodied in the qualitative definitions. The parameters employed in this classification process must be simple and available for extraction from Ordnance Survey maps and other related sources.

Parameters of interest include

a) Percentage of local area occupied by buildings defined as the building area index - BAI.

b) Building location distributions - BLD.

c) Building height distributions - BHD.

d) Terrain - TI.

Although these parameters are defined independently, radio propagation characteristics depend on more than one factor simultaneously.

Three classes of environments are proposed, each of which can be further divided into subclasses giving precise characterisation.

3.1 Class 1 Environment

This class comprises the rural areas described as

(A) Flat rural area

(B) Undulating rural area

(C) Hilly rural area

Parameters BAI and TI are of major importance in the characterisation of this class of environments.

3.2 Class 2 Environment

This class defines the suburban areas which are predominantly residential and can be divided into the following categories

(A) Residential area

(B) Residential with parks and open areas

(C) Residential with high rise buildings

(D) High rise residential areas (e.g. housing estates). Characterisation is achieved using the four parameters.

3.3 Class 3 Environment

This class describes the urban/dense urban areas which are mixtures of buildings used for private, commercial and industrial purposes. The categories of environments included in this class are

(A) Shopping with residential area

(B) Shopping with commercial area

(C) Commercial area

(D) Industrial area

Preliminary work has shown that the BAI for class 2 ranges from 15% to 30% while it is over 40% for class 3.

4. Multipath Model

In the simple 2-dimensional geometry of Figure 1, the principal mode of scattering is single reflection. Each scatterer reradiates incident electromagnetic energy and is therefore attributed a reflection coefficient ρ. The spatial co-ordinates of the scatterers are fixed according to the stochastic process p(R) associated with the scatterer location R. The reflection coefficients are also randomly distributed. The dynamic multipath behaviour of the channel emerges as the mobile moves through a sequence of spatial locations.

Expressions for the path variables τ_i, c_i, γ_i defined earlier are obtained using the simple geometry.

4.1 Propagation time delay τ_i

The propagation path length d_p is given by

$$d_p = d_s + r \qquad (4.1)$$

and the delay time is

$$\tau_i = \frac{d_p}{c} \qquad (4.2)$$

c = velocity of light

Using simple geometric relationships

$$\tau_i = \frac{1}{c}\,[d_T + R_i(1+\cos\phi_i) - l\cos(\phi_i - \eta)] \qquad (4.3)$$

4.2 Echo amplitude c_i

The amplitude c_i is a function of the distances d_s and r. However, due to the local nature of the model, the effect of distance r on the reflected signal is of greater importance. To determine the behaviour of the EM wave, we use a geometric wave optics approach which is well justified at the UHF frequency of operation. For the sake of brevity, only the main steps in the derivation will be presented in this paper.

From Maxwell's equations in a source-free isotropic, homogeneous medium, the electric field satisfies the Helmholtz equation

$$\nabla^2 \hat{E} + K^2 \hat{E} = 0 \qquad (4.4)$$

for $\nabla.\hat{E} = 0$ and $k = 2\pi/\lambda$ where λ is the wavelength of the source. The asymptotic expansion of $\hat{E}$ for k apart from the time factor $\exp(j\omega t)$ is [10, 11]

$$\hat{E}(s) = \exp(-jK\psi) \sum_{n=0}^{\infty} \hat{E}_n(s)/(jk)^n \qquad (4.5)$$

The high frequency limit of interest, the geometrical optics term, is obtained for n = 0. Substituting (4.5) in (4.4) and solving the resulting recursive equations for n = 0 gives

$$\hat{E}(s) \sim \exp(-jk\psi(s))\hat{E}_n(s_o)[G(s)/G(s_o)]^{\frac{1}{2}} \qquad (4.6)$$

where

G(s) = curvature of wavefront at point s on the ray

s_o = reference point

Using the assumption that the scatterers are located at a large distance from the transmitting station, then the waves incident on the scatterers are plane EM waves of the form [11]

$$\hat{E}(d) \sim \exp(-jk\psi(d))\hat{E}_o(d); d = (x^2+y^2+z^2)^{\frac{1}{2}} \qquad (4.7)$$

Selecting the time co-ordinate such that the reflected wavefront appears to have its beginning at point $r_o = 0$ at time t = 0, then

$$\psi(r,\theta,\phi) = r \qquad (4.8)$$

The wavefronts r = ct represent a spherical wave propagating outward from r = 0

For this wave

$$G(r) = 1/r^2 \qquad (4.9)$$

substituting (4.7), (4.8), (4.9) in (4.6) and solving, gives the electric field of the reflected wave at distance r from the scatterer as

$$\hat{E}_r(r) = \frac{\rho \hat{E}_i(r_o)}{r} \exp[\psi(r_o)+\psi(r)] \qquad (4.10)$$

The amplitude c_i of the reflected wave varies as the inverse of the distance r and ρ is a function of the scatterer geometry.

4.3 Echo phase γ_i

Referring to equation (4.10), let the initial phase of the echo be defined as γ_o. For a mobile moving a distance l metres in time τ_i, the phase of the echo becomes

$$\gamma_i = \gamma_o + kl\cos\alpha_i \qquad (4.11)$$

where α_i is the angle of wave arrival with respect to the direction of motion of the mobile. For a vehicle speed V, $l = V\tau_i$. Substituting for l and k in (4.11)

$$\gamma_i = \gamma_o + 2\pi f_D \tau_i \qquad (4.12)$$

f_D is the doppler frequency and is given by

$$f_D = \frac{V}{\lambda}\cos\alpha_i \qquad (4.13)$$

5. Multipath Model Simulation

The multipath model was developed for the purpose of predicting the behaviour of the mobile radio channel at UHF in various environments by means of computer simulation methods. The simplicity of the model ensures that this is viable and a program package has been written to simulate it on the IBM3083 mainframe computer at Liverpool University. Using environmental parameters, scatterer location distributions and scatterer sizes extracted from a digitized Ordnance Survey map, statistical results have been obtained in

the following form:-

a) Average power delay profiles

b) Average delays and delay spreads

c) Frequency correlation functions

d) Probability distribution of echo strengths at fixed delays

5.1 Simulation Technique

The simulation technique is based on the hypothetical experiment depicted in Figure 2 which corresponds to a real physical situation. A mobile travels through the channel (a street) and records the received echo profiles at regular intervals. At each spatial location m, the program generates the echo description set (τ_k, a_k, θ_k), the delay, amplitude and phase in the kth bin.

The resolution of the experiment is 0.1μs and the time delay axis is divided into 0.1μs bins with the shortest path or line-of-sight (LOS) delay as the reference (bin 0). Any physical path lying in bin k is deemed to have arrived with 0.1k μs excess delay. This means two paths are resolvable only if $\tau_k - \tau_{k-1} > 0.1\mu s$.

For the scatterer i, the propagation time delay τ_i is calculated using eqn.(4.3) and quantized to the appropriate bin. The corresponding set (c_i, γ_i) is obtained using eqns.(4.10) and (4.11). Since individual subpaths within a delay bin are unresolvable, the resultant a_k and θ_k for the kth bin with N echoes arriving with delay k are obtained using equations (2.5) to (2.8).

The received echo power $p_m(\tau_k)$ is then obtained as

$$p_m(\tau_k) = I_m(\tau_k) + Q_m(\tau_k) \qquad (5.1)$$

where I and Q are the inphase and quadrature components given by

$$I(\tau_k) = a_k \cos\theta_k$$
$$Q(\tau_k) = a_k \sin\theta_k \qquad (5.2)$$

The signal statistics described earlier are obtained by performing the appropriate statistical computations on the I and Q components.

5.2 Simulation program

The simulation program is written in Fortran 77 and is of a modular form. The main module computes the path variables τ_k, a_k, θ_k and the I and Q components. It accesses a data base containing the scatterer locations (w.r.t. a fixed origin) and base areas extracted from a digitized Ordnance Survey map. The base area of a scatterer is a measure of its reflection coefficient. Input control data e.g. route identity, base station transmitter location e.t.c. are supplied at the start of the simulation run. The sampling distance Δ is fixed at 0.2λ (0.066m) to ensure that profiles at slightly separated geographical locations are correlated.

As the mobile moves along the selected route, the nearest 50 scatterers are selected as possible reflectors thus ensuring that the gradual change in principal scatterers which occurs in a real situation is incorporated. However, it is expected that these scatterers will remain the same over a distance of about 10 metres, therefore to save computation time, the scatterers are sampled at every 30λ of mobile movement. The scatterers which contribute significantly to the received signal are determined by the distance r (fig.1). The initial phases of the reflected subpaths in the first profile are assumed apriori uniformly distributed over (0,2π). A random number generator is used to produce a set of numbers over 0-2π which are then assigned to each scatterer. Each new scatterer is assigned a random phase from this set. The I and Q components generated are stored in a data file for access by the other modules.

A second module generates the power profiles and computes the average delays, delay spreads and frequency correlation functions using the method adopted by Cox [8]. A third module computes the probability distributions of echo strengths at fixed delays and the amplitude correlation coefficients of echos in adjacent delay bins. In a typical simulation run, 2000 echo profiles are generated, corresponding to a distance of 132 metres of mobile movement which at 30 mph (13.4 m/s) is a vehicle run time of about 10s. Small scale characterisation is done over 33 metre sections of the street in a typical residential area.

6. Results

Figure 3A shows a series of average power delay profiles obtained over 4 consecutive 33 metre sections of the street. Each profile is the average of 500 individual power profiles. The houses along the street are two storey semi detached houses of roughly the same size, therefore, the statistics are not expected to have a wide variation. The profiles in fig.3A are very similar thus confirming the homogenous nature of the environment. The corresponding frequency correlation functions are shown in figure 3B. The coherence bandwidth B_c is obtained at 0.5 correlation. The values of average delay, delay spread and coherence bandwidth for the profiles are given in Table 1. These values are comparable to those obtained by Cox [8] and Bajwa [12].

The cumulative amplitude distributions at fixed delays exhibit both Rayleigh and log-normal characteristics. For each of the four profiles, the distribution at 0μs show a marked departure from Rayleigh while the distributions at 0.2μs and 0.3μs fit the Rayleigh statistics fairly well. Cox [8] and Turin [3] have shown that this is not uncommon.

7. Conclusions

A simple environment dependent multipath model for wideband propagation at 900 MHz has been developed and simulated on a digital computer. Prediction results show that the model gives a good insight into the channel behaviour.

References

1. Clarke, R.H., 'A statistical theory of mobile reception' BSTJ, vol.47, p.968, pp.957-1000.

2. Jakes, W.C. (Ed)., 'Microwave mobile communications', John Wiley & Sons, 1974.

3. Turin, G.L. et al; 'A statistical model of urban multipath propagation', IEEE Trans., Veh. Tech; VT-21, No.1, 1972, pp.1-9.

4. Ossana, J.F., Jnr, 'A model for mobile radio fading due to building reflections: Theoretical and experimental fading waveform power spectra'. BSTJ, Vol.43, No.6, 1964, pp.2935-2971.

5. Parsons, J.D. and Bajwa A.S.; 'Wideband Characterisation of fading mobile radio channels', IEE Proc. F, 129, No.2, 1982, pp.95-101.

6. Zander, J. 'A statistical model of the urban UHF radio channel', IEEE Trans. Veh. Tech, VT-30, No.4, 1981, pp.145-155.

7. Kennedy, R.S., 'Fading dispersive Communication Channels, John Wiley, 1969.

8. Cox, D.C., 'Delay doppler characteristics of Multipath Propagation at 910 MHz in a suburban mobile radio environment, IEEE Trans. Ant. Prop, Vol.AP-20, No.5, 1972, pp.625-635.

9. Bello, P.A., 'Characterisation of Randomly time variant linear channels, IEEE Trans. Com. Syst, Vol.CS-11, Dec. 1963, pp.360-393.

10. Kline, M and Kay, I.W., 'Electromagnetic theory and Geometrical Optics', Krieger Pub-Co., New York, 1979.

11. Keller, J.B.; Lewis, R.M. and Seckler, B.D.; 'Asymptotic solution of some diffraction problems, Comm. Pure and App. Maths, Vol.9, 1956, pp.207-265.

12. Bajwa, A.S.: 'Wideband Charaterisation of UHF mobile radio propagation in Urban and Suburban areas'. Ph.D. thesis, Department of Electronic and Electrical Engineering, University of Birmingham, U.K., 1979.

Average Profile	Average delay d μs	Delay spread s μs	Coherence bandwidth B_c MHz
1	0.21	0.29	3.80
2	0.22	0.28	2.25
3	0.21	0.27	2.85
4	0.20	0.27	2.85
Overall average	0.21	0.27	3.20

Table 1: Average power delay profile characteristics

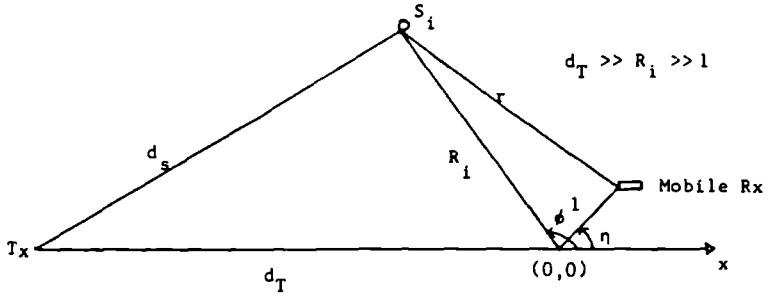

Fig. 1: Multipath geometry of the model

Fig. 2: Hypothetical Experiment for simulation.

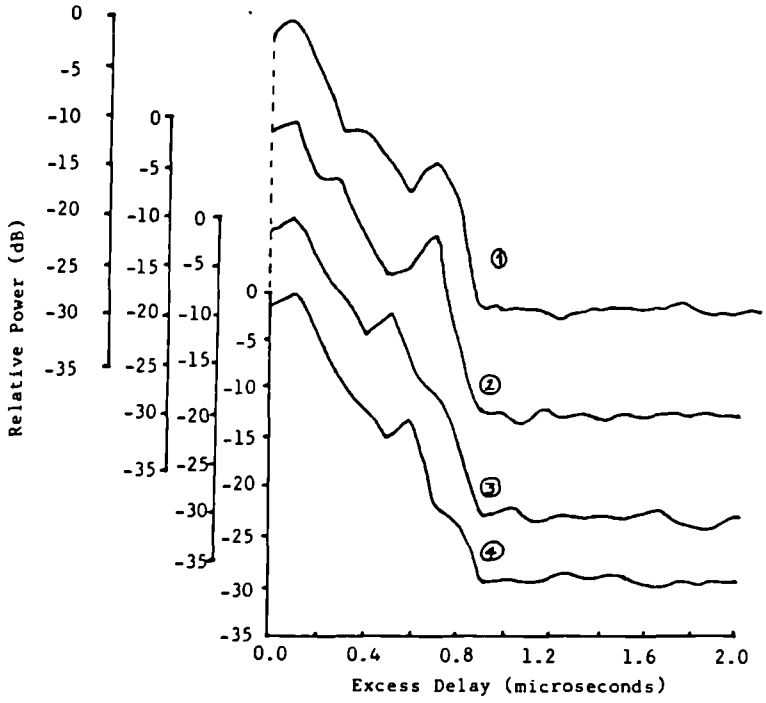

Fig. 3A: Average power delay profiles.

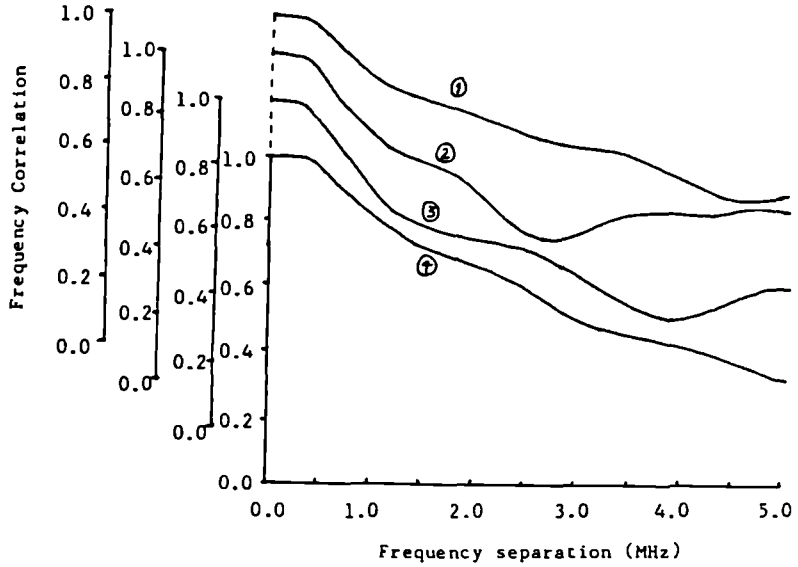

Fig. 3B: Frequency correlation functions.

CHANNEL MODELLING AND SIMULATION FOR WIDEBAND SYSTEMS

O.O Kafaru

1. Introduction

In mobile radio communications, the design of wideband digital data transmission systems for optimum performance under the conditions established by the propagation channel, depends largely on a good understanding of the channel behaviour over a wide bandwidth. If the channel is well characterised, the system can be designed to reduce the effects of any disturbance, in particular, frequency selective fading which causes intersymbol interference and its attendant limits on BER performance.

In the past, to achieve this objective, it has been necessary to carry out extensive costly and time consuming measurements in various carefully selected areas, such as would typify the environment in which the system is to be implemented. Analysis of the data yields system design parameters that describe the dispersive behaviour of the channel. The results collected in one area cannot necessarily be applied in another. This suggests the need for alternative ways of studying the channel behaviour.

An attractive option is that of the use of a suitable propagation model, either in a mathematical analysis, or a simulation study. It is well known that buildings and other structures in the mobile radio environment, greatly influence the wave propagation between base station and mobile [1,2]. A model of the propagation channel will, for the sake of completeness and accuracy, need to include parameters which are functions of the environment. Previous models [3,4,5] have omitted this factor, but Zander [6] proposed a model based on randomly located scatterers. The model presented in this paper, is based on the features of the local environment of the mobile, namely the scatterer locations and their reradiating capabilities. It also allows for distance-dependent wave intensity variations and doppler shifts caused by vehicle movement [7].

2. Channel propagation model

The derivation of the model required the identification of the fundamental mechanism of wave propagation between base station and mobile unit. The use of simple geometry, and a recourse to ray-optics methods, ensured that an accurate representation of the channel could be obtained. The principal mode of scattering is single reflection. Figure 1 shows the 2-dimensional geometry of the model. Each scatterer reradiates incident electromagnetic energy and is therefore attributed a reflection coefficient ρ_i, which is a function of the size of the scatterer. In addition, its location is fixed at a distance R_i from a reference origin. The random scatterer locations suggest that a stochastic process p(R) can be associated with R. Likewise, we associate a process $p(\rho)$ with ρ. Each propagation path can be characterised by a set of path variables, namely, propagation time delay τ_i, amplitude c_i and phase shift γ_i. The derivations of the expressions for these variables have been presented elsewhere [7], but for the sake of brevity, only the representative expressions will be given herein.
Referring to figure 1, the echo time delay is obtained as

$$\tau_i = 1/c[Z + R_i(1 + \cos\varphi) - m\cos(\varphi_i - \eta)] \qquad (2.1)$$

and the corresponding path amplitude is

$$c_i = \rho_i E_i / r_i \qquad (2.2)$$

where E_i is the field incident on the scatterer.
The phase shift due to vehicle movement of Δm metres is

O.O Kafaru is with the Department of Electrical Engineering and Electronics, University of Liverpool.

$$\gamma_i = \gamma_o + \Delta\gamma = \gamma_o + \beta(\Delta m)\cos\alpha_i \qquad (2.3)$$

where γ_o is the phase at the previous location.
The dynamic multipath behaviour of the channel emerges as the mobile moves through a sequence of spatial locations. The received signal is the sum of these time delayed, attenuated and phase shifted versions of the transmitted signal. In characterisation studies, this multipath effect is measured in the time domain as the impulse response of the channel, given by the equation

$$h(t,\tau) = \sum_{k=0}^{\infty} a_k(\tau)\delta(t - \tau_k)\exp(-j2\pi f_c\tau_k) \qquad (2.4)$$

In terms of the physical environment, the kth propagation path, recieved in the time interval (τ_k, $\tau_k + d\tau$) which is the delay resolution of the receiver, is the superposition of i = 1,...,N subpaths.

The random nature of the channel implies that its behaviour should be studied by stochastic methods, in particular, using the autocorrelation function of the impulse response (or transfer function in the frequency domain). The mathematical expression for this function, in terms of the parameters obtained earlier, is complex and difficult to handle analytically. Therefore, recourse has been made to software simulation, to obtain the impulse response from which the correlation function can be obtained using Fourier Transform techniques.

3. Channel simulation

The multipath propagation model was developed for the purpose of predicting the dispersive behaviour of the radio channel at UHF in various types of environments. The basis of the simulation is therefore a statistical map of the service area being investigated. This map, obtainable either by extraction from Ordnance Survey maps or generated using random number generators of a desired distribution, comprise essentially of the building locations and sizes (base areas). The transmitter site and vehicle routes are also fixed. The mobile, empowered to move along the routes at a specified constant speed, records the received echo profiles at spatial points spaced 0.06 metres apart. Ray tracing techniques are used to identify the valid ray paths. Each echo profile is described by the parameter set { τ_k, a_k, θ_k } where k numbers the distinguishable ray paths. The time resolution of the simulation is 0.1μs, which means that two paths are resolvable only if $\tau_k - \tau_{k-1} > 0.1\mu s$. The time delays are referred to the shortest or line of sight path if it exists. This simulated impulse response is analysed in the same manner as for experimental data to obtain three system design parameters of interest, namely average delay, delay spread and coherence bandwidth of the channel. These parameters explicitly describe the dispersiveness of the particular environment.

4. Example results

Simulations have been carried out for various types of environments in the city of Liverpool. The results presented, in the form of average power profiles and frequency correlation functions, are for two different sample locations. The average power profiles are for 6 metre sections of the street.

Figure 2 shows a profile obtained on Melville Street in a residential area on the edge of the university precint. The street is almost radial to the direction of the transmitter. A block of 4-storey flats lies on the right hand side of the mobile while there's an open space on its left with a couple of large buildings set approximately 100 metres and 80 metres from the road. The profile shows a small degree of dispersion with most of the energy arriving within 1 μs excess delay. The smoothly decaying correlation function and corresponding large 0.5 coherence bandwidth is as expected.

The second location, Everton Road, is situated about 1.5 km from the transmitter and is also in a residential area. Figure 3 shows the average power profile obtained. The two peaks at about 1.4μs and 2.0μs are due to two 8-storey buildings, located approximately 220 metres and 250 metres ahead and on the edge of a vast open space on the left of the mobile. These peaks result in the large delay spread and a smaller 0.5 coherence bandwith than that of figure 3. Their effect is not overly pronounced as as they lie about 15dB below the peak power value. The oscillation in the frequency correlation function is due to the peak at 0.4μs.

Comparing these two sets of results, it is seen that the simulation model is capable of predicting the effect of prominent terrain features on the received signal.

5. Conclusion

An environment-dependent multipath propagation model has been developed and used in the simulation of the wideband mobile radio propagation channel. Results show that the model predicts very well, the effect of the environment on the mobile received signal.

References

[1] COX.D C :' Delay Doppler Characteristics of Multipath Propagation at 910 MHz in a Suburban Mobile Radio Environment', IEEE Trans., Vol. AP-20, No.5, Sept. 1972, pp 625-635.

[2] BAJWA.A.S :' Wideband Characterisation of UHF Mobile Radio Propagation in Urban and Suburban Areas', Ph.D Thesis, Department of Electronic and Electrical Engineering, University of Birmingham, UK, 1979.

[3] CLARKE.R.H :' A Statistical Theory of Mobile Radio Reception', Bell Syst. Tech. Jnl., Vol. 47, July 1968, pp 957-1000.

[4] TURIN.G.L .CLAPP.F.D JOHNSTON.T.L .FINE.S.B .LAVRY. D.:' A Statistical Model of Urban Multipath Propagation', IEEE Trans., Vol. VT-21, No.1, Feb. 1972, pp 1 - 9.

[5] SUZUKI.H. :' A Statistical Model for Urban Radio Propagation', IEEE Trans., Vol. COM-25, No. 7, July 1977, pp 673-680.

[6] ZANDER.J. :' A Stochastical Model of the Urban UHF Radio Channel', IEEE Trans., Vol. VT-30, No 4, Nov. 1981, pp 145-155.

[7] KAFARU.O.O, BAJWA.A.S and PARSONS.J.D :'An Environment- Dependent Approach to Wideband UHF Multipath Propagation Modelling', IERE Fourth International Conference on Land Mobile Radio, University of Warwick, Dec. 1987, pp 121-127.

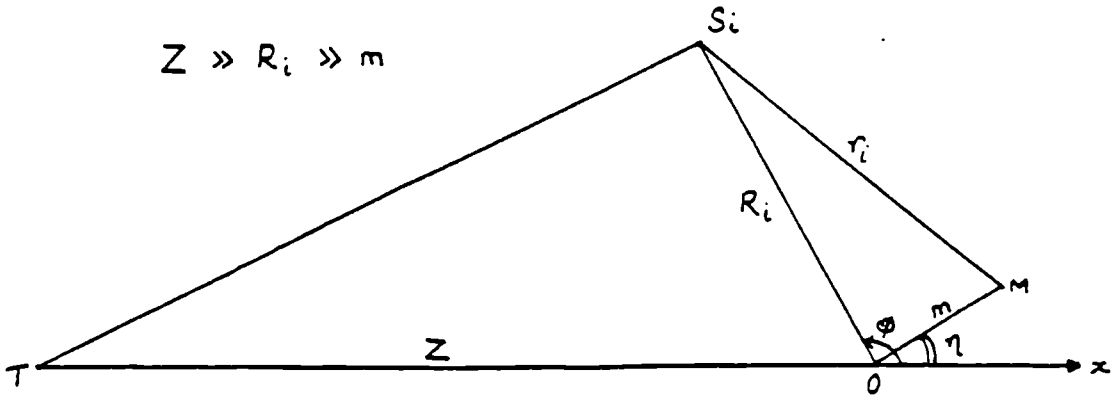

Figure 1. Geometry of the multipath model

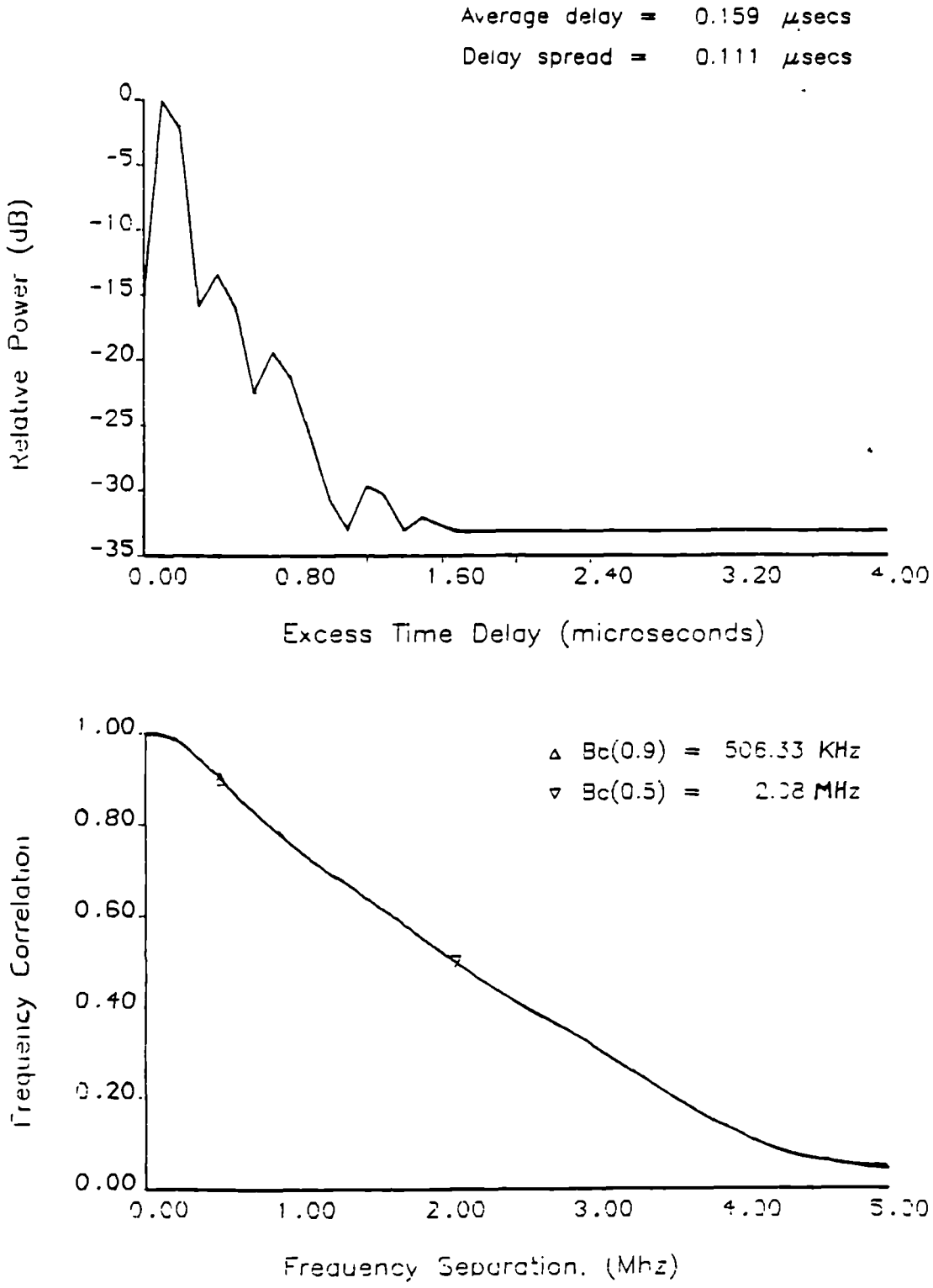

Figure 2. Average power delay profile and frequency correlation function for Melville Street.

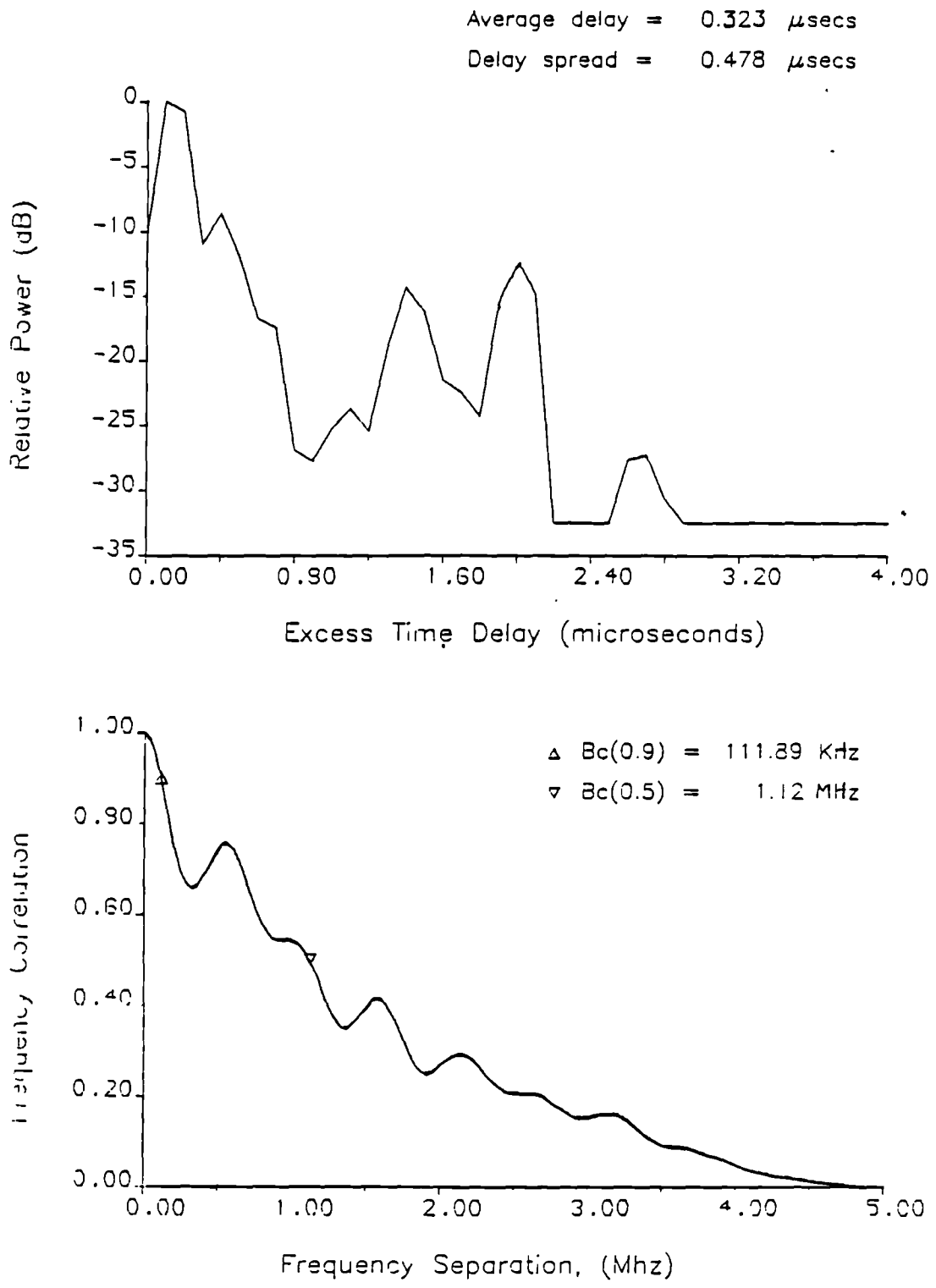

Figure 3. Average power delay profile and frequency correlation function for Everton Road.